AD-A028 095

ABBREVIATED FULL-SCALE FLIGHT TEST INVESTIGATION OF THE LOCKHEED L1011 TRAILING VORTEX SYSTEM USING TOWER FLY-BY TECHNIQUE

NATIONAL AVIATION FACILITIES EXPERIMENTAL CENTER

PREPARED FOR
FEDERAL AVIATION ADMINISTRATION

MAY 1976

Report No. FAA-AFS-1-76-2

ABBREVIATED FULL-SCALE FLIGHT TEST INVESTIGATION OF THE LOCKHEED L1011 TRAILING VORTEX SYSTEM USING TOWER FLY-BY TECHNIQUE

Leo J. Garodz

MAY 1976

FINAL REPORT

Prepared for

U. S. DEPARTMENT OF TRANSPORTATION

FEDERAL AVIATION ADMINISTRATION

Systems Research & Development Service

Washington, D.C. 20590

Technical Report Documentation Page

1. Report No.	2. Government Accession No.	3. Recipient's Catalog No.
FAA-AFS-1-76-2		

4. Title and Subtitle	5. Report Date
ABBREVIATED FULL-SCALE FLIGHT TEST INVESTIGATION OF THE LOCKHEED L1011 TRAILING VORTEX SYSTEM USING TOWER FLY-BY TECHNIQUE	May 1976
	6. Performing Organization Code
	8. Performing Organization Report No.
7. Author(s)	FAA-NA-75-14
Leo J. Garodz	
9. Performing Organization Name and Address	10. Work Unit No (TRAIS)
Federal Aviation Administration National Aviation Facilities Experimental Center Atlantic City, New Jersey 08405	11 Contract or Grant No 214-531-070
	13 Type of Report and Period Covered
12. Sponsoring Agency Name and Address	Final June 1972
U.S. Department of Transportation Federal Aviation Administration Systems Research and Development Service Washington, D.C. 20590	14 Sponsoring Agency Code

15 Supplementary Notes

16. Abstract

A brief flight test program was conducted at the National Aviation Facilities Experimental Center (NAFEC) to investigate the time-history characteristics of the vortex system of a Lockheed L1011 airplane in terminal area-type operations using a 140-foot high instrumented tower. Vortex rotational flow velocities were measured by hot-film anemometers, vortex flow visualization--as outlined by tower-mounted smoke granades--was documented, and meteorological data was recorded. In addition, data on aircraft track, performance, and configuration were gathered. The test results show that: (1) the L1011 vortex system was more persistent and intense than that of other heavy jet transport (300,000 lb) aircraft tested by NAFEC, but did not persist for more than 2 minutes; (2) vortex dissipation was due primarily to vortex breakdown (bursting); (3) vortex core diameters were on the average about 5, 4, and 2 feet in diameter for the landing, approach, and takeoff configurations, respectively; (4) peak recorded tangential velocities, V_θ, were 126, 135, and 224 feet per second for these same respective configurations; (5) vortex lateral movement in-ground effect was approximately $(\pi/6.6)b$, above ground level; and (6) average vortex descent velocities approached 6 feet per second out of ground effect.

COLOR ILLUSTRATIONS REPRODUCED IN BLACK AND WHITE

17. Key Words	18. Distribution Statement
L1011 Wakes L1011 Turbulence L1011 Trailing Vortices L1011 Full-Scale Flight Tests Hot-Film Anemometry	Document is available to the public through the National Technical Information Service, Springfield, Virginia, 22151 **PRICES SUBJECT TO CHANGE**

19. Security Classif. (of this report)	20. Security Classif. (of this page)	21. No. of Pages	22. Price
Unclassified	Unclassified	234	8.00

Form DOT F 1700.7 (8-72) Reproduction of completed page authorized

NOTICE

This document is disseminated under the sponsorship of the Department of Transportation in the interest of information exchange. The United States Government assumes no liability for its contents or use thereof.

TABLE OF CONTENTS

LIST OF ILLUSTRATIONS

LIST OF ILLUSTRATIONS (continued)

LIST OF ILLUSTRATIONS (continued)

LIST OF ILLUSTRATIONS (continued)

SYMBOLS

AR	=	Wing Aspect Ratio, b^2/S
b	=	Aircraft wingspan, feet
b'	=	Separation of vortex pair, feet, $\pi b/4$
C_L	=	Airplane lift coefficient,
h	=	Height above ground level (AGL), feet
$\bar{c}$	=	Wing mean aerodynamic chord, feet
L	=	Lift pounds (=nW)
n	=	Normal load factor
q	=	Dynamic pressure, lb/ft^2 $(=\frac{1}{2}\rho V^2)$
r	=	Distance from vortex center, feet
r_c	=	Vortex core radius where V_θ is a maximum, feet
S	=	Wing area, feet
t	=	Vortex age, seconds
V	=	True airspeed, knots or feet per second
$\hat{V}_\theta$	=	Absolute recorded vortex tangential velocity, feet per second
V_θ	=	Vortex tangential velocity, feet per second
W	=	Gross weight of aircraft, pounds
y	=	Lateral distance from aircraft flightpath or centerline, feet
$\dot{y}$	=	Lateral velocity, feet per second
Z	=	Vertical distance measured downward from aircraft flightpath feet
$\dot{Z}$	=	Downward vertical velocity, feet per second
Γ	=	Vortex circulation, square feet per second
Γ_o	=	Initial midspan vortex circulation, $\frac{4W}{\pi\rho Vb}$ square feet per second
ρ	=	Air density, slugs/per cubic foot

Subscripts:

max = maximum

v = vortex

w = wind

ind = induced

a/c = aircraft

INTRODUCTION

PURPOSE.

The National Aviation Facilities Experimental Center (NAFEC) has performed an abbreviated flight test program to gather data on and analyze the relatively "long" time-history characteristics of the vortex system of a Lockheed L1011 airplane in terminal area-type operations. The results thereof are of potential value to further refine, if necessary, air traffic control operation criteria associated with simultaneous operations of various mixes of other aircraft with this airplane in the National Airspace System (NAS).

Major parameters for consideration were: aircraft vortex tangential flow velocities, their field of influence, i.e., radial distribution of the tangential velocity; vortex persistence and low-altitude meteorological data. In addition, it was desired to obtain discrete flow-field data on vortex core diameters for potential math modeling of the L1011 vortex wake.

BACKGROUND.

In 1970 NAFEC jointly participated with the National Aeronautics and Space Administration (NASA) and the Boeing Company to investigate the vortex wake characteristics of the then newly-arrived "jumbo jets," the Lockheed C5A and Boeing 747, and some of the older, large jet transport-type aircraft. Full-scale flight testing was necessary because, although relatively expensive compared to other vortex investigations, e.g., wind tunnel, water tank, analytical studies, etc., it produced the needed results quickly and with confidence in their application in NAS.

NAFEC flight test teams primarily concentrated on measuring vortex characteristics at low altitudes using the tower fly-by technique. Tests were performed at both the Environmental Science Services Administration (ESSA) site at the Nuclear Reactor Test Station (NRTS) of the Atomic Energy Commission (AEC) facility at Idaho Falls, Idaho (reference 1), and at NAFEC at Atlantic City, New Jersey (references 2 and 3). The other investigations (NASA and Boeing) primarily used the in-flight vortex probe technique (references 4 and 5).

In 1972, with the advent of the "wide-body" jets (i.e. the L1011 and DC10), the Federal Aviation Administration (FAA), Flight Standard Service (AFS), initiated a request to NAFEC for an investigation of the L1011 airplane's vortex wake characteristics inasmuch as NAFEC had the necessary experience and equipment to accomplish this investigation expeditiously.

The flight tests were conducted on June 3, 1972, at the NAFEC 140-foot, full-scale flight test vortex measurement facility (figure 1); and preliminary results, in the form of a data report, were submitted to AFS on June 16, 1972. Because of the limited availability of the L1011 test aircraft, only 19 data runs were made during a single early morning test period. The data acquired forms the basis for this report.

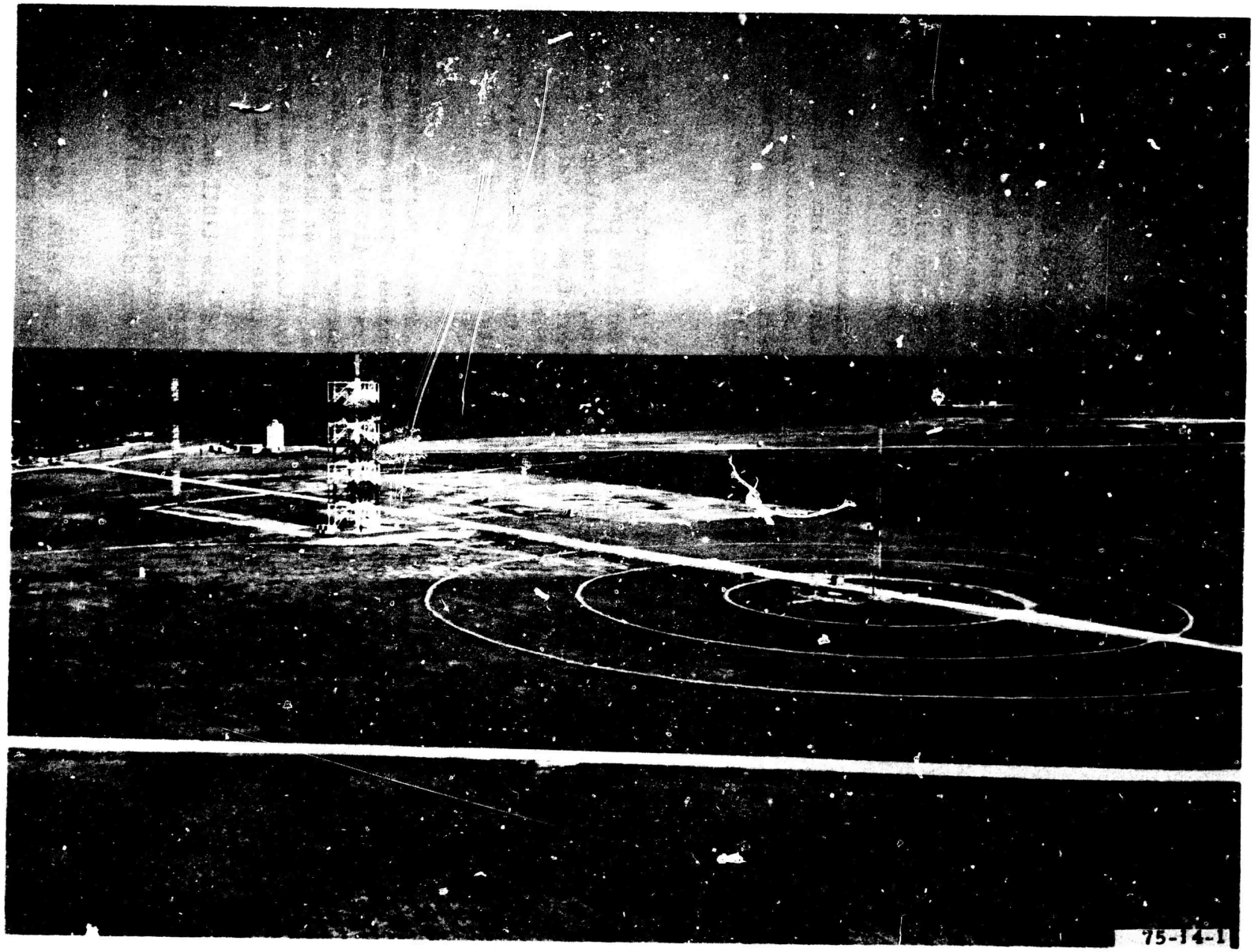

FIGURE 1. NAFEC 140-FOOT HIGH FULL-SCALE FLIGHT TEST VORTEX MEASUREMENT FACILITY

DISCUSSION

FLIGHT TEST PROGRAM.

TEST AIRPLANE. The Lockheed Aircraft Company provided the airplane (destined for Eastern Airlines) for this flight test program. Photographs of the L1011-1 airplane are shown in figures 2 and 3. Three-view, general arrangement drawings are shown for the L1011 with flaps up and flaps down in figures 4 and 5, respectively.

The wing is of cantilever low-wing monoplane design with high lift devices. The dihedral at the trailing-edge is 7° 31 min on the inner wings, 5° 30 min on the outboard panels. Wing sweepback is 35° at the quarter-chord. The high-lift system incorporates large chord double-slotted Fowler trailing-edge flaps and full-span leading edge slots which provide substantial lift augmentation for takeoff and landing.

Tracks are mounted on the forward segment of the trailing-edge flaps to permit extension and rotation of the aft segment. Four leading-edge slots are installed outboard of the engine pylon on each wing. Each segment is mounted to two roller-supported tracks and extends in a circular motion down and forward for takeoff and landing. Three Krueger leading-edge flaps are installed inboard of each engine pylon on each wing. Six spoilers are installed on the upper surface of each wing, two inboard and four outboard of the high-speed aileron.

The L1011 also has a direct lift control (DLC) system for glide-slope control. For the landing approach at constant airspeed and pitch angle, DLC is accomplished by modulation of the flight spoilers about a nonzero nullpoint and greatly improves glidepath control. The DLC function is possible only in the landing configuration.

TEST PROCEDURE. The tower fly-by technique was used for this test. The technique basically consisted of flying the L1011 airplane perpendicular to the ambient surface wind, as measured at the top of the tower --140 feet above ground level (AGL) -- at an appropriate distance vertically and upwind laterally from the tower and preferably under light-ambient wind conditions, the latter being most conducive to vortex persistence.

Figure 6 depicts the L1011 flying abeam of the test tower on a data run. Six of the seven levels of vortex flow visualization smoke generators have been ignited. A "High Ranger," used for close-up, detailed vortex structure photograph coverage, is visible on the right-hand side. (Figure 7 vividly depicts the assistance that colored smoke vortex flow visualization provides for subsequent data analysis.) Further details on this test technique can be obtained in reference 6.

FIGURE 2. LOCKHEED L1011 TRISTAR AIRPLANE ON GROUND

FIGURE 3. LOCKHEED L1011 TRISTAR AIRPLANE IN FLIGHT

During the test period relatively low ambient winds did prevail, ranging from 16 feet per second (ft/s) (11 miles per hour (mi/h)) to 20 ft/s (14 mi/h) as measured at the tower top and decreasing to a range of 1 ft/s (0.7 mi/h) to 6 ft/s (4 mi/h) at 23 feet AGL.

For this task it was intended to gather vortex data of at least 2 minutes of age. The relatively low height of the test tower (140 feet AGL) for this size (wingspan=155 feet) airplane made it difficult, if not impossible, to achieve that "age" with a vortex that was out of "ground effect" for the entire period between generation and interception of the tower.

FULL-SCALE VORTEX MEASUREMENT FACILITY. A photograph of the facility is shown in figure 1. The focal point of the facility is the test tower, which is 140 feet high and whose base is 76 feet above sea level. It is an equilateral triangle tower tapering from 5 feet on a side at its base to about 1 1/2 feet on a side at the top. This tower is constructed of steel, of cantilever design and requires no guy wires. The tower is, in reality, a large aerodynamic rake.

The adjacent area is relatively flat terrain for a radial distance of about 1,000 feet from the tower base. Three concentric circles at radii of 100, 200, and 300 feet are visible in the photograph and are used to facilitate tower identification on the part of the test pilots and airplane lateral positioning on the part of both the pilot and site project manager.

INSTRUMENTATION.

AIRPLANE. The Lockheed L1011 airplane was not specially instrumented for the tower fly-by testing nor was there any need for it to be. Pilot knee-pad data on time abeam of the vortex tower, airplane configuration, indicated airspeed, radar altitude above the ground, pressure altitude (29.92 inches of mercury) magnetic track, lateral distance from the tower, and engine performance were found to be sufficient for subsequent data correlation and analysis. The phototheodolite data were used in lieu of pilot recorded data on airplane track, altitude, and position abeam of the tower. In addition, the pilot was requested to note the stability or smoothness (turbulence level) of the atmosphere when performing a tower fly-by. The indicated airspeed (IAS) was converted to equivalent airspeed (EAS).

TOWER VORTEX MEASUREMENT. The hot-film airflow anemometry used for vortex measurements in the series of tests is described in reference 6. However, there were two major differences in this tower configuration for the L1011 flight tests. The sensors were spaced at 1-foot intervals, and signals were deleted at the lower levels. Because of limitations on available signal data recording system capability of 210 signals and the need to obtain additional high resolution data not acquired in the reference 6 flight tests, the hot-film airflow sensors at levels 41 feet AGL and below were inactivated. This was felt to be a valid choice of signal deletion inasmuch as it was assumed,

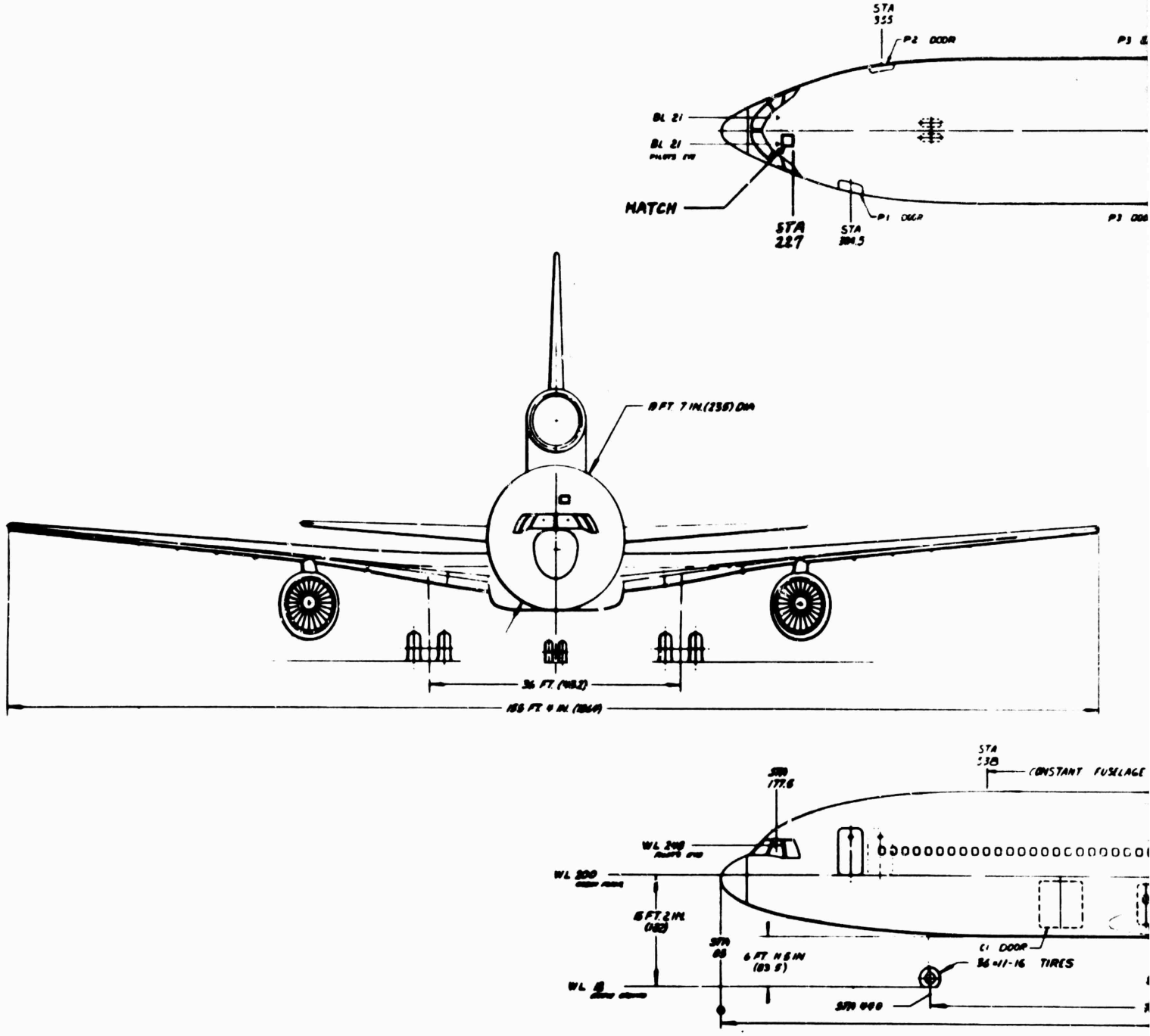

FIGURE 4. THREE-VIEW DRA

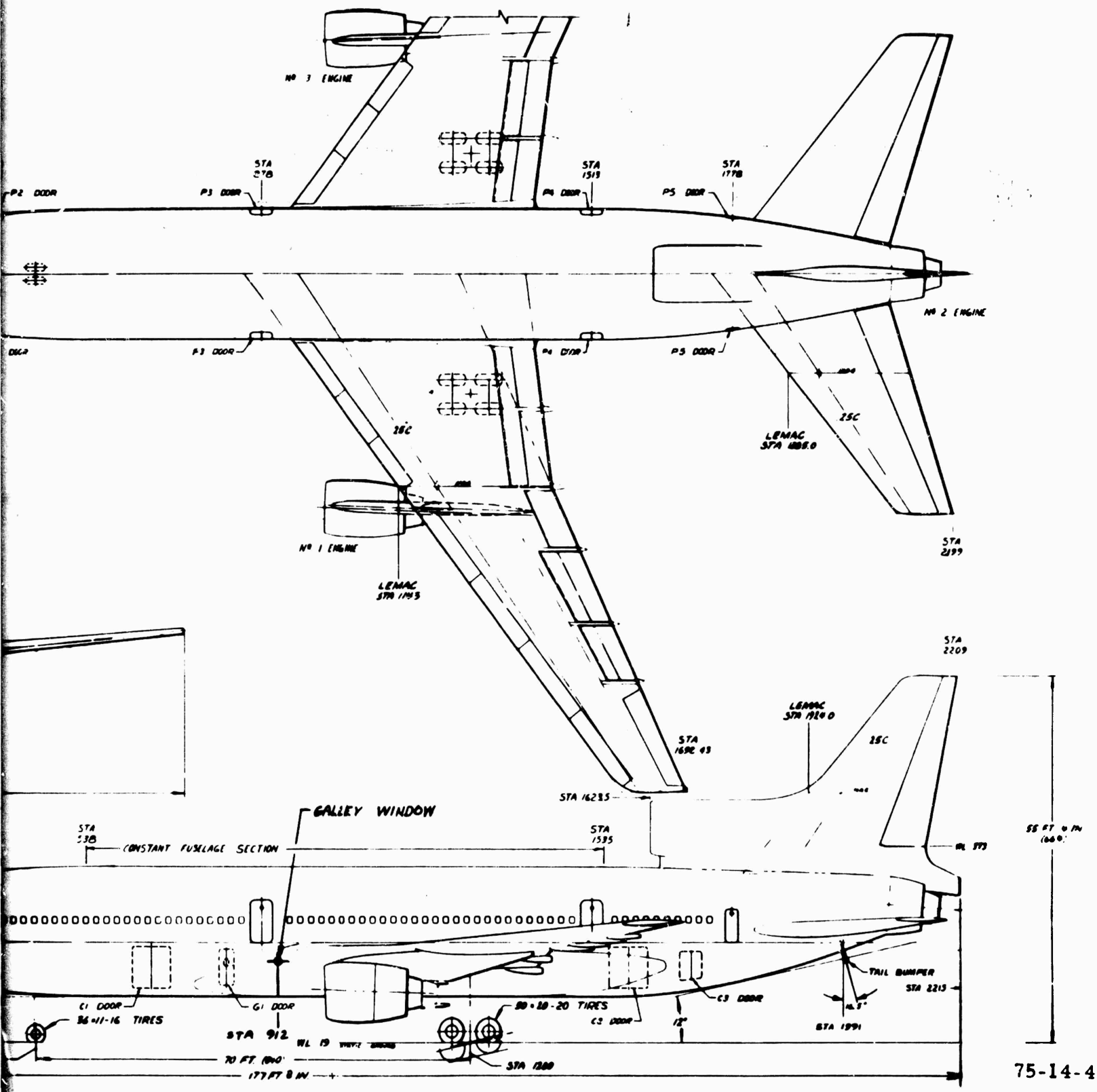

75-14-4

RE 4. THREE-VIEW DRAWING L1011, FLAPS UP

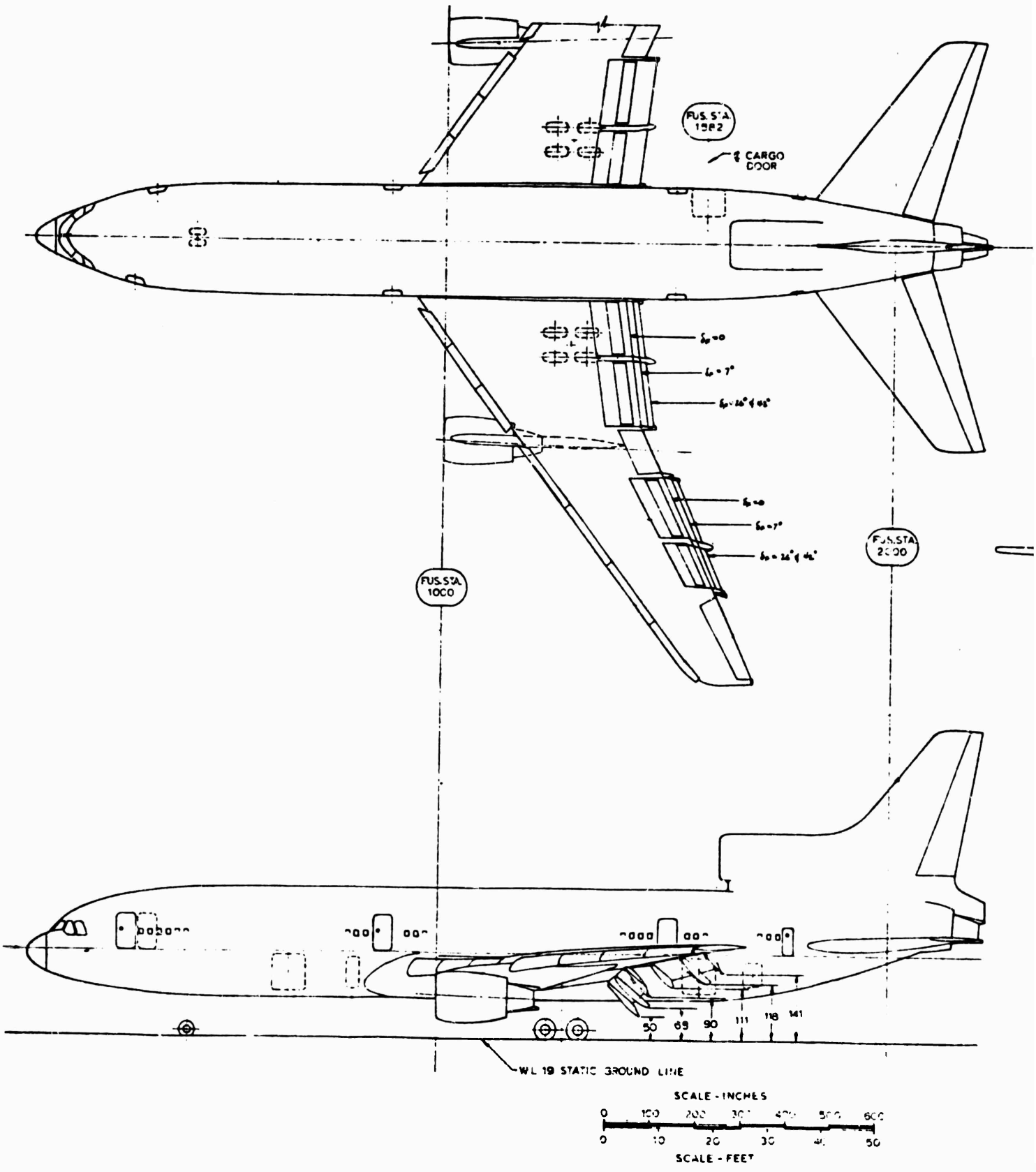

FIGURE 5. THREE-VIEW DRAWING L1011, FLA

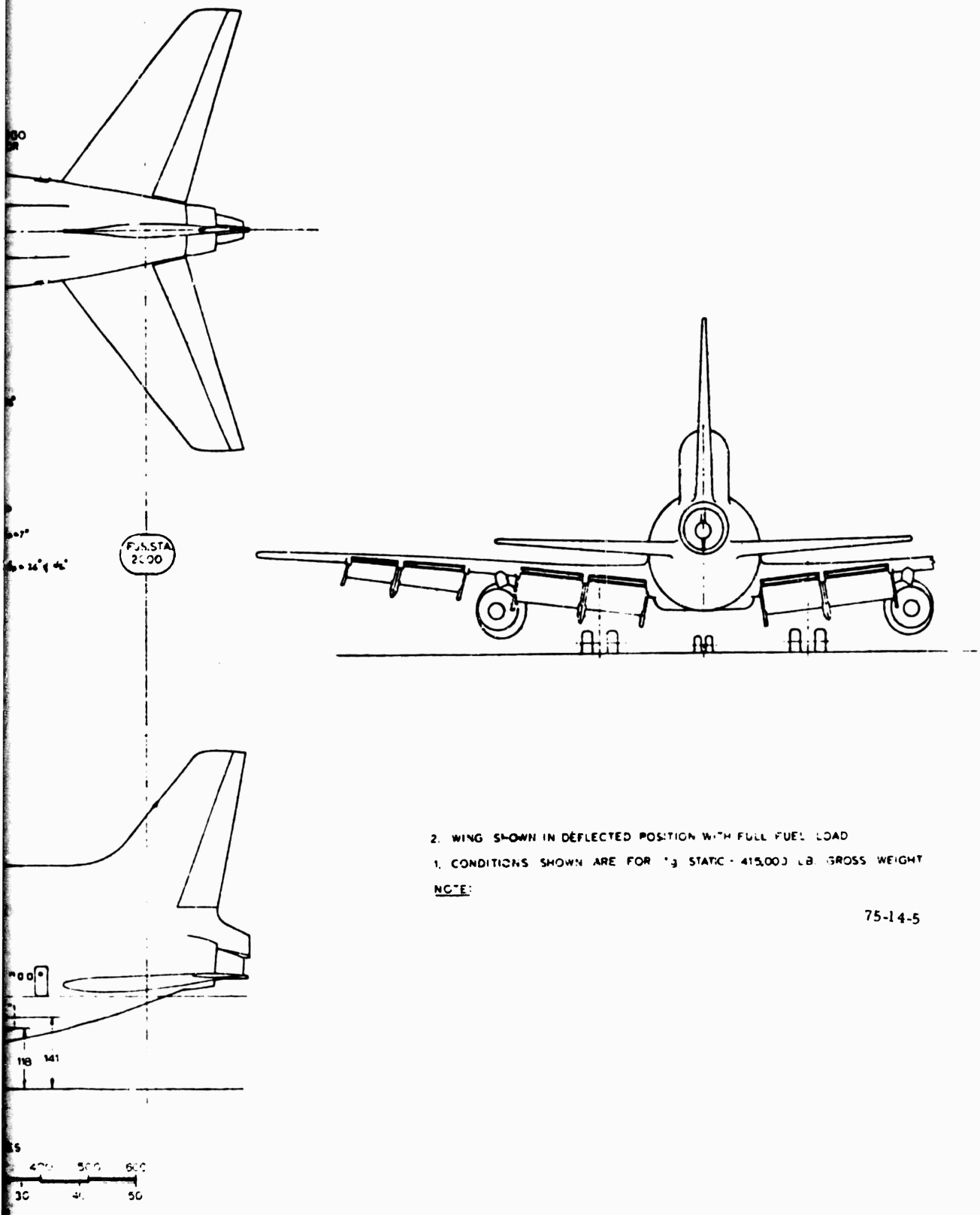

2. WING SHOWN IN DEFLECTED POSITION WITH FULL FUEL LOAD

1. CONDITIONS SHOWN ARE FOR 1g STATIC - 415,000 LB. GROSS WEIGHT

NOTE:

75-14-5

E-VIEW DRAWING L1011, FLAPS EXTENDED 42°

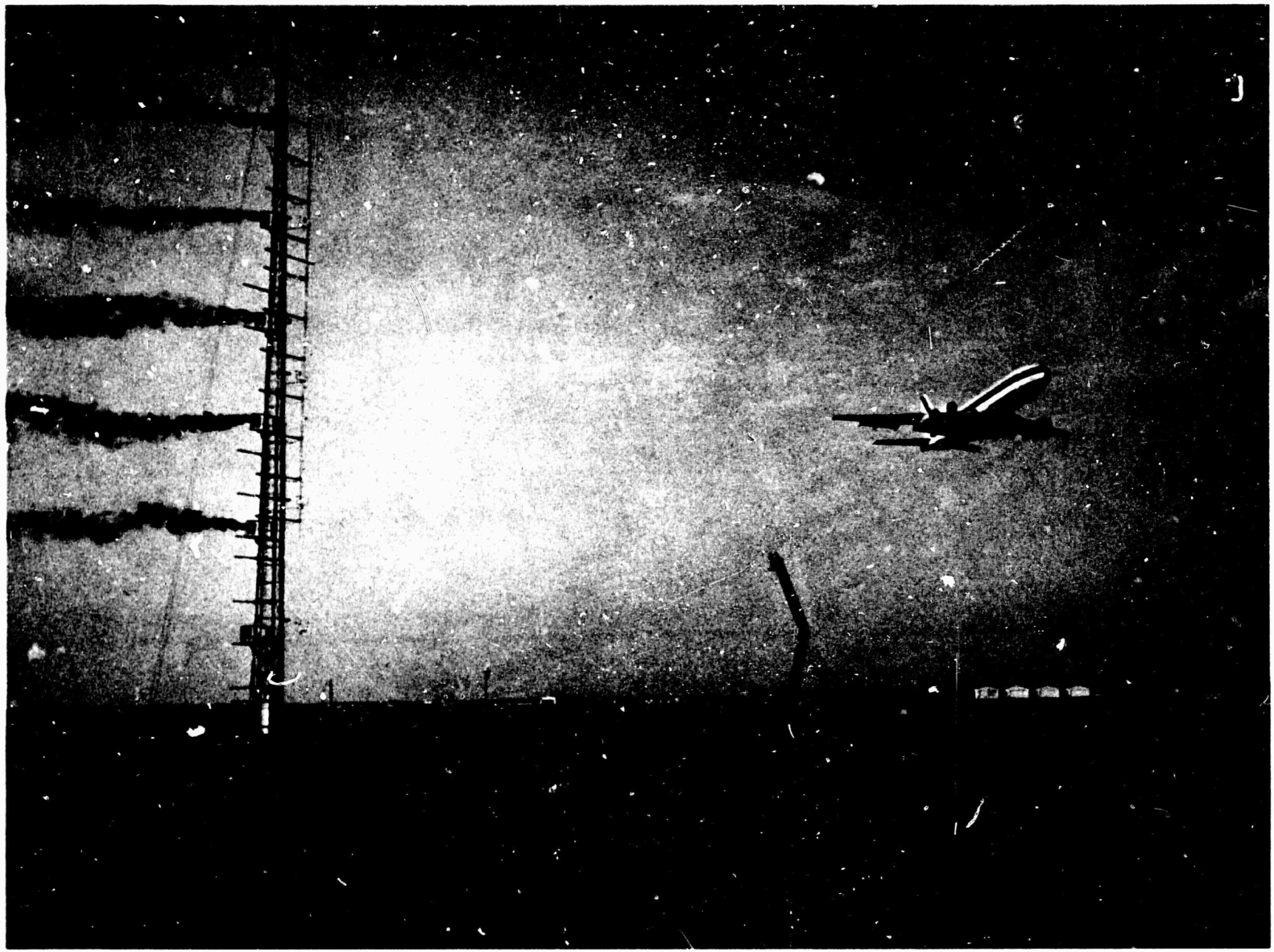

FIGURE 6. L1C11 FLYING ABEAM OF THE NAFEC TEST TOWER

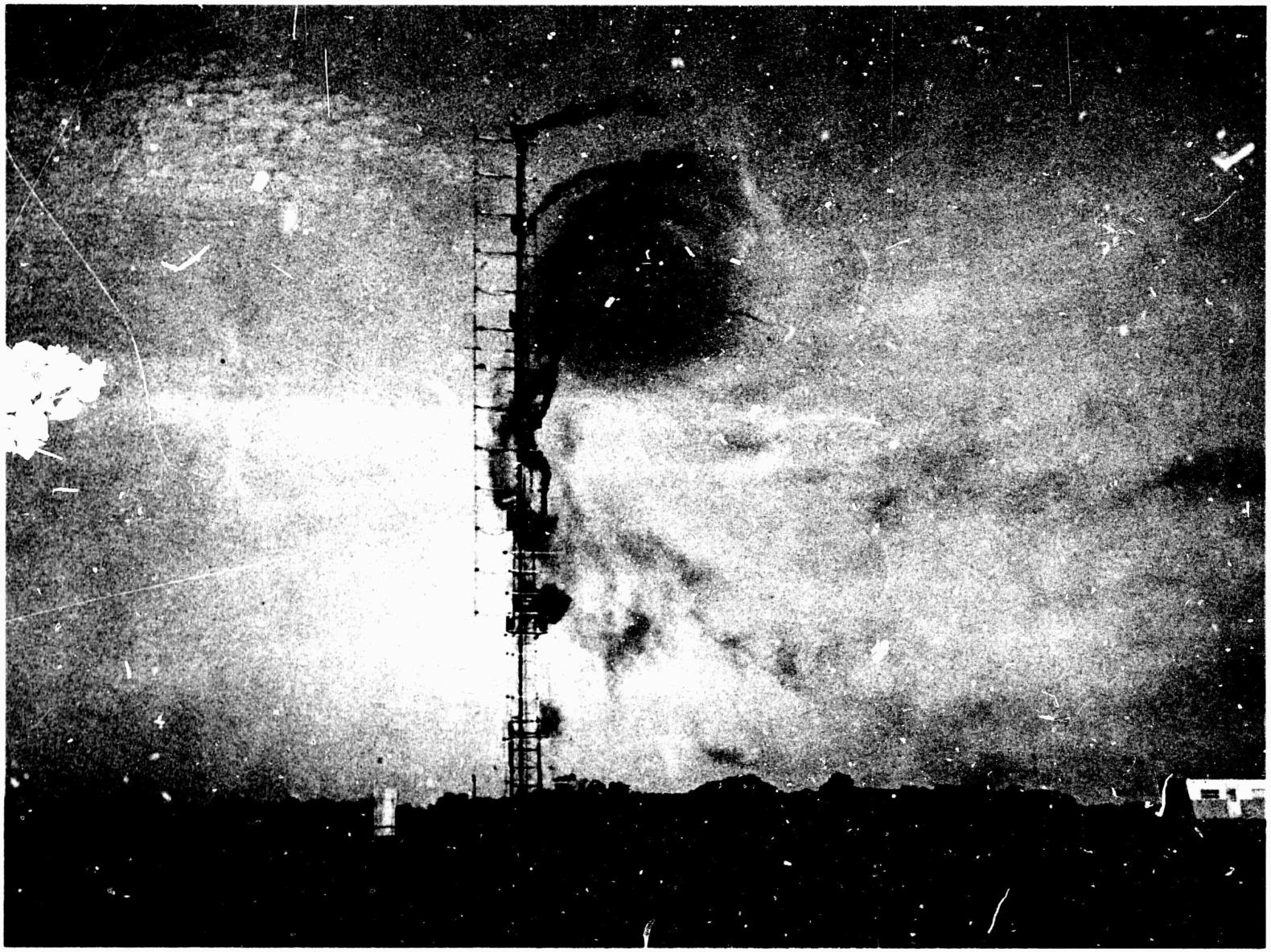

FIGURE 7. L1011 PART WING VORTEX SYSTEM AS VISUALIZED BY VORTEX

based on previous flight tests with other large aircraft, that the majority of the vortex hits would be above this level. This assumption proved to be valid, as one can see upon screening the enclosed data on the height of vortex hits on the tower.

In addition to the planned signal deletion from these lower sensors, additional lower signals were inadvertently lost. Hot-film anemometer sensor levels 42 to 55 AGL were not recorded on the magnetic tape due to improper patching of the tape recorder. This was not discovered until the tests were completed and the data processed. As discussed in reference 6, on-line real-time oscillograph recordings were made for each tower fly-by for signal sensor operational reliability and validity checks. However, because of data acquisition instrumentation circuitry design, the presence of recorded vortex velocity signals on the oscillograph did not necessarily mean that these signals were being recorded on magnetic tape. Because of concern for the accuracy of the hot-film anemometors used in these tests when the sensors were immersed in a field of reverse airflow -- i.e., when the flow was impinging on the sensor from the direction of the horizontal support arm -- a series of calibrations was conducted in the NAFEC 20X28 inch wind tunnel. The calibration procedure and results thereof are discussed in detail in appendix A and further in the body of this report.

METEOROLOGY: TOWER ATMOSPHERIC MEASUREMENT. Meteorological instrumentation was installed at five levels (ground level to 140 feet AGL) along the vertical span of the tower. These five levels were 23, 45, 70, 100 and 140 feet above the ground. Ambient temperature, wind velocity, and direction were recorded for these five levels. In addition, atmospheric relative humidity measurements were made for levels 23 and 140 foot AGL. Additional information on meteorological measurement instrumentation is described in reference 6.

METEOROLOGY: UPPER ATMOSPHERIC MEASUREMENT (>140 feet AGL). Meteorological data above the 140-foot vortex tower was obtained from the upper air facility, which was located approximately 2 miles southeast of the vortex tower. The upper air measurements were made with a standard Weather Bureau radiosonde, using a 600-gram balloon. Tracking was accomplished with a model WBRT-57 radio theodolite. Measurements, including temperature, humidity, and pressure were transmitted to the ground station by the radiosonde and elevation and azimuth angles were obtained from the theodolites.

The information transmitted by the radiosonde occurs as a nonperiodic interval known as a contact point. These points are based upon pressure of the atmosphere and usually occurred at approximately 300-foot increments up to an altitude of 3,000 feet when data collection was stopped. As a result of this type operation, atmospheric data was not available from the 140-foot level of the tower to the first contact point which occurred at an altitude of 300 feet.

A radiosonde was released before and after each vortex flight test period. If the test flights were scheduled for a long period, such as 4 hours, a third radiosonde would be released in the middle of the test period.

PHOTOGRAPHY. Vortex flow visualization was provided by the colored smoke grenades mounted at 20-foot intervals along the vertical span of the tower and both motion- and still-photography were used to record the results. This made it possible to determine when and at what level the vortex systems passed through the tower and proved to be a valuable aid in confirming the interpretation of recorded data. Two 16 mm colored motion picture cameras were located 90° apart on 325 feet radii from the tower to provide this coverage. An elapsed time clock was within the field of view of each camera (for example, see figures 8 and 9 for vortex "age" time correlation). A third 16 mm colored motion picture camera, using a zoom lens, was installed on a "Hi-Ranger" crane to provide closeup coverage of the vortices.

The still-photographic coverage was primarily of targets of opportunity, i.e., coverage of vortices with an obviously unusual structure.

DATA TIME CORRELATION. Correlation between aircraft fly-bys and vortex generation and movement was accomplished by "central time" which was recorded concurrently with airflow and meteorological sensor outputs on magnetic tape and on the phototheodolite data. An event marker switch was triggered when the L1011 was abeam of the tower, denoting "zero time." This concurrently ignited a flash bulb located within the field of view of the motion picture cameras on the ground and started the elapsed time clocks cited earlier.

DATA PROCESSING. Data processing methods are discussed in reference 7.

DATA ANALYSIS/RESULTS.

DATA PRESENTATION. The flight test data output and presentation consist primarily of:

1. Computer printouts (not included in this report) of peak recorded vortex tangential velocity versus time, as recorded by the sensors from the levels of 56 to 142 feet;

2. Plots of recorded tangential velocity scalar magnitude against time for the 87 hot-film sensor levels. An example of these is shown for tower fly-by data run 12 in figure 10,, wherein both starboard and port wing vortices passed through the sensor array at approximately 74 feet above the ground. The L1011 was in takeoff/approach configuration, which uses 22° landing flap deflection. Other select examples are shown in appendix B;

3. Still photography and motion picture coverage of the visualized vortices in the tower vicinity. Figure 7 is an example of the former. No photographic coverage was obtained on L1011 data runs 16 and 17, due to the expenditure of the smoke grenades on the previous 15 fly-bys. Tower fly-bys were continued and data collected during smoke grenade replenishment on data runs 16 and 17 to avoid loss of flight test time;

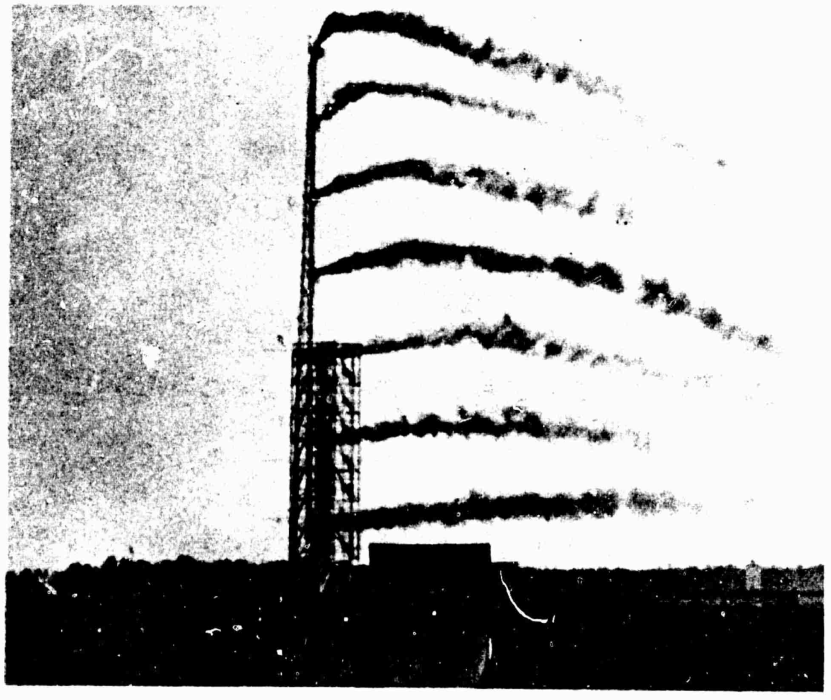

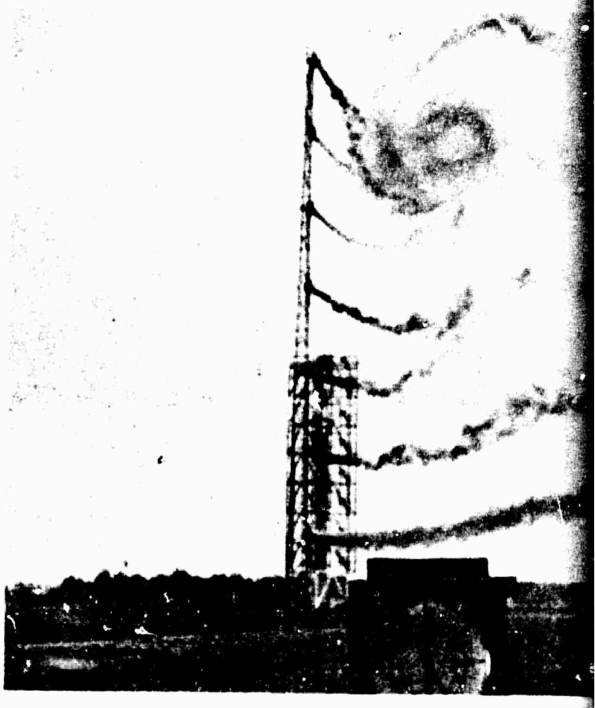

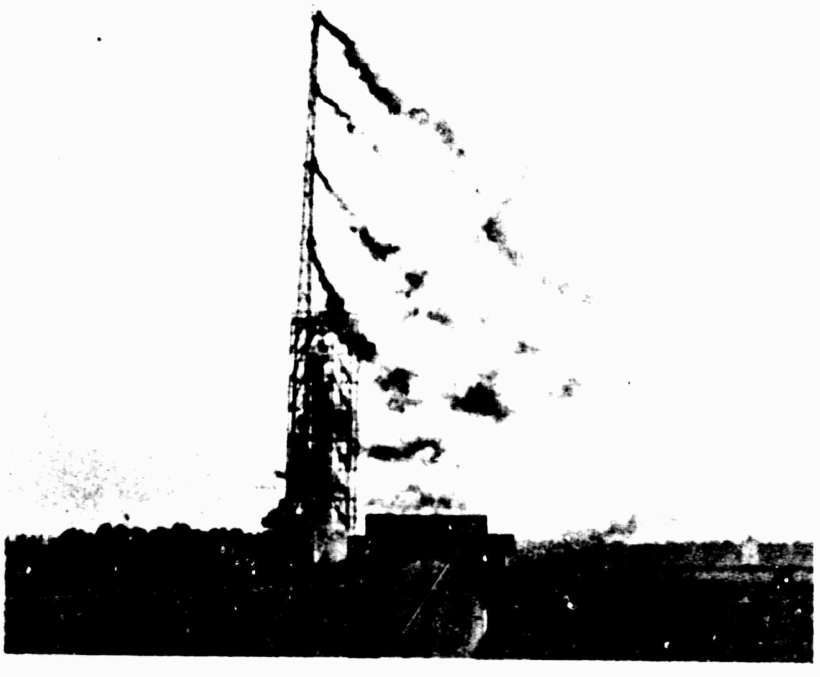

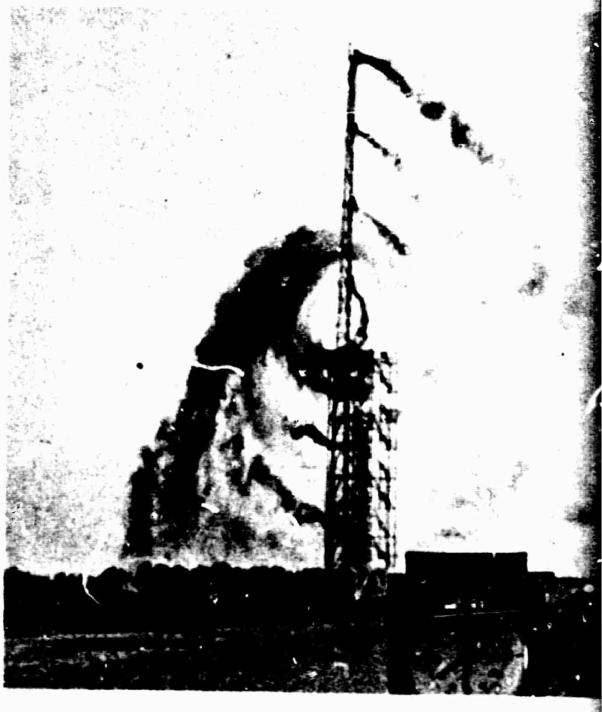

FIGURE 8A. PHOTOGRAPHIC (16mm) COVERAGE OF L1011 VORTICES

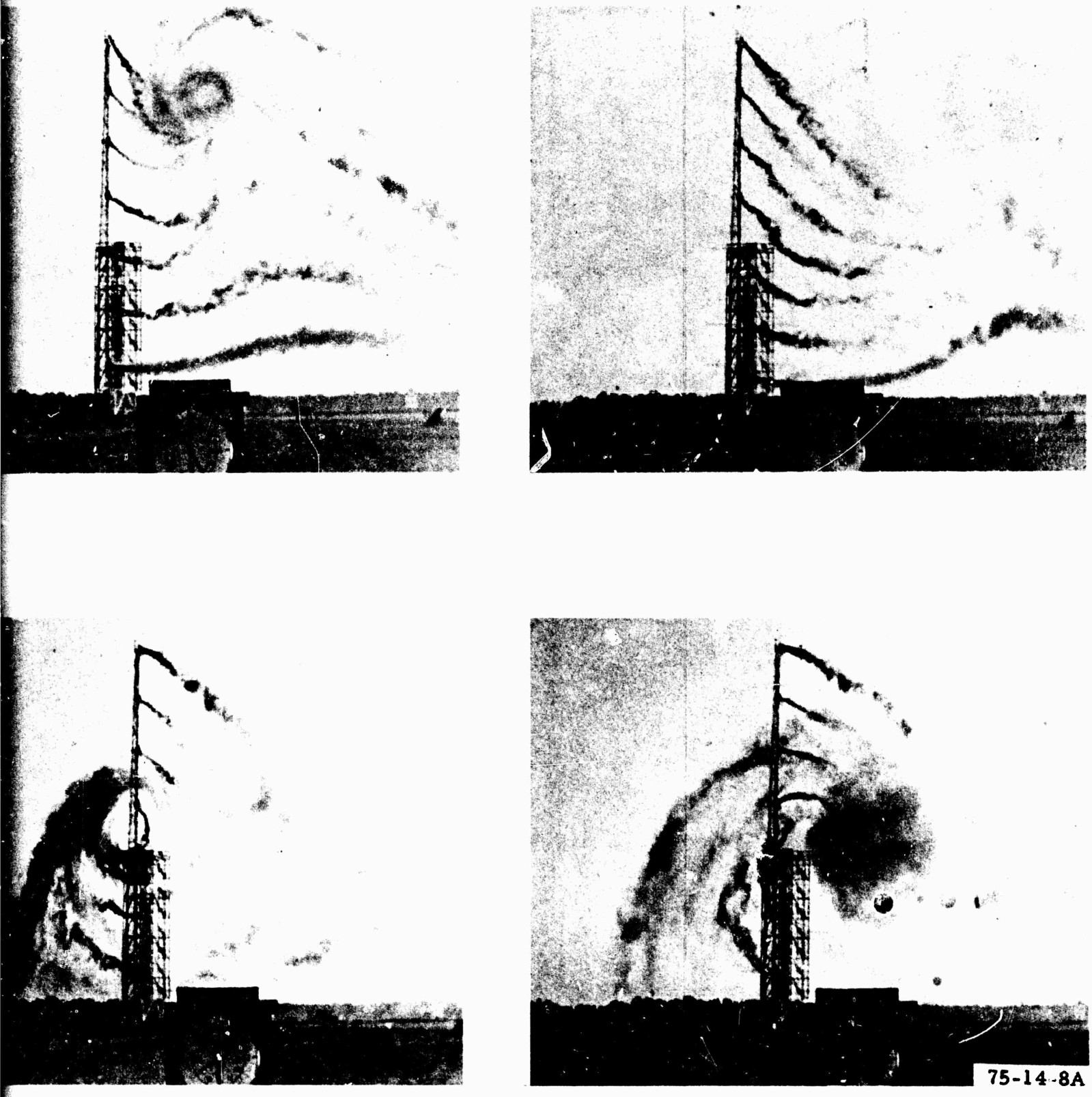

) COVERAGE OF L1011 VORTICES FOR DATA RUN 6, LANDING CONFIGURATION, $\delta_f=42°$

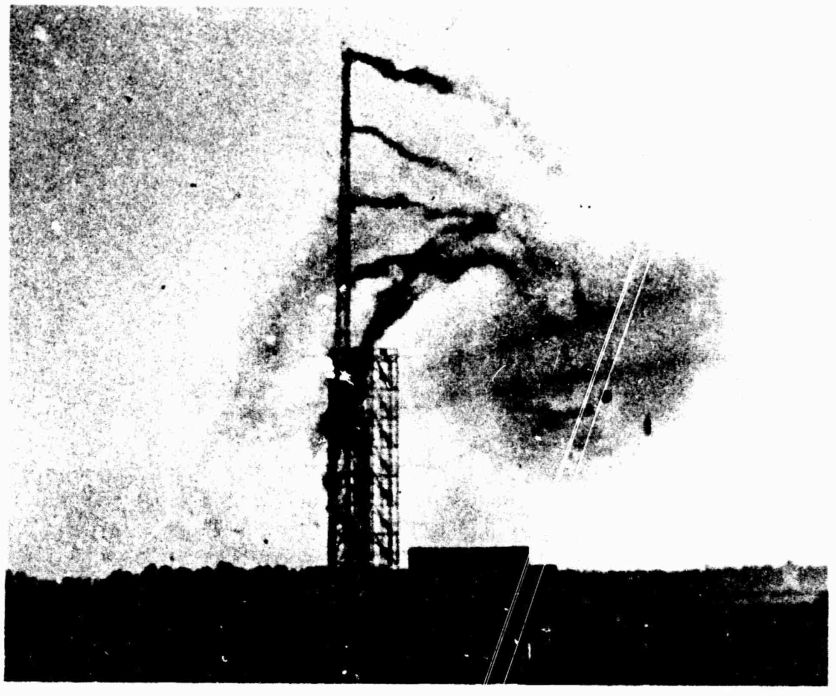

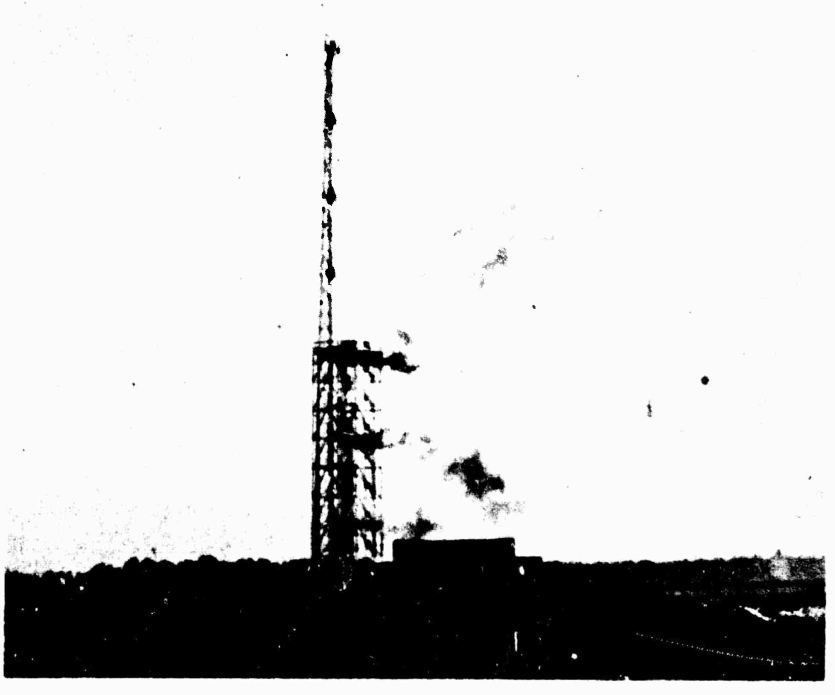

FIGURE 8B. PHOTOGRAPHIC (16mm) COVERAGE OF L1011 VORTICES FOR DATA RUN

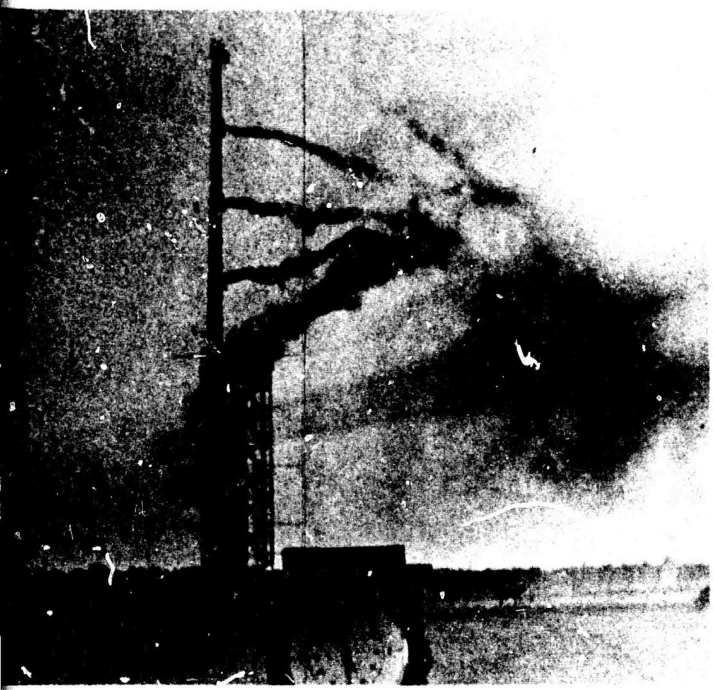

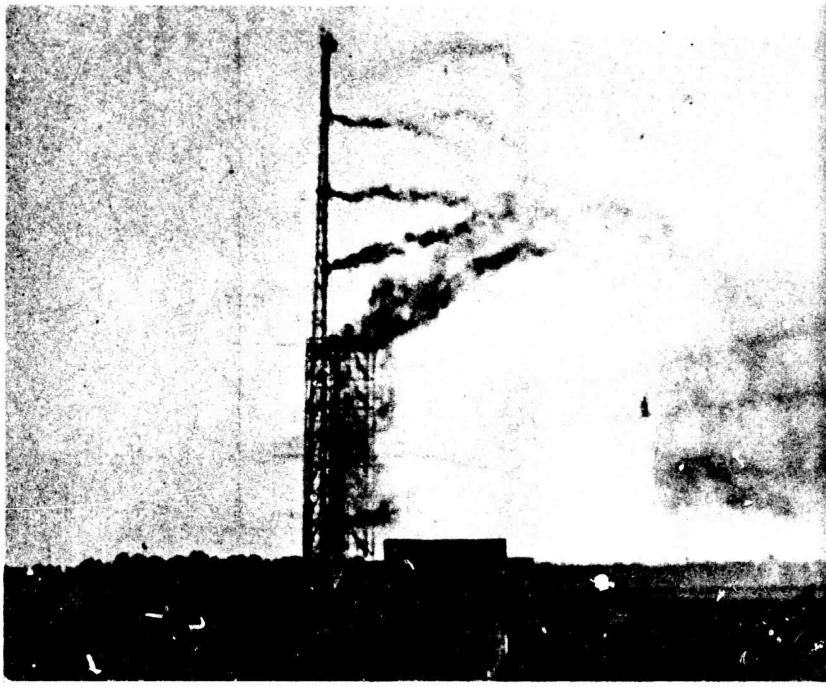

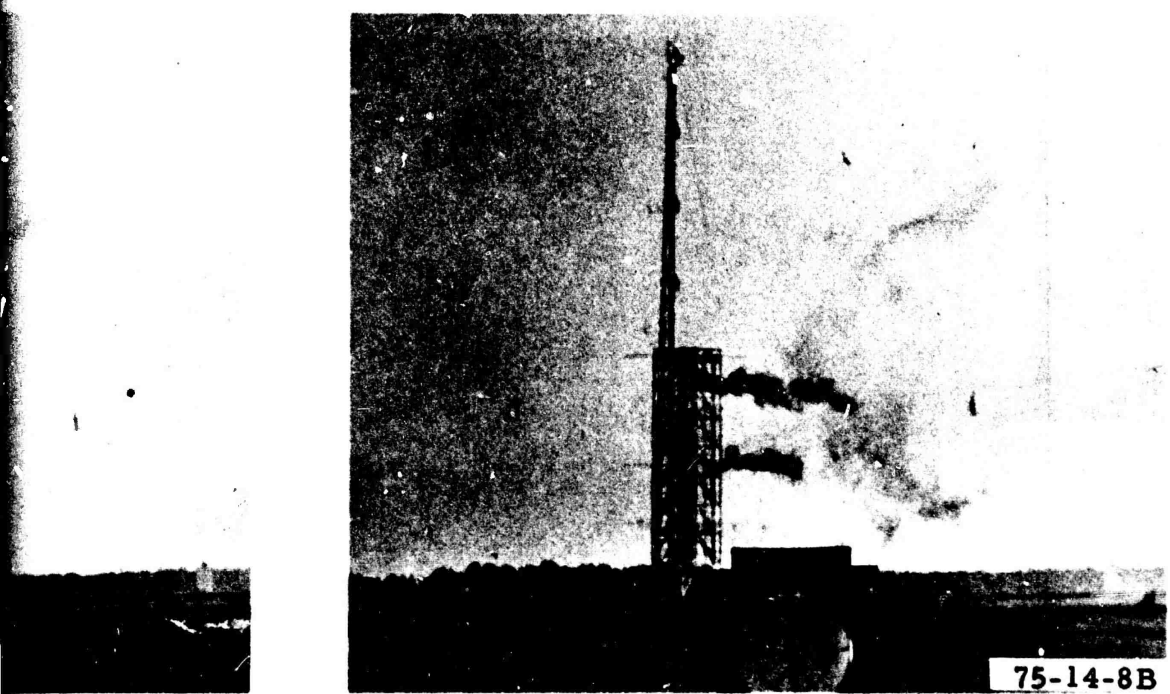

GE OF L1011 VORTICES FOR DATA RUN 6, LANDING CONFIGURATION, δ_f=42°

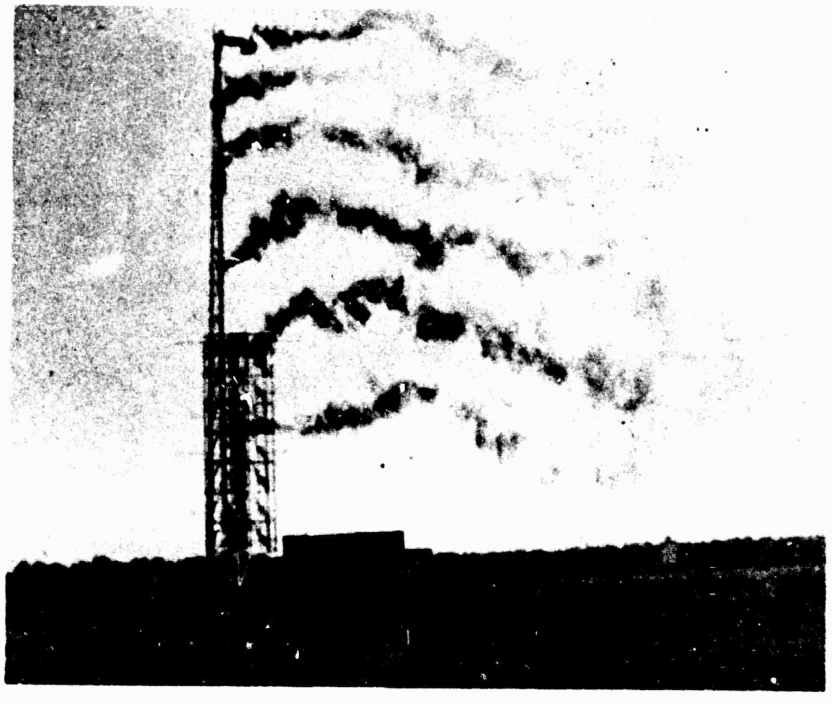

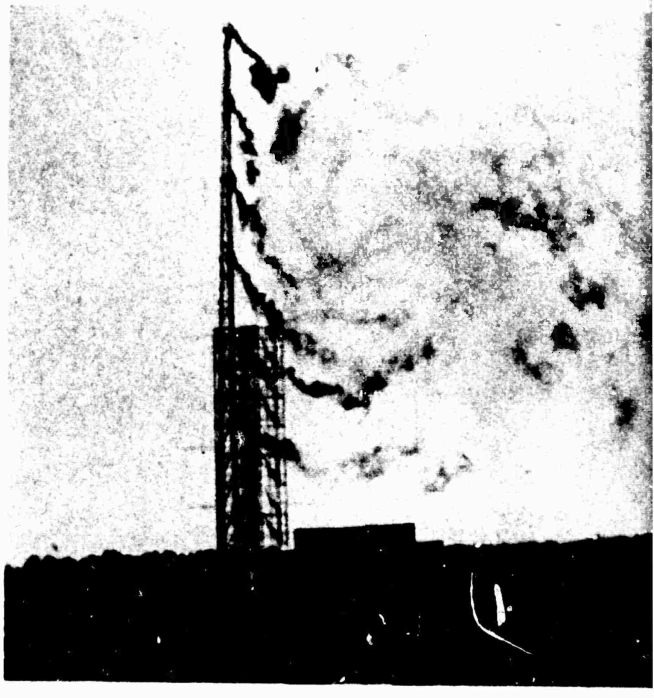

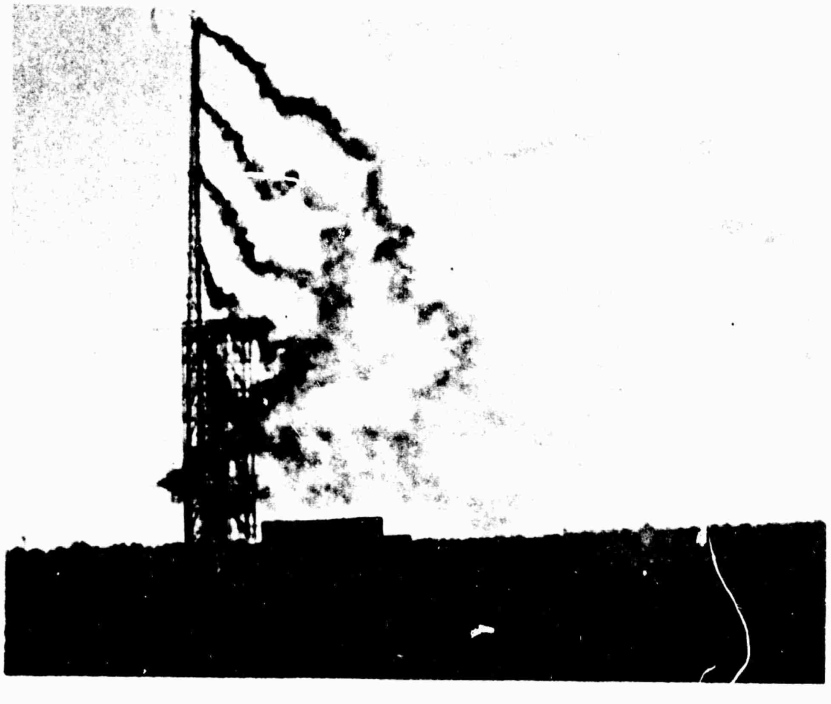

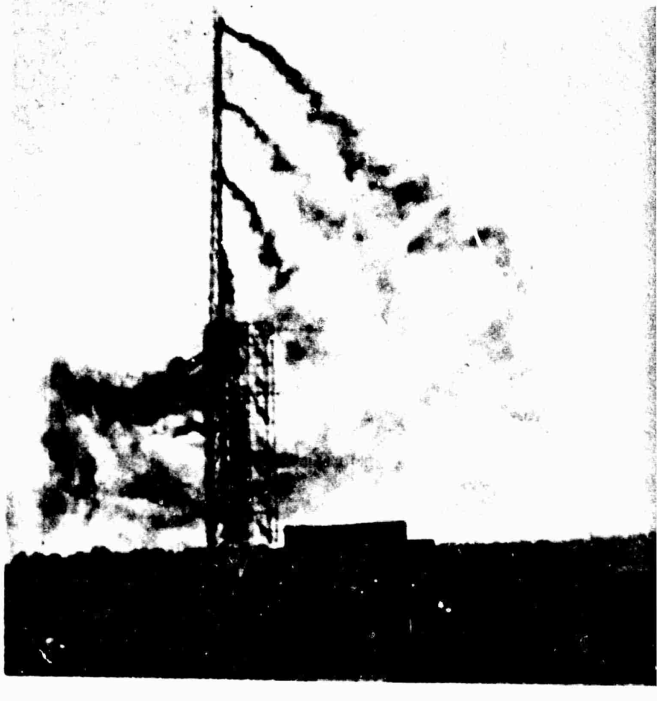

FIGURE 9A. PHOTOGRAPHIC (16mm) COVERAGE OF L1011 VORTICES FOR DATA

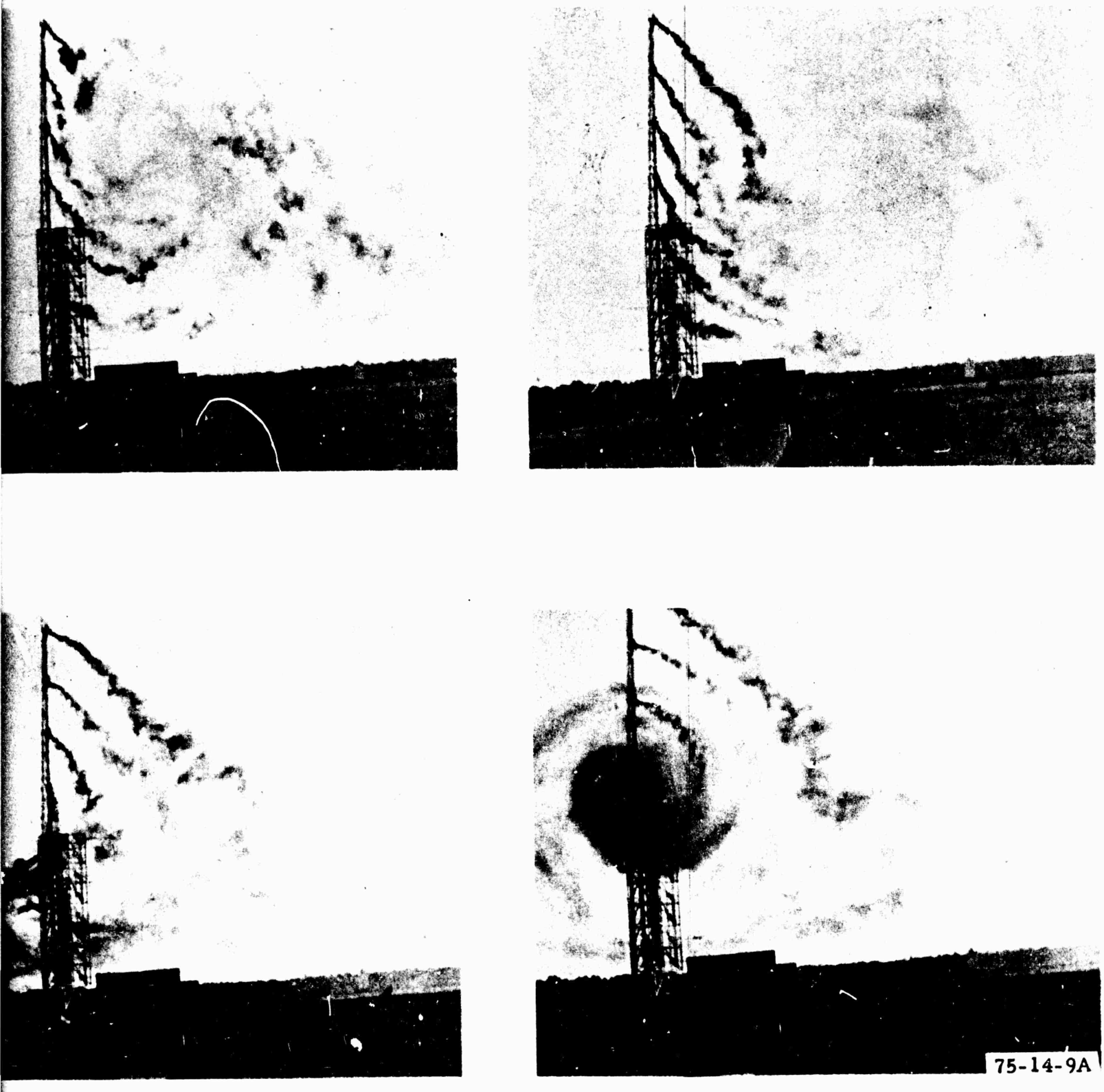

VERAGE OF L1011 VORTICES FOR DATA RUN 11, TAKEOFF/APPROACH CONFIGURATION, δ_f=22°

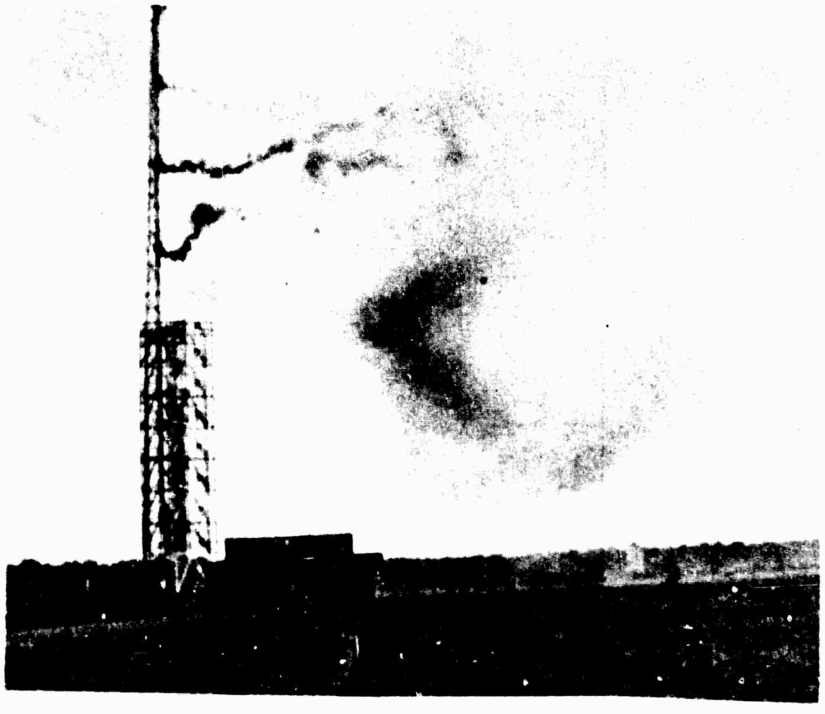

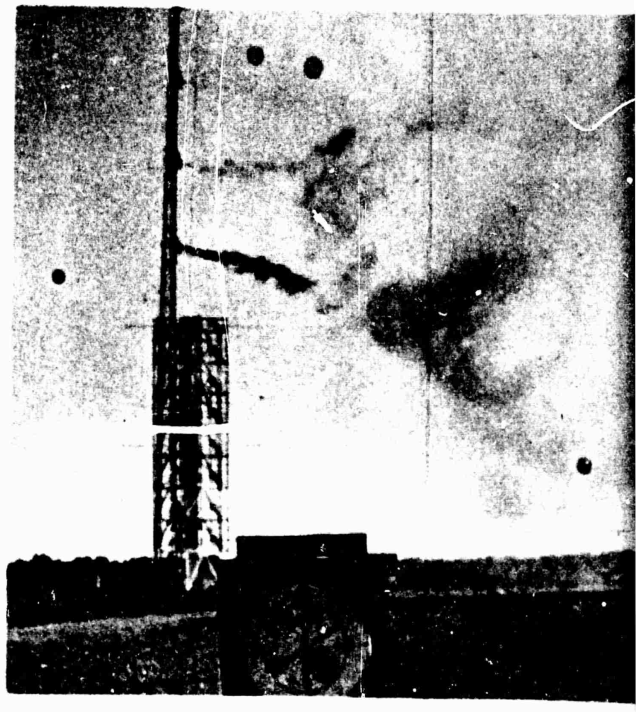

FIGURE 9B. PHOTOGRAPHIC (16mm) COVERAGE OF L1011 VORTICES FOR DATA RUN 11, TAKE

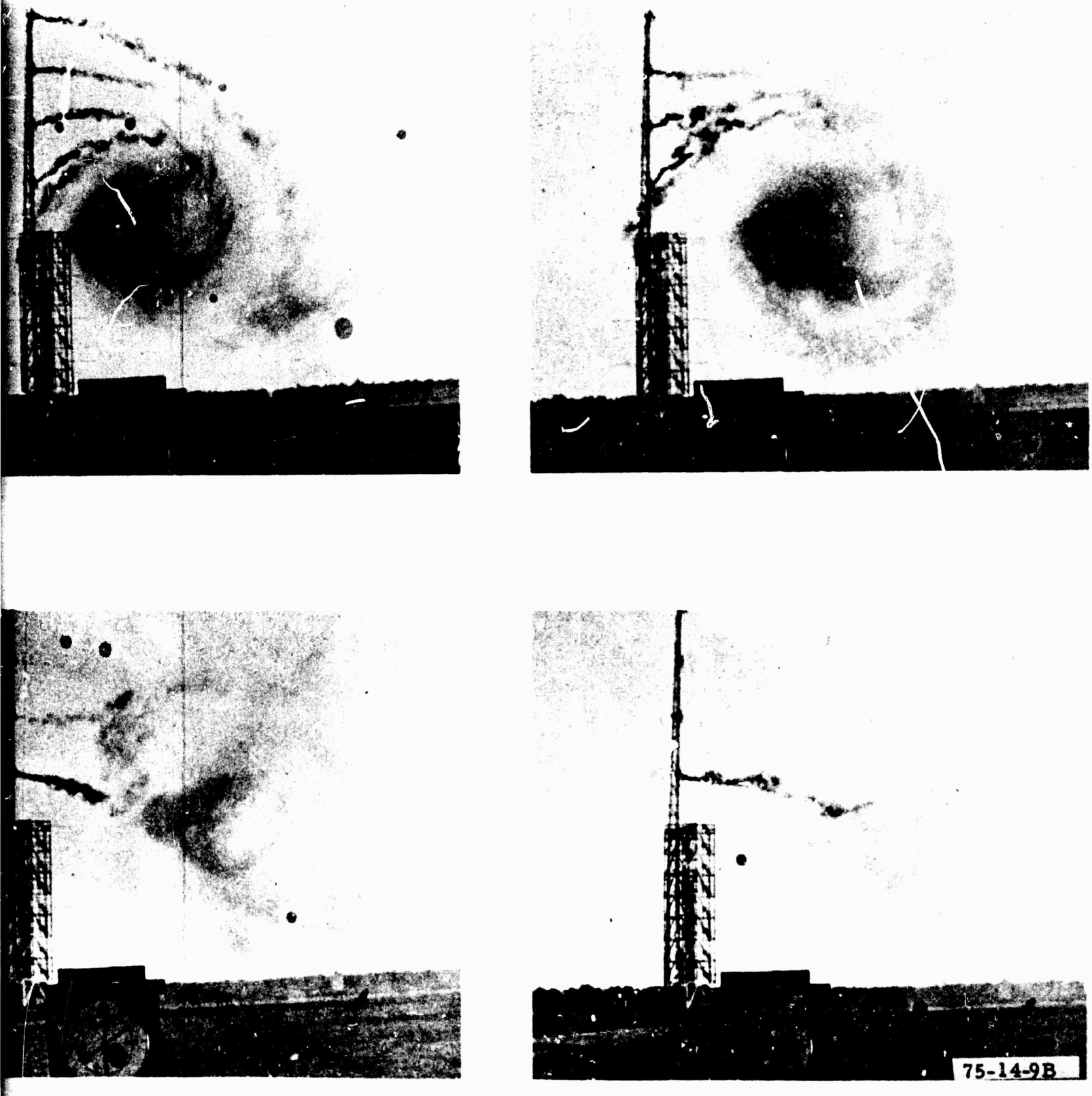

VORTICES FOR DATA RUN 11, TAKEOFF/APPROACH CONFIGURATION, $\delta_f=22°$

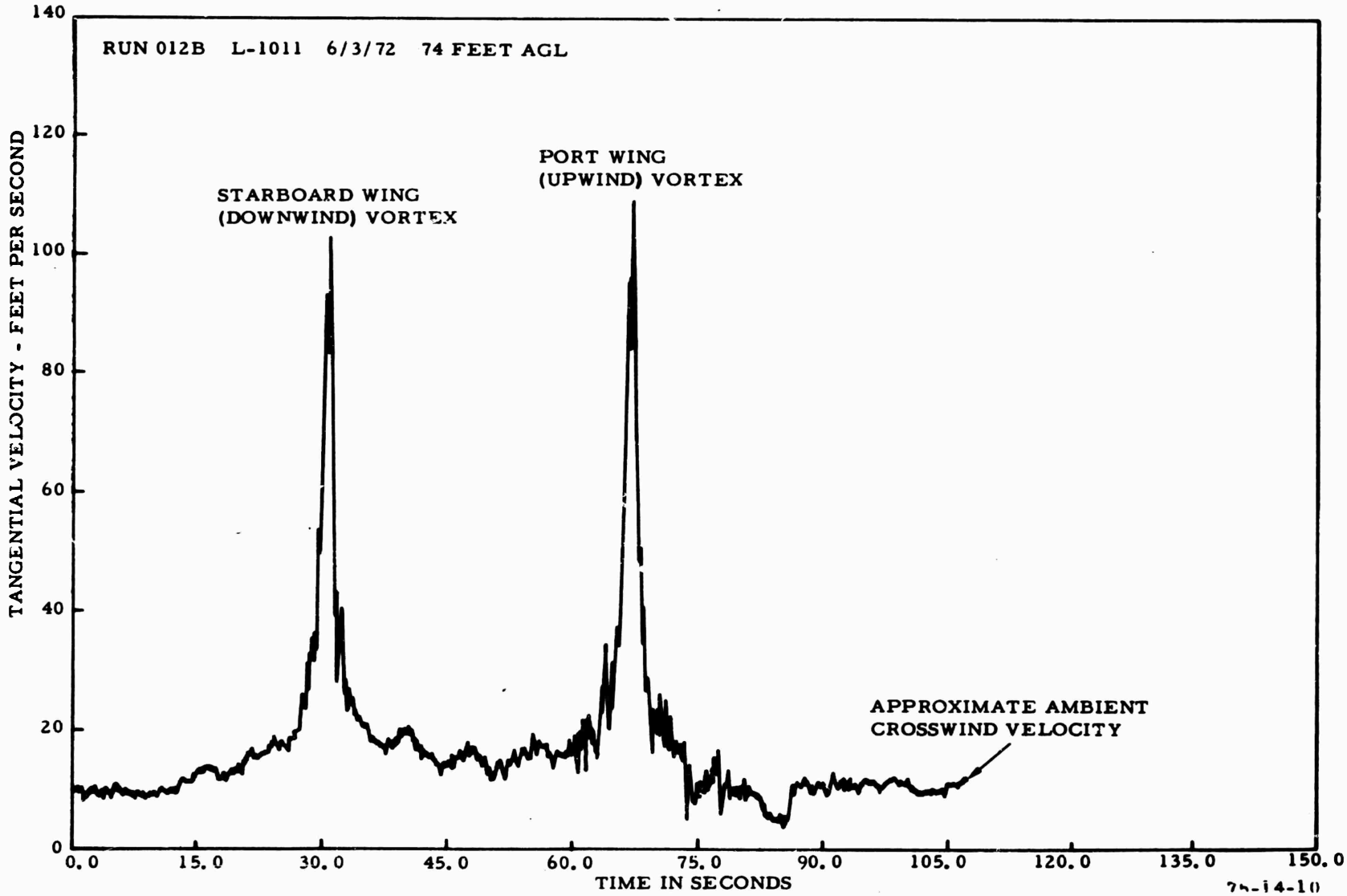

FIGURE 10. TYPICAL SENSOR (74 FEET AGL) VELOCITY TIME-HISTORY PLOT (CALCOMP) L1011 TAKEOFF/APPROACH CONFIGURATION, $\delta_f = 22^o$

4. A summary flight test data sheet (appendix C), which lists L1011 airplane performance, configuration, gross weight and position data relative to the test tower, starboard and port wing vortex ages, peak recorded vortex tangential velocities (uncorrected for wind, mutually induced effects, or ground effect), and approximate height AGL where the vortex intercepted the tower hot-film anemometer array;

5. Plots of vortex tangential velocity, corrected for wind, as a function of sensor height above the ground. (The resultant tangential velocity profiles are presented in appendix D.);

6. Expanded plots of the recorded vortex tangential velocity scalar magnitude against time for the vicinity of the sensor levels AGL where it was determined that the vortices passed through the sensor array. Again for data run 12 (cited in paragraph 4) we have expanded the plots for the two vortices' starboard and port, and they are shown in figures 11 and 12. Other select examples are depicted in appendix E. (Still other examples, for other tower fly-bys, are available at NAFEC.);

7. Composite plots of the vortex tangential velocity time-history profiles for the sensor levels in the vicinity of the vortex core passage through the sensor array. These composite plots cover an elapsed time of 15 seconds in the vicinity of peak recorded vortex tangential velocity. Some examples of these composite plots are listed in appendix F. (Other examples are available at NAFEC, if required by other investigators.); and

8. Low altitude meteorological data are listed in appendix G and includes ambient temperature, wind velocity and direction at five levels (23, 45, 70, 100, and 140 feet AGL) on the tower, and relative humidity at two levels (23 and 140 feet AGL). An attempt was made to record additional meteorological data from 300 feet to 3,000 feet AGL in order to obtain an indication of the nature of the atmosphere, particularly stability, in which the airplane flew and the vortices were generated. However, the data obtained by means of a radiosonde, were not considered satisfactory for the purpose in that data acquisition did not, unfortunately, commence until 1,200 feet AGL.

DATA ANALYSIS. This airplane has at least four possible operational configurations (1) holding/cruise (clean) with δ_f=0°, (2) takeoff with δ_f=10°, (3) takeoff/approach with δ_f=22°, and (4) landing with δ_f=42°. Nineteen tower fly-bys were conducted, with primary emphasis on acquiring data for the approach and landing configurations. As can be seen in the summary data sheet of appendix C, the 19 L1011 data runs consisted of 10 in landing, 5 in approach, 3 in takeoff, and 1 in cruise configuration. Thirty-two vortex "hits" were noted on the tower--a hit being defined as where it is believed that at least one-half (vertical velocity distribution) of the vortex passed through the hot-film anenometer sensor array.

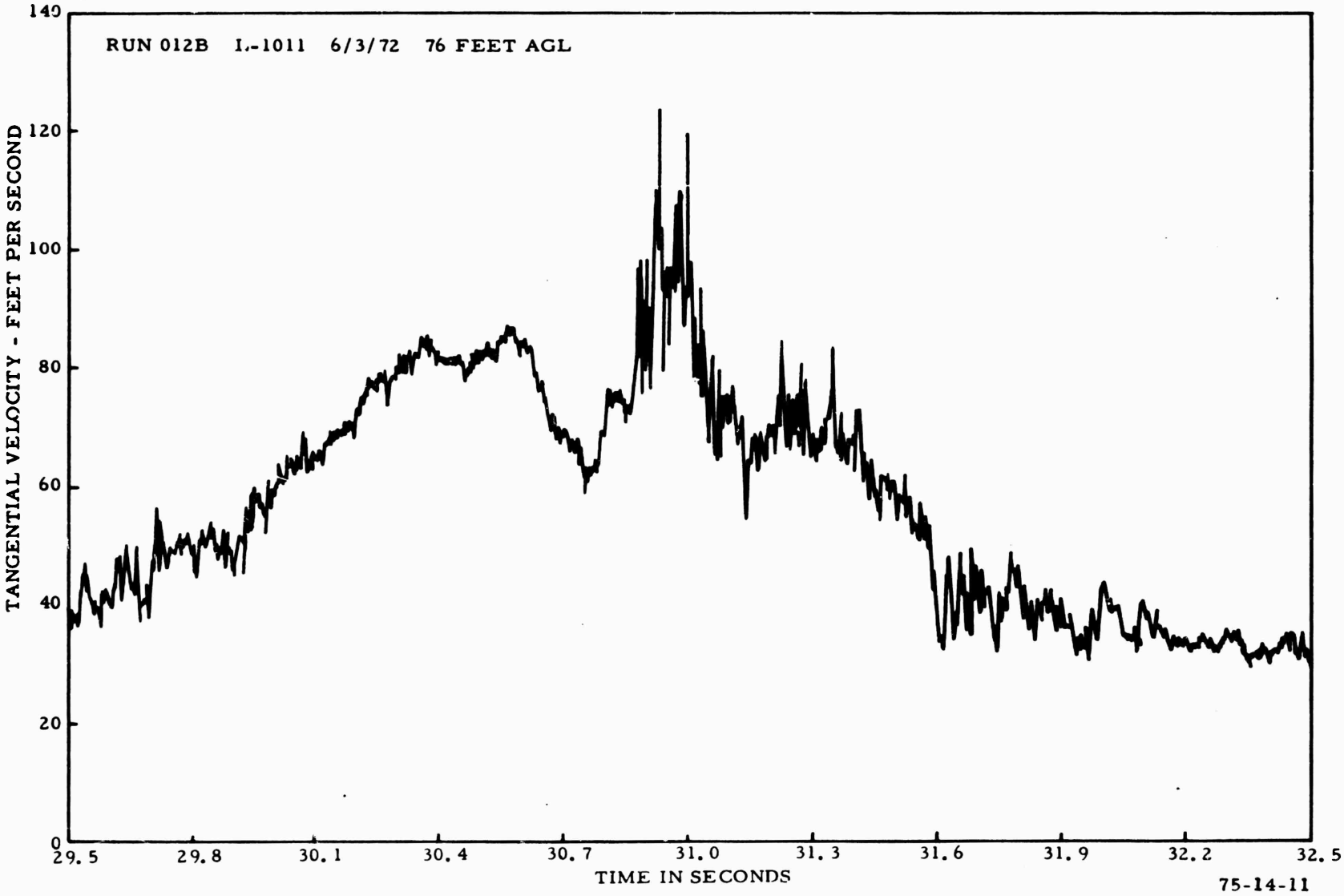

FIGURE 11. COMPUTER EXPANDED VORTEX TANGENTIAL VELOCITY VS. TIME PLOT OF L1011 STARBOARD WING DOWNWIND VORTEX $\delta_f = 22^\circ$

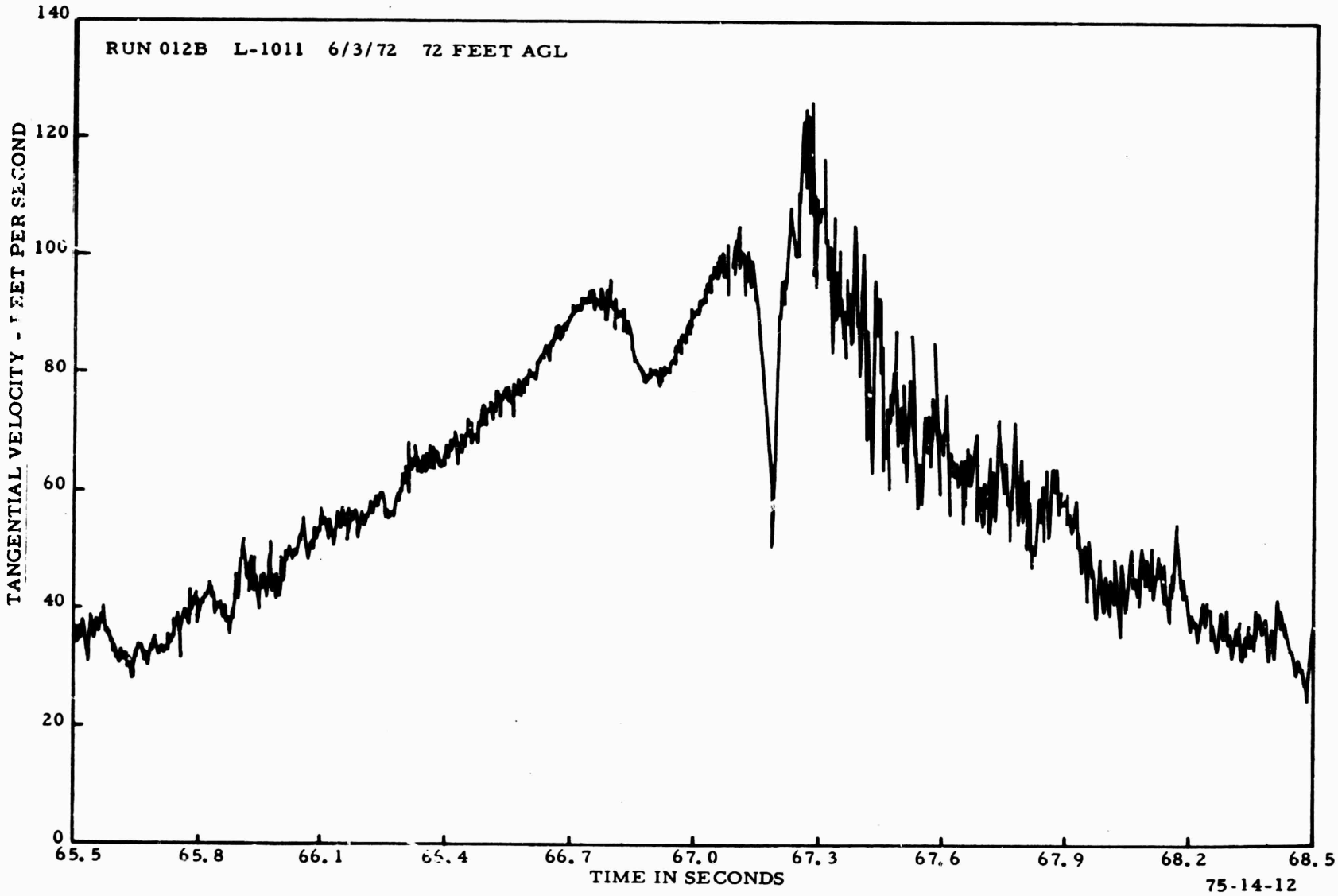

FIGURE 12. COMPUTER EXPANDED VORTEX TANGENTIAL VELOCITY VS. TIME PLOT OF L1011 PORT WING (UPWIND) VORTEX $\delta_f = 22^o$

With such a limited amount of data it is difficult, if not impossible, to attempt certain types of parametric data display and data correlation. However, even with the limited number of flight tests, data runs past the tower and recorded vortex rotational velocities, certain significant items were noted, both visually and in the recorded data. The following objectives for L1011 vortex data analysis would be attempted, given sufficient data, but were not obviously achievable because of the limited data and/or anomalies which presented themselves during the course of the analyses:

1. Vortex persistence per se.

2. Vortex persistence as a function of atmospheric conditions.

3. Vortex characteristics as a function of L1011 configuration.

4. Vortex movement, vertically and laterally, as a function of atmospheric conditions, airplane configuration, and airplane proximity to the ground.

GENERAL VORTEX CONSIDERATION.

Before one can proceed further, one must have a general idea of vortex movement in space and in close proximity to the ground under various atmospheric conditions, how this movement affects the recorded data, and what are the certain assumptions made in the data analysis included herein.

Figures 13 and 14 are fairly basic with regard to the vortex phenomena and show the trajectory of a vortex pair for no crosswind and various crosswind conditions, respectively. The curvature of the vortex path trajectory commences upon the vortex encountering "ground effect" which is that distance above the ground at which the vortex pair is influenced by forces other than those produced by vortex mutual interaction and atmospheric characteristics. These ground effect forces are produced by the close proximity of the vortex to the ground and commence at a distance which has theoretically and experimentally been found to be on the order of a wingspan height of the generating aircraft above the ground.

With regard to vortex vertical and horizontal movement and associated descent and translational velocities and vortex height during tower passage as a function of time, one can readily see in figures 15 and 16 that the L1011 space position abeam of the tower must be considered in the subsequent data analyses.

For example, positioning the aircraft in close to the tower as in position (1), or too high further away from the tower has the disadvantage that it can cause one or both of the vortices to pass over the tower. However, the potential advantage of such airplane positioning is that one might obtain data on both vortices with the least influence of ground effect.

Positioning the airplane further away from the tower or at lower altitudes will make it difficult, if not impossible, to calculate vertical descent velocities or translational velocities because of ground effect influences as

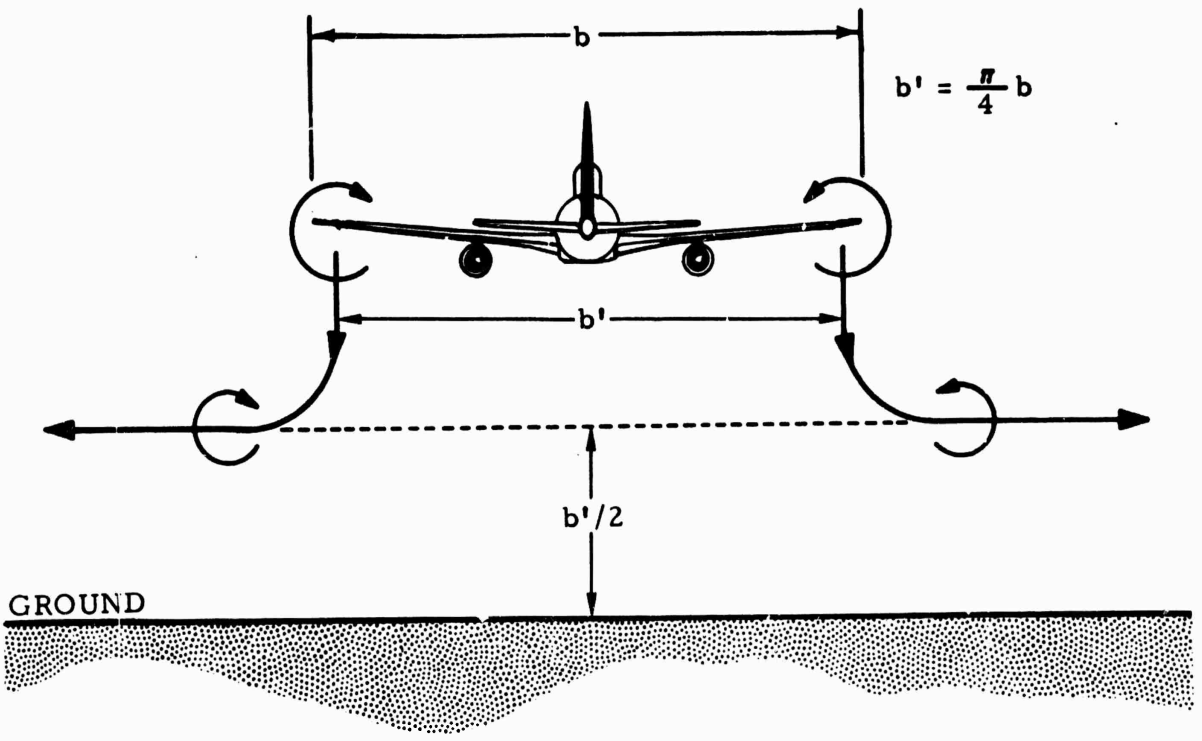

75-14-13

FIGURE 13. VORTEX TRAJECTORY IN SPACE WITH NO CROSSWIND

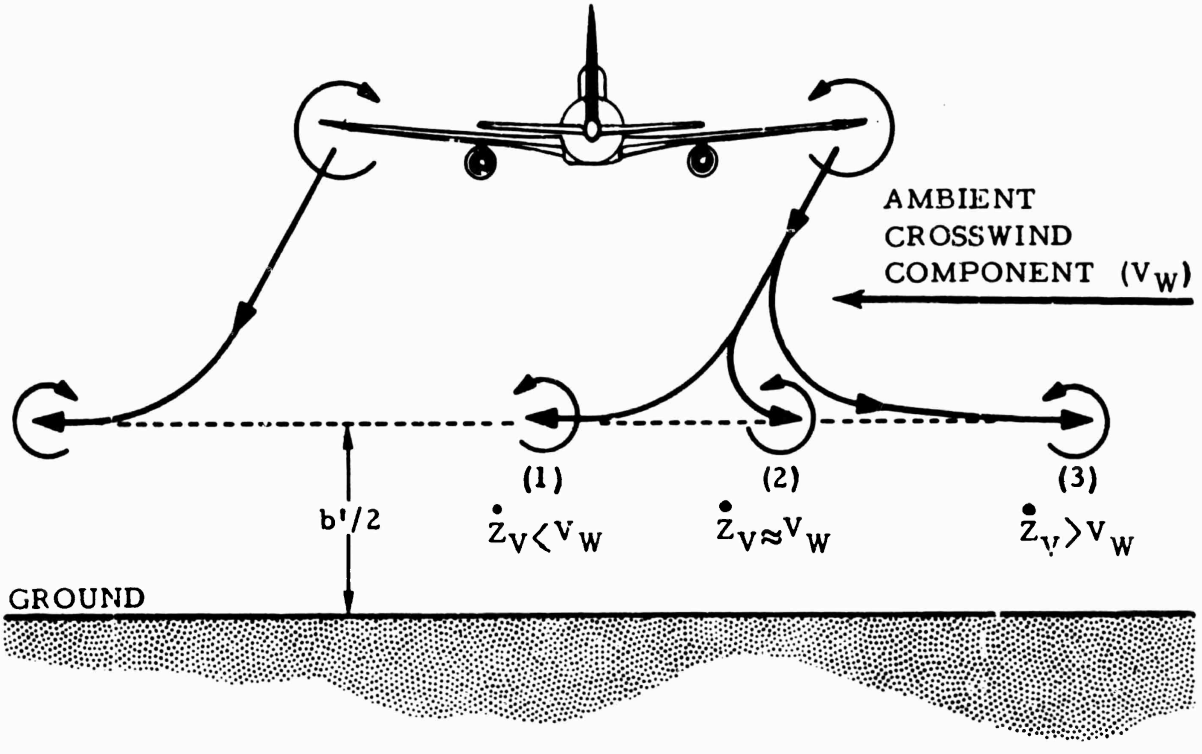

75-14-14

FIGURE 14. VORTEX TRAJECTORY IN SPACE UNDER VARIOUS CROSSWIND CONDITIONS

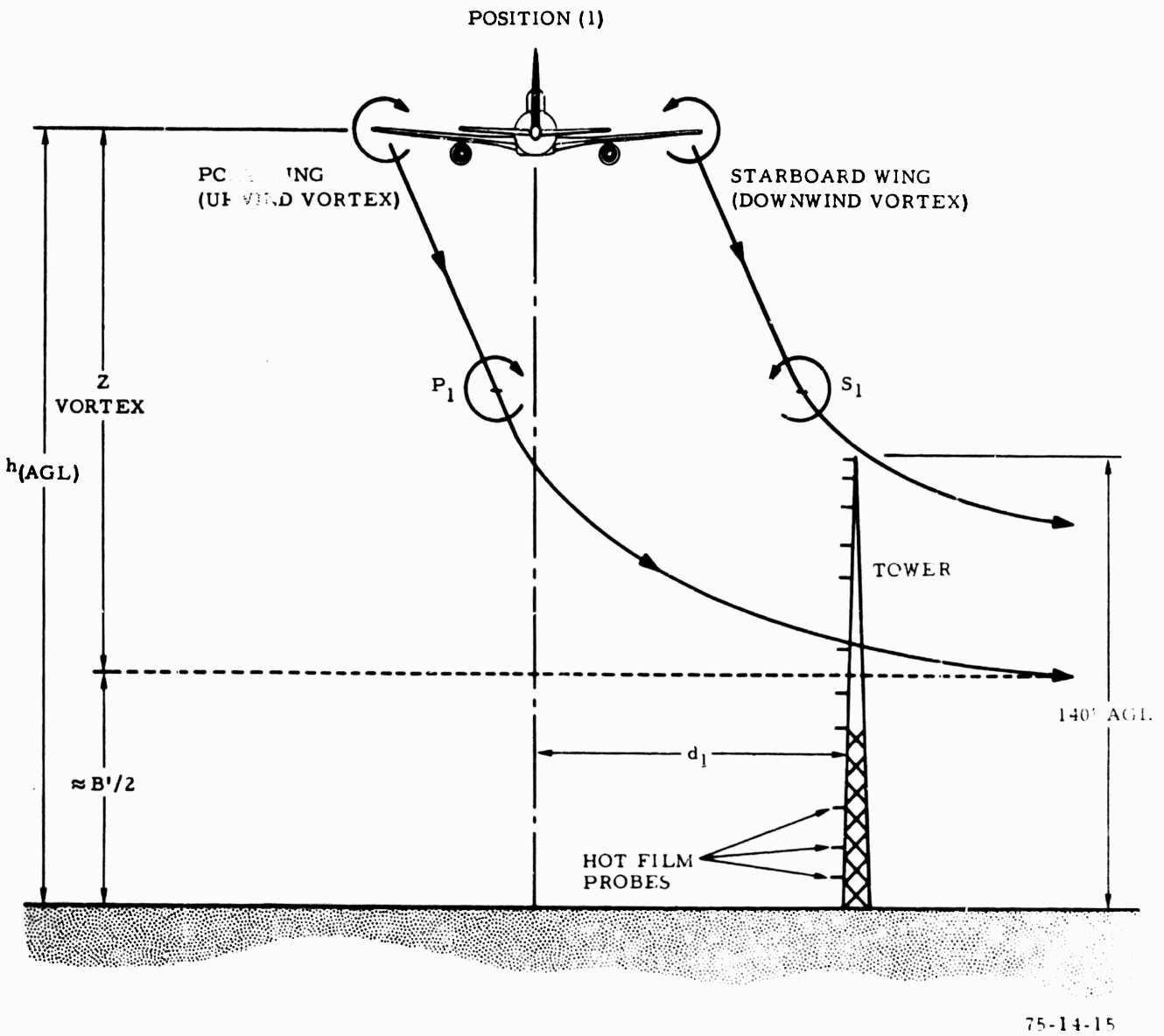

FIGURE 15. VORTEX TRAJECTORY IN SPACE WITH AIRCRAFT IN CLOSE PROXIMITY TO TOWER (POSITION 1)

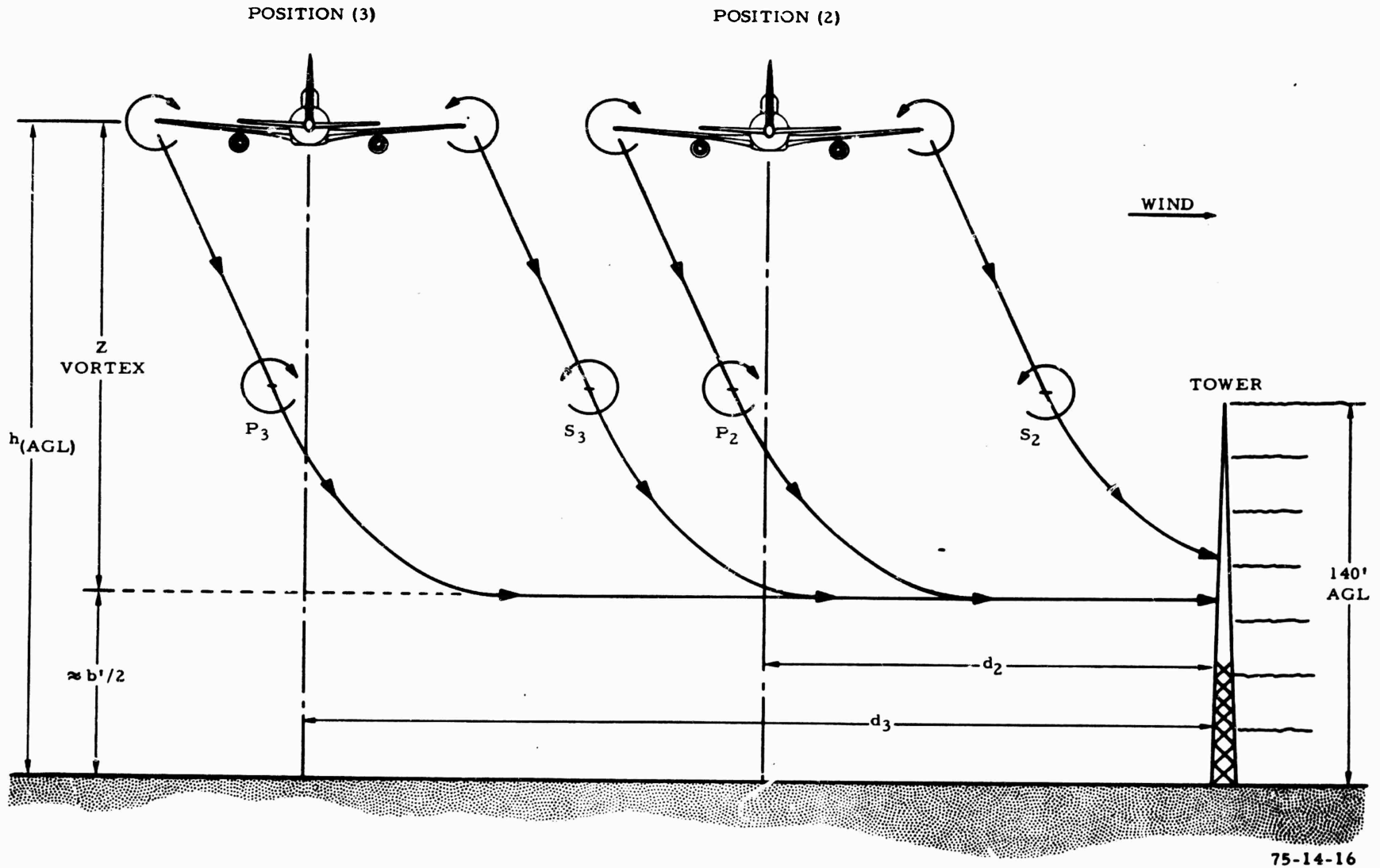

FIGURE 16. VARIOUS TRAJECTORIES IN SPACE WITH AIRCRAFT FURTHER UPWIND FROM TOWER (POSITIONS 2 AND 3)

in position (2) for the port wing vortex and position (3) for both wing vortices. The descent time for vortices P_2, S_3, and P_3 would be the same, however, since we only measure elapsed time between aircraft tower passage and vortex tower strike and, therefore, cannot accurately determine how to break up this elapsed time into descent and translations movement times.

However, wherein the vortices intercept the tower near the top one can, with some reservation, have a greater confidence in arriving at a fairly reasonable vortex descent velocity, Z_V, inasmuch as variation in crosswind components would least affect this vertical movement direction as compared to horizontal velocity, $\bar{Y}_V$.

The vortex system mutual interaction, including the image vortices resulting from ground effect due to vortex proximity to the ground does affect the vortex tangential velocity flow field and what the individual hot-film anemometer sensors "feel."

It is important to look at what comprises the velocity flow field at a sensor which is relatively close to a passing vortex.

To orient the reader, figures 15 and 16 discussed earlier, are general schematics of the L1011 abeam of the tower (flying into the paper) and depict the starboard wing (downwind or No. 1) vortex and the port wing (upwind or No.2) vortex. For this discussion we assume that we have both vortices passing through the tower. The components which make up the resultant velocity can be significant and have been considered in previous vortex data analysis, e.g., reference 2 and 10. As depicted in figure 17, resultant velocities composed of five components: V_1 is the velocity induced by the opposite (upwind) vortex, V_2 the velocity induced by the mirror image of the upwind vortex in ground effect, V_3 is the velocity flow field induced by the vortex under consideration, V_4 is the velocity induced by the mirror image of the downwind vortex, and V_w is the ambient wind velocity. Applying this same logic, we can arrive at the composition of the upwind vortex flow field as shown in figure 18.

Multiple vortices normally can be expected to be shed from the wing of an airplane with some degree of landing flap deflection. However, analysis of the flight test data indicates two discrete and predominant vortices passing through the tower when the trailing vortex system intercepts it. A case in point is clearly evident in figure 10 for L1011 data run 12.

Figures 19 and 20 depict the velocity components which contribute to the resultant velocity to which the hot-film sensor responds for the downwind and upwind vortices, respectively. For a particular vortex, using the notation in the two cited figures, we have

$$U^1 + \sqrt{v_\theta^{1\,2} - v_{ind}^2} \qquad (1)$$

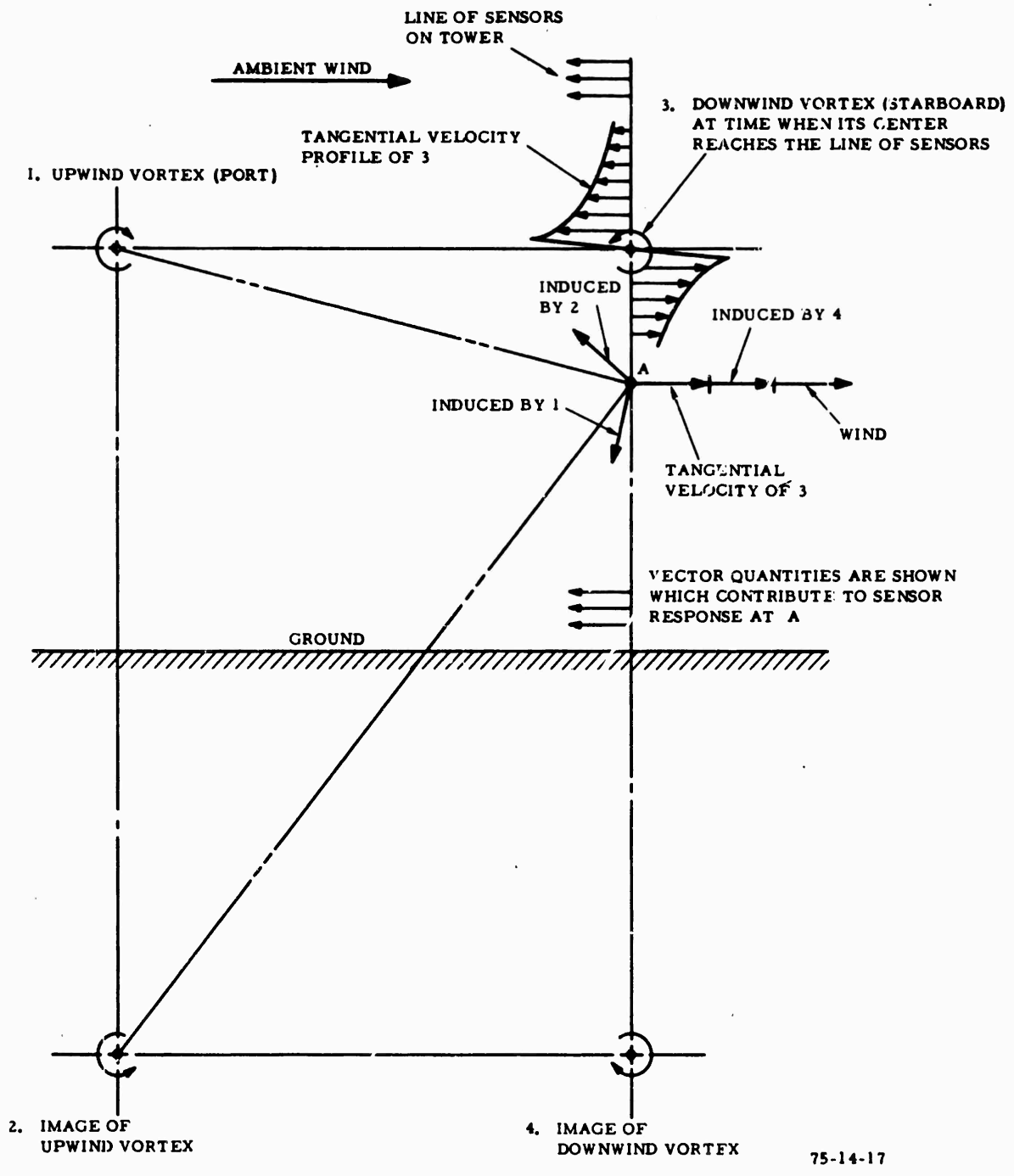

FIGURE 17. SCHEMATIC OF THE VORTEX WAKE SYSTEM AT THE TIME CENTER OF THE DOWNWIND VORTEX REACHES THE VERTICAL ARRAY OF SENSORS ON THE TOWER

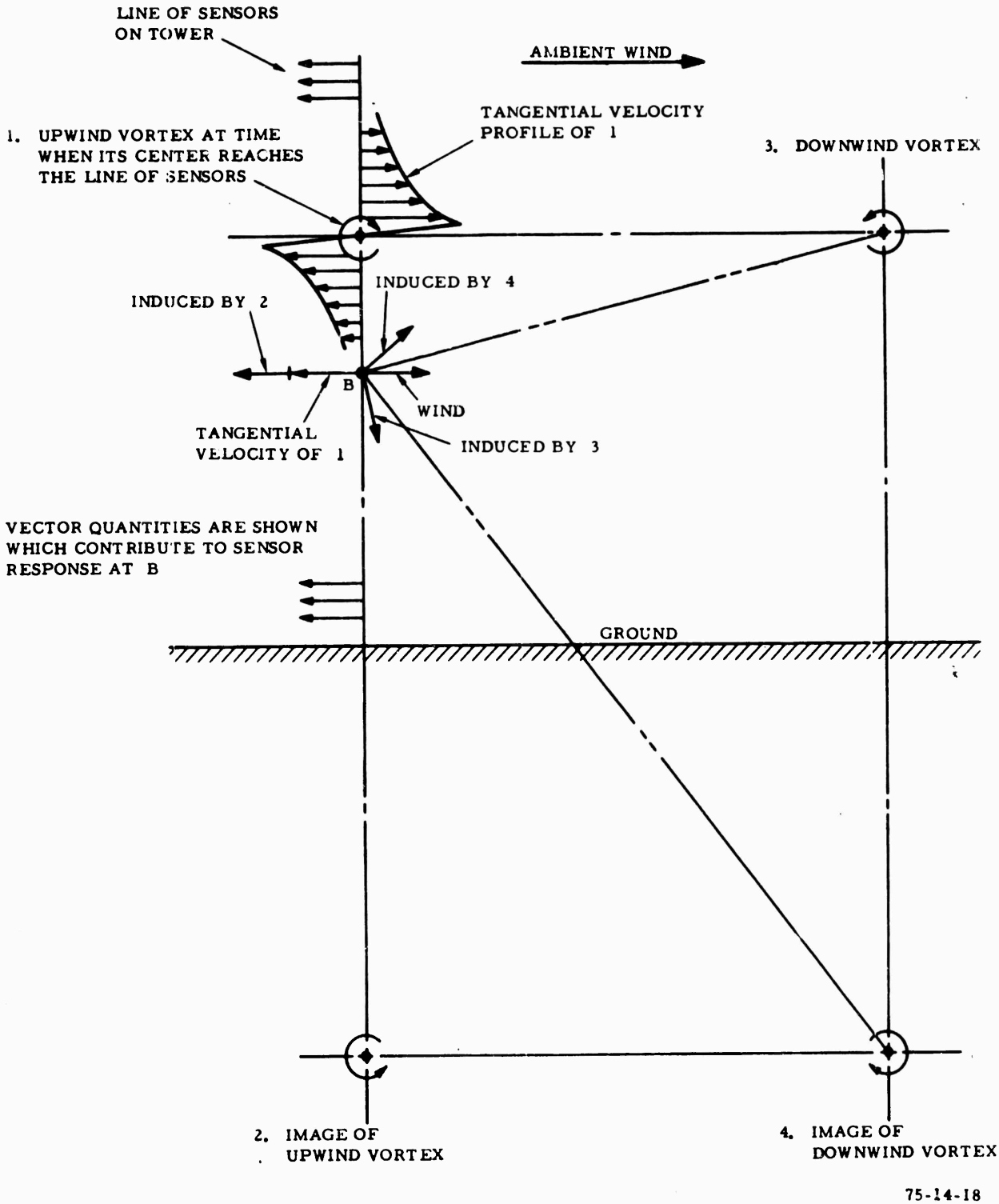

FIGURE 18. SCHEMATIC OF THE VORTEX WAKE SYSTEM AT THE TIME THE CENTER OF THE UPWIND VORTEX REACHES THE VERTICAL ARRAY OF SENSORS ON THE TOWER

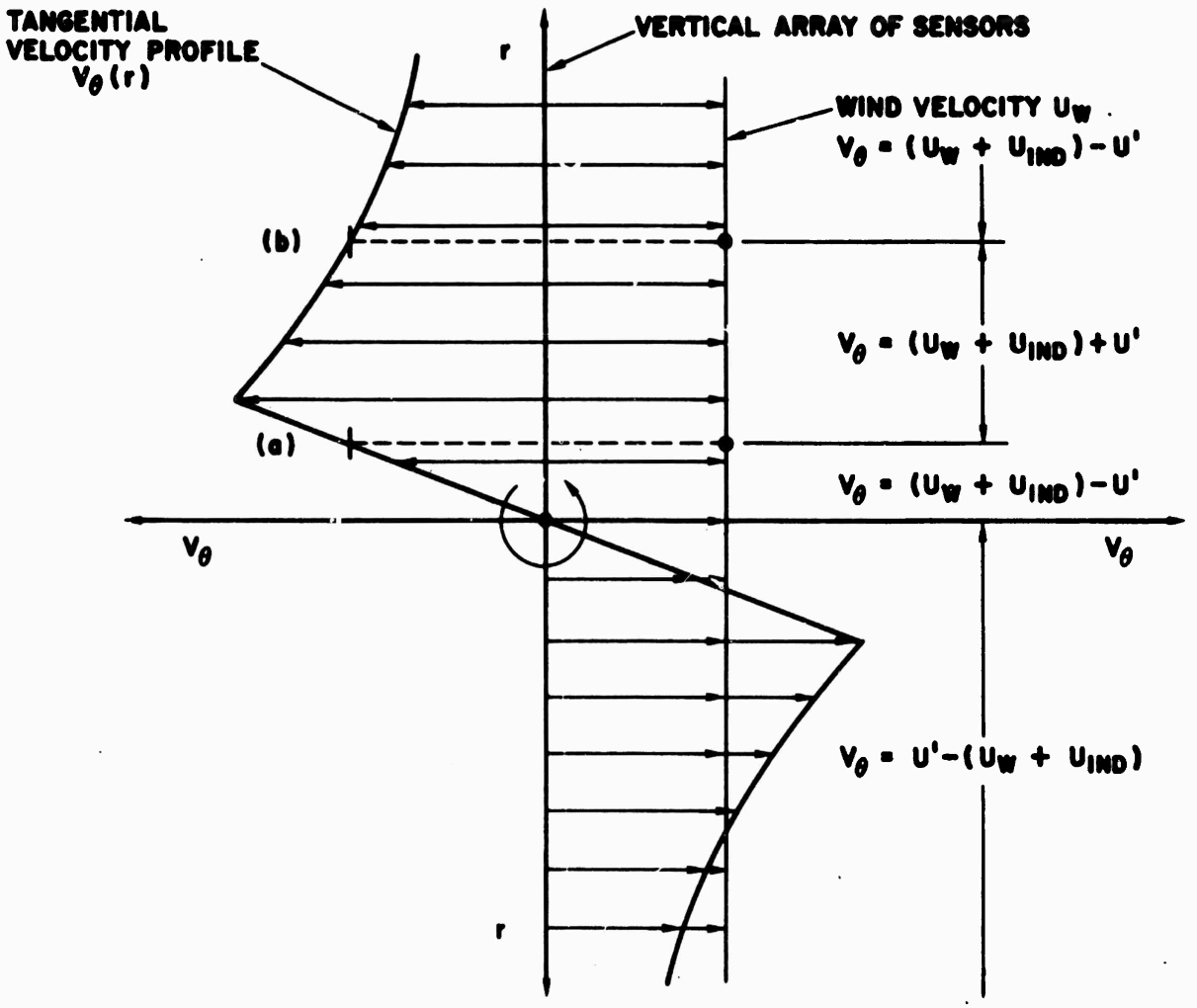

$$V'_\theta = \sqrt{(U_W + U_{IND} \pm V_\theta)^2 + V_{IND}^2}$$

U_W = WIND VELOCITY PARALLEL TO GROUND.

U_{IND} = TOTAL HORIZONTAL COMPONENT OF INDUCED VELOCITIES FROM UPWIND VORTEX AND BOTH IMAGES.

V_θ = LOCAL TANGENTIAL VELOCITY IN VORTEX.

V_{IND} = TOTAL VERTICAL COMPONENT OF INDUCED VELOCITIES FROM UPWIND VORTEX AND ITS IMAGE.

75-14-19

$$U' = \sqrt{V'^2_\theta - V_{IND}^2}$$

FIGURE 19. VELOCITY COMPONENTS COMPRISING RESULTANT VELOCITY TO WHICH HOT-FILM SENSOR RESPONDS, DOWNWIND VORTEX

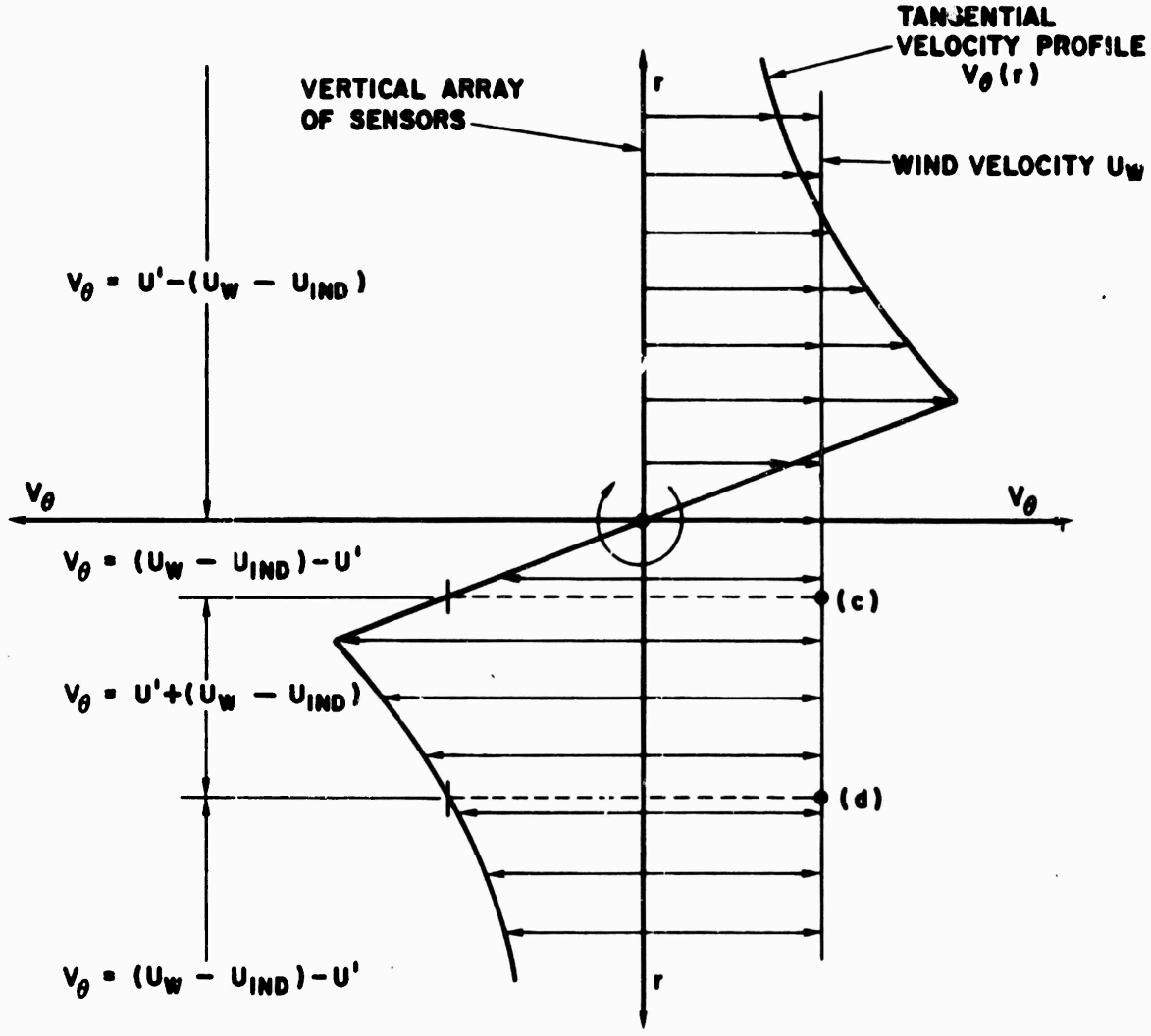

U_W = WIND VELOCITY PARALLEL TO GROUND.

U_{IND} = TOTAL HORIZONTAL COMPONENT OF INDUCED VELOCITIES FROM DOWNWIND VORTEX AND BOTH IMAGES.

V_θ = LOCAL TANGENTIAL VELOCITY IN VORTEX.

V_{IND} = TOTAL VERTICAL COMPONENT OF INDUCED VELOCITIES FROM DOWNWIND VORTEX AND ITS IMAGE.

$$U' = \sqrt{V'^2_\theta - V_{IND}^2}$$

75-14-20

FIGURE 20. VELOCITY COMPONENTS COMPRISING RESULTANT VELOCITY TO WHICH HOT-FILM SENSOR RESPONDS, UPWIND VORTEX

$$V_\theta^1 = \sqrt{(U_w + U_{ind} \pm V_\theta)^2 + V^2} \qquad (2)$$

or (1) $$U^1 = U_w + U_{ind} \pm V_\theta$$

For this particular investigation, the total horizontal component of the induced velocities U_{ind} from the opposite vortex and both images was neglected because of the uncertainty of the position due to ground effect of the opposite vortex and, therefore, its mirror image in relation to the vortex located on the line of sensors at that particular instantaneous point in time and the relatively insignificant contribution of the horizontal velocity component of the mirror image vortex on the vortex tangential velocity distribution for the vortex under consideration.

Accordingly, the data reduction and analyses for the vortex tangential velocity versus radial distance plots (appendix D) were reduced by using equation (1)

$$U^1 = U_w \pm V_\theta \qquad \text{or} \qquad V_\theta = \pm U^1 \pm U_w$$

wherein U_w signifies the crosswind component of the ambient wind.

Even then there was difficulty in data reduction and plotting of the tangential radial distribution plots V_θ versus h of appendix D because of the inability of the hot-film sensors to resolve a 180° ambiguity in the sensed horizontal airflow components at the instantaneous time that a vortex was axisymmetric about the vertical array of sensors, and because of the interference produced by the probe support arms, as discussed later in the text as well as in appendix A.

Because of the crosswind present during the testing (except for runs 1 and 2) there should be two points at which the ambient wind velocity, U_w and the tangential velocity, V_θ, should be of equal magnitude. One point would be within the vortex core and the other outside the vortex core, but both points would be on the same side of the vortex axis. These points would lie above the vortex axis for the downwind vortex as can be noted in figure 19, points (a) and (b), and below the vortex axis for the upwind axis, points (c) and (d) in figure 20.

However, such nullpoints were rarely identified distinctly within the vortex core for any of the vortices passing through the tower. The closest approach to a nullpoint within the core was observed in the data covering L1011 runs 5 and 10, figures 21 and 22, respectively. These two plots could actually be depicting a centered vortex core passage across these two sensors at level 97 and 133, respectively. However, as discussed earlier in this report, since the instantaneous vortex translational velocity is difficult to determine when the vortices are immersed in an ambient wind and under the influence of ground effect, one cannot definitely conclude that this is a vortex core

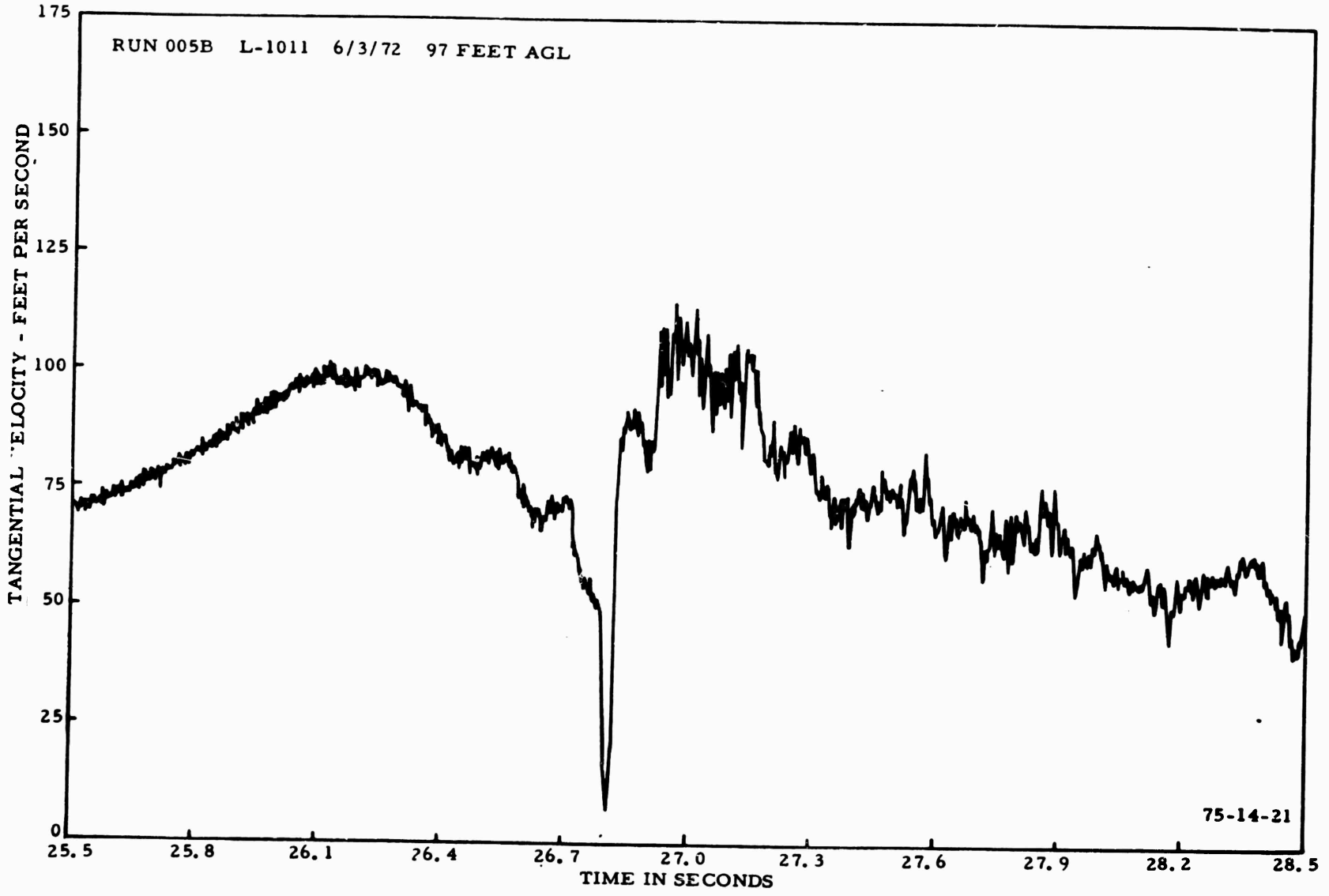

FIGUR 21. EXPANDED V_θ VS. t PLOT DEPICITING APPARENT "NULLPOINT" WITHIN VORTEX CORE, PORT WING (UPWIND) VORTEX, LANDING CONFIGURATION, $\delta_f = 42^\circ$ DATA RUN 5

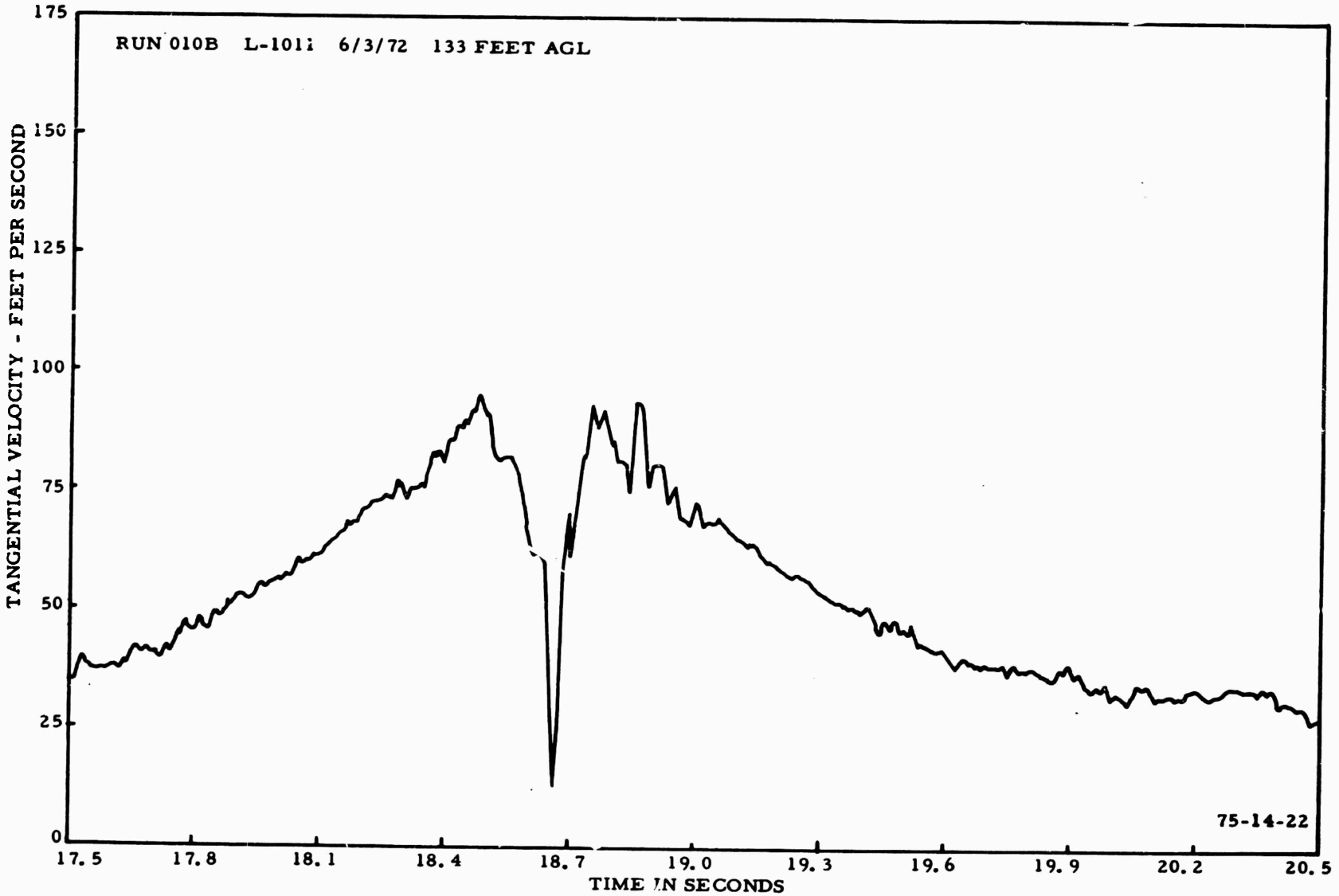

FIGURE 22. EXPANDED V_θ VS. t PLOT DEPICTING APPARENT "NULLPOINT" WITHIN VORTEX CORE, STARBOARD WING (DOWNWIND) VORTEX, APPROACH CONFIGURATION, $\delta_f = 22^\circ$, DATA RUN 10

passage, although the probability is high that it is. Outside of the vortex core, certain cases did reveal themselves wherein the resultant recorded horizontal velocity component did approach zero--to within approximately 2 ft/s. For example, looking at L1011 data run 009 in appendix C, we see that the downwind vortex intercepted the tower 21 seconds after generation, at approximately the 116-foot sensor level. The Vθ time-history plot for this run is shown in figures B-1 through B-3 of appendix B. The field of reverse vortex flow, i.e. (against the ambient wind) would be in the top half of the vortex. Looking at the Vθ- time-history plot for the 140 to 142-foot sensor levels for the same vortex age (figures B-4 through B-6 of appendix B), we see practically zero recorded velocity for this vortex at these levels. Thus the tangential velocity is approximately equal to the ambient wind velocity at that level, or about 20 ft/s. Figures B-7 through B-12 of appendix B depict the same vortex/ambient wind interaction for the first vortex of data run 15.

In this vein, it is pertinent to point out an apparent anomaly in the V_θ versus time plots for the sensor levels in the vicinity of vortex passage through the tower. Whenever the vortex flow direction was from the rear of and concurrently, along the horizontal hot-film anemometer support arm, or calling it the field of reverse flow, a velocity defect was noted for about one-half of the vortex (vertical projection) at the instantaneous point of time when the vortex was axisymmetric along the vertical array of sensors.

For these tests, this velocity defect would be above the vortex axis for the first (downwind) vortex and below the vortex axis for the second (upwind) vortex, and is clearly evident in several selected composite plots of appendix F. For example, taking a look at figures F-1 and F-2 (in appendix F) L1011 data run 10, note the smooth peaks for the recorded tangential velocity in the lower half of the vertical array of sensors in figure F-1, the downwind vortex, and the upper half of figure F-2. The vortex flow field is approaching the sensor from the front in the semi-vortex array cited. Conversely, note the raggedness and velocity defect in the upper half of the vertical array of sensors of figure F-1, and the lower half of signals of figure F-2. Similar results are shown for both vortices of runs 12 and 15, figures F-3 through F-6. The flow field, at vortex/sensor passage time, is from the rear of the sensor. Expanded plots show this velocity defect to be similar to a vortex core passage and, therefore, one must be careful in interpreting this particular part of the recorded vortex tangential velocity flow field. The limited wind tunnel studies at NAFEC, cited earlier, and in appendix A, have substantiated the appearance of a velocity flow defect during reverse flows on the sensor/sensor support arm. This defect is apparently due to a combination of flow blockage and boundary layer formation on the horizontal support arm. Accordingly, this anomaly should be considered when one analyzes the radial distribution plots of vortex tangential velocities in appendix D and the expanded Vθ- versus time plots in appendix E.

VORTEX PERSISTENCE PER SE. Figure 23 is a summary plot of all the L1011 vortex "hits" on the tower and depicts peak recorded tangential velocites versus vortex age. Figures 24 through 26 show the peak recorded tangential

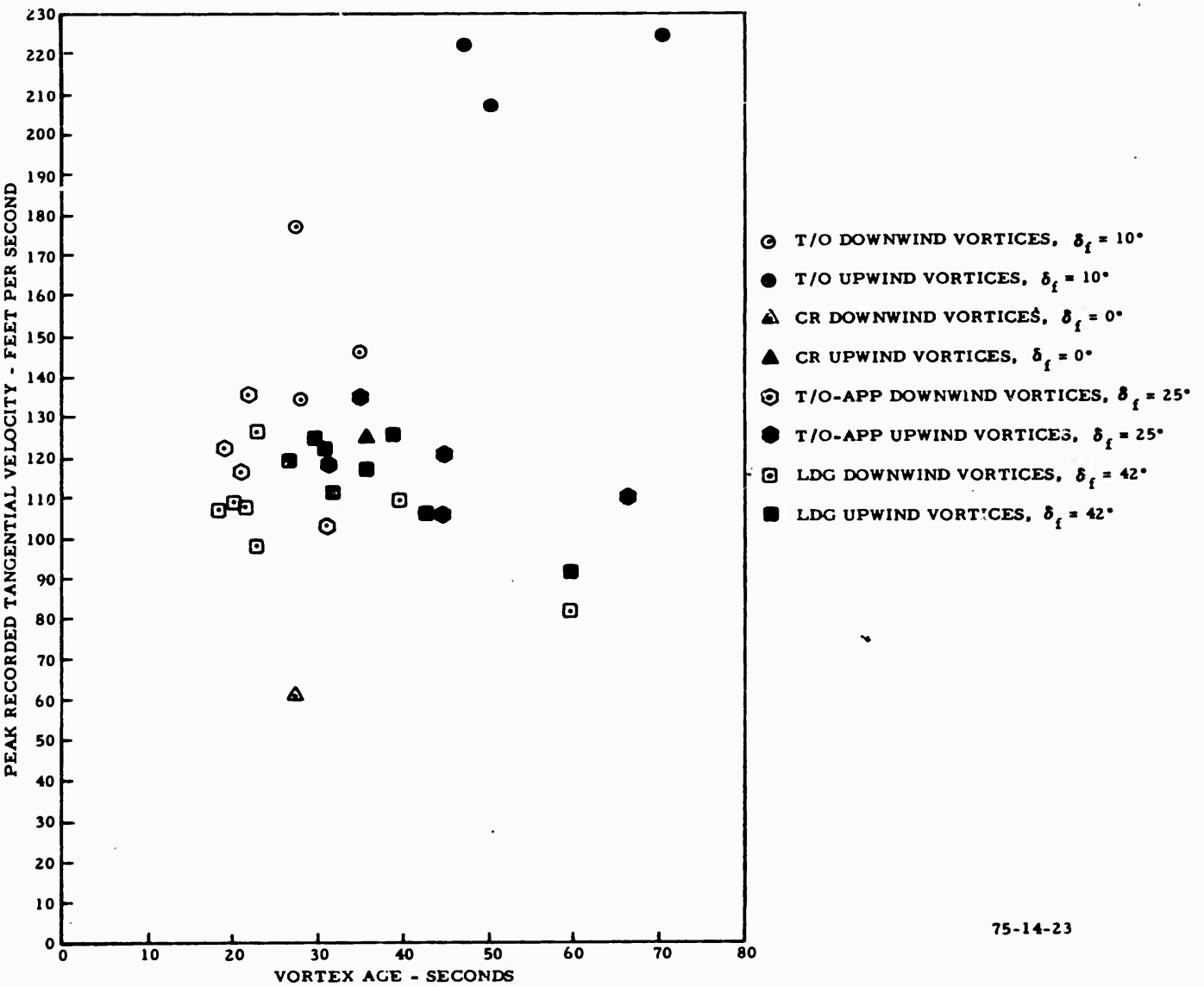

FIGURE 23. SUMMARY PEAK RECORDED TANGENTIAL VELOCITY VS. AGE (ALL CONFIGURATIONS)

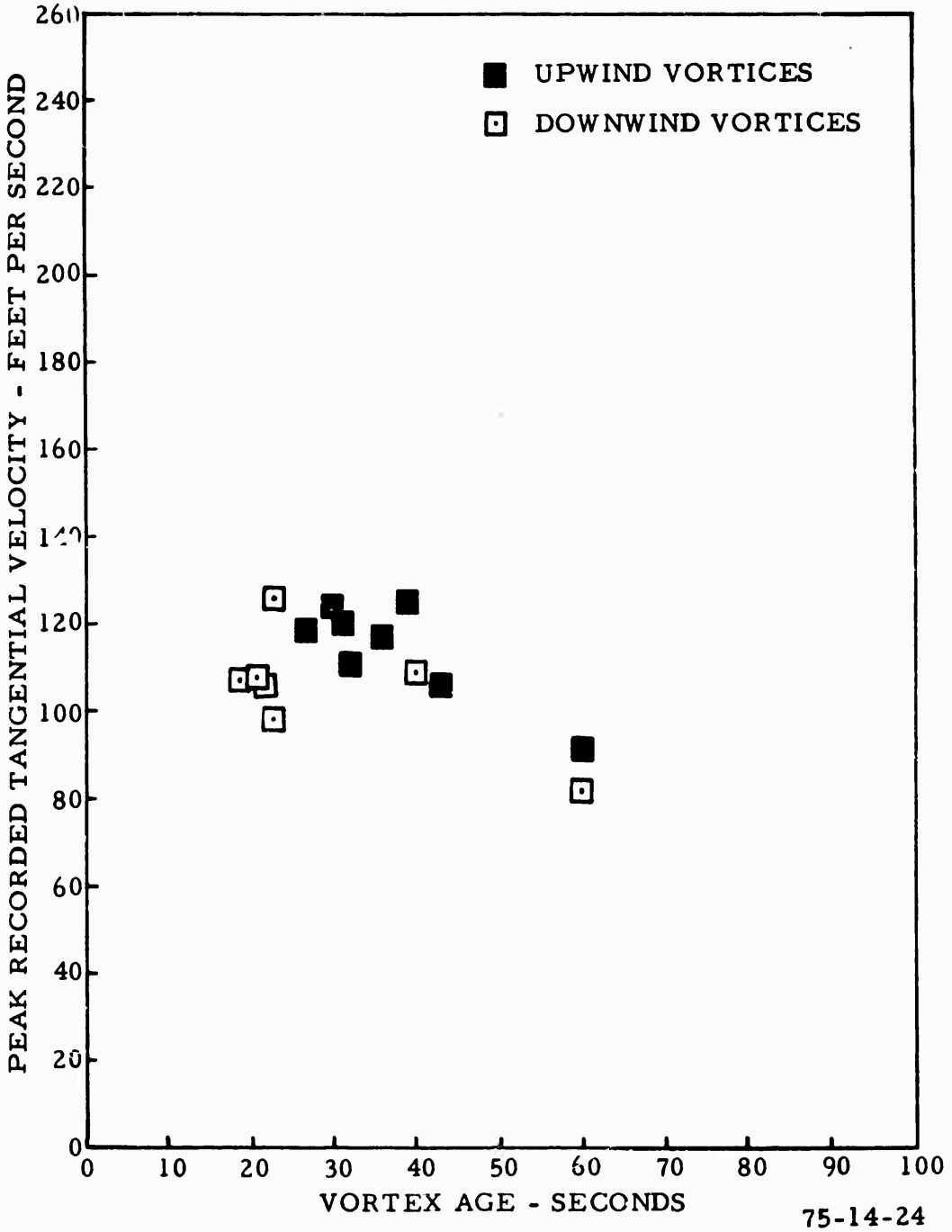

FIGURE 24. PEAK RECORDED TANGENTIAL VELOCITIES VS. AGE (LANDING CONFIGURATION $\delta_f = 42^o$)

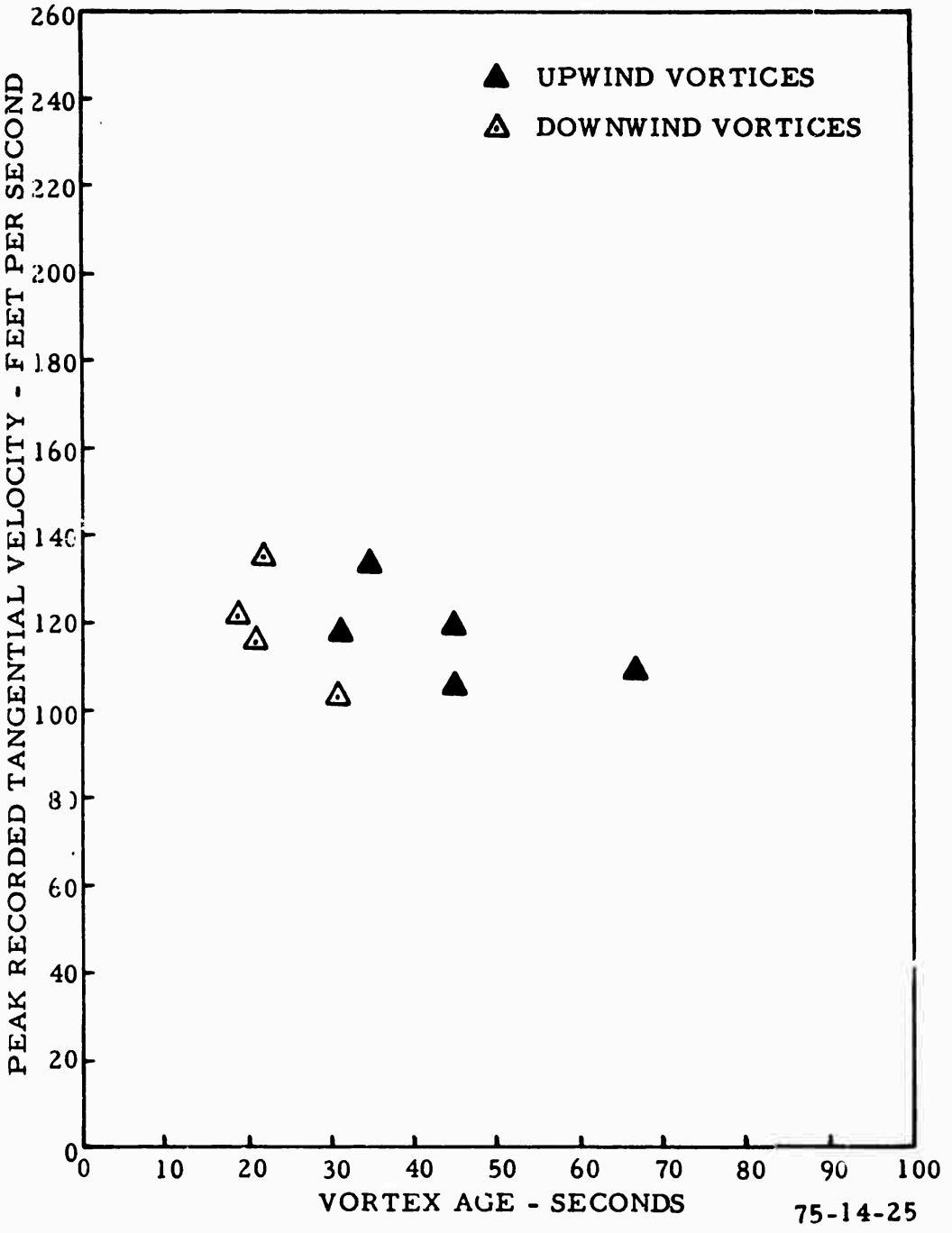

FIGURE 25. PEAK RECORDED TANGENTIAL VELOCITIES VS. AGE (TAKEOFF/APPROACH CONFIGURATION, $\delta_f = 22^o$)

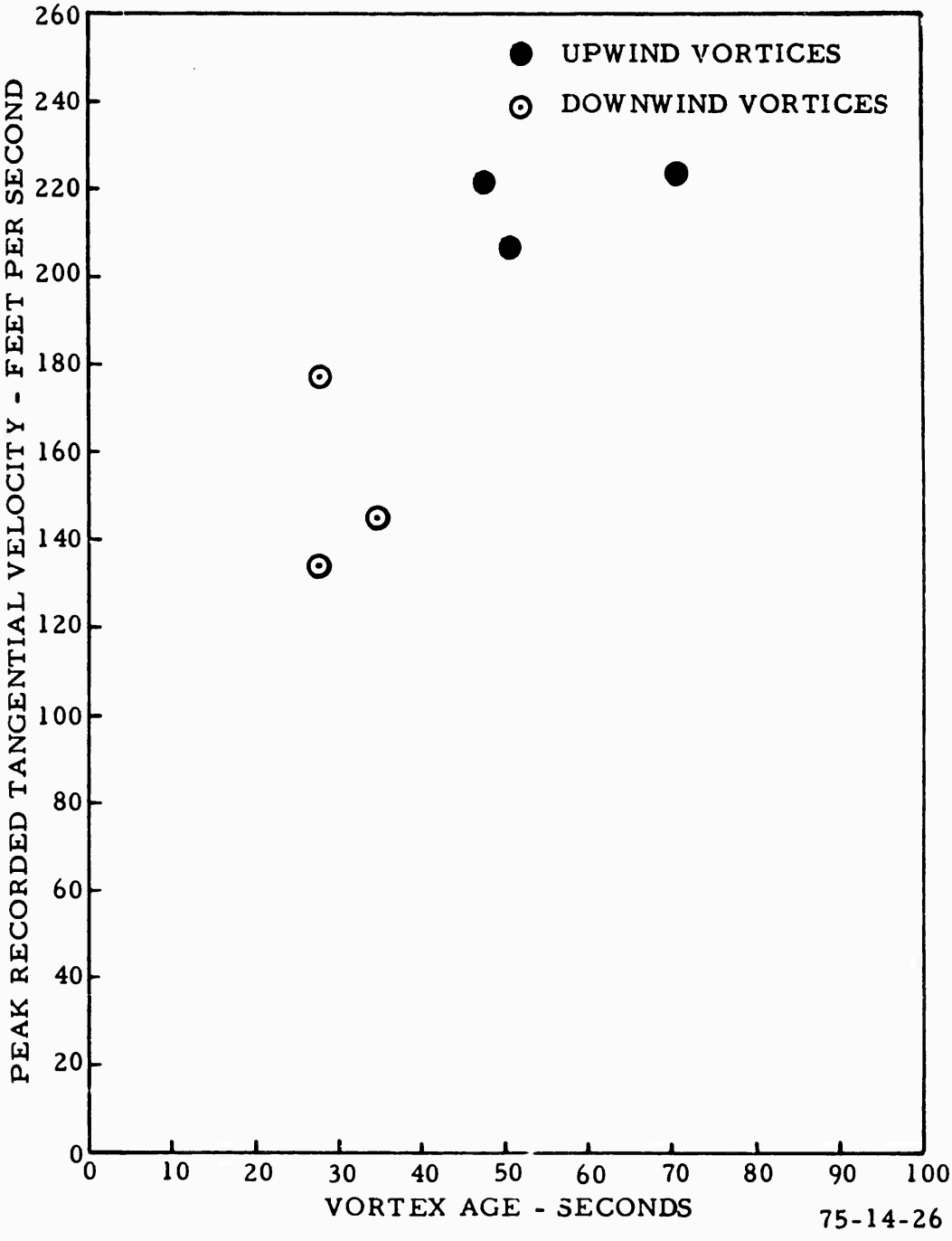

FIGURE 26. PEAK RECORDED TANGENTIAL VELOCITIES VS. AGE (TAKEOFF CONFIGURATION, $\delta_f = 10^o$)

velocity for the downwind vortex (first vortex, starboard wing) and the upwind vortex (second vortex, port wing) for the landing, takeoff/approach and takeoff configurations, respectively. Without exception the upwind vortices, for similar life spans, are more intense than the downwind vortices for this airplane. This has been noticed in other vortex flight tests conducted by NAFEC at low altitudes using the tower fly-by technique with other aircraft, and has been noted in earlier reports on vortex investigations, (references 6 and 7). This subject is discussed further in the next section, and figure 27.

The longest time-history data points acquired for the landing configuration were at 60 seconds concurrently for runs 1 and 17, 67 seconds for run 12 for the takeoff/approach configuration, and 71 seconds for the takeoff configuration. It is interesting to note that no decay in peak tangential velocity is noted for the takeoff configuration (10° δ_f). However, a decay trend is noted for the landing (42° δ_f) and takeoff/approach (22° δ_f) configuration.

Of great significance was the persistence of the vortices after they passed through the tower. Although quantitative data on vortex intensity can not be obtained after tower passage, the vortex flow visualization system on the tower permitted determination of the age of the system prior to vortex instability onset and subsequent rapid disintegration to random turbulence. The visualized flow fields shown in figures 7 and 28 through 31 are typical of these visualized vortices prior to breakdown. The predominant dissipation mode was observed to be vortex breakdown or bursting. Dissipation due to vortex/atmosphere interaction, and dissipation due to diffusion, were the other two modes. No vortex linking and subsequent breakdown due to sinsoidal instability was observed.

The "tubular-type" vortex structure was observed to slowly grow in diameter until it reached what appeared to be a constant core diameter (e.g., see figures 8 and 9), of about 8 to 12 feet for the landing configuration and lasted up to just under 2 minutes, at which time rapid breakdown was noted. The breakdown or bursting normally was as follows: just prior to breakdown a spiralling-type flow was distinctly noted to appear suddenly around the perimeter of the core cylinder as noted in figure 32. This was followed by a widening of the core axisymmetrically to about double its original diameter with the spiral flow still evident around the now enlarged vortex core. This lasted for about 2 to 5 seconds, after which rapid disintegration of this laminar-type flow field to random turbulence was noted. This overall decay can be seen in figure 32. Although the photograph shows the bursting of a B727 vortex system, as outlined by CORVUS oil and photographed with a K-38 camera during NAFEC flight tests with this aircraft at Edwards Air Force Base (AFB), it is representative of the vortex breakdown mode noted at NAFEC.

The contribution of the vortex test tower to vortex dissipation time or decay, due to tower/vortex intersection during vortex passage through the tower, has always been of concern using this test technique. The tower definitely disturbs or "ruptures" the vortex tube, to some extent, upon vortex passage,

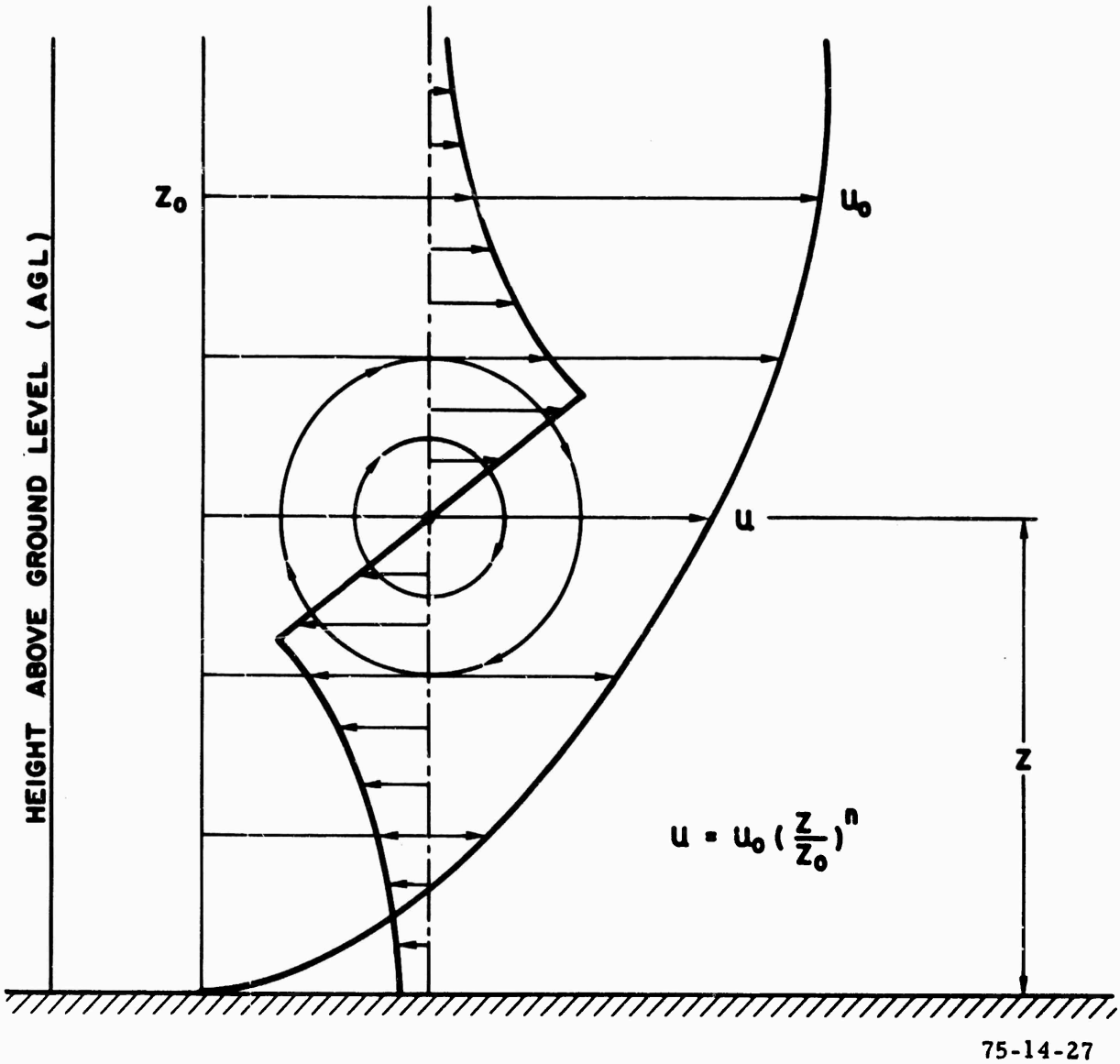

FIGURE 27. SCHEMATIC OF UPWIND VORTEX IMMERSED IN EARTH'S BOUNDARY LAYER FORMED BY PREVAILING AMBIENT WIND (CROSSWIND FLIGHT)

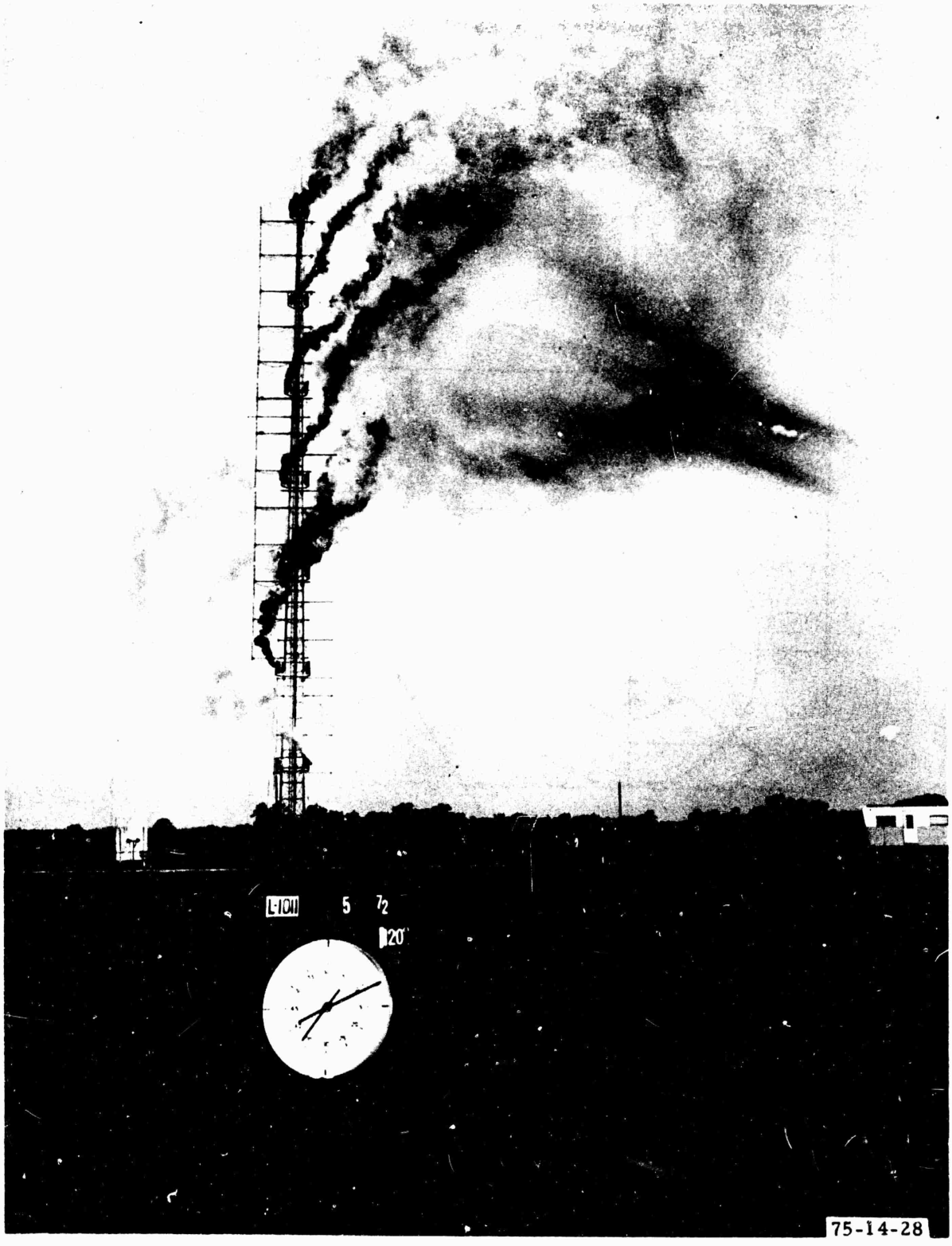

FIGURE 28. LOCKHEED L1011 PORT WING (UPWIND) VORTEX STRUCTURE RUN LANDING CONFIGURATION, δ_f=42°, VORTEX AGE 37 SECONDS

FIGURE 29. LOCKHEED L1011 PORT WING (UPWIND) VORTEX STRUCTURE, RUN 10, TAKEOFF/APPROACH CONFIGUREATION (δ_f=220°) EXACT AGE UNKOWN BUT >35 SECONDS

FIGURE 30. LOCKHEED L1011 PORT WING (UPWIND) VORTEX STRUCTURE RUN 14, TAKEOFF CONFIGUREATION (δ_f=10°), EXACT AGE UNKNOWN BUT >51 SECONDS

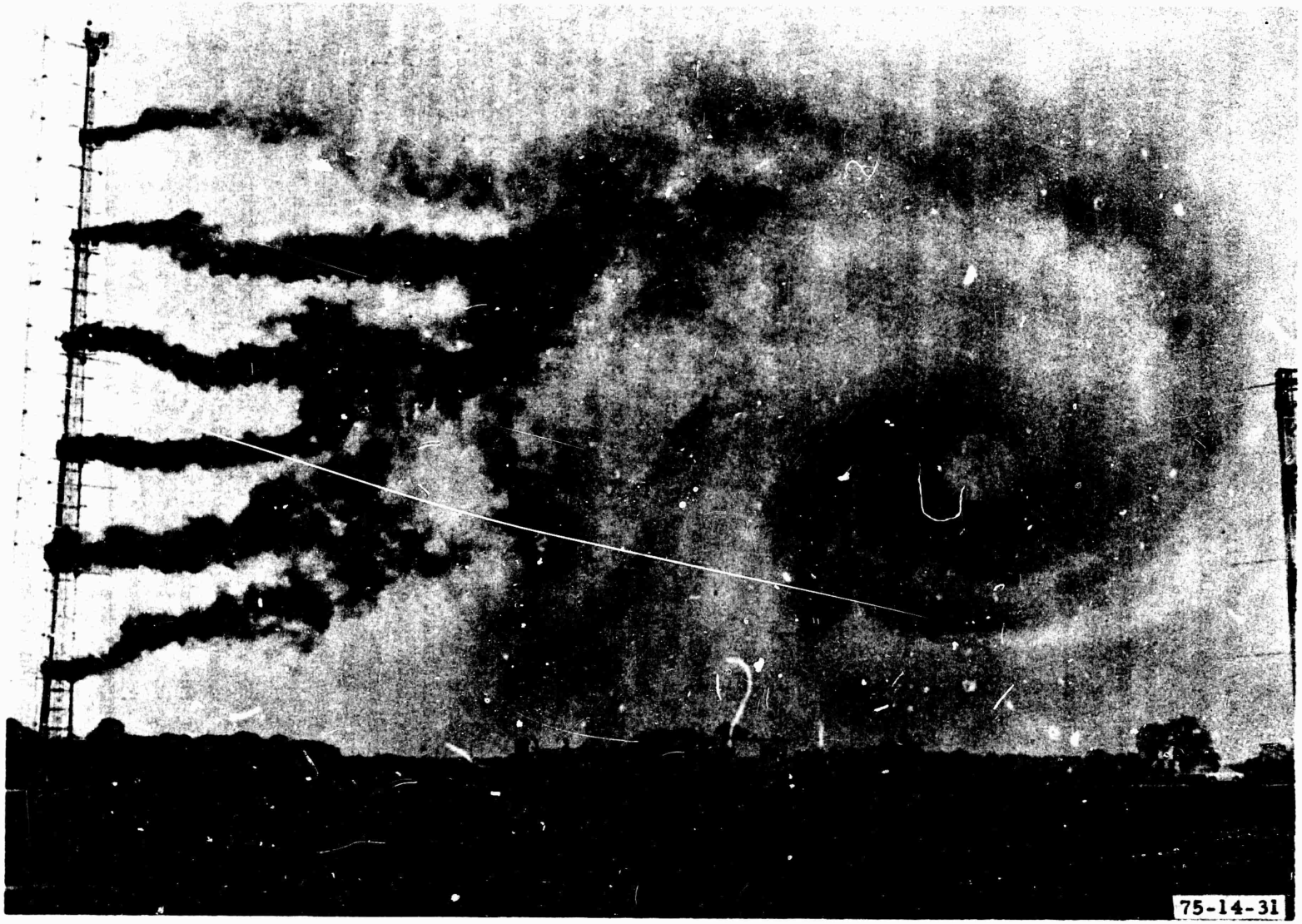

FIGURE 31. VISUALIZED PORT WING (UPWIND) VORTEX, L1011 CRUISE CONFIGURATION INDICATED AIRSPEED 305 KNOTS

and permits, although only momentarily, relatively higher ambient air pressure to enter the vortex core. This increased air pressure appears, at times,to accelerate vortex decay. However, this has been found to be the exception rather than the rule. Some of the unusual core and concentric tube vortices noted with flow visualization, as in figure 30 for example, are believed to be caused by vortex/tower interaction. In figure 8, however, one will note that this type of phenomenon is not observed after vortex passage for this data run.

VORTEX PERSISTENCE AS A FUNCTION OF ATMOSPHERIC CONDITION. It has always been NAFEC's intent to correlate aircraft vortex intensity with some parameter which would be indicative of atmospheric conditions. Certain indices such as Richardson number (Ri), temperature gradient, wind direction-speed index (DSI), and power spectral density of atmospheric turbulence are indicative of some parameters considered.

In view of the limited number of data runs flown during this time, any comprehensive attempt at correlation of L1011 vortex persistence as a function of various atmospheric conditions could be misleading.

However, correlation of vortex persistence in close proximity to the earth's surface with ambient wind velocity and direction reveals a significant result. That is, there is a definite relationship between the L1011 upwind and downwind vortices characteristics and the wind direction in relation to the aircraft flightpath. Looking at data runs 1 and 2, we see that the L1011 track was 310° and 309°, respectively, and the ambient wind velocity/direction was 16 ft/s/317° and 16 ft/s/310°, respectively, as measured at the 140-foot sensor level on the test tower. These data runs can be considered to have been flown into the wind and, accordingly, only one of the two-wing vortices (starboard) passed through the tower on each fly-by, and this passage was due to ground effect. Test site personnel, positioned approximately 500 feet northwest of the tower, felt the port wing vortices pass them by, moving in a direction perpendicular to and away from the airplane flightpath. Obviously, no correlation for this condition is possible between the port and starboard wing vortices because of lack of quantitative data on the former for these two runs. Intuitively, one would hypothesize that they were both of equal strength for the same age.

The aircraft flightpath was reoriented to the north (000°) after test run 2, in order to produce a crosswind condition which would cause both vortices to move towards the tower and thereby obtain quantitative data thereon. As can be seen in appendix G, for the 140-feet level, the wind direction changed from 295°M, run 3, to approximately 270°M for run 18. For all practical purposes data runs 3 through 19 are considered to have been conducted under crosswind conditions.

A brief explanation for the intensity and persistence difference between the downwind and upwind vortices is as follows: with a prevailing ambient wind as shown schematically in figure 27 (and actually in figure 33 for L1011 data run 4), due to viscous forces, a boundary layer is formed adjacent to the earth's surface. The boundary layer profile varies according to some

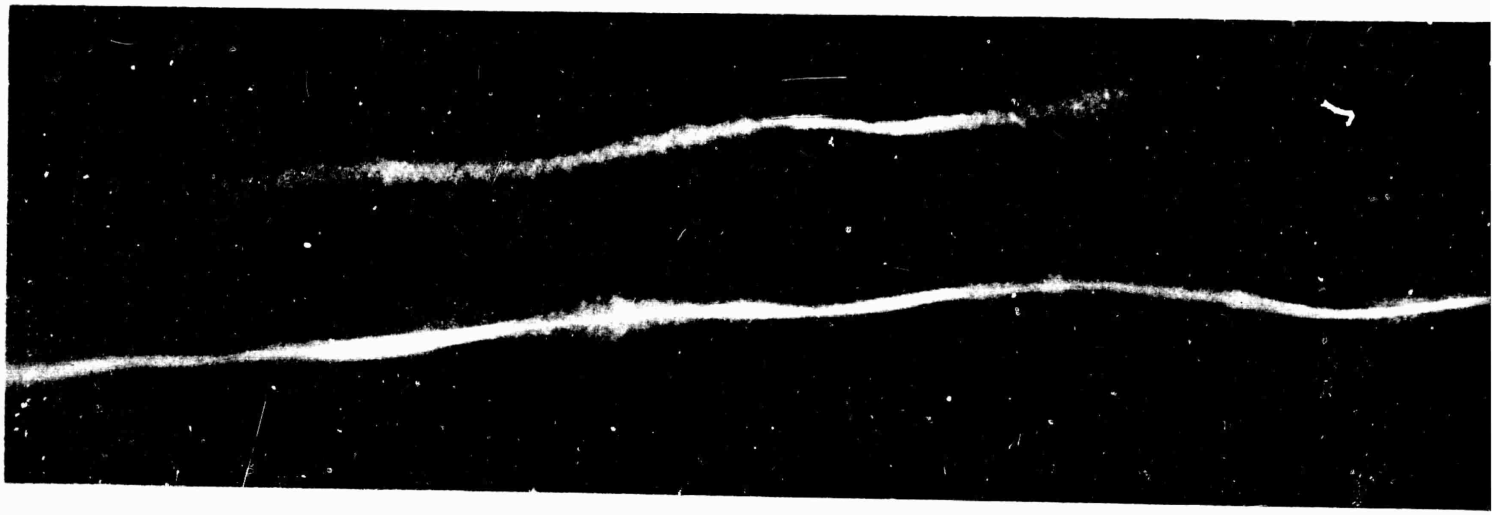

FIGURE 32. SPIRAL BREAKDOWN OF B727-200 VORTICES AT APP
AIRCRAFT FLIGHTPATH LEFT TO RIGHT, CLEAN CON

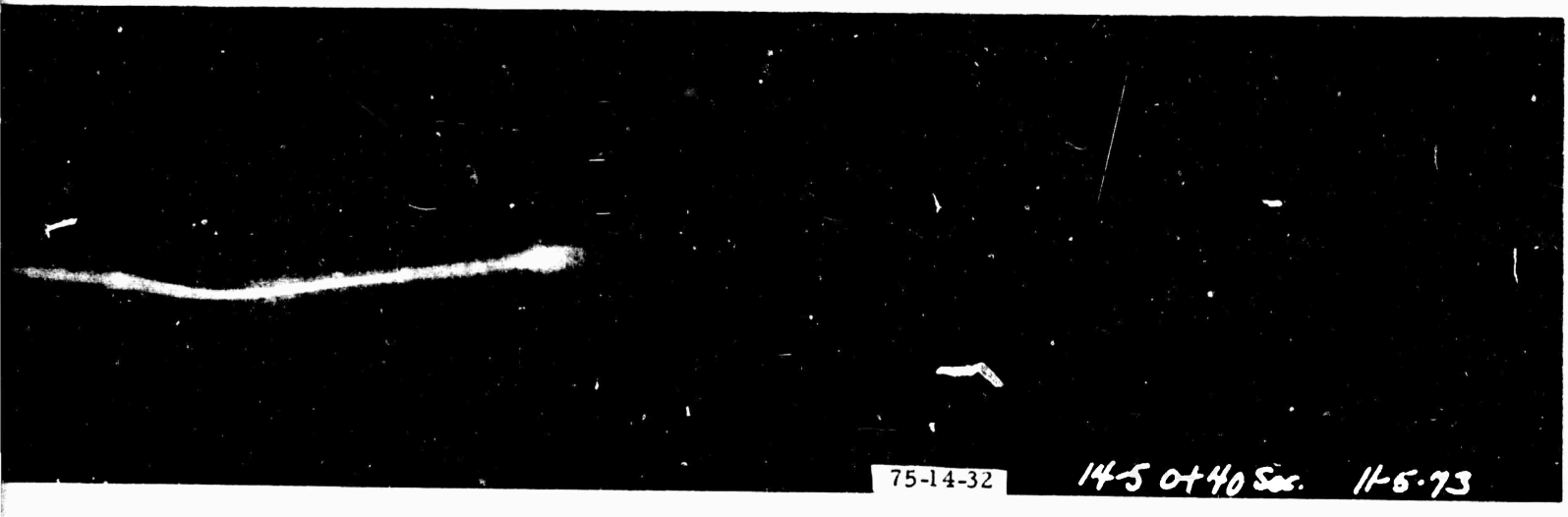

B727-200 VORTICES AT APPROXIMATELY 5,000-6,000 FEET AGL. AGE 40 SECONDS.
LEFT TO RIGHT, CLEAN CONFIGURATION

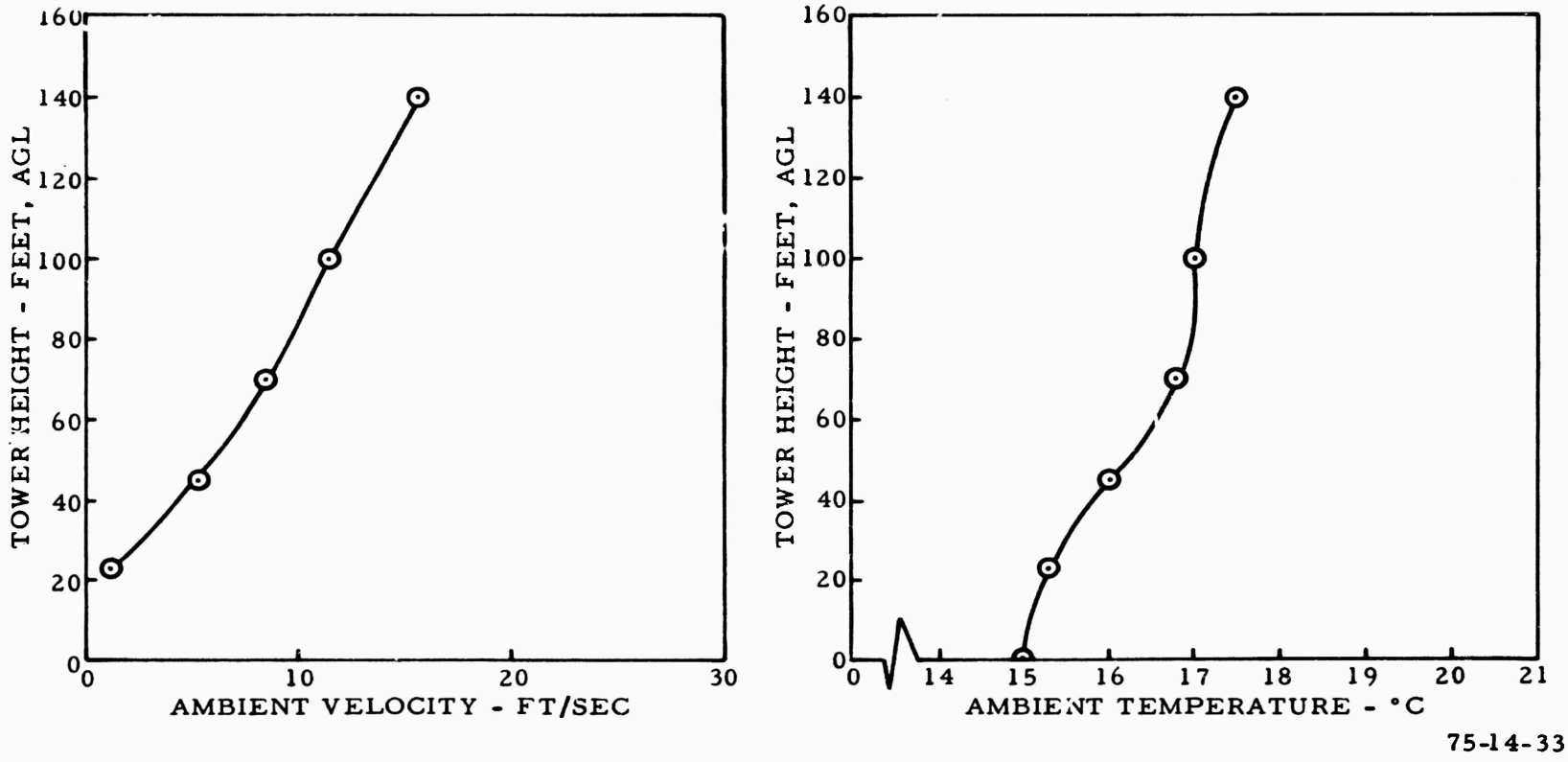

FIGURE 33. TEMPERATURE AND WIND VELOCITY PROFILE OBTAINED AT 0620 HOURS ON JUNE 3, 1972, TESTS WITH THE L1011 AIRPLANE, DATA RUN 4

power law depending upon, among other things, the characteristics of the earths' surface over which the wind is blowing. For the particular case in point, wherein the L1011 was flown approximately perpendicular to the ambient wind, the upwind vortex due to its direction of rotation would appear to have energy fed into it as it rolled along the ground. In addition, the upwind vortex, under the conditions cited, appears to be of a more orderly flow nature.

This can be seen in the photographic movie coverage (16 mm) of L1011 data runs 6 and 11, figures 8 and 9, respectively. The clock within the field of view shows elapsed time in seconds (small hand) and one second per revolution (large hand). The tower in the background is used for meteorological measurements and is approximately 500 feet away from the vortex tower.

The following items are worthy of note for these two data runs. For the downwind vortices, one can see how different the vortices are and how quickly they change to a random, turbulent type flow after tower passage. However, for the upwind vortices, note how much more orderly the flow is and more persistent the vortices are after tower passage.

Notice that for both runs, the upwind vortices were 2 seconds apart (43 and 45 seconds for runs 6 and 11) (figures 8 and 9), had the same peak recorded velocity of 106 ft/s, and were within 1 foot of each other (72-73 feet AGL) for tower intercept (appendix C).

It is to be noted that the L1011 flight test data were obtained from tests conducted early in the morning (sunrise), under smooth, steady wind and stable atmospheric conditions during which a temperature inversion existed. The smooth steady wind and stable stratified atmospheric conditions can be observed in figure 6 and inversion conditions are plotted in figure 33 for L1011 data run 4.

Based upon observations and recorded data at the test site during vortex flight testing, it is beginning to become more apparent that inversion conditions contribute to the persistency of aircraft vortices in close proximity to the ground. However, even though the vortex wake becomes more buoyant as it descends through such an atmosphere, for the L1011 airplane they did, in fact, descend as discussed later in this report.

VORTEX CHARACTERISTICS AS A FUNCTION OF L1011 CONFIGURATION. L1011 configurations are stated in appendix H and shown schematically in figures 4 and 5. The vortex characteristics as a function of airplane configuration are depicted in figures 24 through 26 and in the various figures of appendixes B, D, E and F. Select recorded vortex tangential velocity time-history plots (CalComp) are shown in appendix B. Several of these were discussed earlier. These are plots covering the entire data run from time zero (airplane abeam of the tower) until stop data signal was initiated after vortex (one or both) passage through the tower. Several of the time histories selected are for the sensor level closest to where the vortex peak tangential velocity was recorded and/or a vortex core was assumed to pass. The benefit of this complete velocity time-history profile

is that one can obtain a better understanding of the airflow field surrounding the vortex itself, the downwash field between the vortices, and the flow field induced by aircraft passage on the ambient wind flow field. This lateral wind velocity increment can produce a higher and, therefore misleading conception of what the actual ambient wind velocity was at time zero on these V_θ versus time plots. A similar type of phenomenon was observed by Zwieback, reference 8, during DC8 vortex measurements in the field at Long Beach, California.

A series of complete V_θ versus time plots is shown in figures B-13 through B-27 of appendix B for L1011, run 12 for sensor levels 68-82. This particular run was selected because both vortices intercepted the test tower at approximately the same height AGL (about 74 feet) and, therefore the result provides a better picture of what the vortex flow field looks like behind the L1011 while moving laterally in ground effect under crosswind conditions. However, one must view with caution further analysis of these plots, as discussed earlier in this section, with regard to the various induced velocities and ambient wind velocity contribution to what the sensor "feels." Freezing the vortex at a particular sensor level and trying to model it laterally has the disadvantage that what is seen on these appendix B plots is a varying age vortex, and one which is descending unless stabilized in height due to ground effect. However, if the vortex passes by the sensor fairly rapidly at a particular level, then the age does not vary laterally by more than a few seconds from one extreme of the field of influence on one side of the vortex axis to the other.

Peak Recorded Tangential Velocities. Figures 24 through 26 depict the differences that L1011 flap configuration has on the peak recorded tangential velocity between the landing configuration, δ_f=42°, figure 24, and the takeoff/approach configuration, δ_f=22°, figure 25. However, even though the amount of data is limited, there is a noticeable difference in peak tangential velocities between the takeoff configuration, δ_f=10°, and the two previous configurations cited. This corresponds to previous findings reported in references 1, 3, and 7 with the latter giving a detailed explanation covering this change in vortex tangential velocities with airplane configuration.

However, there have also been found exceptions to this characteristic of increased $V_{\theta_{max}}$ and smaller vortex cores with decreased flap deflection, e.g., as reported for the DC7 and B727 in references 6 and 9, respectively. For the former, the highest peak velocites occurred in the landing configuration, while the lowest peak velocities were recorded in the takeoff configuration. For the B727, little or no change in vortex velocity characteristics with airplane flight configuration was noted. Similar results were noted in other B727 vortex measurements as reported in reference 2.

Vortex Field of Influence. The field of influence of a vortex is defined to be double that area which extends radially from the vortex axis to a point where the tangential velocity approximates the ambient wind velocities, the field of influence diminishes, and one expects greater vortex flow-field/atmospheric-turbulence interaction at the lower altitudes.

Taking a look at the V_θ versus time Calcomp plots for the operational sensor levels from 56 to 142 feet AGL, it could be seen that for the landing configuration, $\delta f=42°$ (the majority of the runs in this configuration), the vortex field of influence extends for a distance of approximately 70 feet up the tower, or about 35 feet on either side of the peak recorded velocity. Approximately the same vertical span field of influence was noted for the takeoff/approach configuration, $\delta f=22°$; and to a slightly lesser degree, about 50 feet, for the takeoff configuration, $\delta f=10°$.

There is a significant difference noted in the field of influence, however, for the one data run 19, performed in the cruise configuration, δf=zero degrees. In this particular case, the total vertical field was only about 20 feet in diameter for both the downwind and upwind vortices. The composite plot for run 19 in appendix F, figures F-7 and F-8, provides an indication of how small these rotational velocity flow fields are in intensity and velocity distribution.

These findings on field of influence appear to correlate well with those reported in reference 2, wherein, with the exception of the B727 and DC9 aircraft, the vortex characteristics of the jet transport aircraft tested revealed the following:

Aircraft Configuration	Approximate Field of Influence (Based on Wingspan of Generating Airplane)
(1) Landing Configuration. Full landing flaps.	1/3 - 1/2 Wingspan
(2) Takeoff/Approach Configuration. Flaps approximately 1/2 - 1/3 of full flap.	1/3 Wingspan
(3) Takeoff/Clean Configuration. Flaps approximately zero to 1/2 full flaps.	1/6 - 1/3 Wingspan

Vortex Core Size. Aircraft vortex core radius is considered to be that radial distance at which the vortex tangential velocity, V_θ, is a maximum and within which the rotational flow field velocity distribution approximates that of a rotating solid body. Previous full-scale flight test vortex measurements, using the tower fly-by technique have revealed that an earlier theory on vortex core diameters, e.g., reference 10, was in error by approximately an order of magnitude.

For this analysis, four methods of vortex core diameter determination were considered:

1. Scaling of vortex core in movie coverage of the vortex flow field as outlined by the tower smoke which was entrained in the vortices during vortex passage through the tower.

2. Determination of the core size by using the expanded plots some of which are in appendix E combined with vortex translational velocities and the technique used in reference 11.

3. Using the results of reference 12 that the circulation varies logarithmically with radius.

4. Using a curve fitting technique on the V_θ versus radial distance plots of appendix D wherein the equation of the curve includes core radius, r_c. Primary emphasis was placed on using method 4. A brief discussion of the four methods follows.

Method 1. Where tower smoke was available on a particular test run, the 16 mm colored photographic coverage obtained with the two movie cameras placed 90° apart from each other, as discussed earlier, was reviewed. Using a combination of the known tower height of 140 feet and tower base width, 5 feet, measurements of the vortex core size were attempted. It was assumed that the vortex core was outlined by the most densely smoke-packed cylinder visualized in the vortex flow field. Certain investigators have questioned whether the smoke entrained in the vortex, as shown in various photographic coverage of the vortices, does in fact outline the vortex core. Previous analysis on the subject during NAFEC's 1970 vortex measurement tests has revealed that the colored smoke particles, in general, have the same characteristics as the air particles, i.e., size and density, and therefore can be expected to assume the same rotational flow characteristics of a vortex, and thus depict them visually.

Using this technique, it is difficult at times to ascertain what constitutes the vortex core, particularly where multiple concentric cylinders are noted, e.g., as portrayed in figure 30. Core size determinations were made immediately upon vortex passage through the tower when the entrained smoke had formed and outlined a cylindrical structure. The vortex core size estimates using this technique are listed in table C-2 in appendix C.

Method 2. This technique, described in detail in reference 2, uses basically the following equations. Referring to figures 34 and 35, we have for an exact core passage by sensor A

$$d_c = \Delta_t \cdot \dot{y}_v \tag{3}$$

where Δt = time interval between velocity peaks, V_1 and V_3,
and $\dot{y}_v$ = vortex lateral transport velocity

For a partial core penetration by sensor B, as shown in figure 35, we have

$$d_c^2 = \frac{\left[\dot{y}_v \cdot \Delta t\right]^2}{\left[1 - \frac{V_{min}}{V_{max}}^2\right]} \tag{4}$$

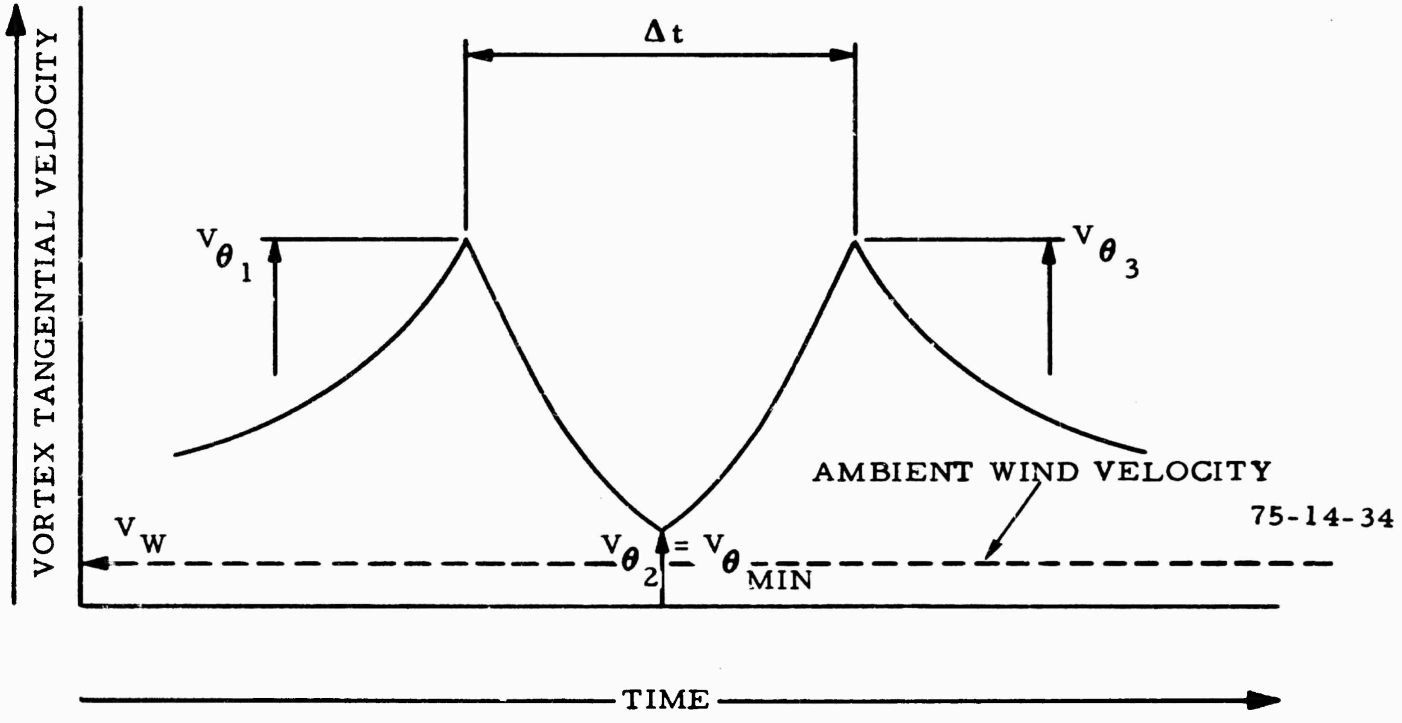

FIGURE 34. EXPANDED TIME HISTORY OF RECORDED VORTEX TANGENTIAL VELOCITY AT A SENSOR

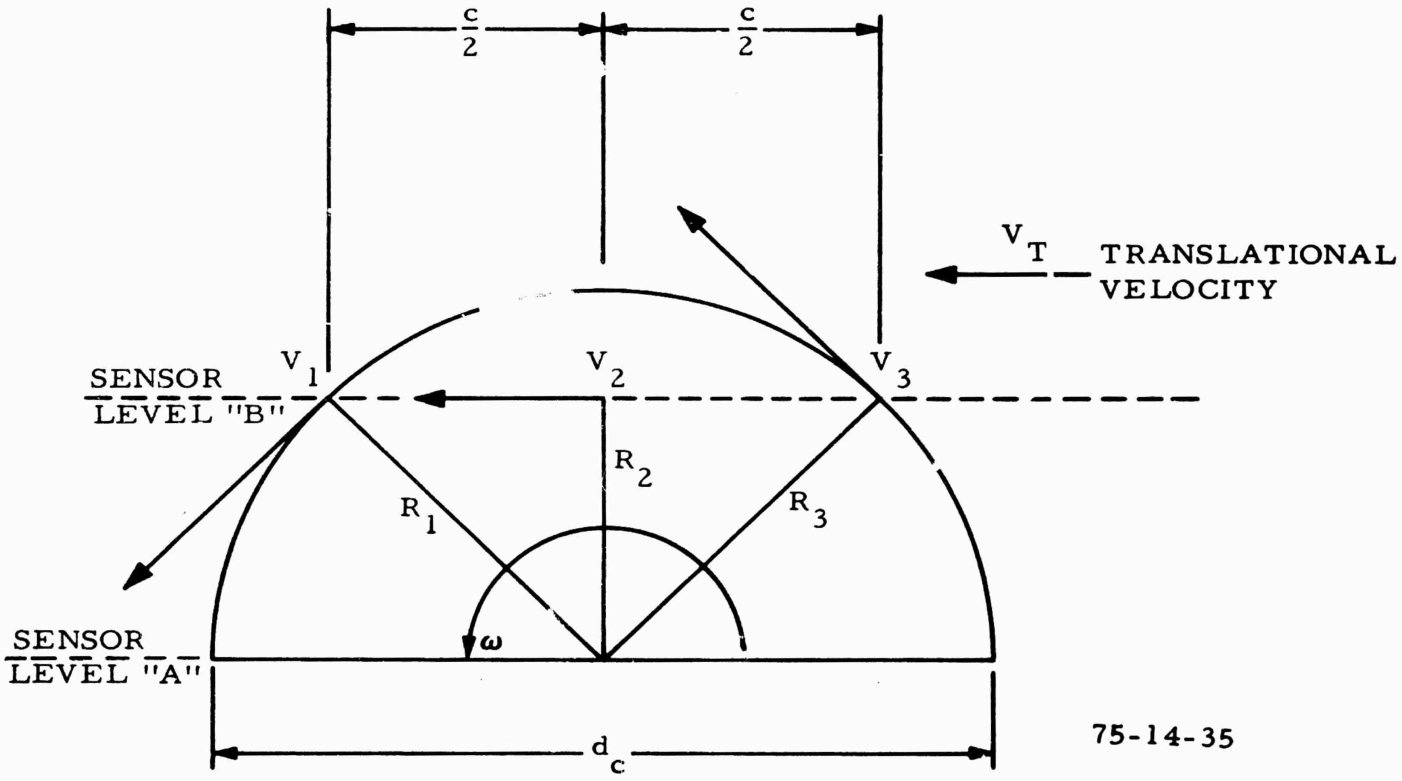

FIGURE 35. VORTEX PASSAGE ACROSS A PAIR OF SENSORS AND ASSOCIATED GEOMETRIC RELATIONSHIP FOR SENSOR VELOCITIES

Three difficulties arise, using this technique for core radius determination:

1. The instantaneous vortex lateral transport velocity across the sensor y_v is difficult to obtain because of a varying windspeed and direction and ground induced effects on vortex movement. Accordingly, where vortex core size is calculated using this technique, some careful analyses and judgment must be made as to what comprises the instantaneous y_v. Where an average y_v was used, this average was based on the distance between the point where a particular vortex is shed from the wing $y_{a/c} \pm 1/2 + b'$ and the vortex test tower divided by the elapsed time for the vortex to traverse this distance.

2. In addition, it is difficult to determine the sensor level closest to which vortex core passage occurred, for reason cited earlier, i.e., a vortex tangential velocity decrement, the point V_2 or V_{min} in figure 34 may be due to probe support arm interference.

3. Taking into account the hot-film sensor alignment, the sensor still does respond, although minutely, to axial and radial flows associated with vortex core characteristics as well as the vortex transport velocity itself which would preclude determination of an accurate $V_{\theta_{min}}$ in figure 34.

In other cases it is not possible to discern any significant V_θ decrement so as to be able to select points V_1 and V_3 and likewise a Δt; i.e., see runs 14 and 16 appendix E.

An example of this calculation is shown in figure 36, for L1011 run 9. Using table C-2 of appendix C, we see that y_v=18.6 ft/s for the first vortex. Inasmuch as this is the downwind vortex, we would expect its lateral velocity to be greater than the crosswind at that level. However, we have no way of accurately knowing the instantaneous transport velocity at the level and instant of tower passage. Accordingly, using average y_v values in our calculations, it would tend to make the vortex cores appear to be larger in radius than they actually are. In this particular example, we arrive at a core radius of approximately 3.6 feet. However, using the average wind velocity of approximately 13 ft/s at 100 feet AGL (appendix G) we calculate a core radius of about 2.7 feet.

Method 3: Based on the quality of the L1011 data, particularly the V_θ versus h plots, and the excellent results obtained using the approach of McCormick, et. al,., references 11 and 13 as expanded upon from Hoffman and Joubert's work, reference 12, that the velocity field around the vortex obeys a logarithmic variation of circulation with radius

$$\Gamma = \Gamma(r_c)\left[\ln\left(r/r_c\right) + 1\right] \tag{5}$$

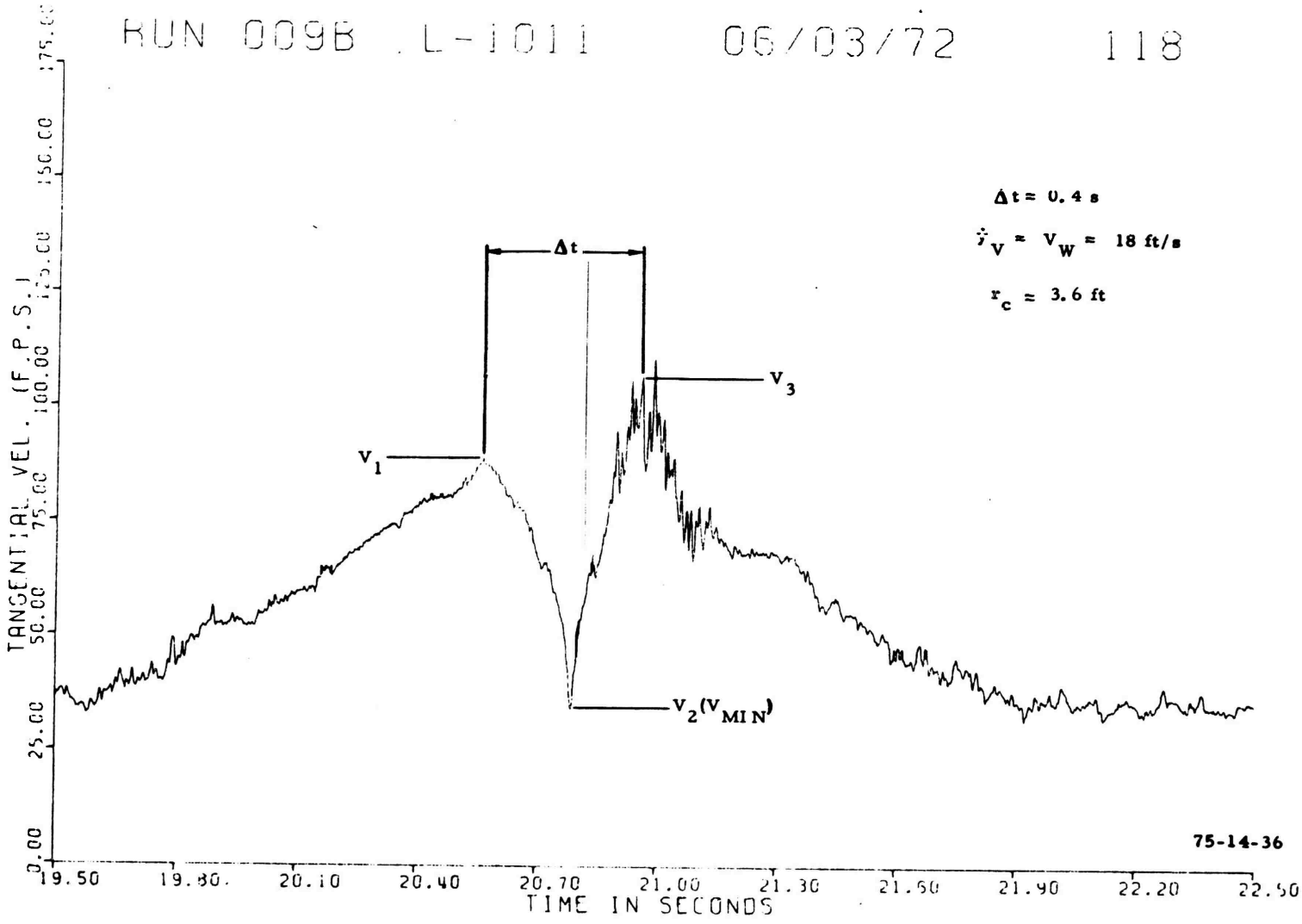

FIGURE 36. EXPANDED TIME-HISTORY PLOT OF RECORDED VORTEX TANGENTIAL VELOCITY, SENSOR LEVEL 118, L1011 RUN 9, APPROACH CONFIGURATION, STARBOARD (DOWNWIND) VORTEX

it is possible to estimate the core radius from a plot of Γ versus $\ell n\ r$ as follows :

$$\Gamma = 2\pi r\ V_\theta \tag{6}$$

Differentiation in equation (5) with respect to $\ell n\ r$ we have

$$\frac{d\Gamma}{d(\ell n\ r)} = r\frac{d\Gamma}{dr} = 2\pi r\ (V_\theta + r\frac{dV_\theta}{dr}) \tag{7}$$

for $r_c = r_c$, $\frac{dV_\theta}{dr} = 0$ and

$$\Gamma(r_c) = 2\ r_c\ V_\theta\ (r_c) \tag{8}$$

and

$$\left[\frac{d\Gamma(r_c)}{d(\ell n\ r)}\right]_{r = r_c} = \Gamma(r_c) \tag{9}$$

Using the $V\theta$ versus r plots of appendix D, Γ can be calculated from equation (6) and a plot of Γ versus $\ell n\ r$ prepared. A straight line is then drawn through the points the slope of which should be equal to $\Gamma\ (r_c)$. Using the value of $\Gamma\ (r_c)$ and the associated value of $\ell n\ r$ on this plot, one may then estimate the value for (r_c). Four such plots were made, selecting four L1011 runs at random, namely L1011 run 7, landing configuration, port (upwind) vortex, L1011 run 9, approach configuration, port (upwind) vortex and run 16, takeoff configuration, both vortices. The plots, shown in figures 37 through 40, respectively, indicate the following:

Run 7, (r_c)=1142 ft^2/s, r_c=2.23 ft
Run 9, (r_c)=1307 ft^2/s, r_c=2.03 ft
Run 16, (r_c)=1071 ft^2/s, r_c=1.57 ft
Run 16, (r_c)= 847 ft^2/s, r_c=0.9 ft

These values of core radii appear to correlate well with those determined by curve fitting technique with the logarithmic radial distribution of tangential velocity profiles discussed under method 4.

Method 4: In view of the success achieved previously in applying the Hoffman-Joubert theory (reference 14) that the tangential velocity field in a turbojet vortex obeys a logarithmic variation of circulation with

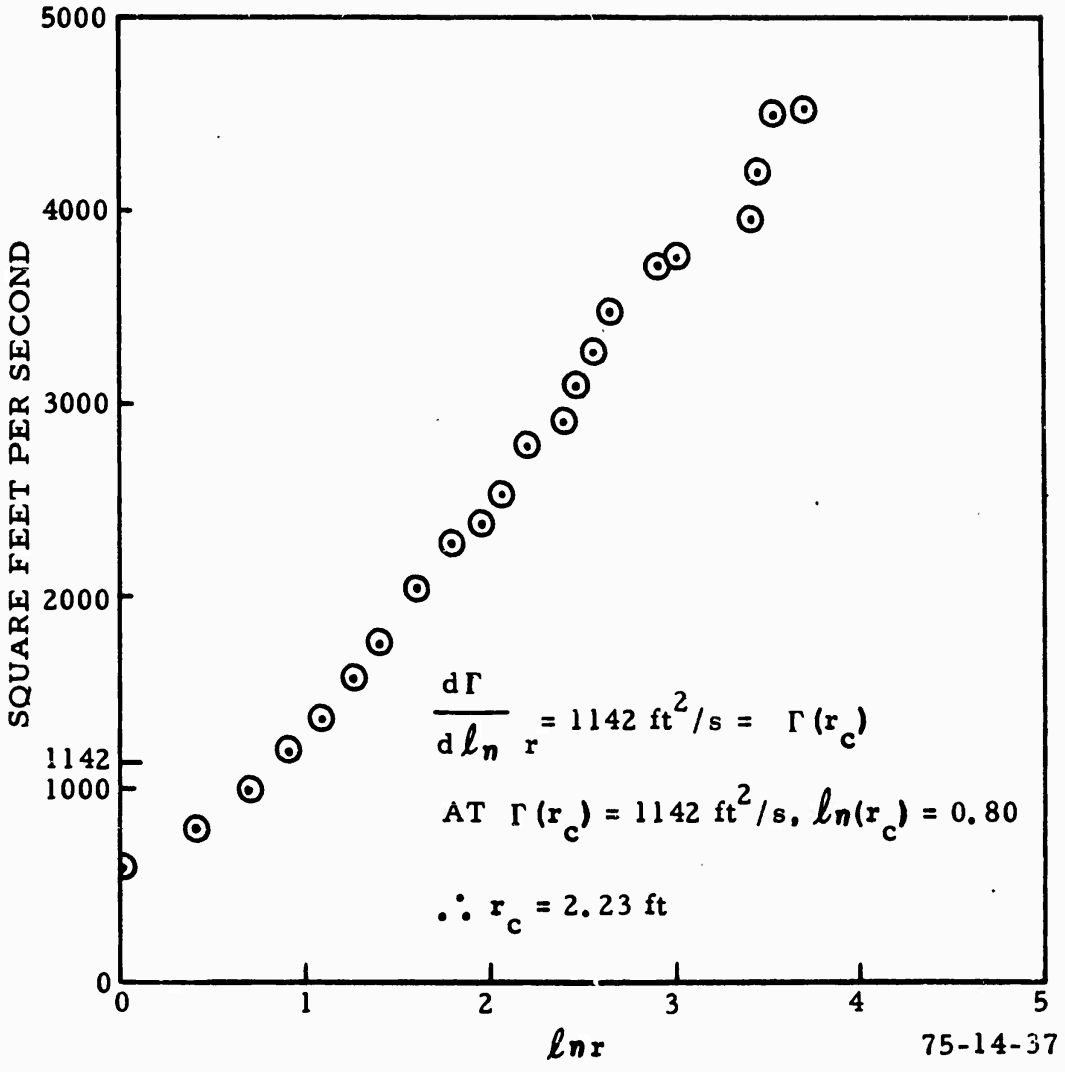

FIGURE 37. L1011 RUN 7, Γ VERSUS ℓn r, LANDING CONFIGURATION, PORT (2nd) VORTEX

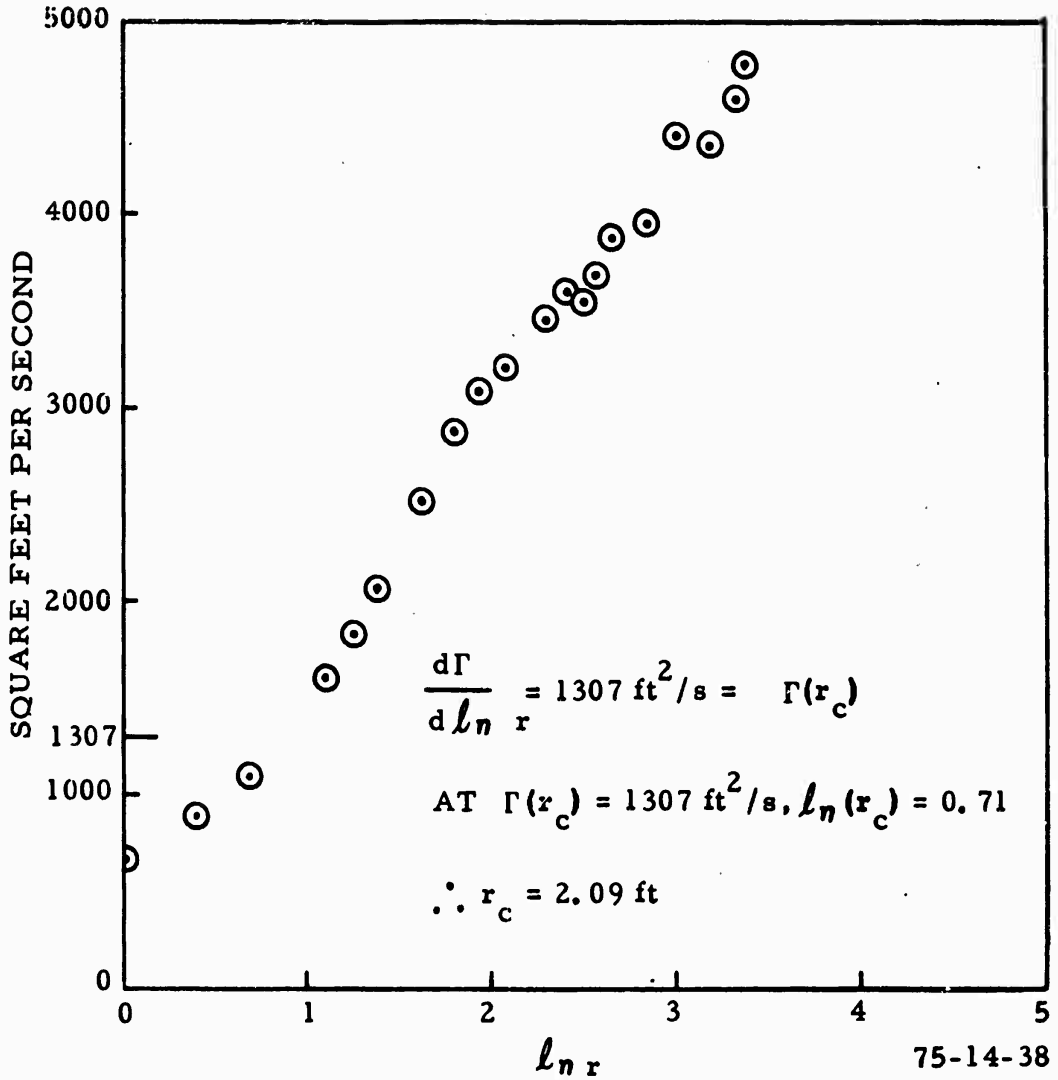

FIGURE 38. L1011 RUN 9, Γ VERSUS ℓn r, APPROACH CONFIGURATION PORT (2nd) VORTEX

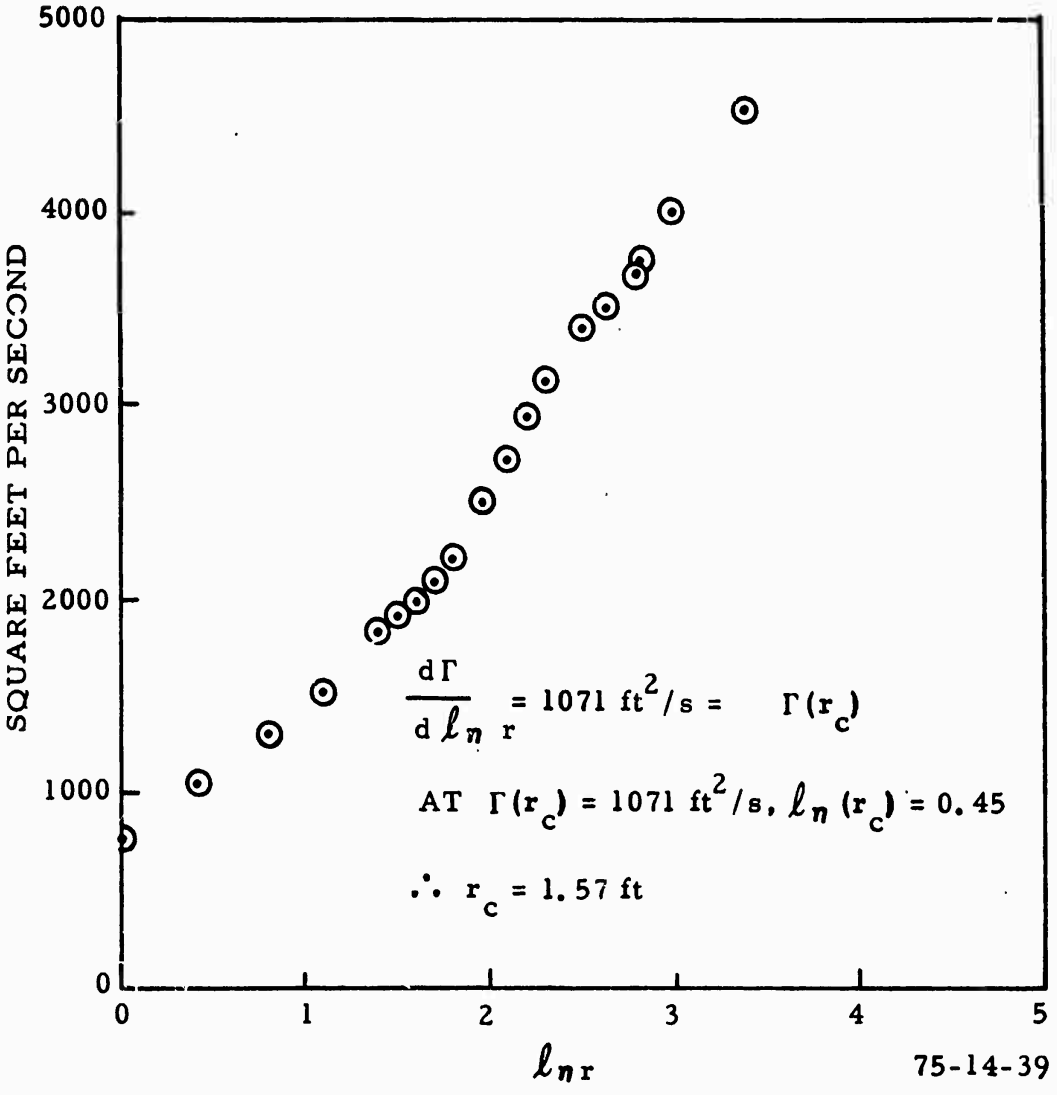

FIGURE 39. L1011 RUN 16, Γ VERSUS ℓn r, TAKEOFF CONFIGURATION STARBOARD, (1st) VORTEX

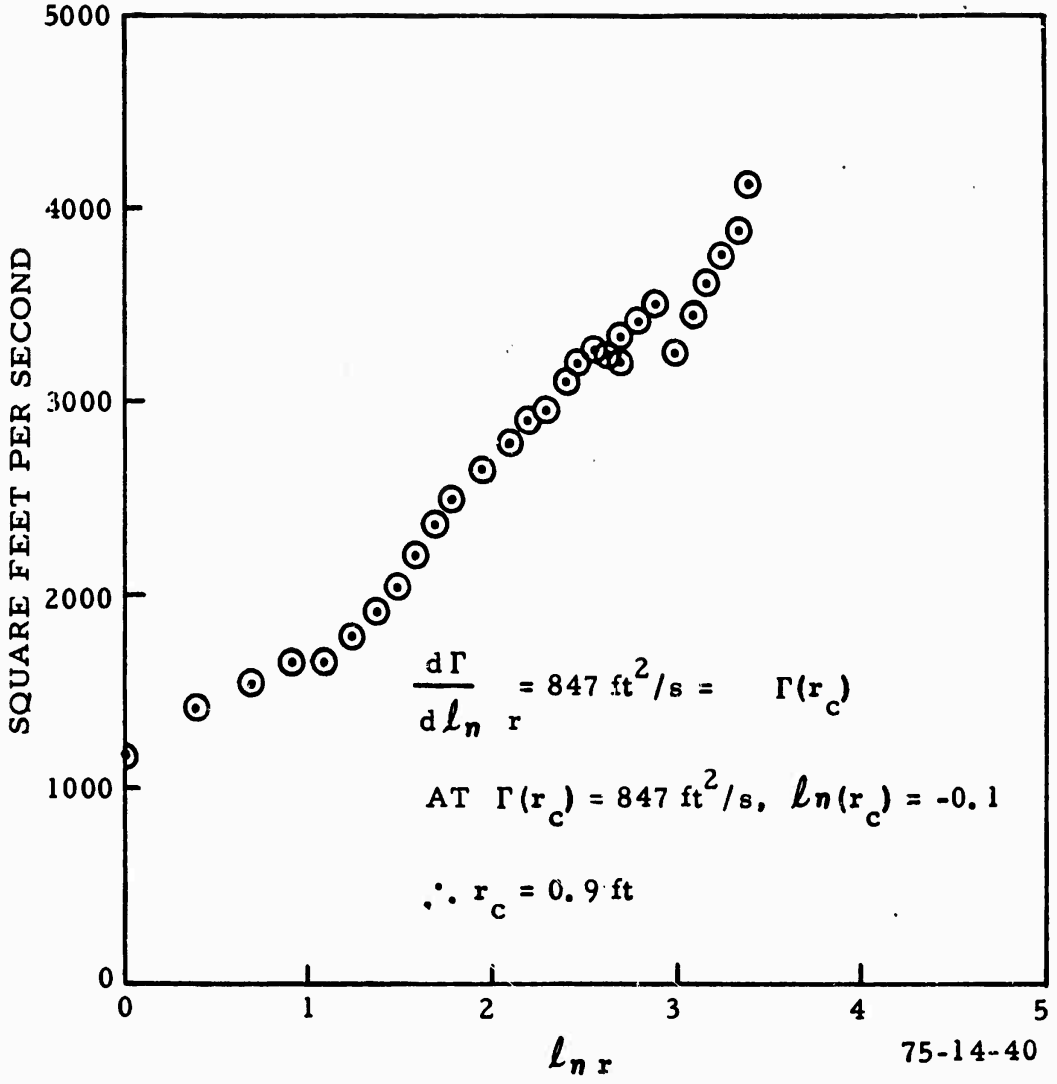

FIGURE 40. L1011 RUN 16, Γ VERSUS $\ell n\ r$, TAKEOFF CONFIGURATION PORT (2nd) VORTEX

radius, the same theory was applied in the analysis of L1011 tangential velocity distribution plots, appendix D. It was found that in the majority of these plots the tangential velocity distribution profiles did indeed follow this logarithmic distribution. Examples of this excellent correlation are shown in figures 41 through 44 for L1011 runs 3, 4, 9, and 10, respectively.

Knowing this, and using the V_θ versus radial distance curves generated by a computer program, the following technique was used for core radius determination. If one were to make a plot of $V_\theta/V_\theta(r_c)$ versus r/r_c using the logarithmic distribution as shown in figure 45, one finds that for a value of $V_\theta/V_\theta(r_c)$ of 1/2, r/r_c=5.4. Accordingly, using the V_θ versus r plots of appendix D, the value of r for which V_θ is equal to 1/2, the value of $V_{\theta_{max}}$ is divided by 5.4 to arrive at the core radius (r_c).

It was found that when the vortex intercepted the test tower at such a height above the ground so as to provide sufficient V_θ data above and below the intercept point for further analysis of that semi-vortex, the upper and lower semi-vortices did not necessarily produce the same profiles of radial distribution of swirl velocities nor, therefore, the same core radii. This non-axisymmetric velocity profile is to be expected because of the distortion caused by the proximity of the vortices to the ground, the interference effects in the field of reverse flow caused by the tower and probe support structure, and the wind shear caused by the earth's surface. In the majority of the runs the core radii were determined for that semi-vortex whose tangential velocities were flowing with the wind and, therefore, subject to minimal tower structure interference effects. The core radii thus obtained are listed in table C-2 of appendix C.

The net result of this particular analysis revealed that the average vortex core radii were found to be on the order of 5, 4, and 2 feet in diameter, for the landing, approach and takeoff (δ_f=10°) configuration, respectively.

Vortex Transport. A vortex pair will normally, under "stationary" atmospheric conditions, move downwards because of mutual interaction between the two vortices. That is, the starboard wing vortex, due to its rotational flow field components in the vicinity of the port wing vortex, will produce a downward flow on the port wing vortex, and vice versa. An isolated vortex will not, under the cited atmospheric conditions, necessarily move downward because there are no outside forces, either vortex or atmospherically induced, to cause it to do so. However, when the vortices are imbedded in a three-dimensional atmospheric flow which is non-homogeneous their movement and paths are difficult to predict. Close proximity of the vortices to the ground, further complicates the picture because of ground effect discussed earlier.

Although considered, this analysis does not address itself in detail to the lateral transport velocity, $\dot{y}_v$, of the L1011 vortex pair. Looking at table C-2 of appendix C, one can see that $\dot{y}_v$ for the upwind vortex is in many cases higher than the ambient wind velocity existing as the tower intercept level. This is primarily attributed to the relatively higher crosswind components with an increase in altitude above ground level as discussed earlier

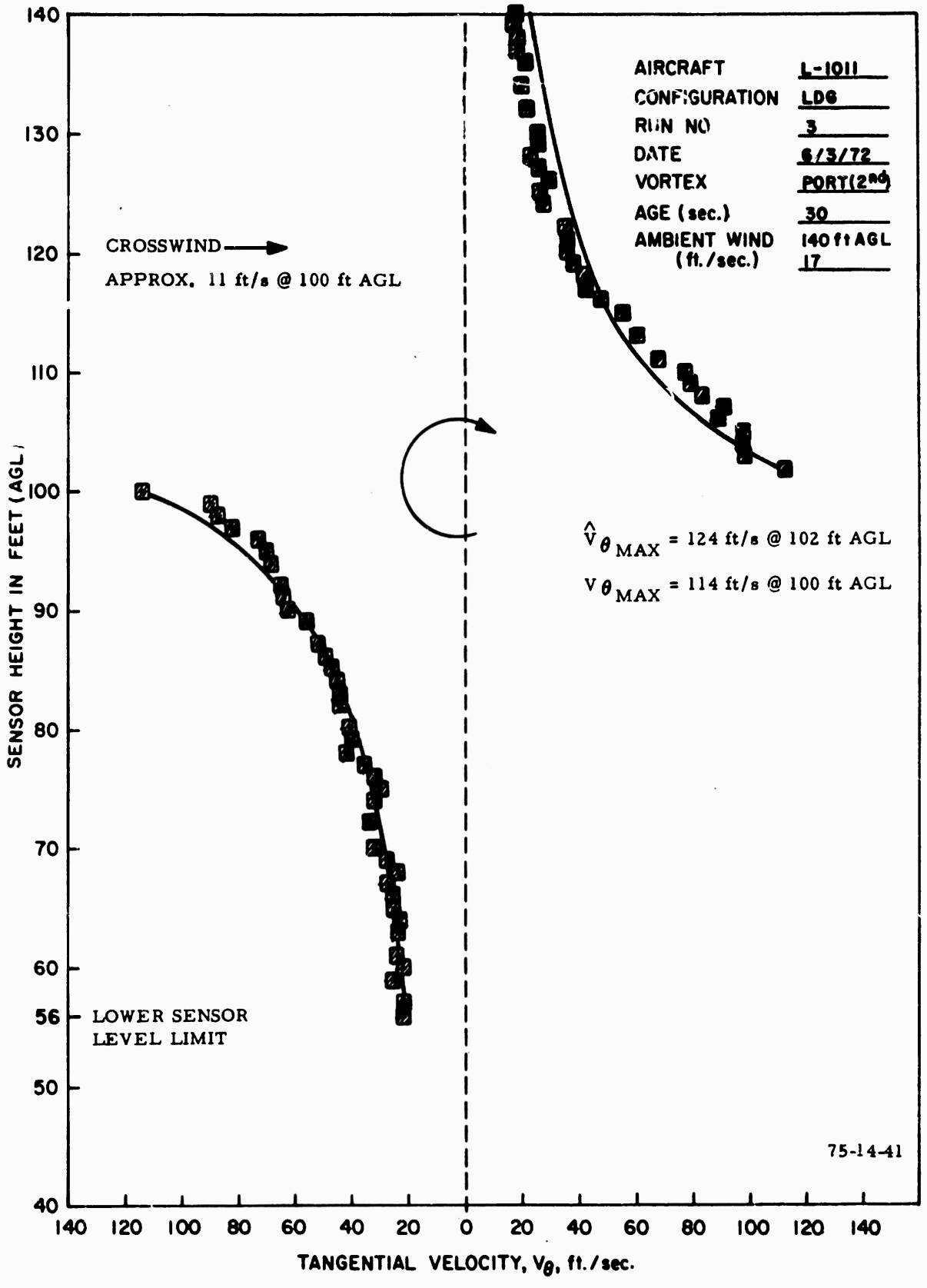

FIGURE 41. L1011 RUN 3, V_θ VERSUS h, LANDING CONFIGURATION PORT (2nd) VORTEX

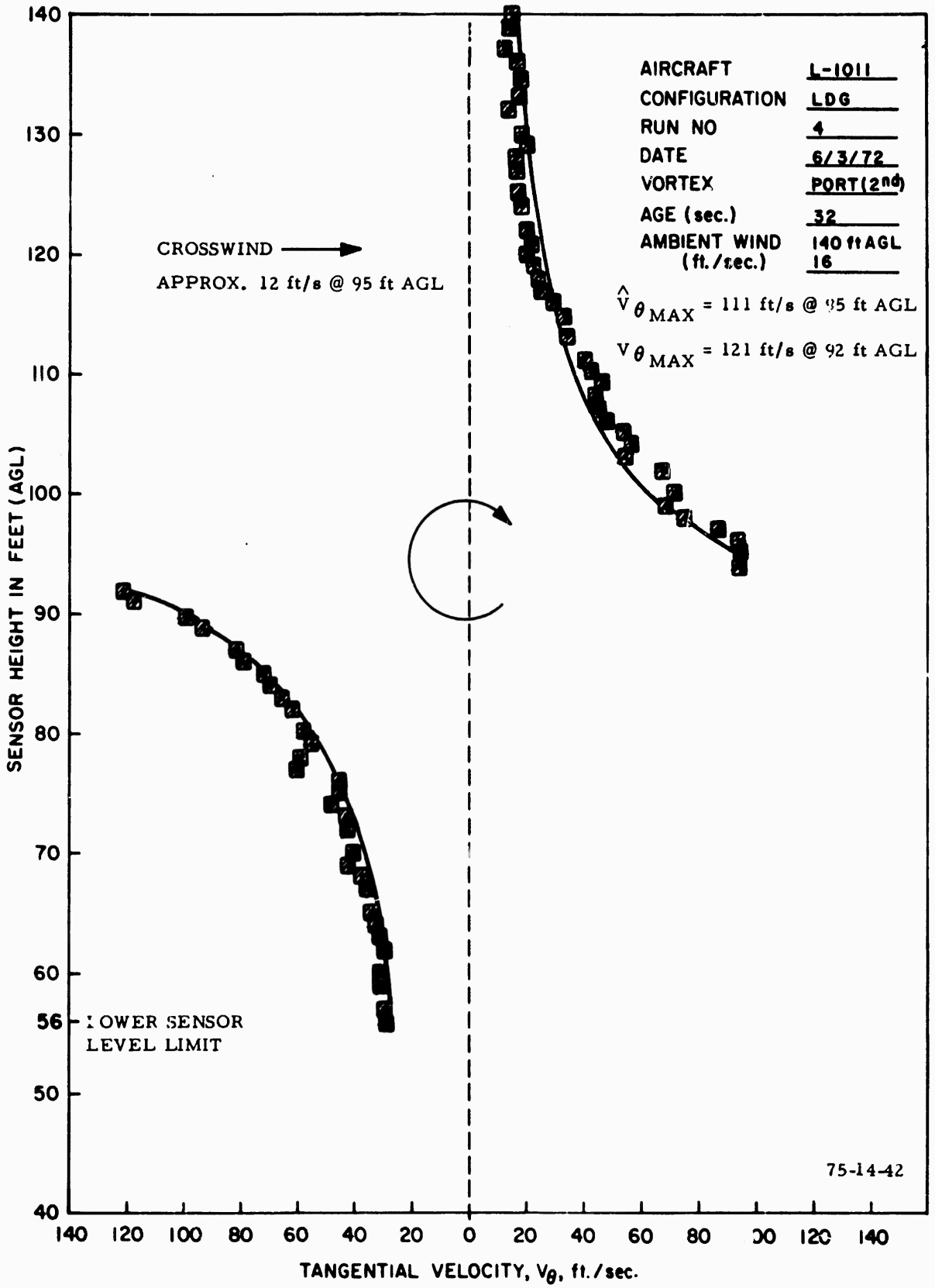

FIGURE 42. L1011 RUN 4, V_θ VERSUS h, LANDING CONFIGURATION, PORT (2nd) VORTEX

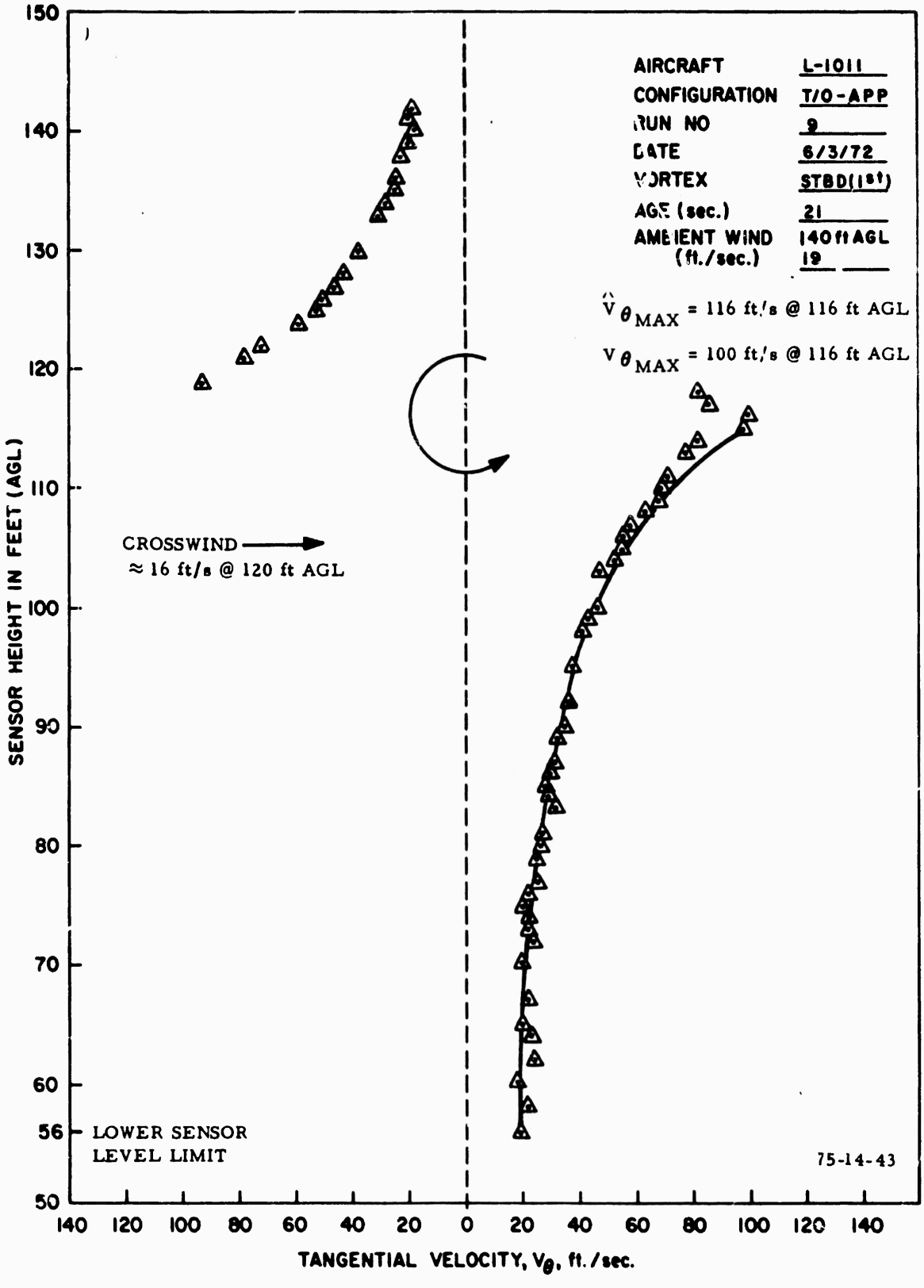

FIGURE 43. L1011 RUN 9, V_θ VERSUS h, TAKEOFF/APPROACH CONFIGURATION, STARBOARD (1st) VORTEX

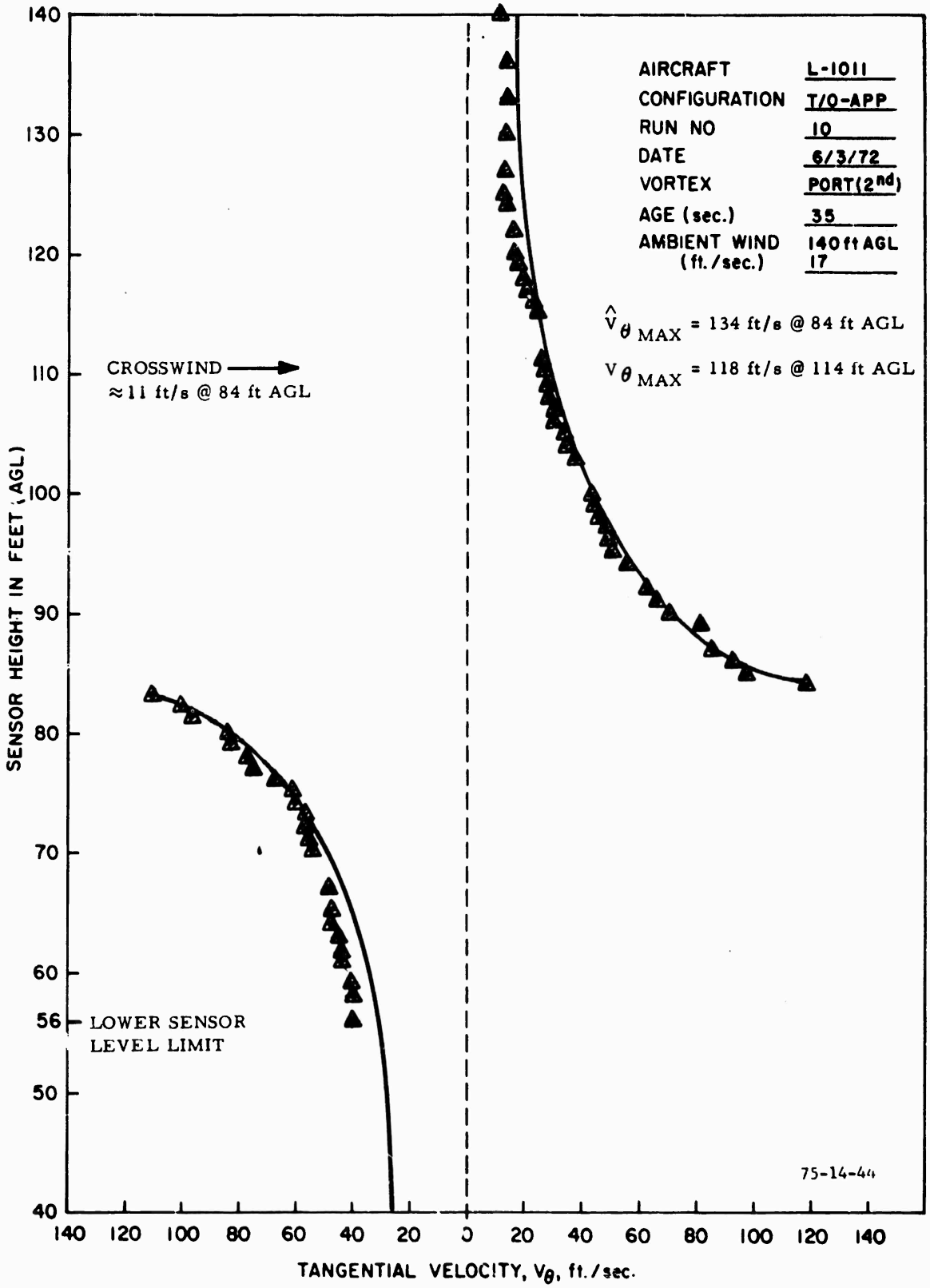

FIGURE 44. L1011 RUN 10, V_θ VERSUS h, TAKEOFF/APPROACH CONFIGURATION VORTEX

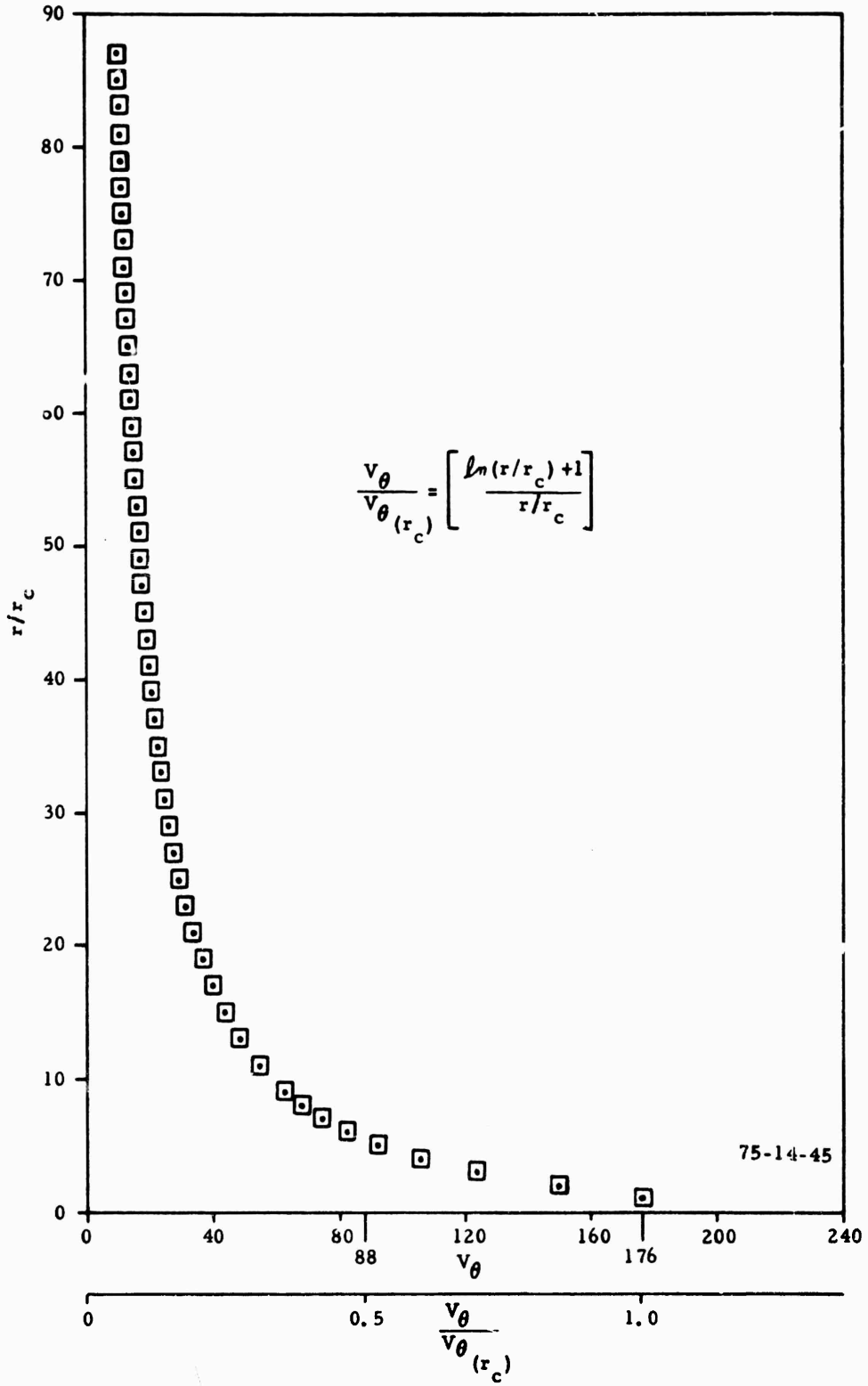

FIGURE 45. DIMENSIONLESS VORTEX VELOCITY DISTRIBUTION

in this report. One can extrapolate the ambient wind data listed in appendix G to the flight test altitude and attempt to calculate the vortex path and velocity.

Primary emphasis was placed on vortex vertical descent calculation, $\dot{Z}_v$, taking into consideration the limitations cited earlier in this report on vortex tower intercept altitude. In addition, it was desired to arrive at an approximate value of vortex transport height above the ground, $K_1 b$, or $K_2 b'$, where K is a constant to be determined.

For the classical assumption of an elliptical loading the sink speed one vortex induces upon another is given by

$$\dot{Z}_v = \frac{\Gamma_o}{2\pi b'} \tag{10}$$

or

$$\dot{Z}_v = \frac{8W}{\pi^3 \rho V b^2} \tag{11}$$

where

$$\Gamma_o = \frac{4}{\pi} \frac{W}{\rho V b} \tag{12}$$

and

$$b' = \frac{\pi}{4} b' \tag{13}$$

However, in reality, the circulation distribution is distorted from the elliptical form due to various modifications of the wing planform, either in the original geometry or as a result of changes in airplane wing configuration during flight operations (i.e., deflection of spoilers, slats, and flaps), either singly or in combination with each other. An example of this can be seen in figure 46 for the L1011 airplane. As a result of this complex change in load distribution, the vortex characteristics and movement vary with a change in airplane configuration. Also of importance is the recent discovery (reference 15), by NASA Flight Research Center, of the unexpected effects the extension of the B747 main landing gear and the change in engine thrust have on the characteristics of the wing vortex system. If either the engine thrust was decreased or the landing gear was extended, the vortex probing pilots found the vortex to persist for a longer period of time. Thus with mutual vortex interaction, one could likewise expect the vortices to descend for a longer period of time.

It should also be evident that vortex descent velocities are not constant and would tend to decrease with vortex age. This was found to be true in the vortex investigation flight tests with the B747 and B707 by Boeing (reference 5), with the C5A and CV990 by NASA-Flight Research Center (reference 4), as well as other flight tests. The descending vortices eventually level off, normally under 2 minutes in age, due to lack of mutual interaction because of vortex dissipation, core linking, breakdown or bursting, atmospheric interaction, or diffusion to insignificant energy levels.

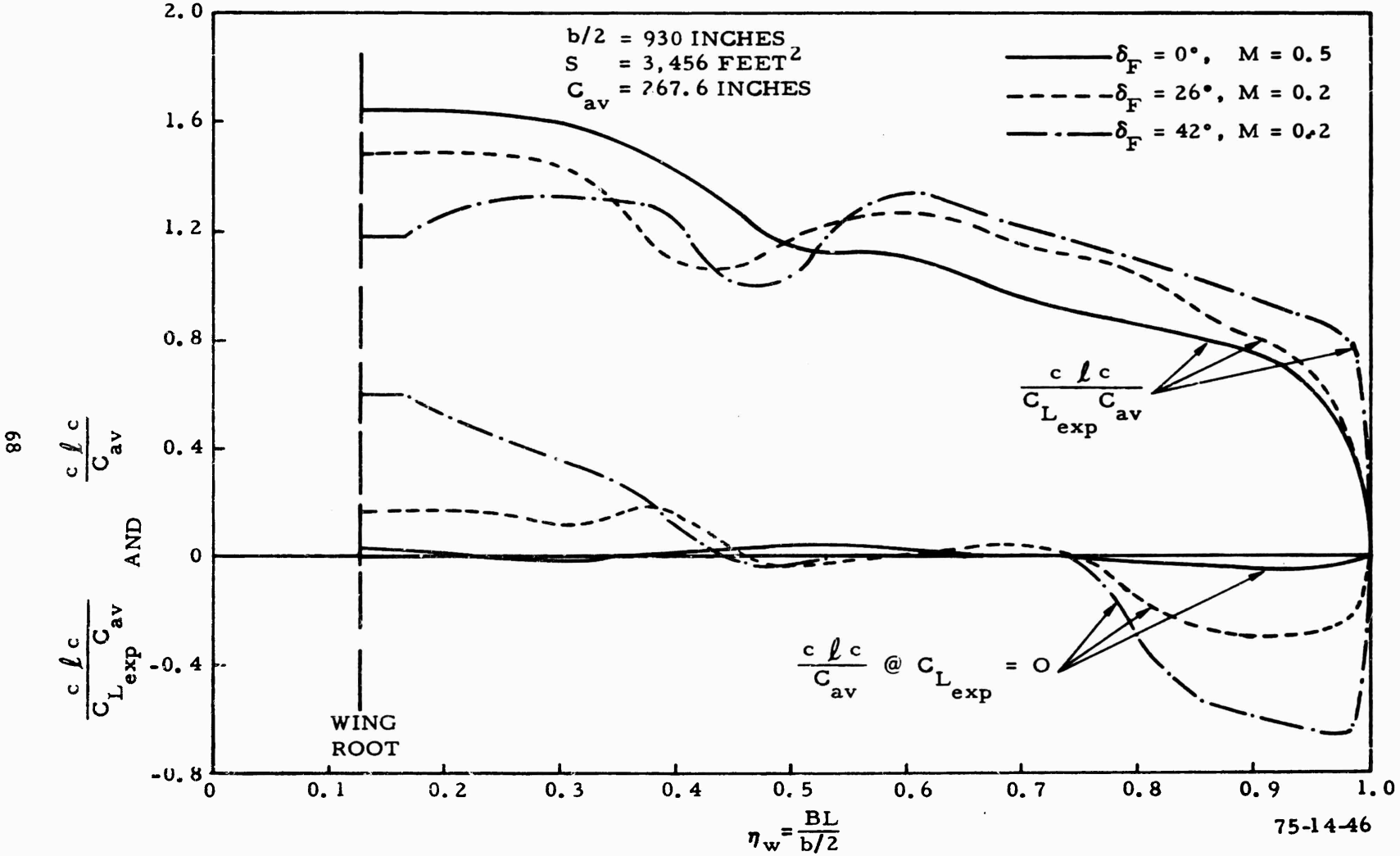

FIGURE 46. L1011 EXPOSED WING BASIC AND ADDITIONAL LIFT DISTRIBUTIONS FOR VARIOUS FLAP SETTINGS

Considering all these effects, one may still obtain some idea of the vortex descent velocity and its altitude AGL of leveling off. Figure 47 is a plot of vortex descent velocity, $\dot{Z}_V$ versus vortex age. From the figure one can readily see that the vortex descent velocity is higher for the landing configuration than for the takeoff or approach configurations. This is to be expected because of the inboard movement of the load distribution with increased flap deflection and, therefore, the decrease in vortex spacing. However, as the vortices come under the influence of ground effect and tend to move apart from each other, the mutually-induced effects would tend to diminish, and concurrently the vortex decrease in velocity. Thus it is not easy to ascertain whether the decrease in $\dot{Z}_V$ is caused by decrease in intensity due to vortex aging, or to proximity to the ground, or to both effects.

Linearly extrapolating the descent velocity data to vortex age of zero seconds leads to an initial $\dot{Z}_V$ of approximately 6.6 ft/s. However, we know, based on previous vortex flow visualization test with our CV880 that there is a finite, although short, time for the vortex sheet to roll up before mutual vortex interaction can occur. Therefore, one would expect a lower initial $\dot{Z}_V$ than 6.6 ft/s. Taking this into consideration, the initial Z_V (not at t=0) is approximately 5.5 - 6.0 ft/s. The theoretical sink speed for an elliptical lift distribution, using equation (11), for L1011 run 4, turns out to be approximately 6.7 ft/s. This compares to 5.3 ft/s for the downwind (first) vortex and 4.6 ft/s. Of course, there is no dissipation term in equation (11).

Figure 48 also provides an indication of the $\dot{Z}_V$ as a function of vortex/test tower intercept altitude. By assuming a decrease of vortex age with an increase in tower intercept height, one can arrive at an estimate of vortex sink speed. However, the greatest benefit of figure 48 is in arriving at the asymptotic path of the vortex lateral transport height above the ground due to ground effect. This tends to be in the vicinity of 65 feet AGL which is approximately the same value predicted by elliptical lift distribution assumptions.

An attempt was made to determine the vortex pair spacing, b', by taking the time interval between the two vortex/tower intercepts and multiplying this by the average wind velocity existing between the two tower intercept levels AGL. However, the vortex spacing, b', turned out to be greater than the wingspan of the L1011, and the scatter was so great that it was impossible to arrive at any conclusive lateral separation distance for the vortex pair. This can be attributed to variation in the wind velocity with time, ground-induced effects on the vortices within the vertical span height of the tower, and possibly, the onset of some sinuous-type oscillation of the vortices with age.

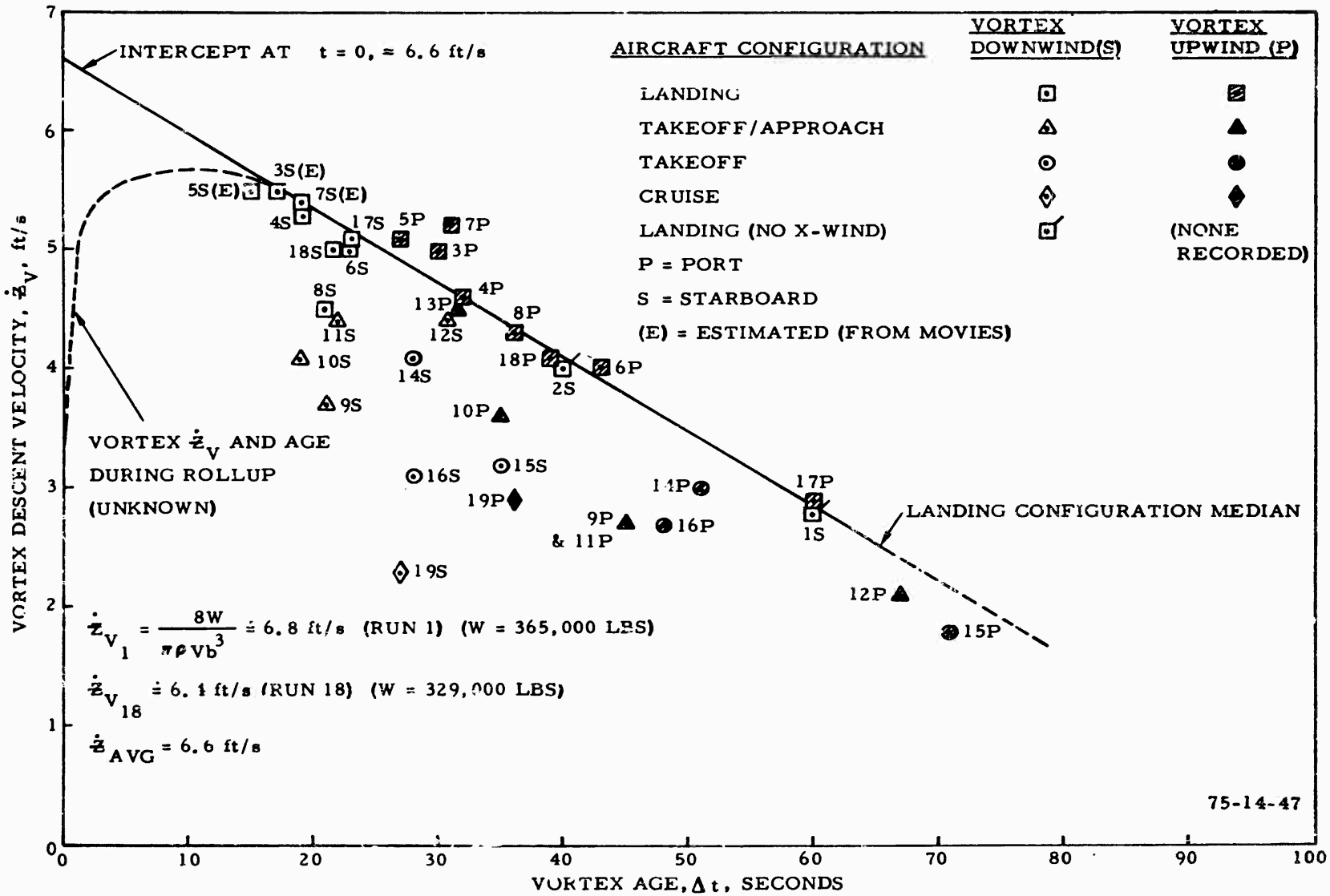

FIGURE 47. L1011 VORTEX DESCENT VELOCITY AS A FUNCTION OF VORTEX AGE; AIRCRAFT ALTITUDE ≤ 253 FT. AGL

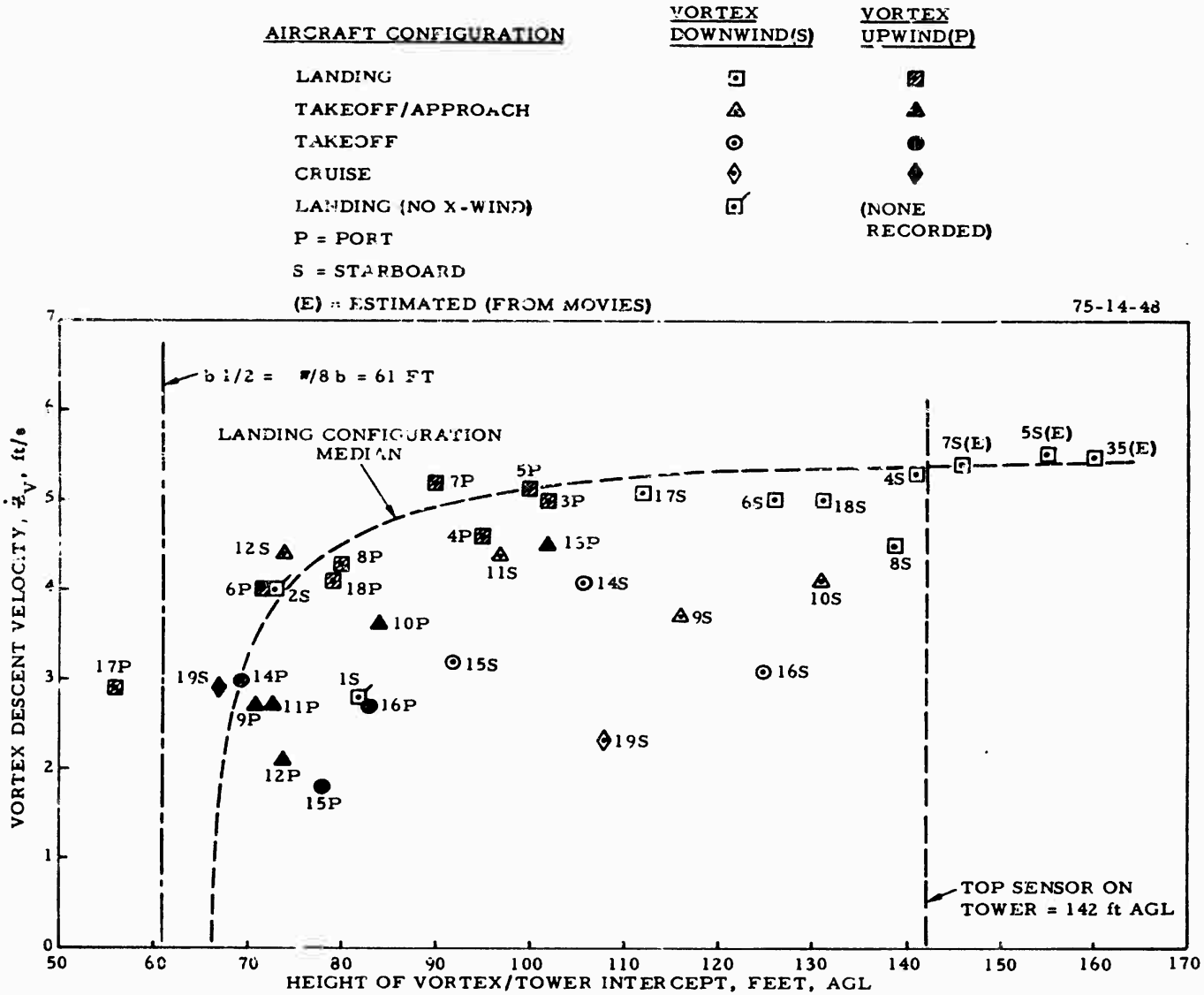

FIGURE 48. L1011 VORTEX DESCENT VELOCITY AS A FUNCTION OF VORTEX/TEST TOWER INTERCEPT HEIGHT

CONCLUSIONS

1. Under crosswind conditions, the upwind vortex of the L1011 airplane was found to be more persistent than the downwind vortex; and for identical vortex ages it was found to be more intense.

2. Peak tangential velocities up to 229 ft/s for takeoff ($10°\delta_f$) configuration, up to 135 ft/s for the takeoff/approach ($22°\delta_f$) configuration, and to 126 ft/s for the landing ($42°\delta_f$) configuration were recorded for the L1011 vortices.

3. The L1011 laminar type vortex flow field exists for less than 2 minutes after generation, as noted visually by observers and by photographic coverage.

4. The L1011 vortex system "core" is approximately 4 to 5 feet in diameter for the landing and approach configuration, and 1 to 2 feet in diameter for the takeoff configuration, $\delta_f=10°$.

5. The field of influence of an L1011 vortex (individual) is approximately 1/3 to 1/2 the wingspan of the L1011 in the landing configuration.

6. The vortex lateral transport height, due to ground effect, was approximately 65 feet above the ground in the landing configuration, which closely approximates that predicted by an elliptical lift distribution, $b' = \frac{\pi b}{4}$

7. The circulation in the vortex varies logarithmically with the radius.

8. The predominant mode of vortex dissipation was found to be vortex breakdown (bursting).

REFERENCES

1. Garodz, Leo J., Measurements of the Vortex Wake Characteristics of the Boeing 747, Lockheed C5A, and Other Aircraft, FAA Data Report, Project No. 177-621-03X, (Special Task No. 1), April 1970.

2. Garodz, Leo J., Investigation of Jet Transport Aircraft Vortex Systems Descending into and Generated in Ground Effect, FAA Data Report, Project No. 504-305-03X, (Special Task No. 2), November 1970.

3. Garodz, Leo J., Investigation of the Relatively Long Time-History Vortex Characteristics of the CV-880 Airplane in Terminal Area - Type Flight Operation, FAA Data Report, Project No. 504-303-03X, (Special Task No. 3), November 1970.

4. Andrews, W. H., Robinson, G. H., and Krier, G. E., Flight Research Center, and Drinkwater III, F. J., Ames Research Center, Flight Test Evaluation of the Wing Vortex Wake Generated by Large, Jet-Transport Aircraft, NASA FWP-18, April 1970.

5. Condit, P. M., Results of the Boeing Wake Turbulence Test Program, Boeing Document Number D6-30851, April 1970.

6. Garodz, Leo J., Miller, N. J., and Lawrence, D., The Measurement of the DC-7 Vortex System Using the Tower Fly-By Technique, FAA/SRDS, FAA-RD-73-141. September 1971.

7. Garodz, Leo J., Lawrence D., and Miller, N. J., The Measurement of the Boeing 747 Trailing Vortex System Using the Tower Fly-By Technique (Tests Sept - Oct 1974), Final Report, Report No. FAA-RD-73-156, June 1974.

8. Zwieback, E. L., Douglas Aircraft Company, Long Beach, California, Trailing Vortices of Jet Transport Aircraft During Takeoff and Landing, AIAA Paper 64-325.

9. Garodz, Leo J., Lawrence D., and Miller, N. J., The Measurement of the Boeing 727 Trailing Vortex System Using the Tower Fly-By Technique , FAA Report No. RD-74-90, August 1974.

10. Sprieter, J. R., and Sacks, A. H., The Rolling Up of the Trailing Vortex Sheet and its Effect on the Downwash Behind Wings, Journal of the Aeronautical Sciences, January 1951.

11. Eisenhuth, J. J., McCormick, B. W., Nelson, R. C., Aero Engineering Associates, State College, Pa, and Garodz, Leo J., FAA, Atlantic City, N.J., Analysis of Experimental Measurements of Trailing Vortex Systems of Large Jet Transport Aircraft.

REFERENCES (continued)

12. Hoffman, E. R. and Joubert, P. N., Turbulent Line Vortices, Journal of Fluid Mechanics, Vol. 16, Pt. 3, pp 395-411, July 1963.

13. McCormick, B. W., Tangler, James L., and Sherrirb, Harold E., Structure of Trailing Vortices, American Institute of Aeronautics and Astronautics, Journal of Aircraft, Volume 5, Number 3, March to June 1968.

14 Garodz, L. J., Lawrence, D., and Miller, N., The Measurement of the McDonnell-Douglas DC-9 Trailing Vortex System Using the Tower Fly-By Technique, FAA Report No. RD 74-179, Nov. 1974.

15. Tymczyszyn, J. J., FAA (Western Region) and Barber, M. R., NASA Flight Research Center, Recent Wake Turbulence Flight Test Programs, Sept 26, 1974, Presented at the 18th Annual Symposium of the Society of Experimental Test Pilots, Beverly Hills, California.

APPENDIX A

WIND TUNNEL CALIBRATION OF THERMO SYSTEMS, INC. (TSI), HOT-FILM ANEMOMETER

PURPOSE.

The purpose of the wind tunnel testing was to verify the hot-film sensor calibrations and also to determine the effects of interference associated with the tower installation.

TEST SETUP. The one-dimensional hot-film sensor Thermo Systems, Inc. (TSI), probe model 1210-60 was mounted in the NAFEC low-turbulence wind tunnel. This tunnel has a test section of 20 by 28 inches and is capable of speeds from 4 feet per second (ft/s) through 250 ft/s. To determine installation interference, four series of tests were performed as follows:

1. Standard Airspeed Calibration. Hot-film axis aligned perpendicular to freestream velocity with probe support downstream (ψ = zero degrees). This test simulates ideal conditions with a minimum of probe/support installation interference.

2. Downstream Calibration. Hot-film axis aligned perpendicular to freestream with probe support upstream (ψ =180 degrees). This test simulates measurements when flight testing was performed in such a flightpath as to cause the vortex to pass through the tower (figure A-1) prior to intercepting the sensor, or when the vortex tangential velocity flow field encompasses part of support hardware (figure A-2).

3. Installation Calibration. Hot-film axis aligned perpendicular to freestream with probe support upstream (ψ =180 degrees) mounted on a 1-inch vertical support rod, figure A-2, on tower. This test most closely simulates actual tower installation and effects when vortex drifts through tower.

4. Yaw Calibration. Angle, ψ between axis of film and freestream is varied from zero through 180 degrees (variable ψ). This test reveals effects of vortex axial flow on calibration.

TEST RESULTS. The results of the calibration may be found in figure A-3 which is the output voltage on the anemometer system (from a TSI model 1080 modified) for various values of wind tunnel velocity. The standard calibration (test 1) was found to agree very closely with the curves obtained during hundreds of calibrations on the vortex tower sensors. Since the hot-film sensing phenomenon is associated with heat transfer, the calibration is seen to be nonlinear. Also shown on figure A-3 are the results of tests 2 and 3 showing reduction in velocity (or reduction in voltage) due to installation interference. It can be seen that the velocity could be reading as much as 40 percent lower than the actual velocity. The addition of the support rod (test 3) adds an additional few percent to the low reading.

The results of the yaw angle calibration (test 4) may be found in figure A-4. The wind tunnel velocity was set at 22 ft/s. The hot-film output indicated 21.6 ft/s at this setting (ψ =zero). The yaw angle was varied and the output is as shown in figure A-4. The minimum output was obtained with the sensor aligned almost parallel to the wind (9.3 ft/s).

The output continued to increase, but at 180-degree position, a decrease in speed was noted caused by sensor probe interference.

SUMMARY OF TEST RESULTS.

1. Vortex flow through the probe support hardware could cause a reduction in recorded velocity (by as much as 40 percent).

2. Axial flow in the vortex causes the sensor to read indicated tangential velocity; i.e., if calm winds were present during testing and a vortex intercepted the sensor, zero velocity might not be achieved due to false reading of axial flow.

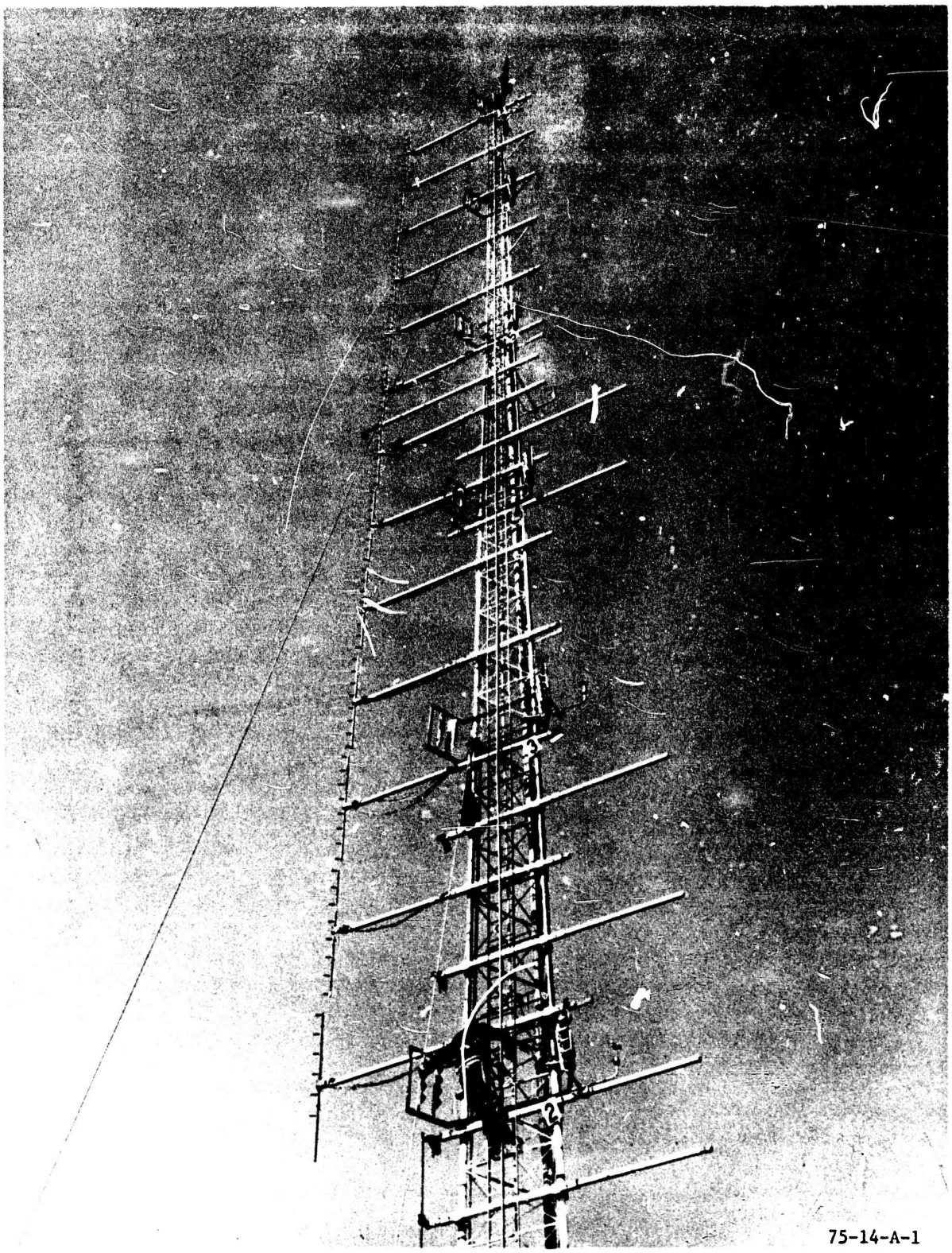

FIGURE A-1. VIEW OF TOWER SHOWING AIRFLOW SENSORS AND GRENADE RACKS.

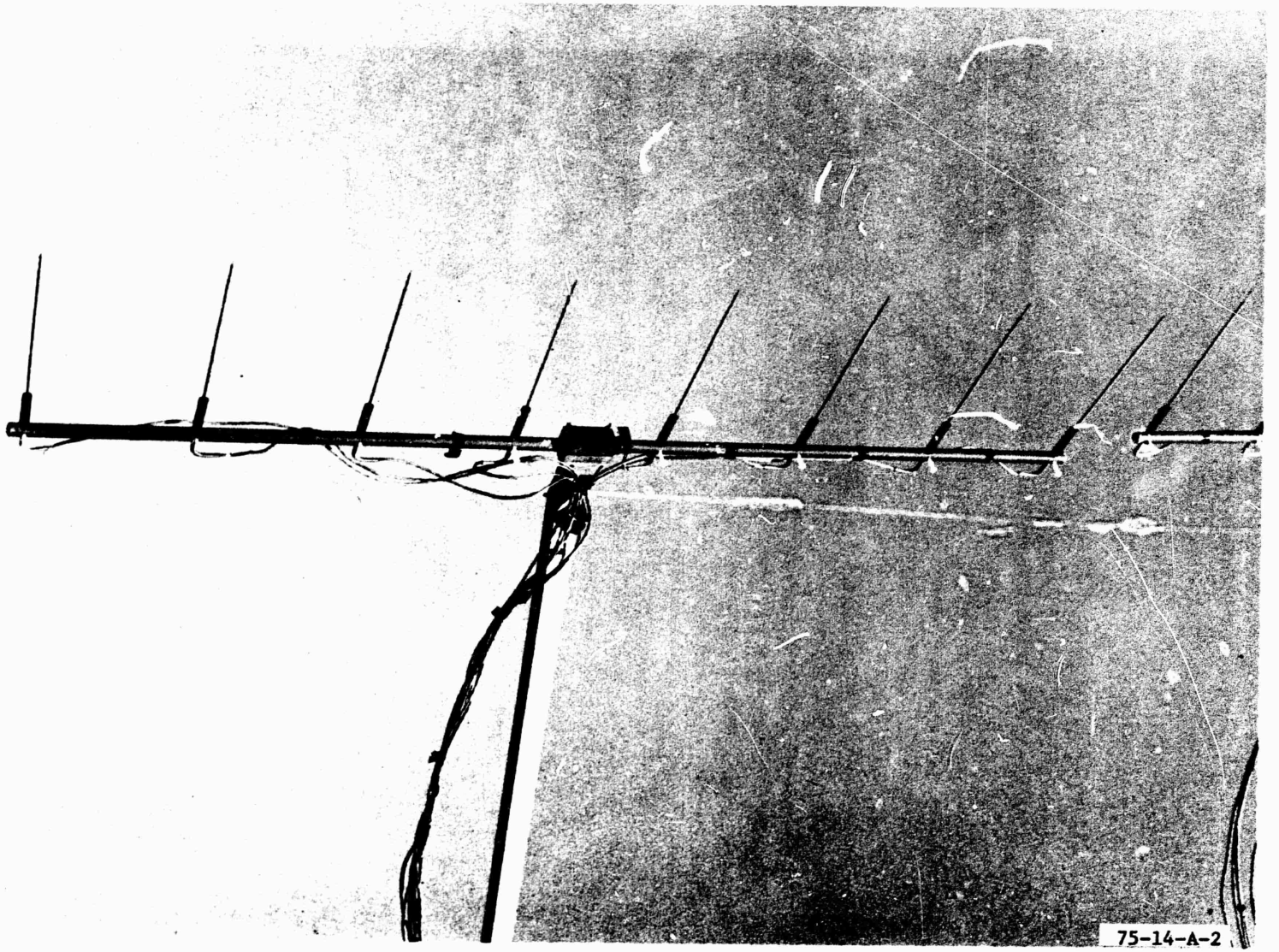

FIGURE A-2. CLOSE-UP VIEW OF AIRFLOW SENSORS.

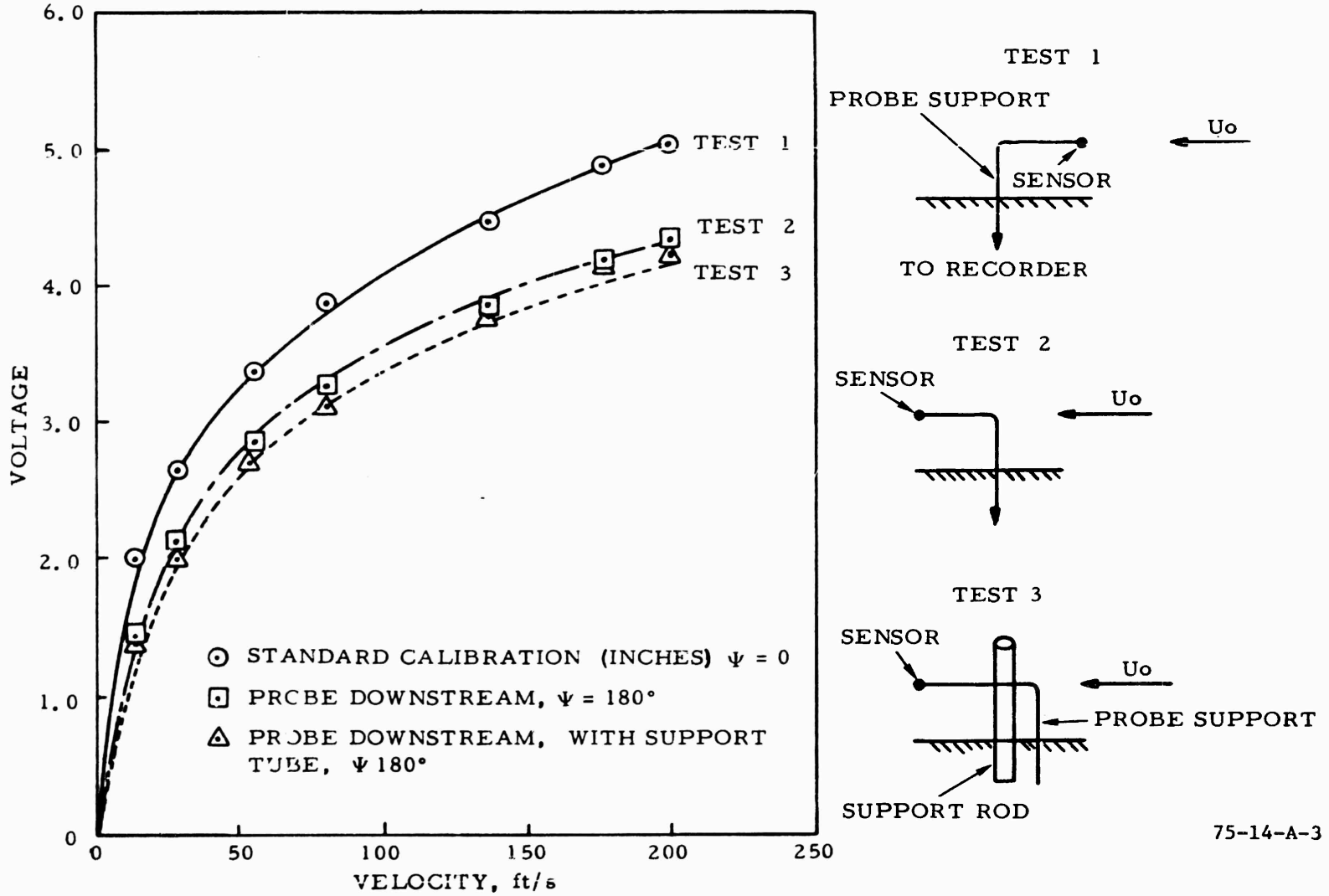

FIGURE A-3. TYPICAL VELOCITY CALIBRATION CURVE FOR A HOT-FILM SENSOR 6 MILS IN DIAMETER IN AN AIRSTREAM (TSI PROBE, MODEL 1210)

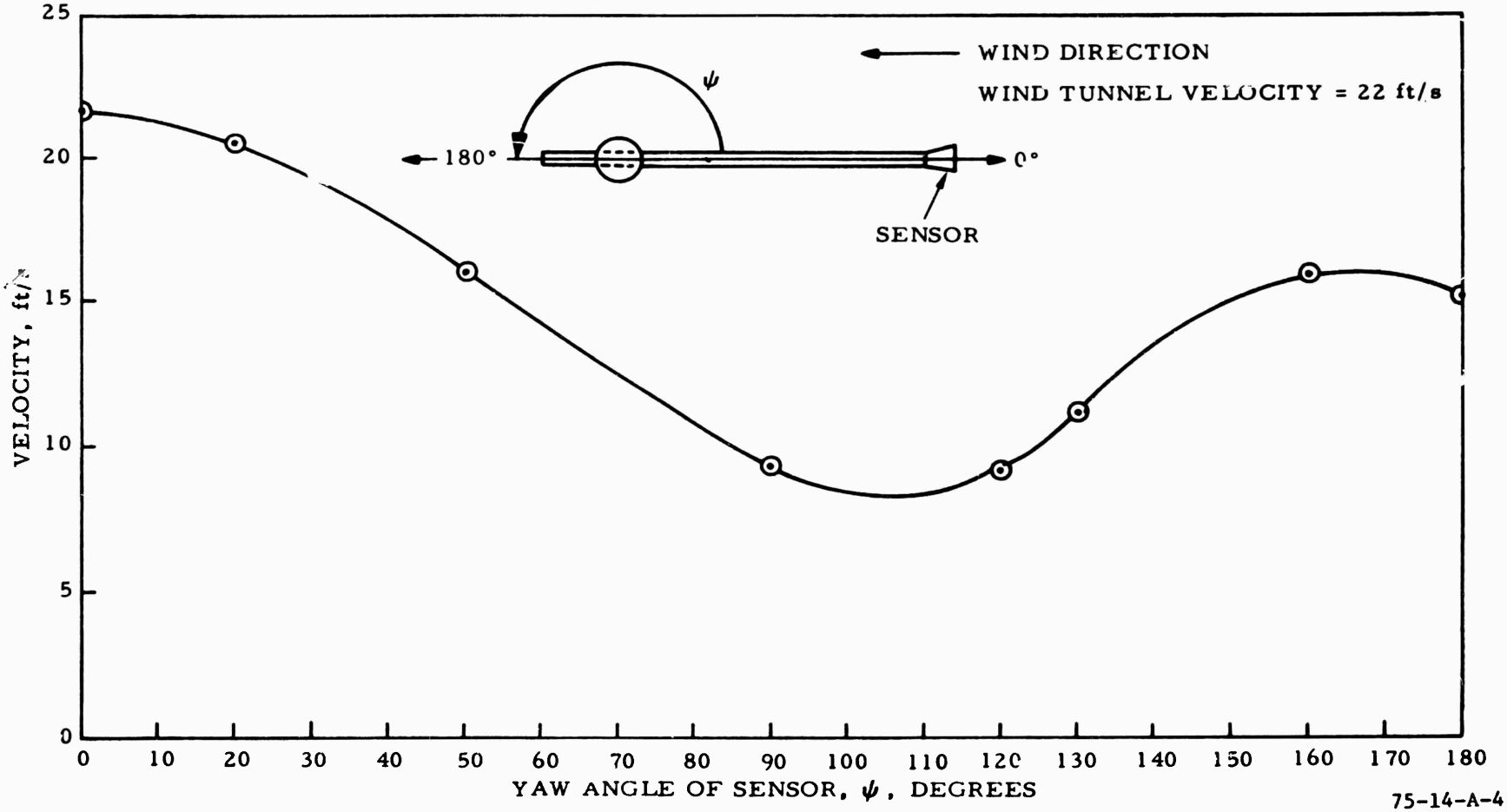

FIGURE A-4. VARIATION OF SENSED AIR VELOCITY WITH YAW ANGLE OF TSI HOT-FILM PROBE MODEL 1210 (WIND-TUNNEL VELOCITY = 22 FT/S)

APPENDIX B

SELECT VORTEX TANGENTIAL VELOCITY VERSUS TIME PLOTS

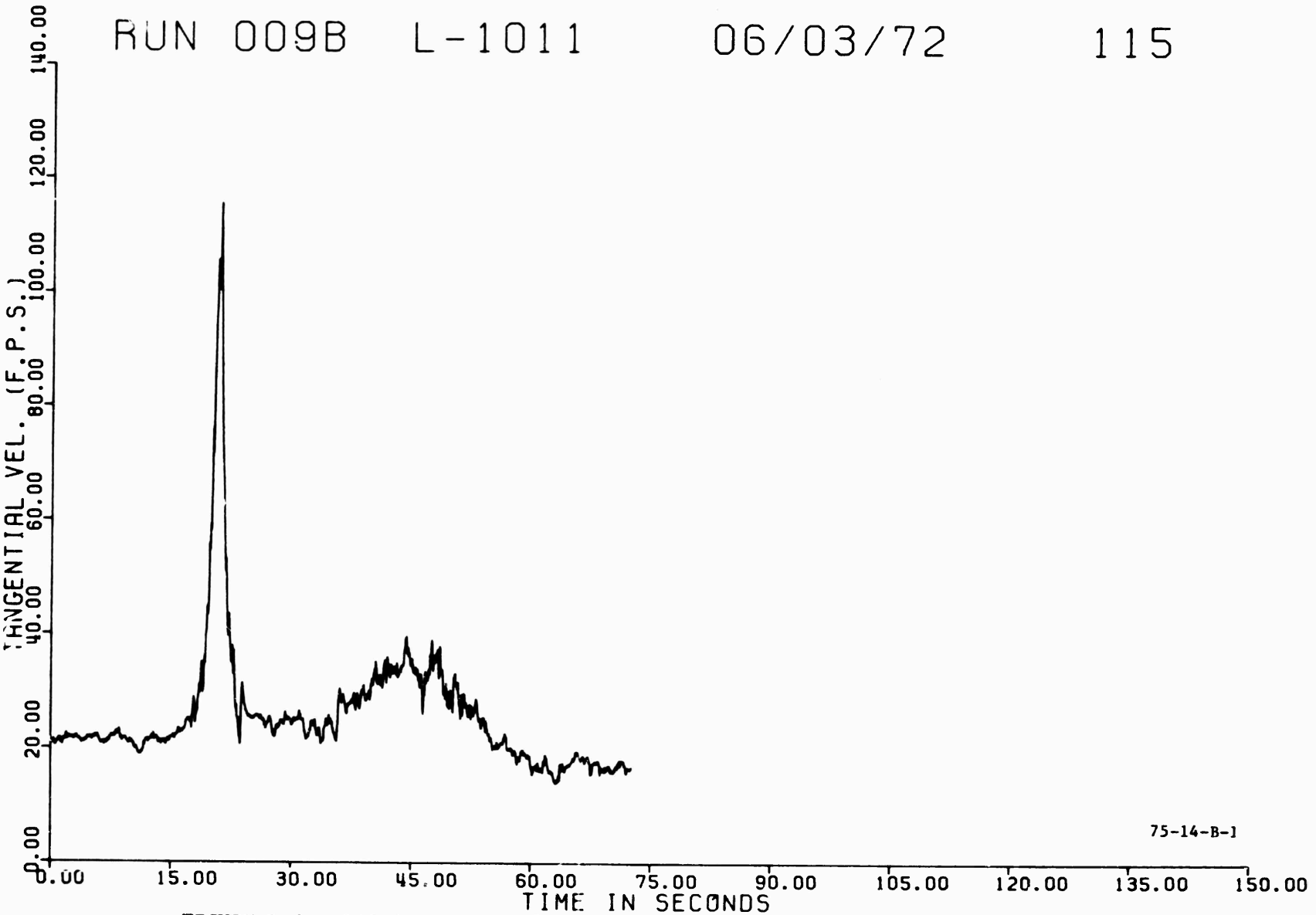

FIGURE B-1. L1011 RUN 9, APPROACH CONFIGURATION, STARBOARD (DOWNWIND) WING VORTEX TANGENTIAL VELOCITY TIME HISTORY AT 115 FEET AGL, VORTEX AGE 21 SECONDS

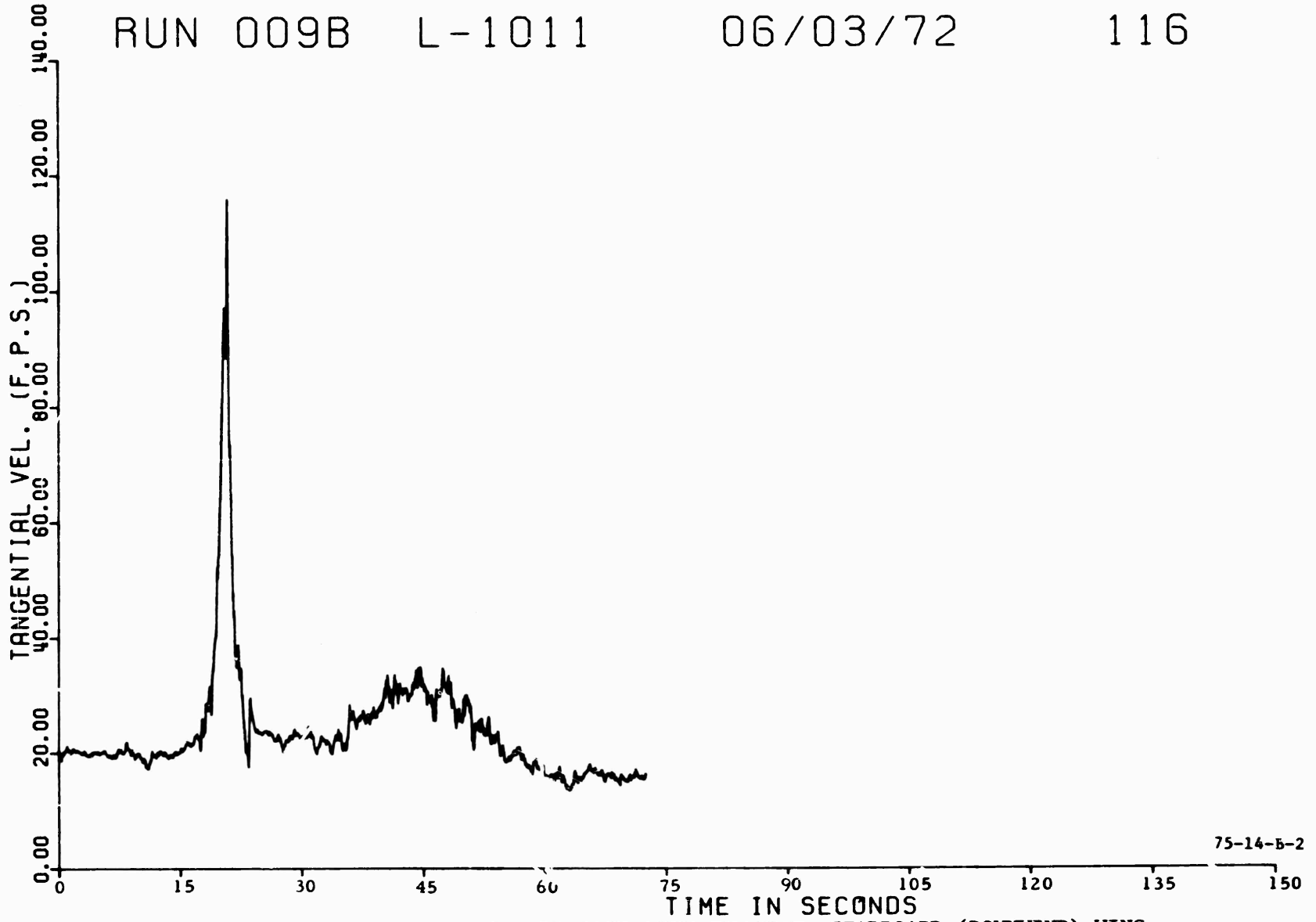

FIGURE B-2. L1011 RUN 9, APPROACH CONFIGURATION, STARBOARD (DOWNWIND) WING VORTEX TANGENTIAL VELOCITY TIME HISTORY AT 116 FEET AGL, VORTEX AGE 21 SECONDS

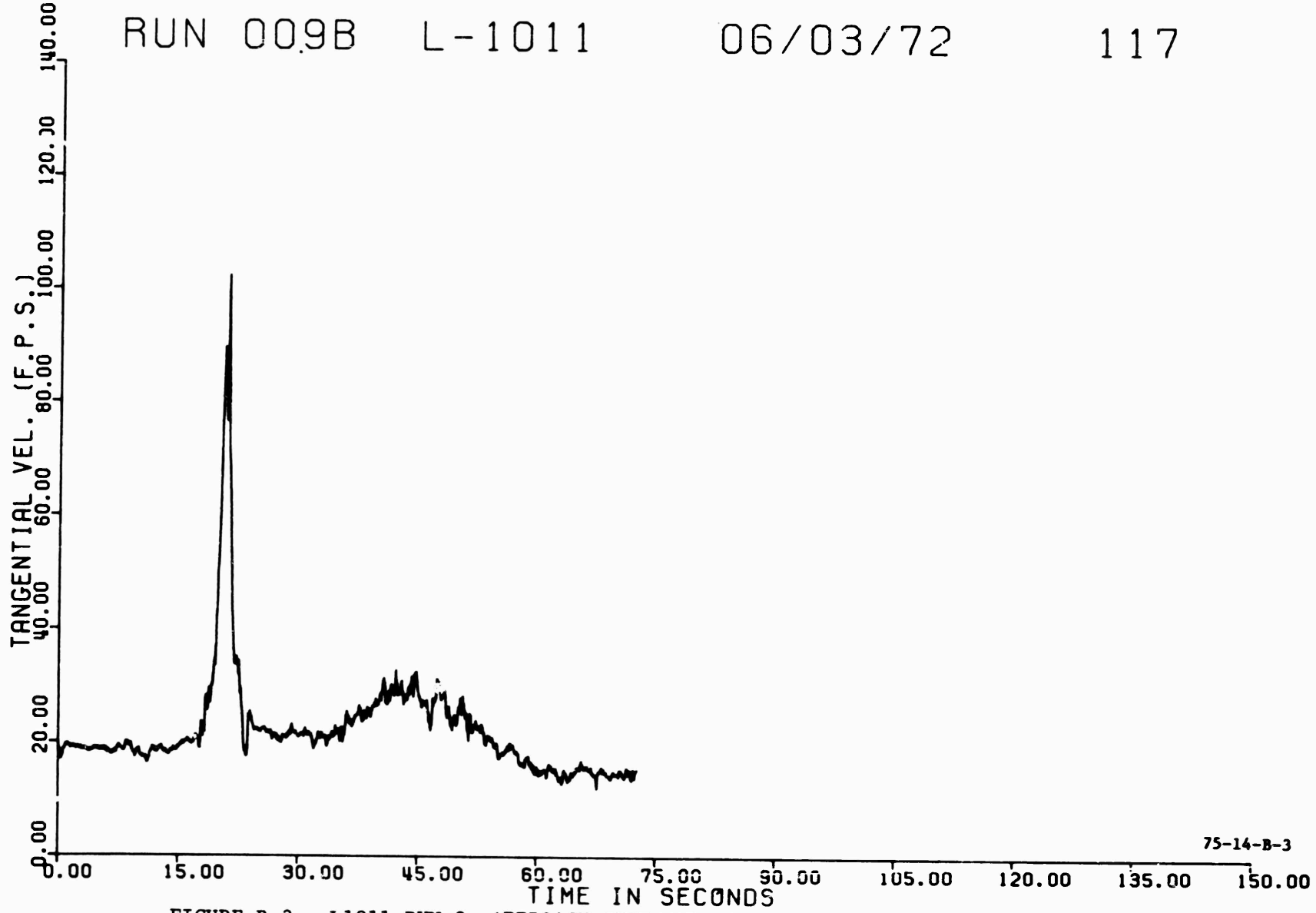

FIGURE B-3. L1011 RUN 9, APPROACH CONFIGURATION, STARBOARD WING (DOWNWIND) VORTEX TANGENTIAL VELOCITY TIME HISTORY AT 117 FEET AGL, VORTEX AGE 21 SECONDS

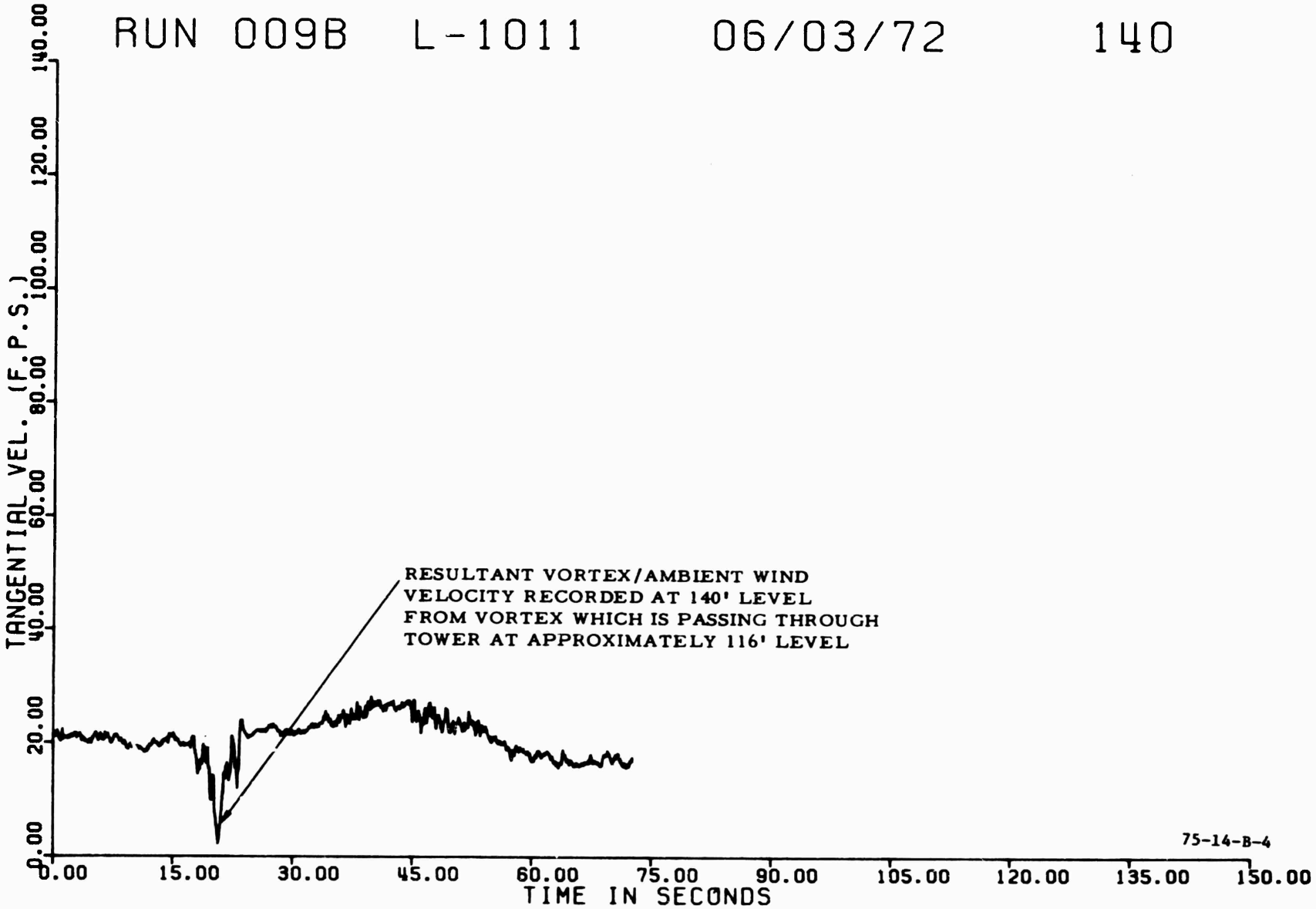

FIGURE B-4. L1011 RUN 9, APPROACH CONFIGURATION, STARBOARD WING (DOWNWIND) VORTEX TANGENTIAL VELOCITY TIME HISTORY AT 140 FEET AGL

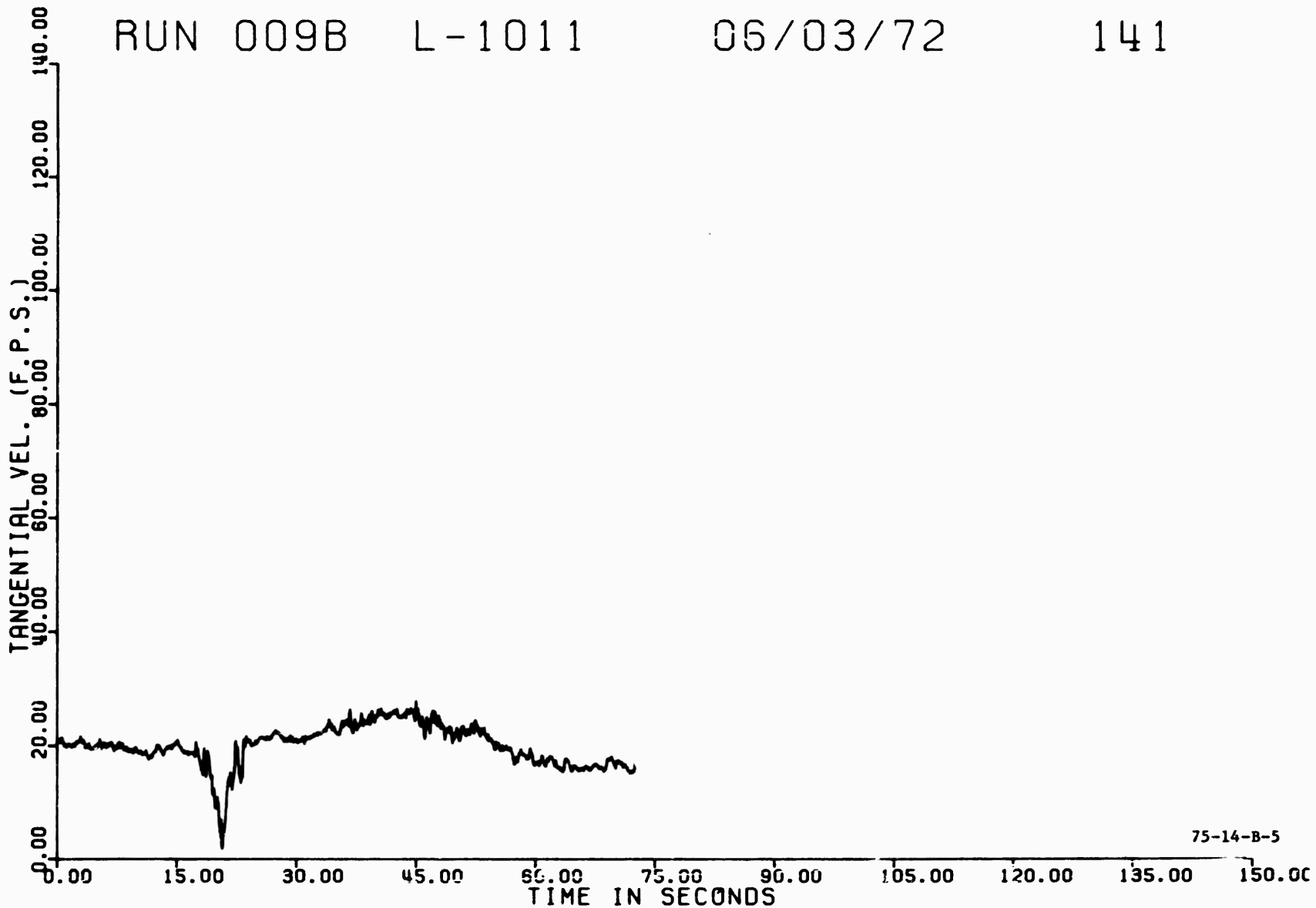

FIGURE B-5. L1011 RUN 9, APPROACH CONFIGURATION, STARBOARD WING (DOWNWIND) VORTEX TANGENTIAL VELOCITY TIME HISTORY AT 141 FEET AGL

FIGURE B-6. L1011 RUN 9, APPROACH CONFIGURATION, STARBOARD WING (DOWNWIND) VORTEX TANGENTIAL VELOCITY TIME HISTORY AT 142 FEET AGL

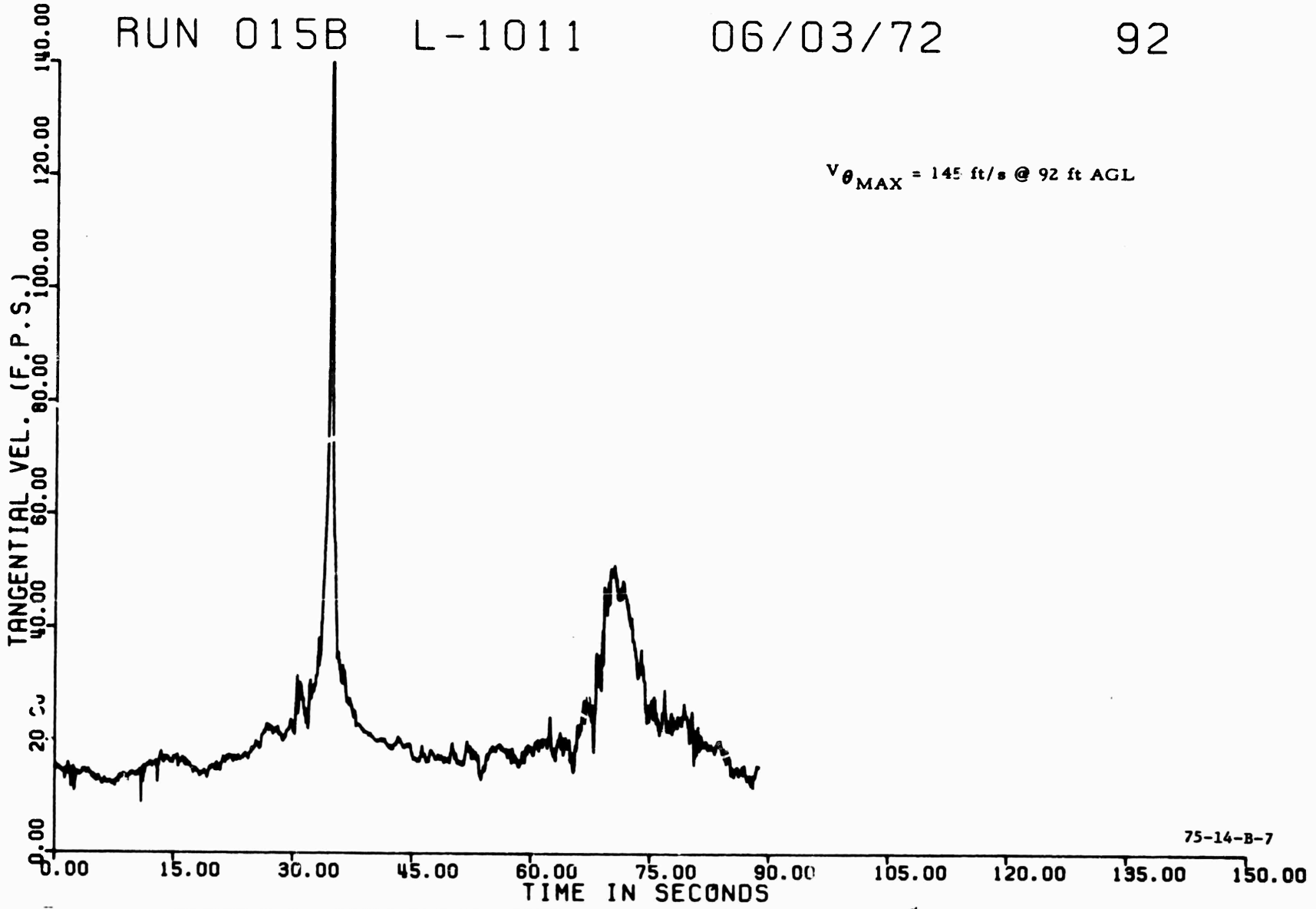

FIGURE B-7. L1011 RUN 15, TAKEOFF CONFIGURATION, STARBOARD WING (DOWNWIND) VORTEX TANGENTIAL VELOCITY TIME HISTORY AT 92 FEET AGL, VORTEX AGE 35 SECONDS

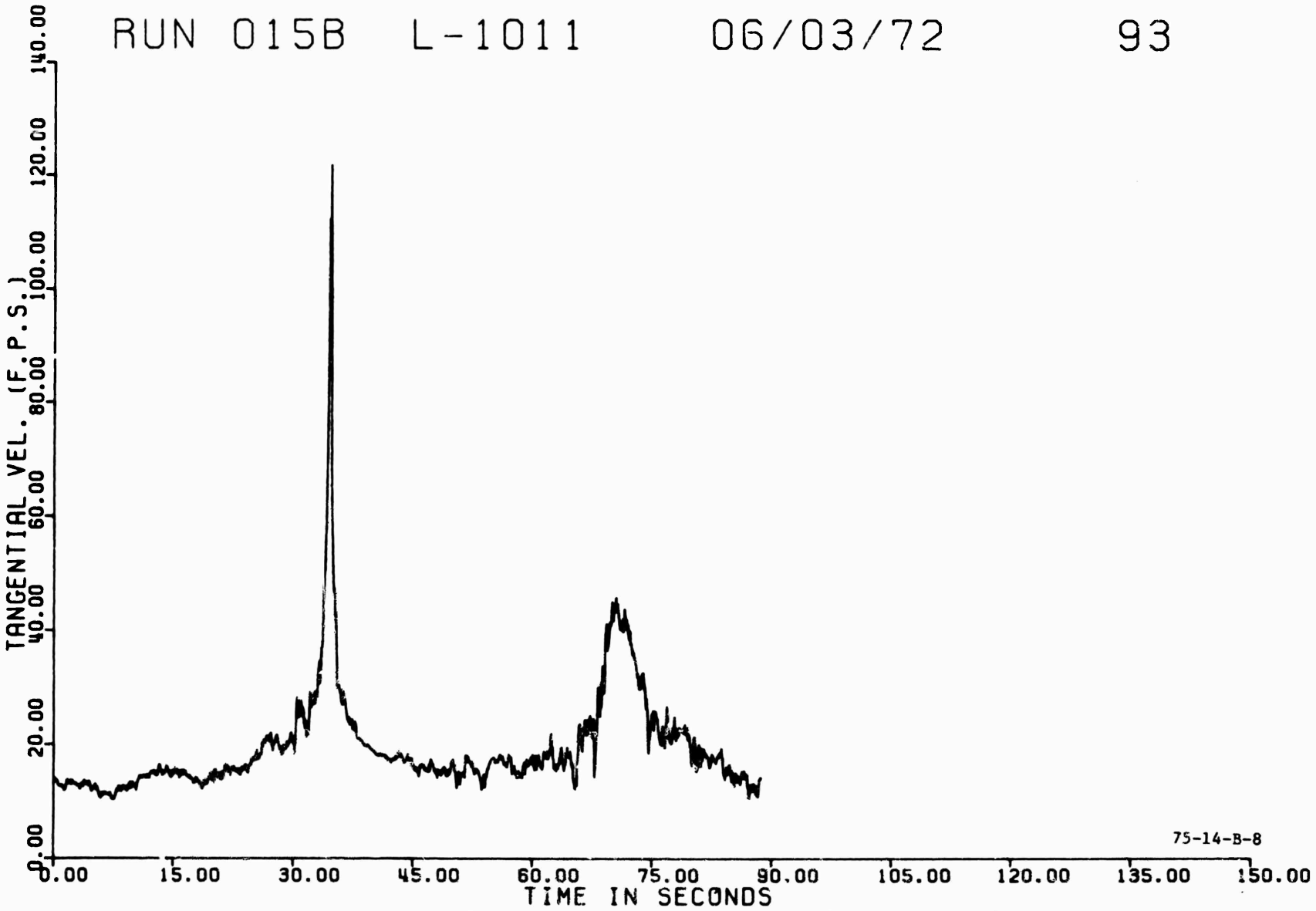

FIGURE B-8. L1011 RUN 15, TAKEOFF CONFIGURATION, STARBOARD WING (DOWNWIND) VORTEX TANGENTIAL VELOCITY TIME HISTORY AT 93 FEET AGL, VORTEX AGE 35 SECONDS

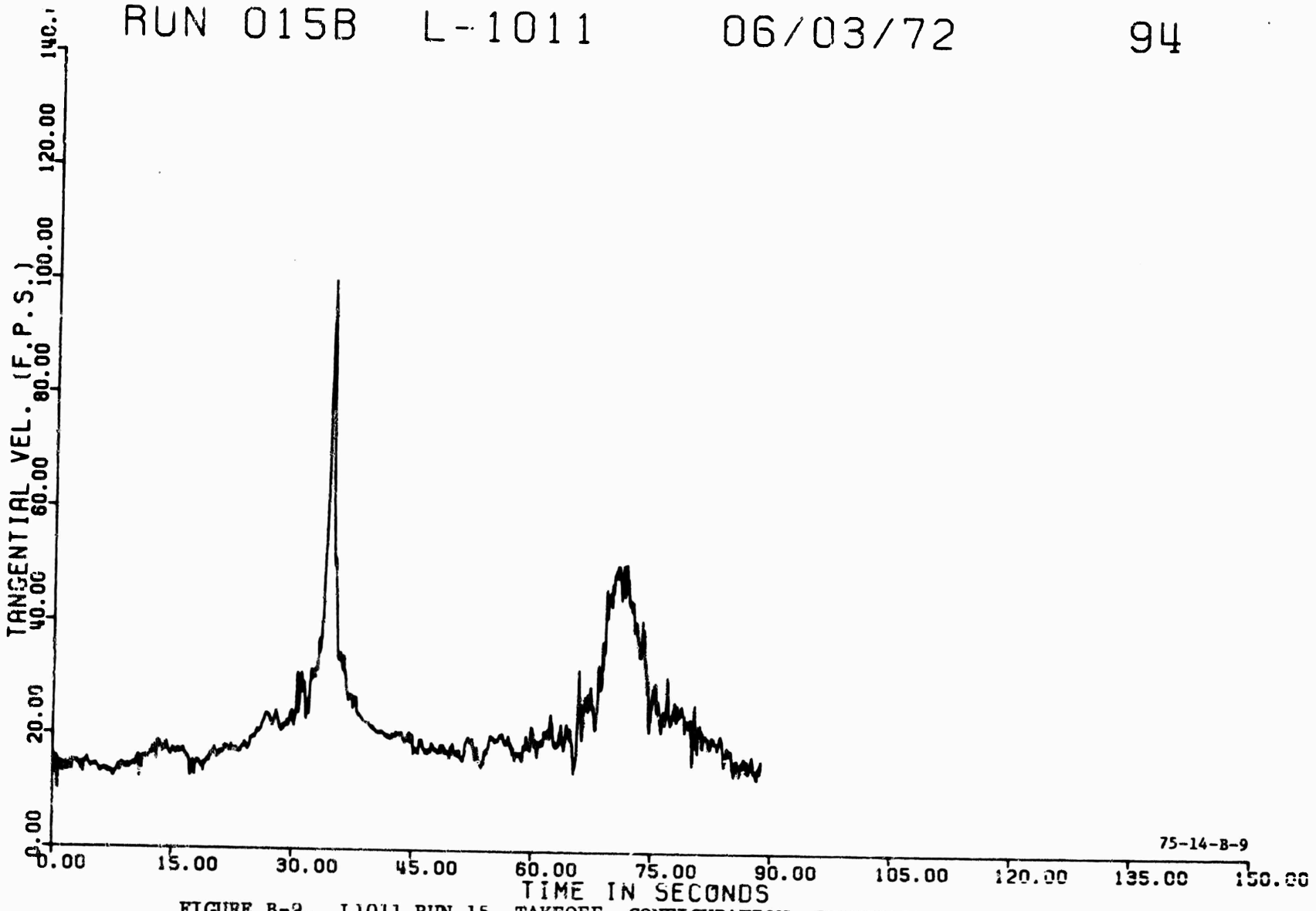

FIGURE B-9. L1011 RUN 15, TAKEOFF CONFIGURATION, STARBOARD WING (DOWNWIND) VORTEX TANGENTIAL VELOCITY TIME HISTORY AT 94 FEET AGL, VORTEX AGE 35 SECONDS

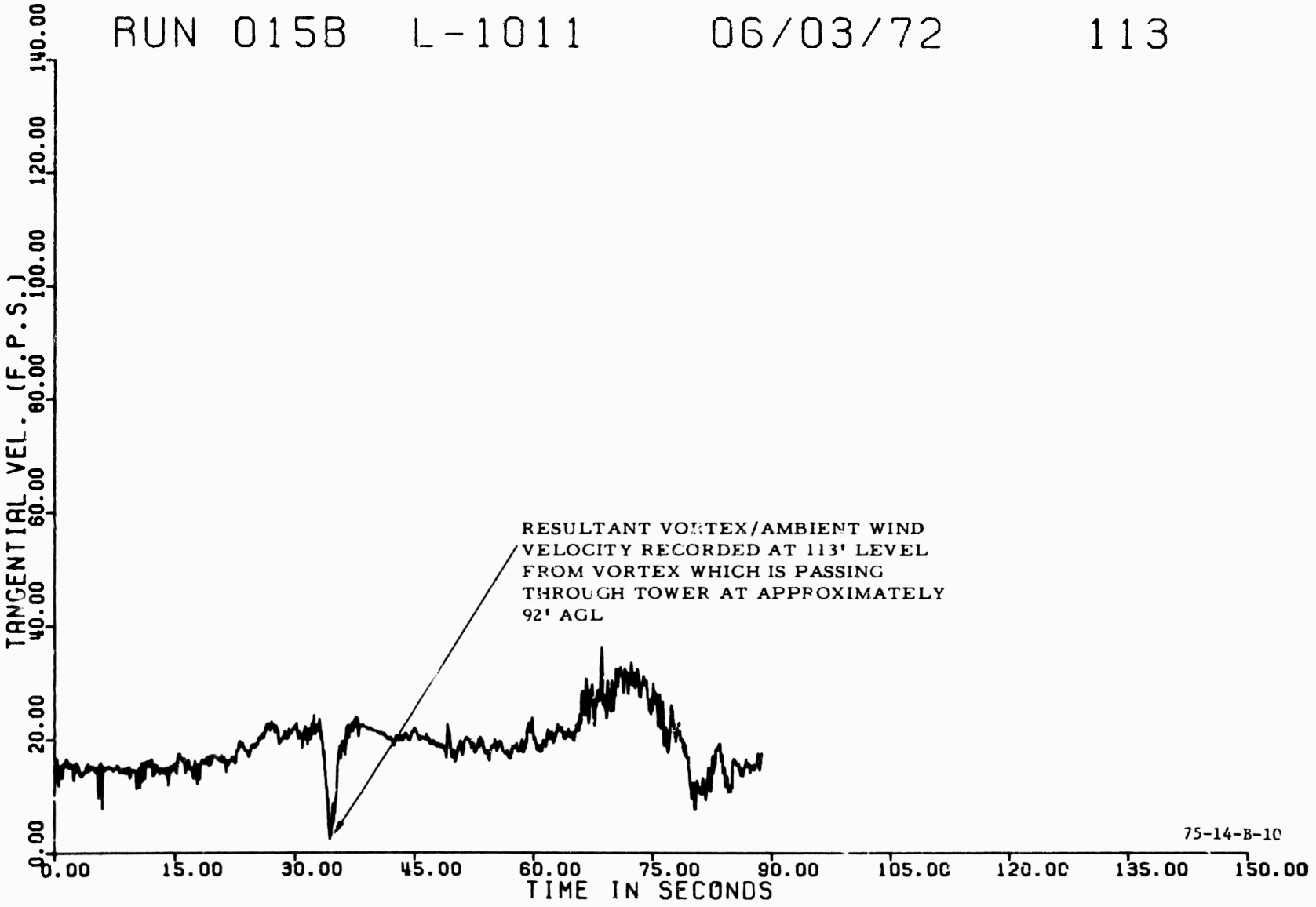

FIGURE B-10. L1011 RUN 15, TAKEOFF CONFIGURATION, STARBOARD WING (DOWNWIND) VORTEX TANGENTIAL VELOCITY TIME HISTORY AT 113 FEET AGL, VORTEX AGE 35 SECONDS

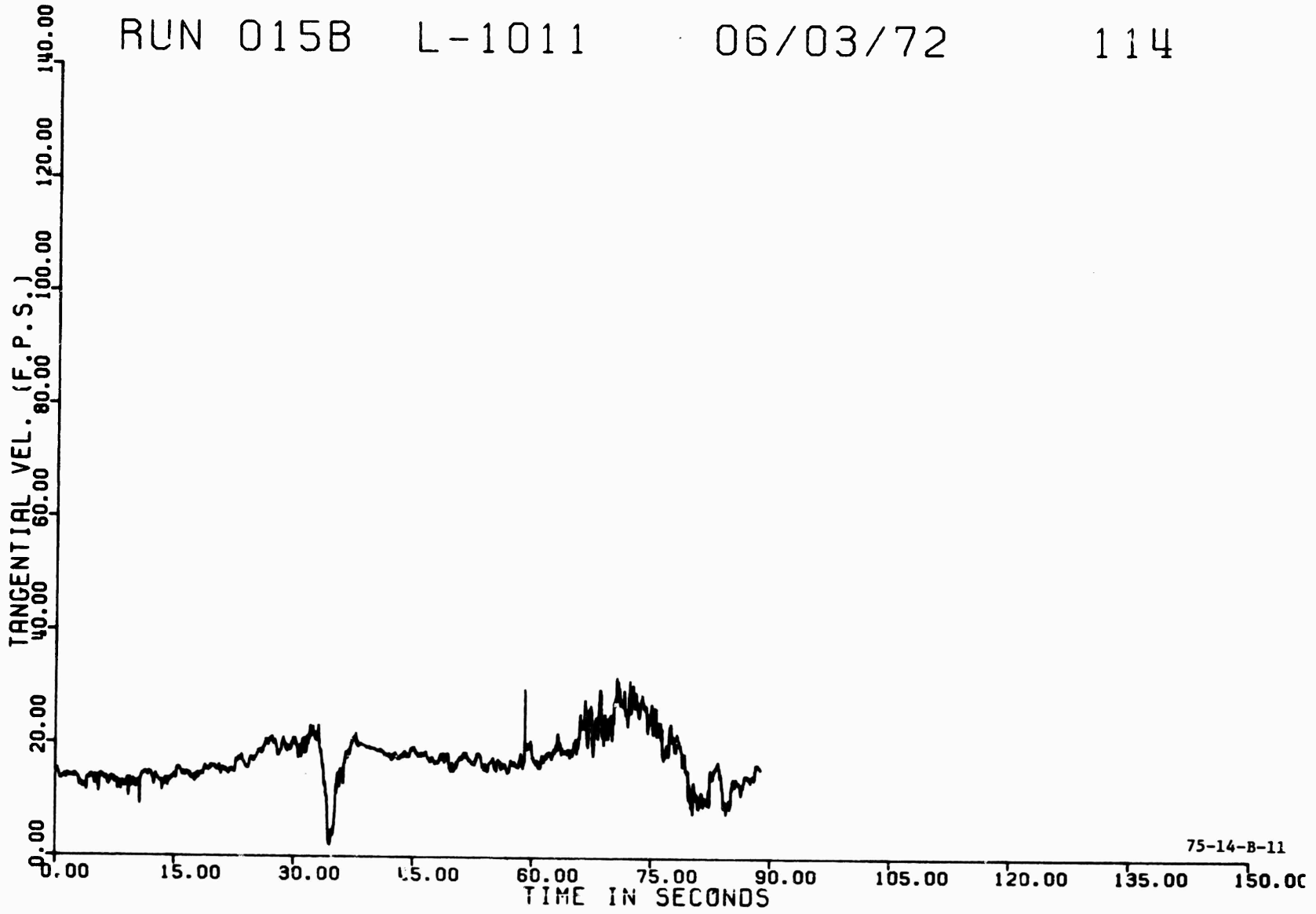

FIGURE B-11. L1011 RUN 15, TAKEOFF CONFIGURATION, STARBOARD WING (DOWNWIND) VORTEX TANGENTIAL VELOCITY TIME HISTORY AT 114 FEET AGL, VORTEX AGE 35 SECONDS

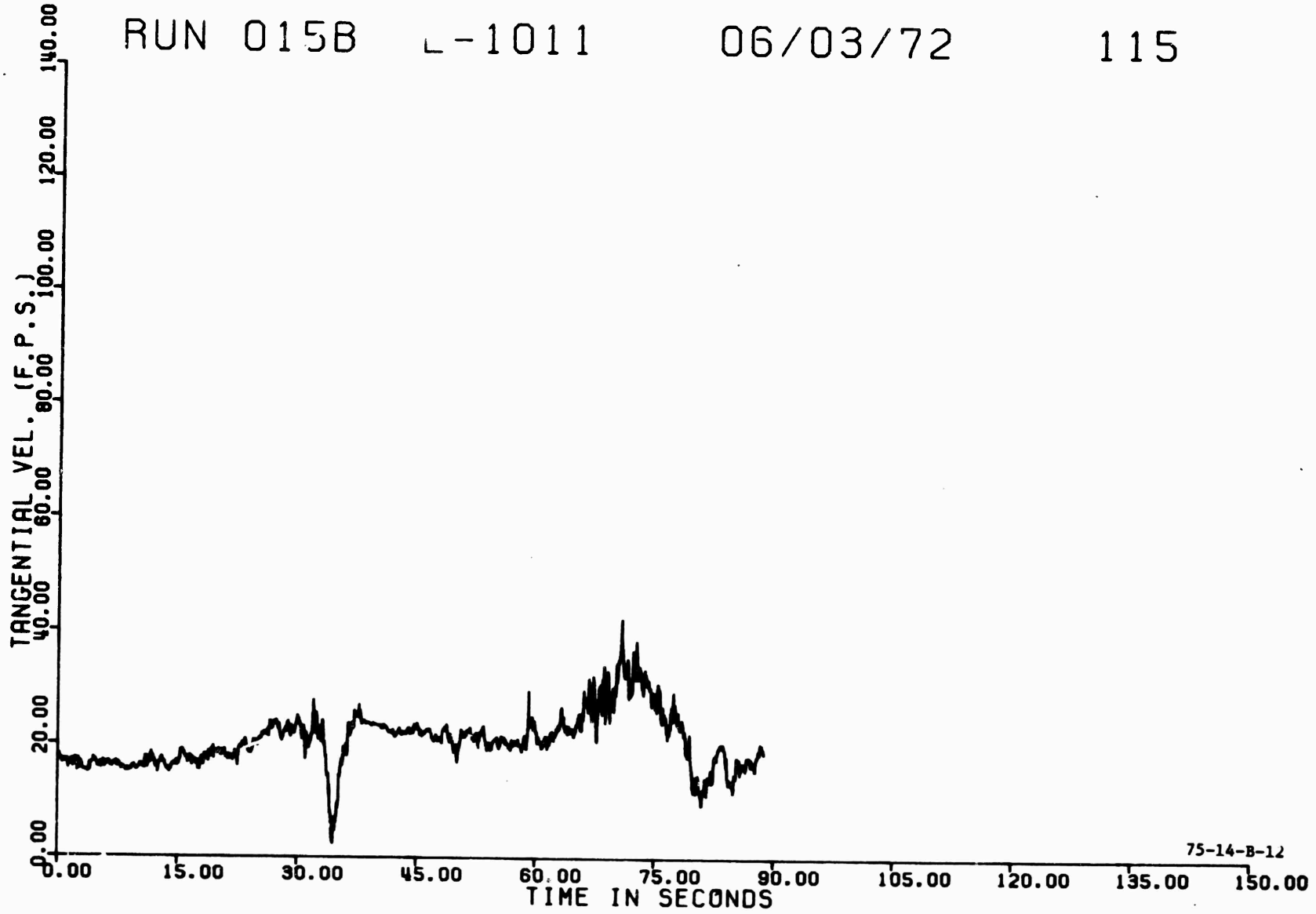

FIGURE B-12. L1011 RUN 15, TAKEOFF CONFIGURATION, STARBOARD WING (DOWNWIND) VORTEX TANGENTIAL VELOCITY TIME HISTORY AT 115 FEET AGL, VORTEX AGE 35 SECONDS

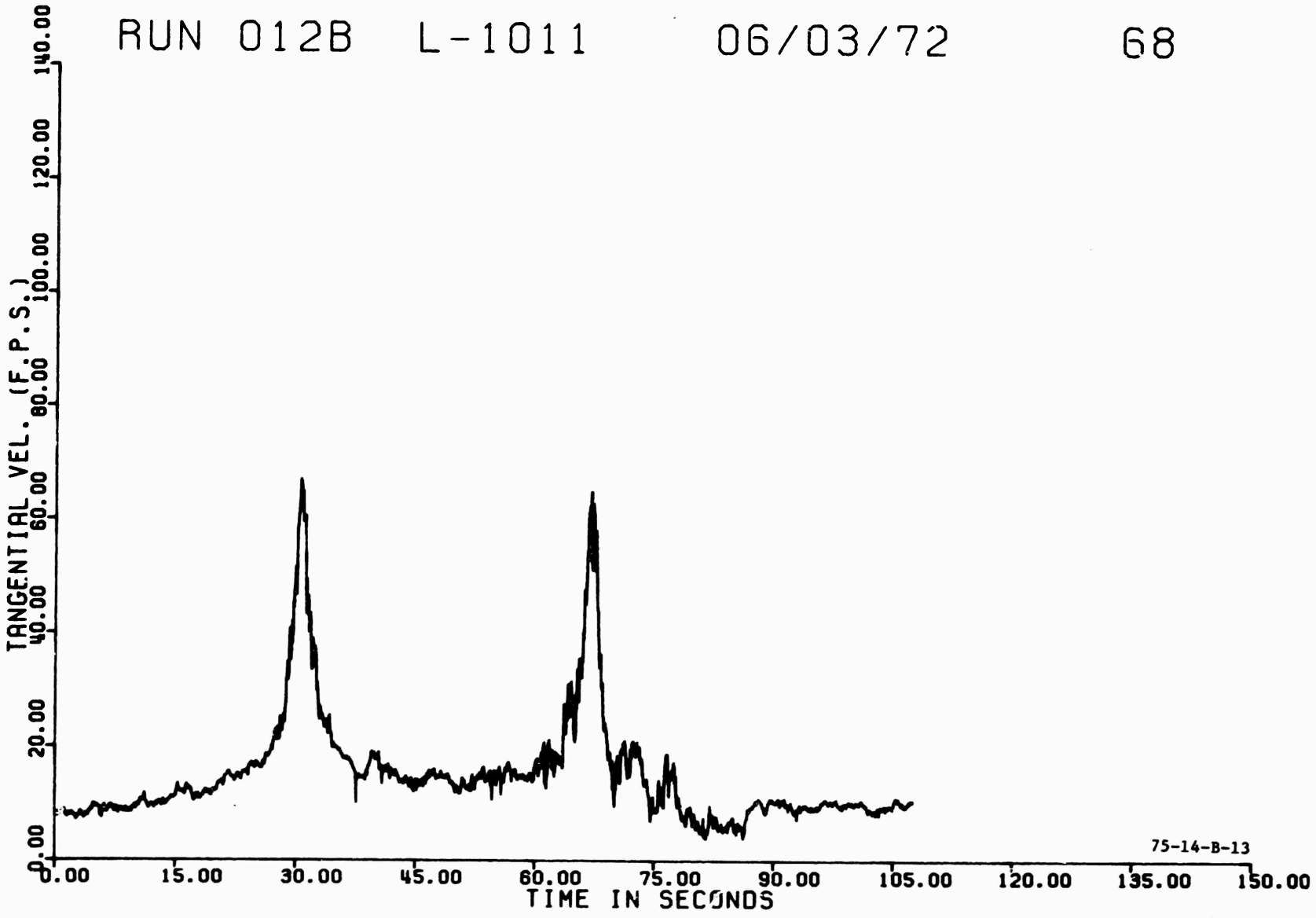

FIGURE B-13. L1011 RUN 12, TAKEOFF CONFIGURATION, STARBOARD WING (DOWNWIND) VORTEX TANGENTIAL VELOCITY TIME HISTORY AT 68 FEET AGL

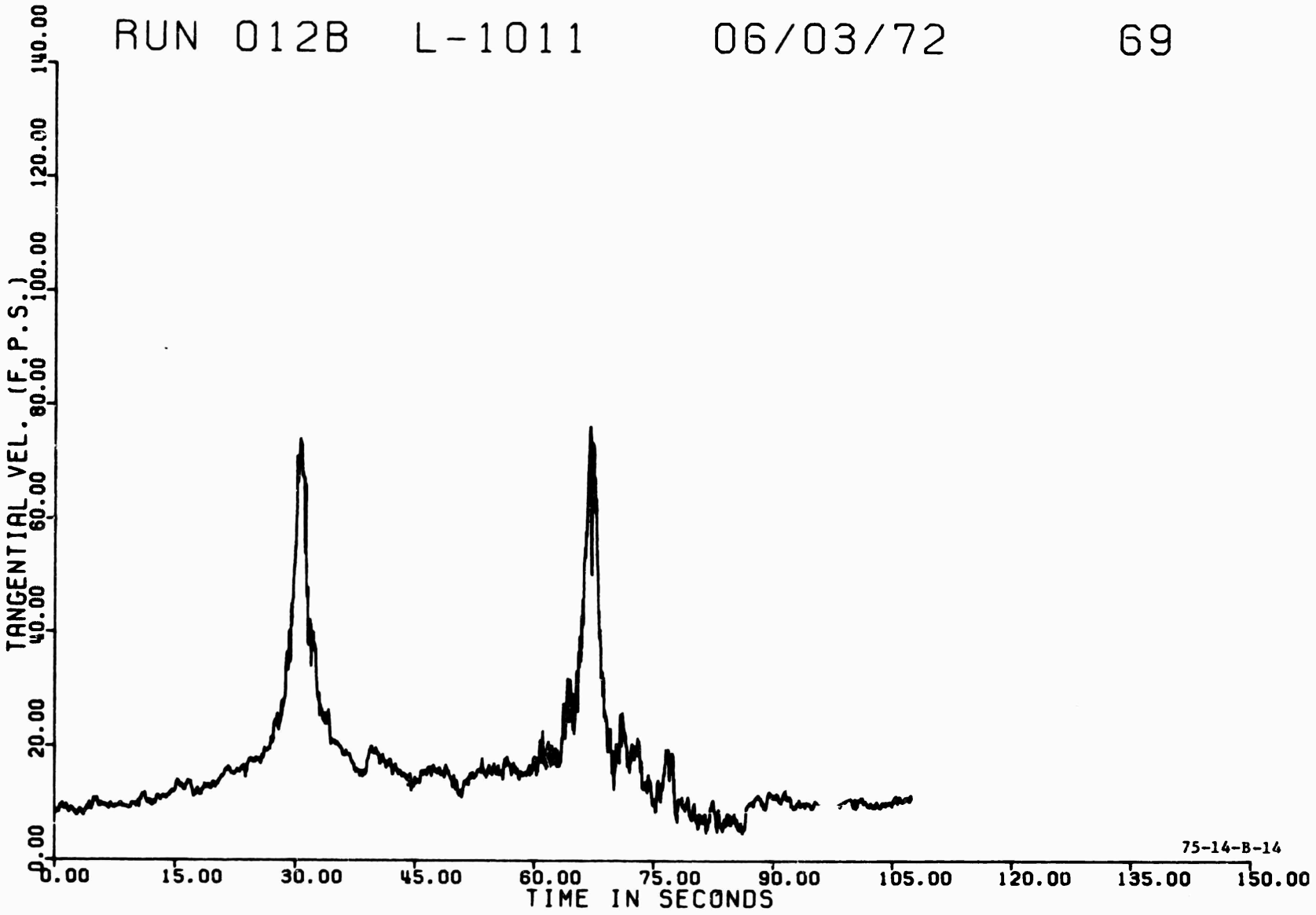

FIGURE B-14. L1011 RUN 12, TAKEOFF CONFIGURATION, STARBOARD WING (DOWNWIND) VORTEX TANGENTIAL VELOCITY TIME HISTORY AT 69 FEET AGL

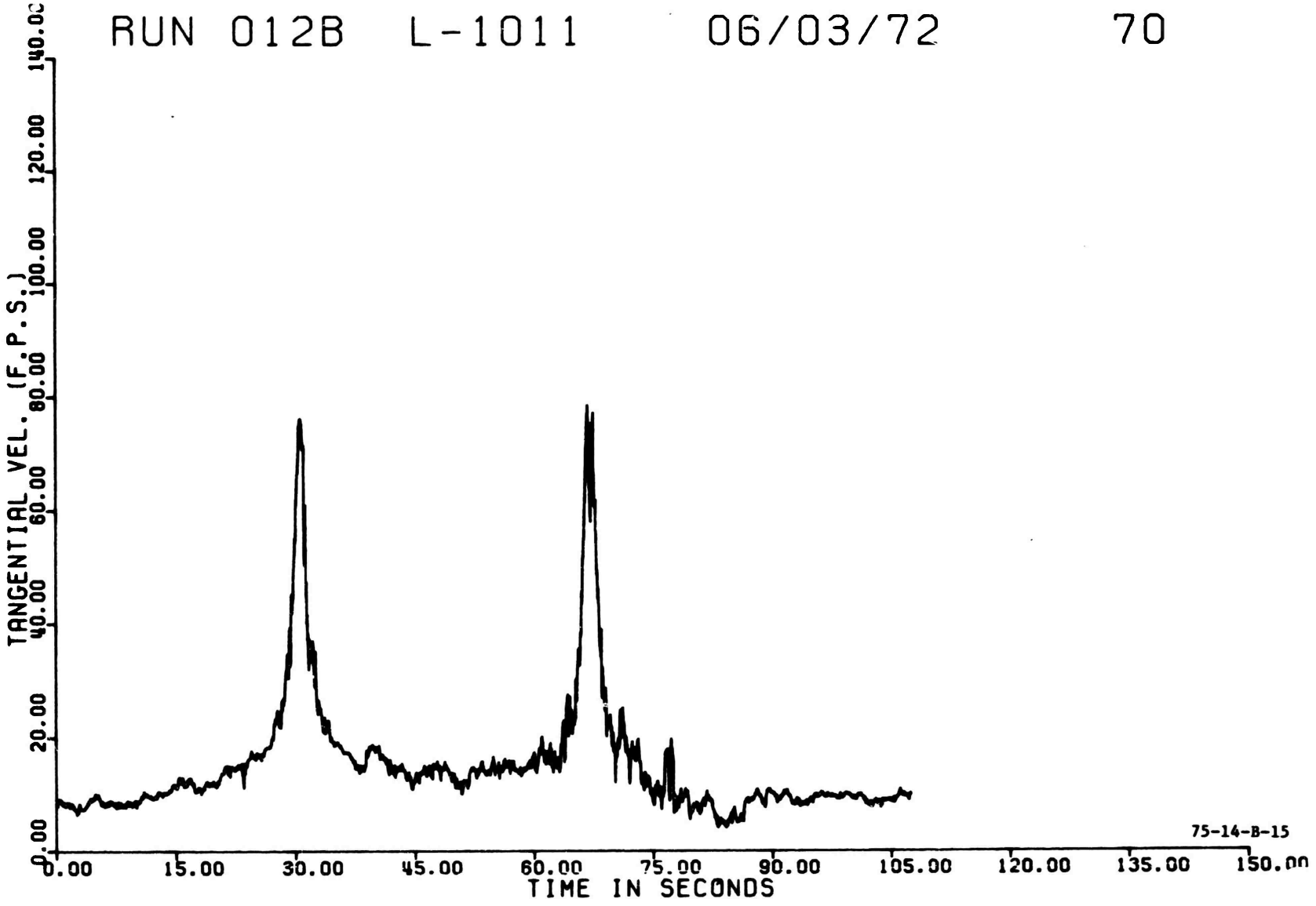

FIGURE B-15. L1011 RUN 12, TAKEOFF CONFIGURATION, STARBOARD WING (DOWNWIND) VORTEX TANGENTIAL VELOCITY TIME HISTORY AT 70 FEET AGL

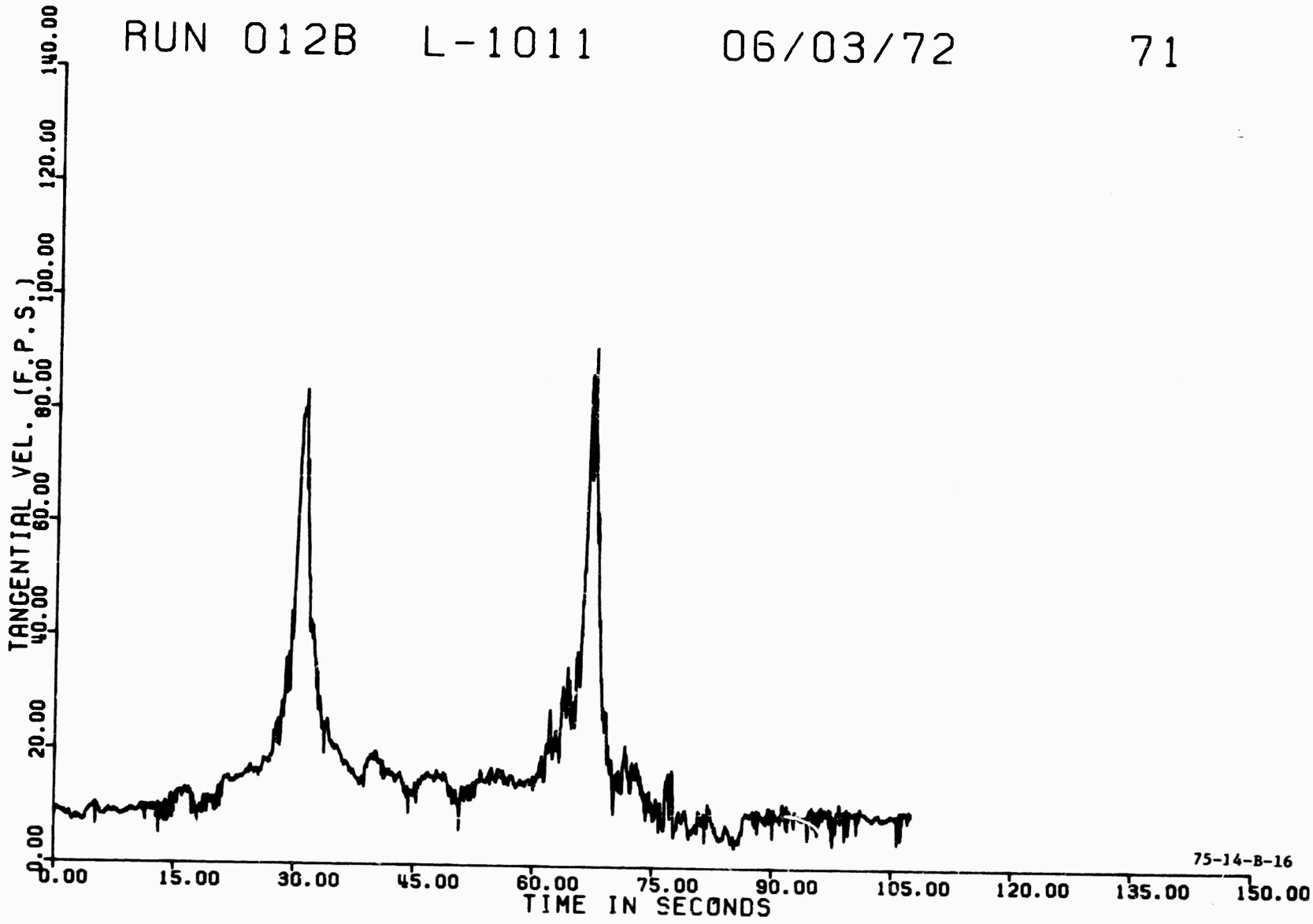

FIGURE B-16. L1011 RUN 12, TAKEOFF CONFIGURATION, STARBOARD WING (DOWNWIND) VORTEX TANGENTIAL VELOCITY TIME HISTORY AT 71 FEET AGL

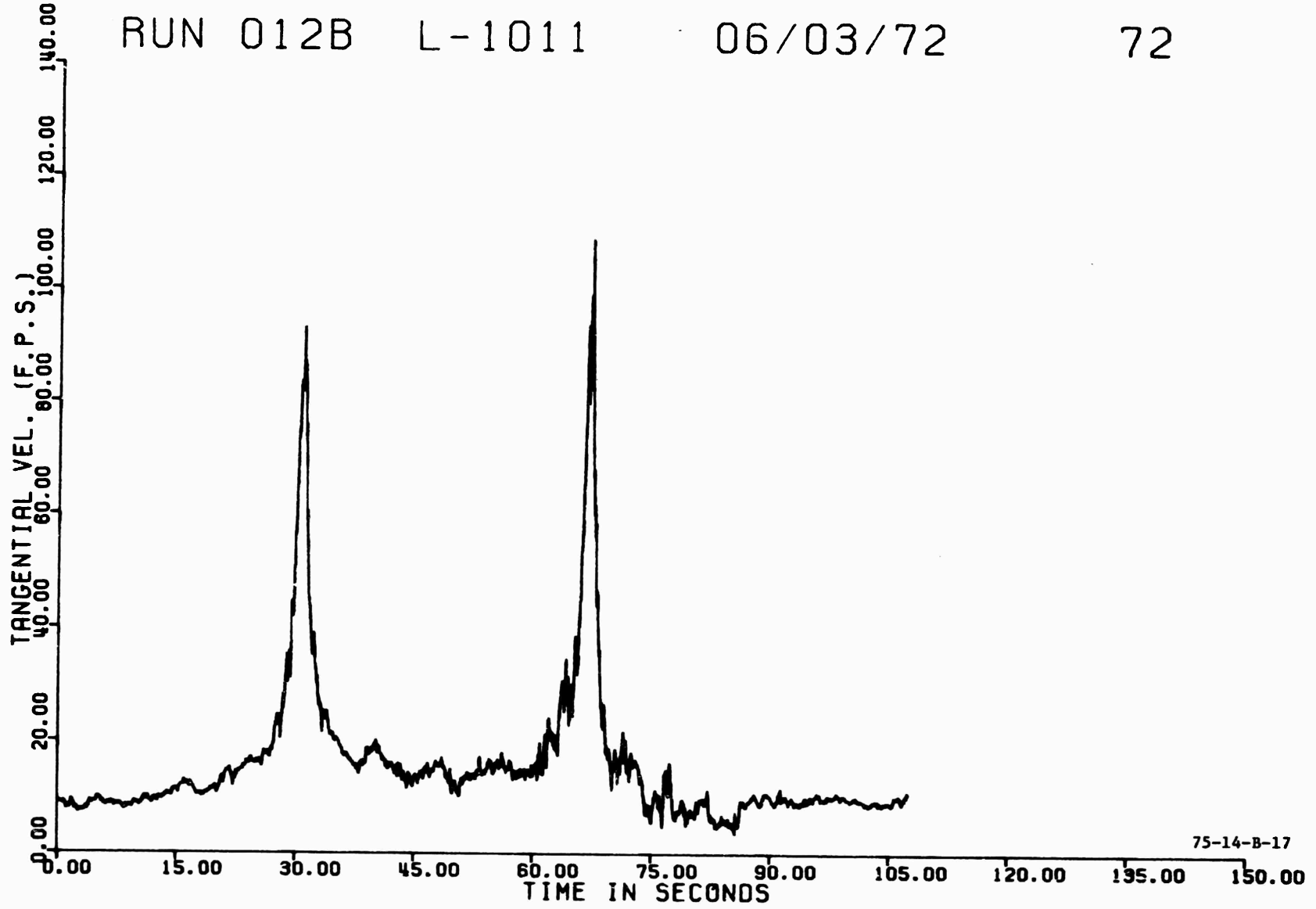

FIGURE B-17. L1011 RUN 12, TAKEOFF CONFIGURATION, STARBOARD WING (DOWNWIND) VORTEX TANGENTIAL VELOCITY TIME HISTORY AT 72 FEET AGL

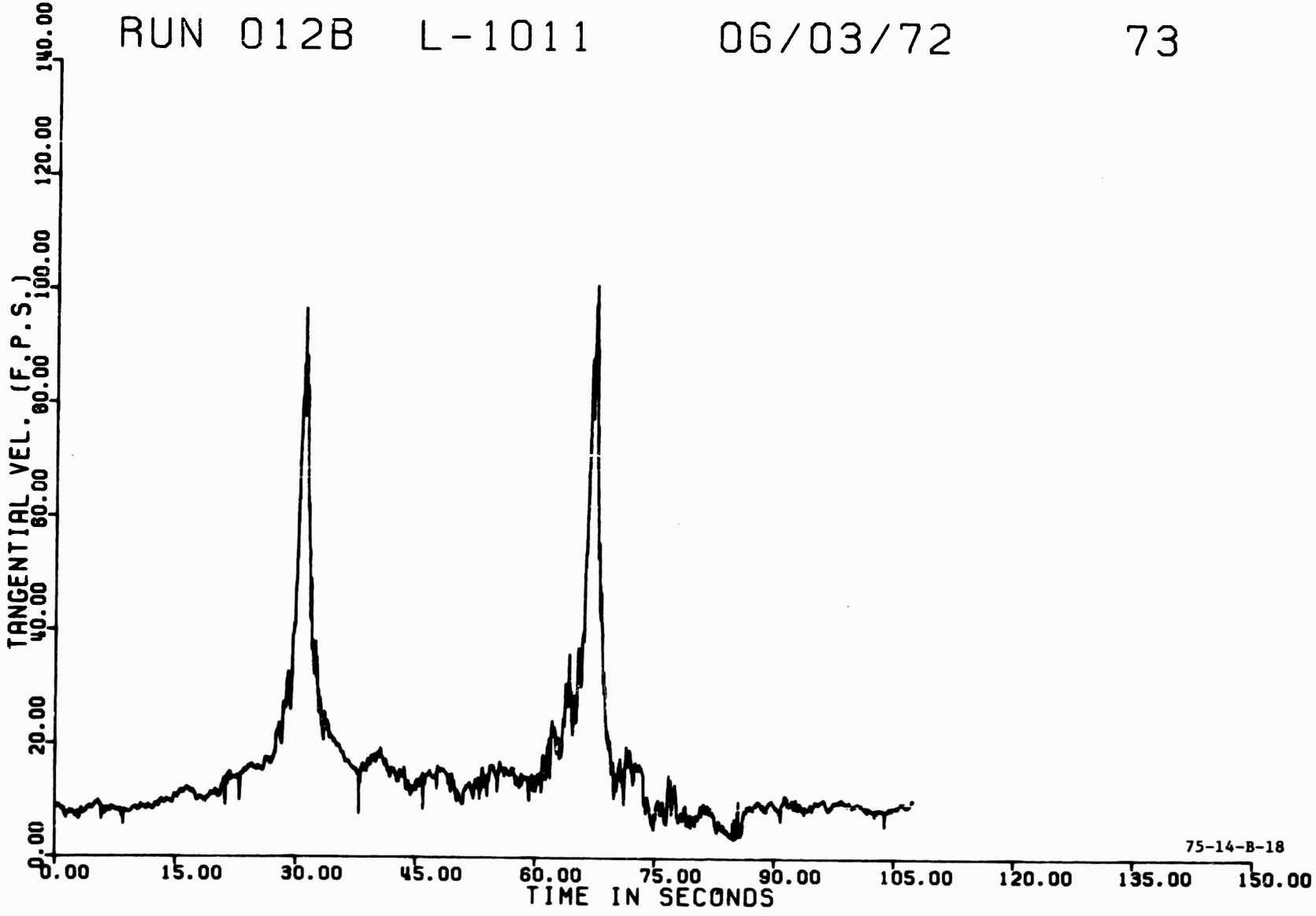

FIGURE B-18. L1011 RUN 12, TAKEOFF CONFIGURATION, STARBOARD WING (DOWNWIND) VORTEX TANGENTIAL VELOCITY TIME HISTORY AT 73 FEET AGL

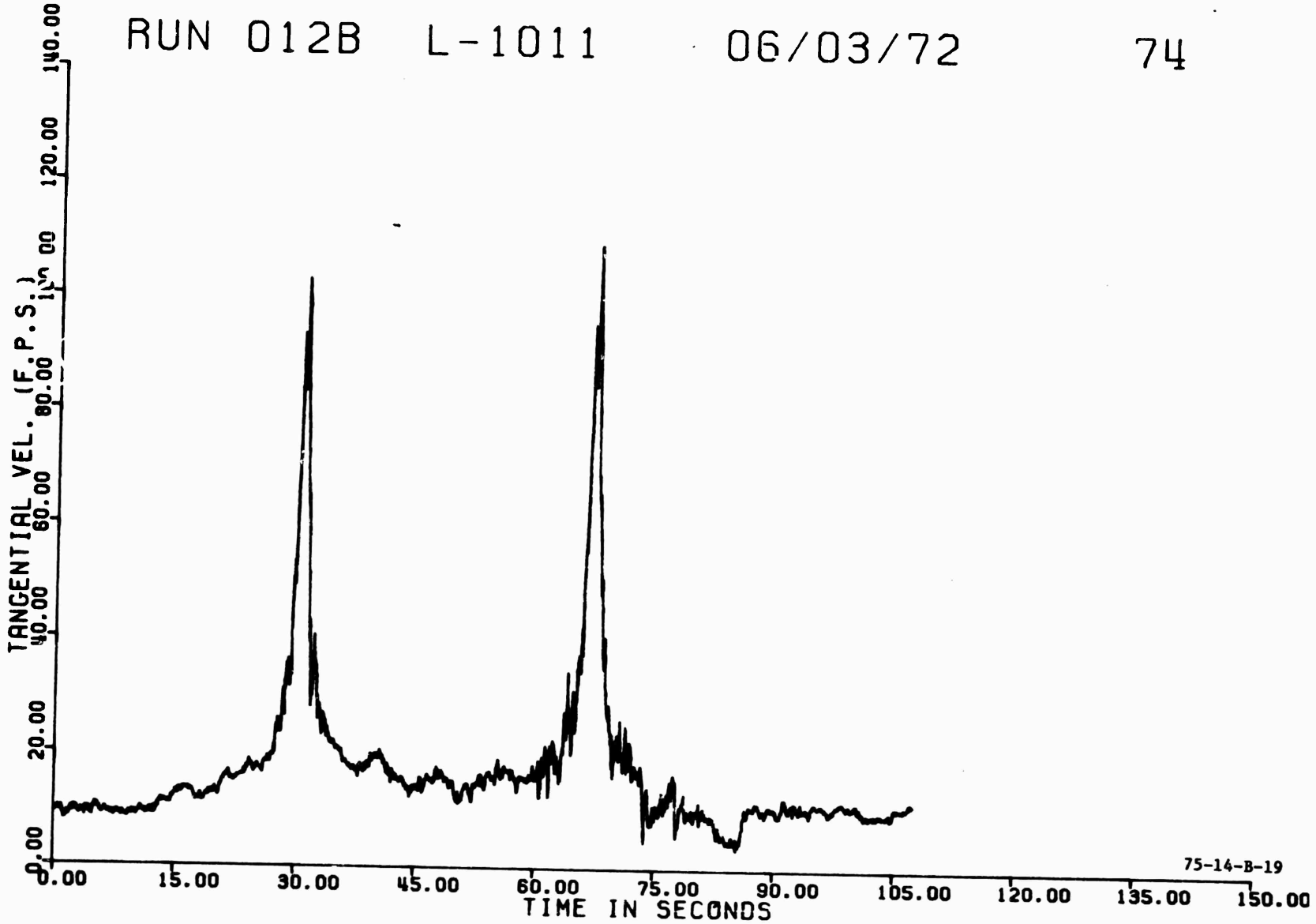

FIGURE B-19. L1011 RUN 12, TAKEOFF CONFIGURATION, STARBOARD WING (DOWNWIND) VORTEX TANGENTIAL VELOCITY TIME HISTORY AT 74 FEET AGL

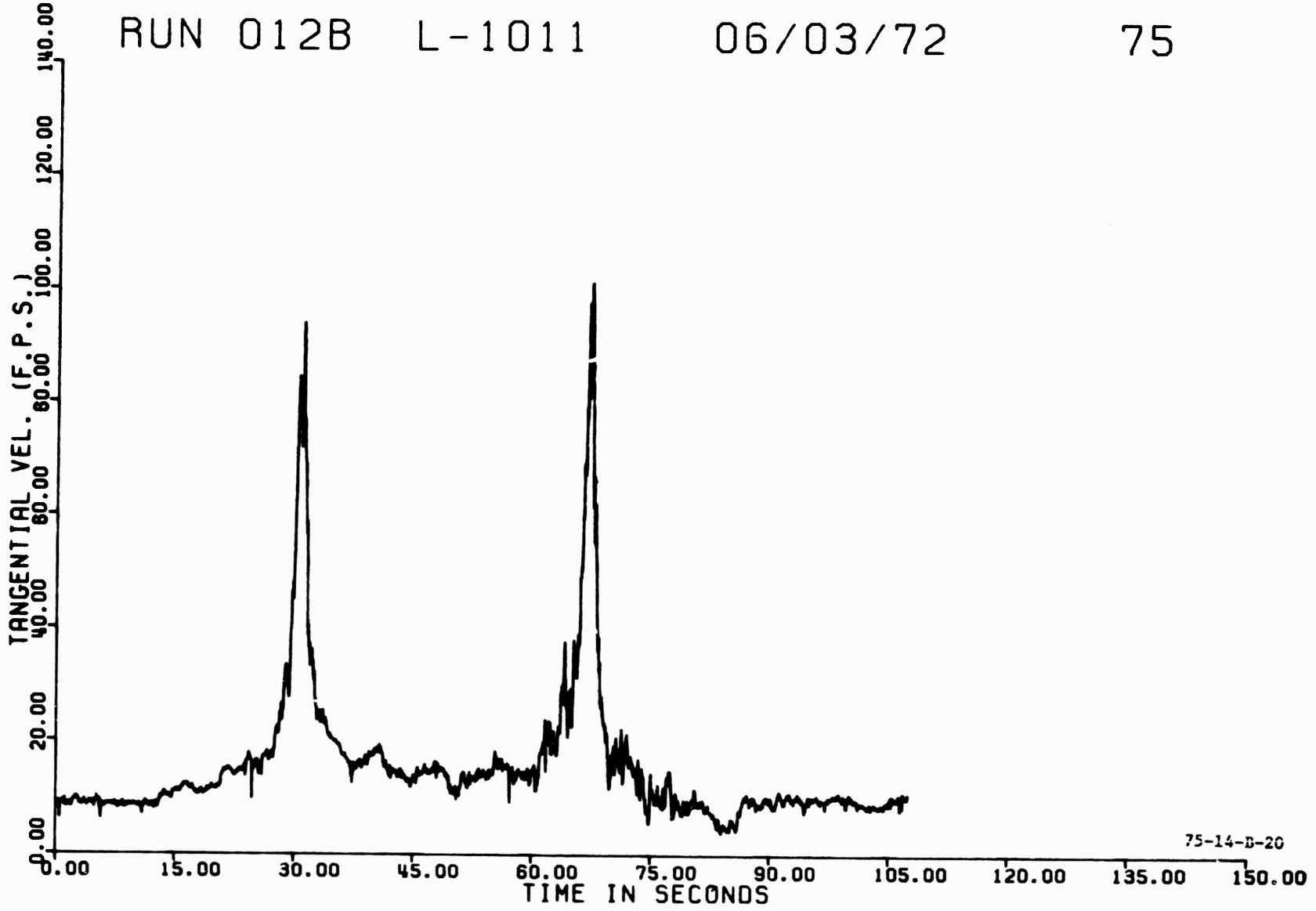

FIGURE B-20. L1011 RUN 12, TAKEOFF CONFIGURATION, STARBOARD WING (DOWNWIND) VORTEX TANGENTIAL VELOCITY TIME HISTORY AT 75 FEET AGL

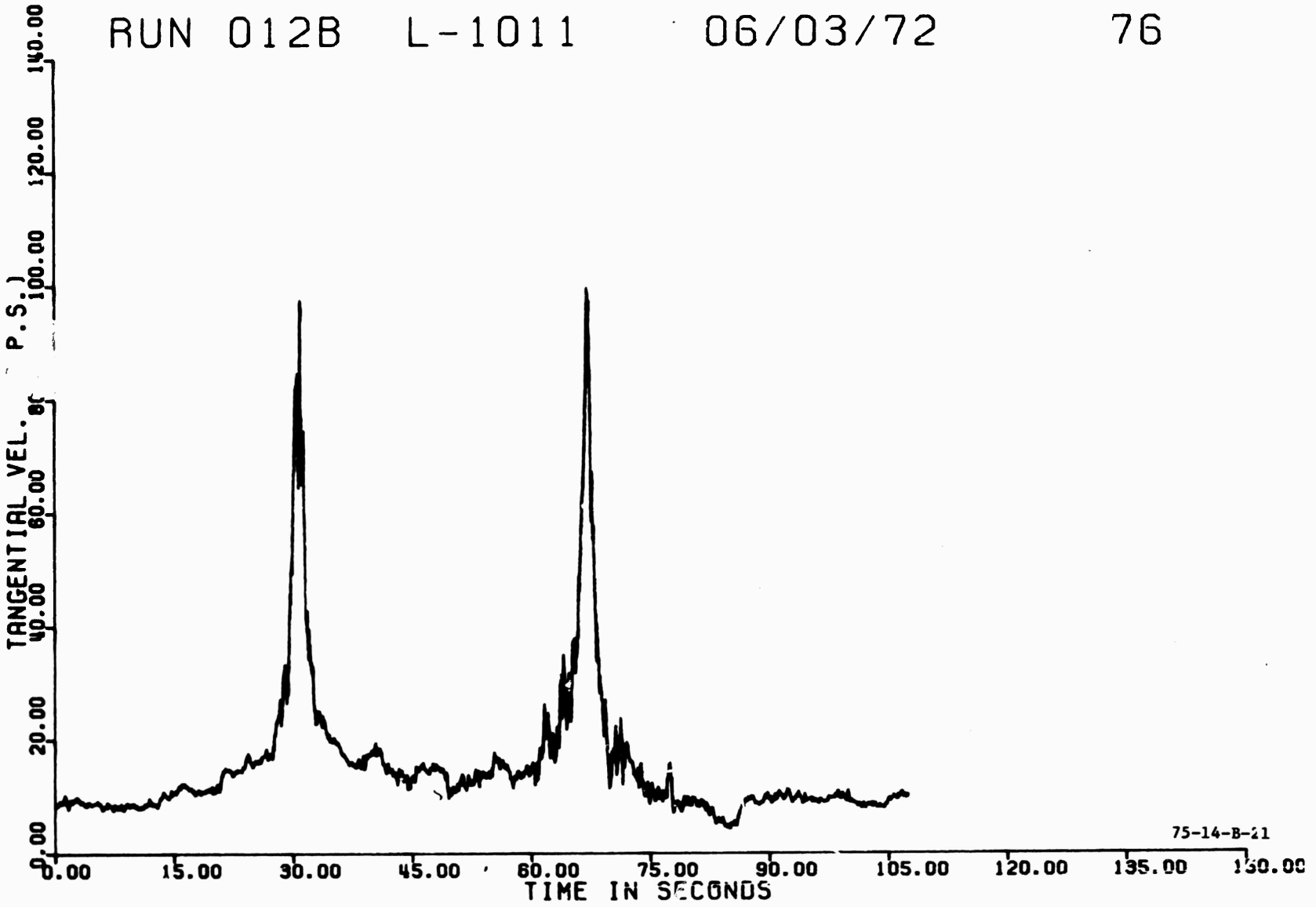

FIGURE B-21. L1011 RUN 12, TAKEOFF CONFIGURATION, STARBOARD WING (DOWNWIND) VORTEX TANGENTIAL VELOCITY TIME HISTORY AT 76 FEET AGL

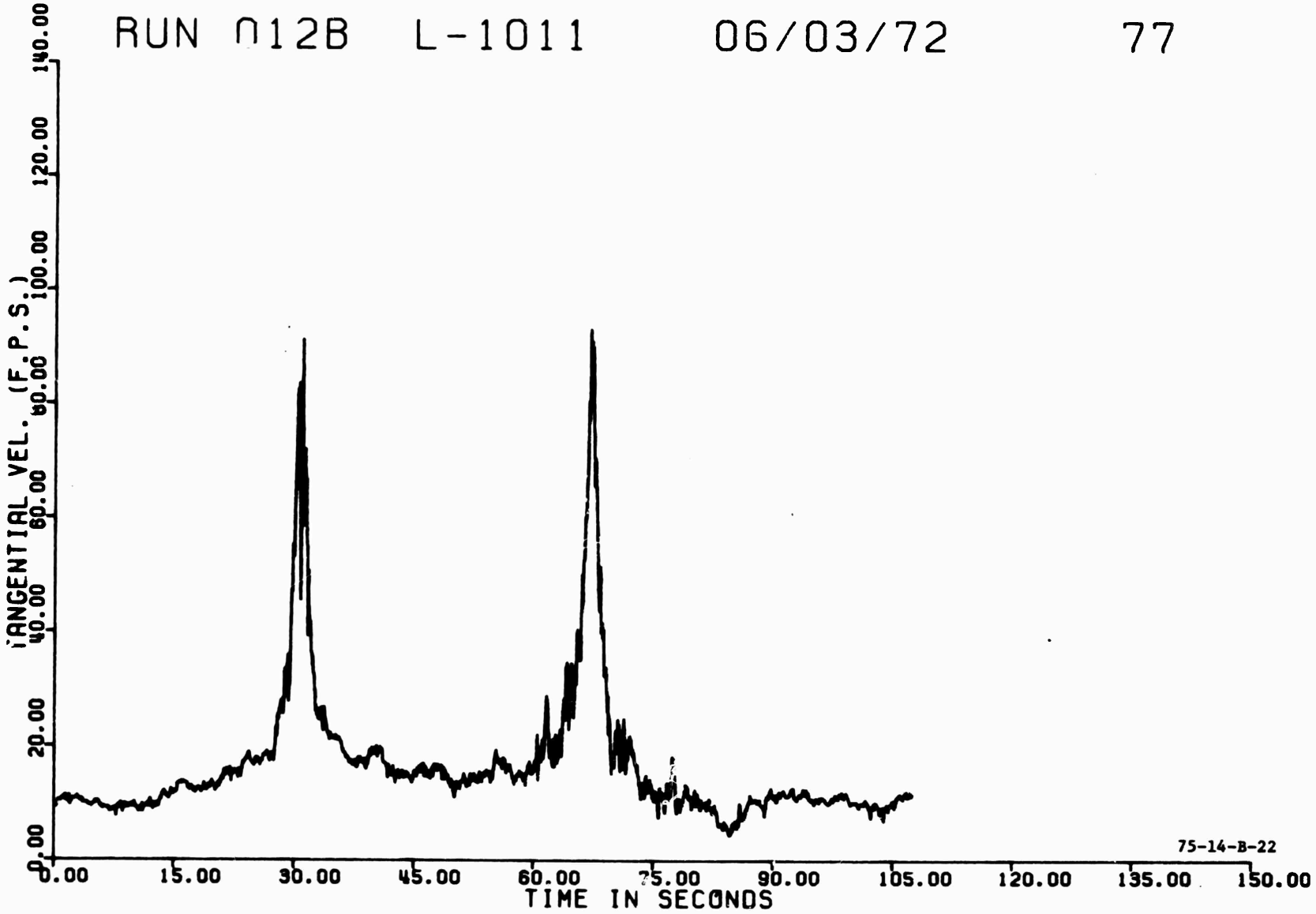

FIGURE B-22. L1011 RUN 12, TAKEOFF CONFIGURATION, STARBOARD WING (DOWNWIND) VORTEX TANGENTIAL VELOCITY TIME HISTORY AT 77 FEET AGL

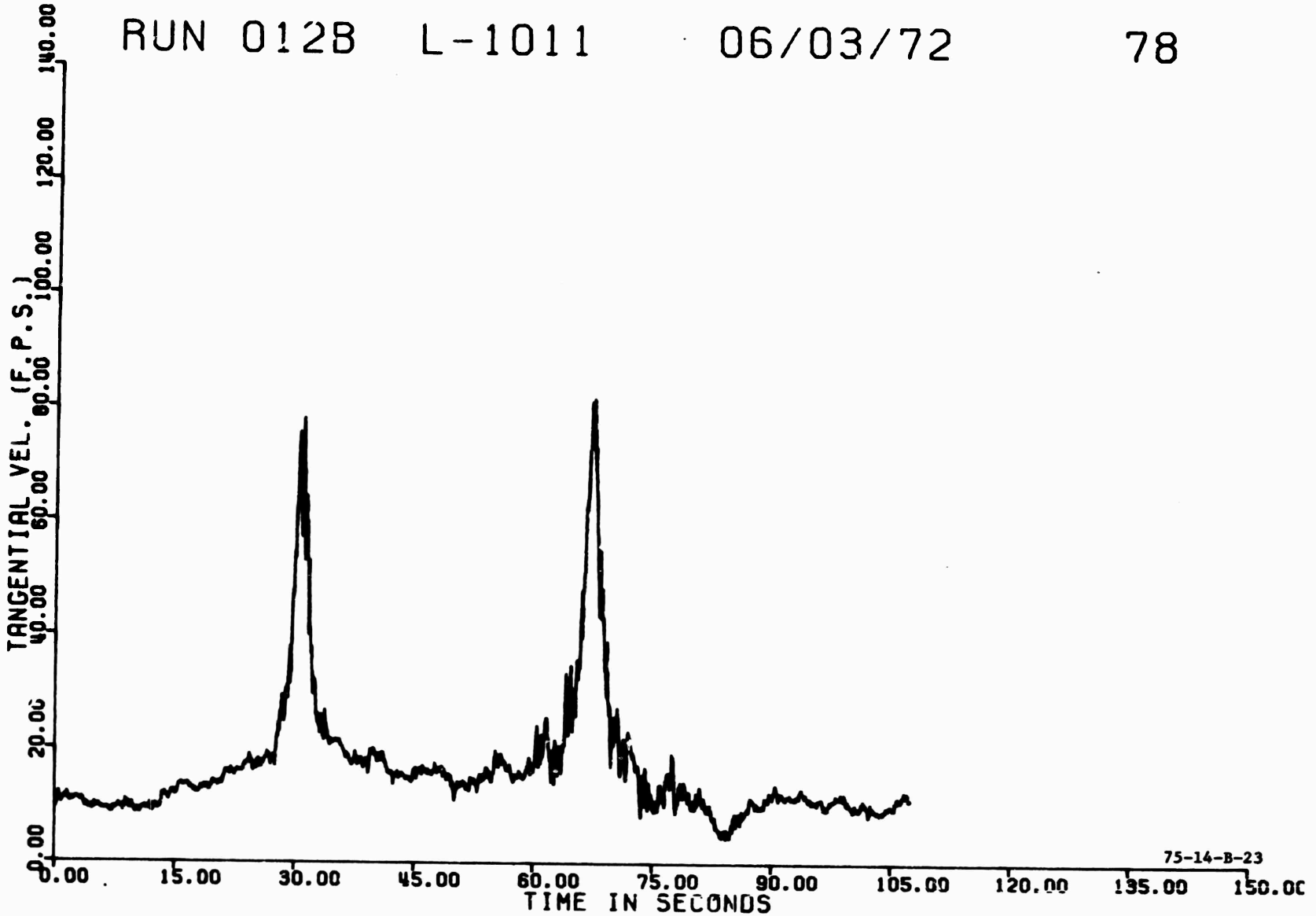

FIGURE B-23. L1011 RUN 12, TAKEOFF CONFIGURATION, STARBOARD WING (DOWNWIND) VORTEX TANGENTIAL VELOCITY TIME HISTORY AT 78 FEET AGL

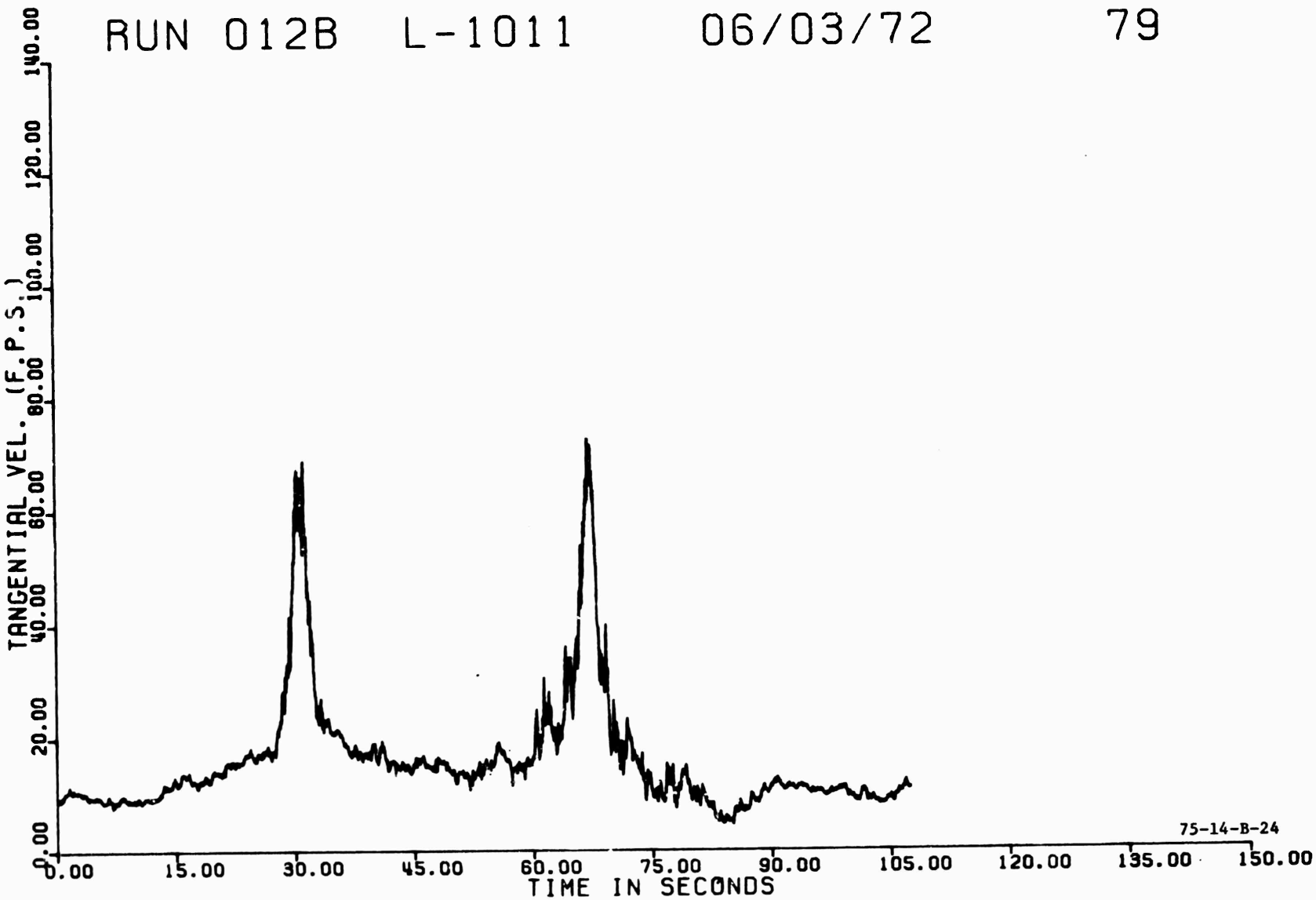

FIGURE B-24. L1011 RUN 12, TAKEOFF CONFIGURATION, STARBOARD WING (DOWNWIND) VORTEX TANGENTIAL VELOCITY TIME HISTORY AT 79 FEET AGL

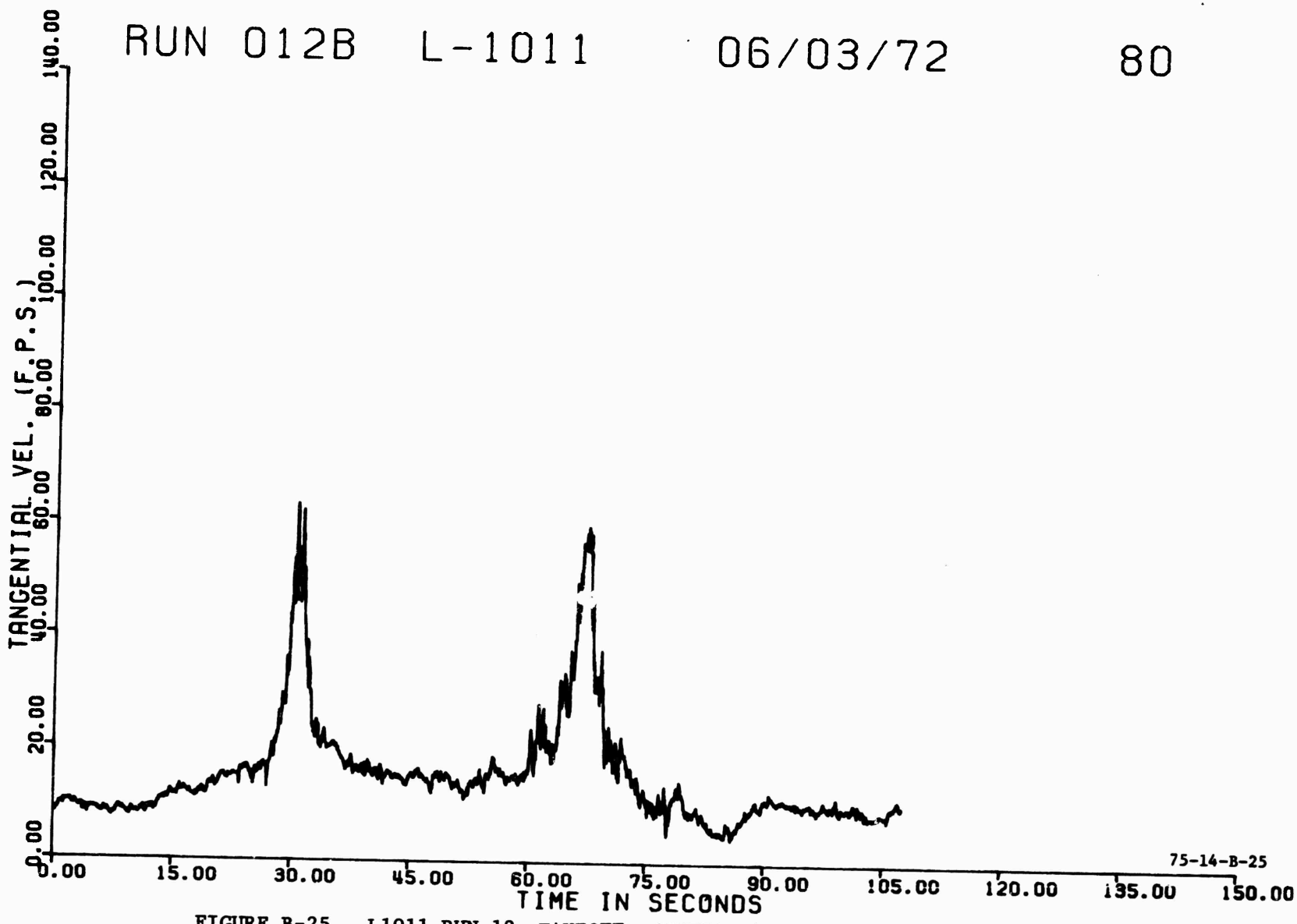

FIGURE B-25. L1011 RUN 12, TAKEOFF CONFIGURATION, STARBOARD WING (DOWNWIND) VORTEX TANGENTIAL VELOCITY TIME HISTORY AT 80 FEET AGL

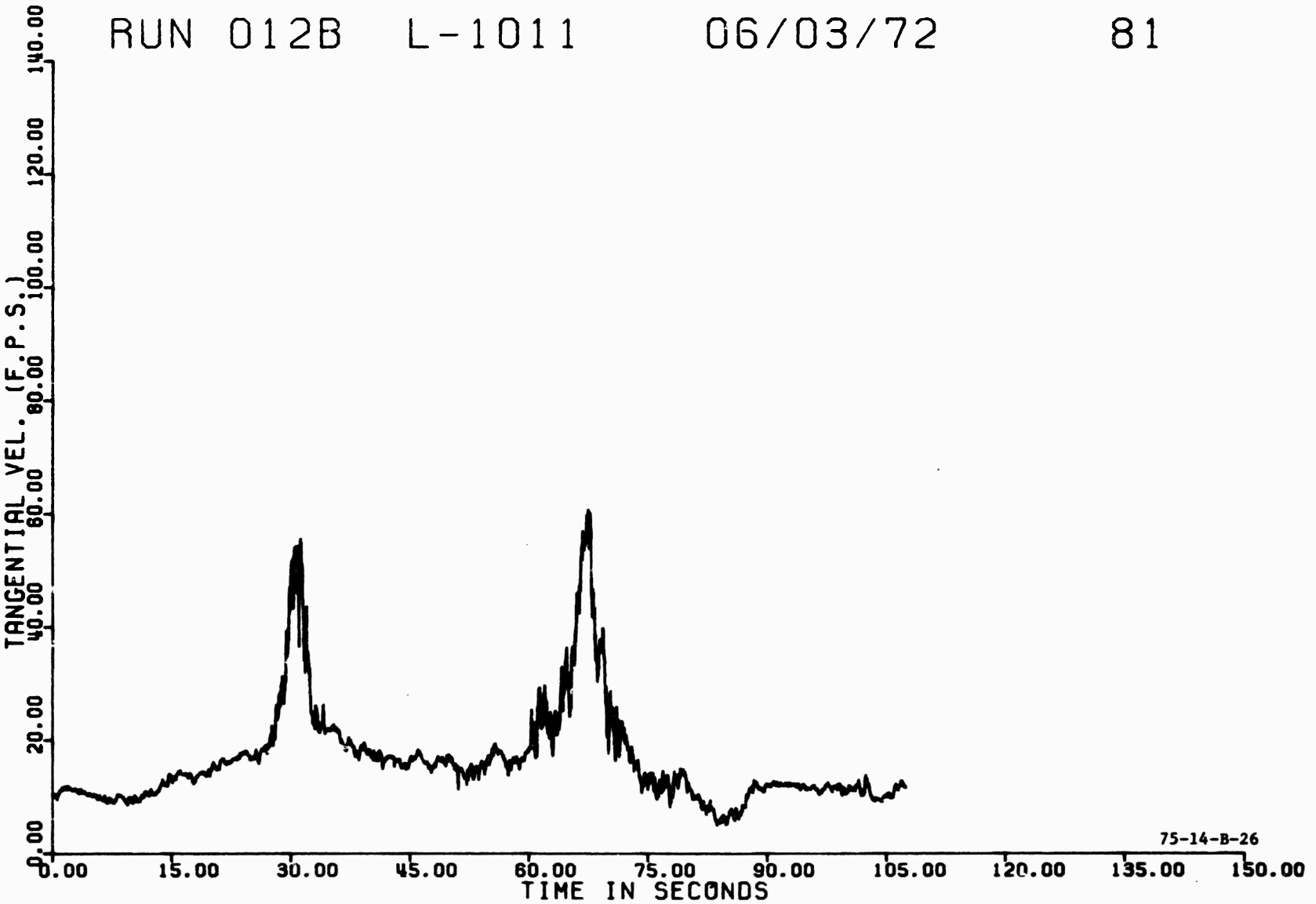

FIGURE B-26. L1011 RUN 12, TAKEOFF CONFIGURATION, STARBOARD WING (DOWNWIND) VORTEX TANGENTIAL VELOCITY TIME HISTORY AT 81 FEET AGL

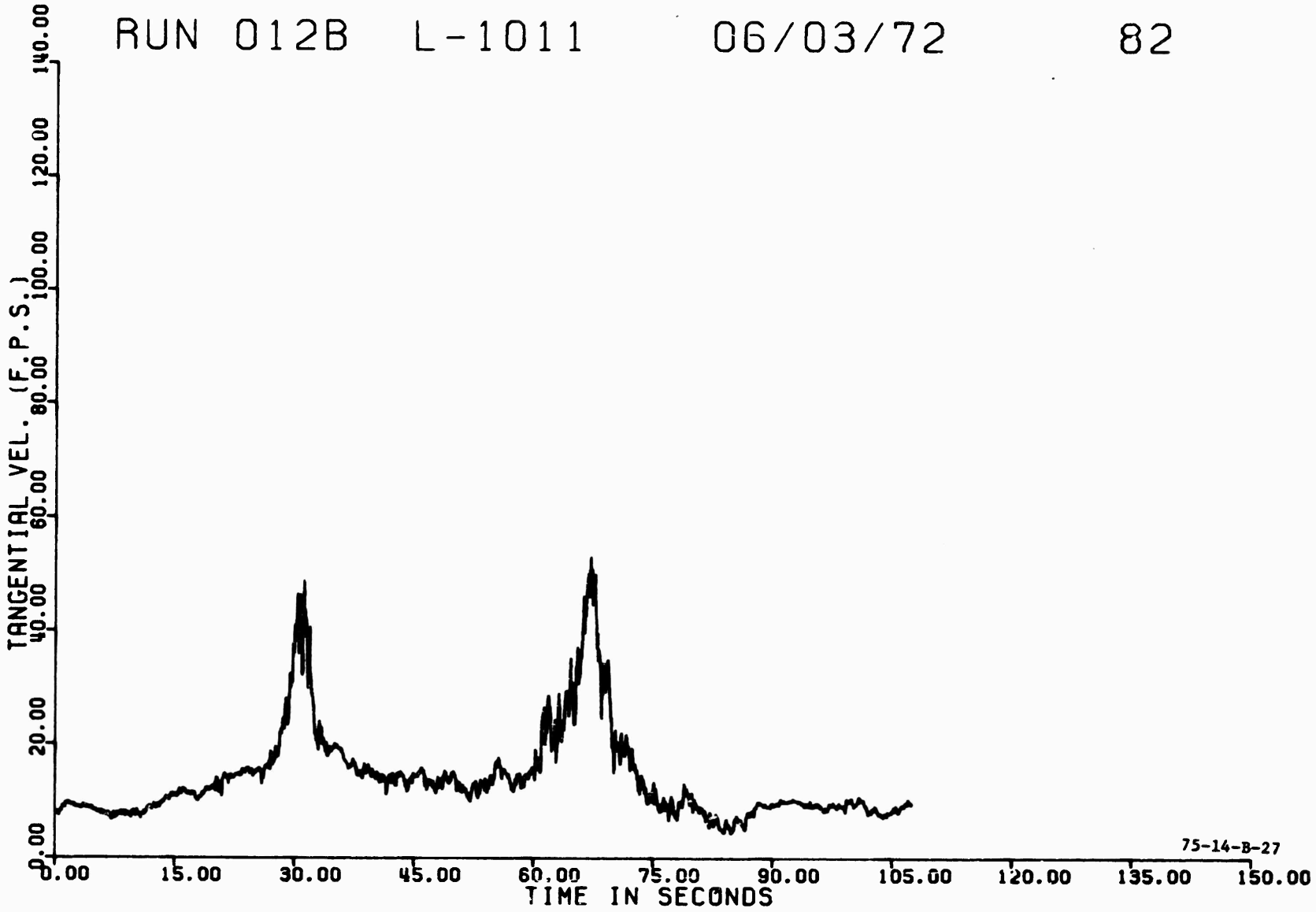

FIGURE B-27. L1011 RUN 12, TAKEOFF CONFIGURATION, STARBOARD WING (DOWNWIND) VORTEX TANGENTIAL VELOCITY TIME HISTORY AT 82 FEET AGL

APPENDIX C

SUMMARY FLIGHT TEST DATA SHEET-VORTEX INVESTIGATION
(Includes Vortex Core Size r_c)

ALT STG: START (0557): 30.00" Hg
FINISH (0733): 30.01" Hg

TABLE C-1

SUMMARY FLIGHT TEST DATA SHEET - VORTEX INVESTIGATION

(PAGE 1 OF 2)

REVISED: 1/10/75

RECORDER: LEO J. GARODZ, PROJ. MGR

DATE [illegible] 1972 **AIRCRAFT** L1011 **COMPANY** LOCKHEED (EASTERN AIRLINES) **REGISTRATION** N305EA

PROJ: JACK WOODMAN

AIRCRAFT CREW C/P: DON MOOR **FIELD ELEVATION** 76 FT **ATM TURB LEVEL AT TEST ALT** NONE (TEMP INVERSION NOTED)

F/E: W. GLUSKIN; TF DIRECTOR: [illegible]; PILOT: JOE BAILEY

TEST LOCATION NAFEC 140' [illegible] FLIGHT TEST SITE; PROBE: 270°M; PROBE: 270°M →

RUN NUMBER	1	2	3	4	5	6	7	8	9	10	11	12
TIME (LOCAL)	0557	0607	0617	0622	0626	0630	0636	0640	0645	0650	0655	0700
AIRCRAFT POSITION (NOTE 1) PHOTOTHEO.	353P	350P	332P	376P	345P	463P	474P	519P	451P	422P	396P	505P
PRESSURE ALTITUDE Hp (Ft) ALTIMETER SET AT 29.92	220	220	240	242	250	240	290	235	190	202	220	205
A/C HEIGHT ABOVE GROUND (Ft) (NOTE 2)	245	231	253	242	238	242	249	234	194	209	194	212
RELATIVE HUMIDITY (140 Ft)	91	88	89	87	84	NR	80	79	79	77	80	NR
OUTSIDE AIR TEMP. (°C) (TEST ALT)	22				→	21						→
AMBIENT PRESSURE (INCHES Hg)	NR											→
WIND DIR./LEVEL (°TRUE) (AVE) *1	293/140	290/140	270/140	/	/	/	/	/	/	→	260/140	260/140
WIND VEL./LEVEL (MPH) (AVE) *1	8/140	10/140	9/140	/	/	/	/	/	/	→	9/140	7/140
EQUIVALENT AIRSPEED (KNOTS) COCKPIT *1 / PHOTO *2	142 / 140	142 / 138	142 / 141	140 / 144	143 / 142	149 / 142	154 / 142	140 / 145	158 / 157	156 / 158	157 / 170	158 / 166
GLIDE PATH ANGLE (DEGREES)	0 (LEVEL)											→
AIRCRAFT TRACK, MAGNETIC (DEGREES)	310	309	001	359	359	000	001	002	000	000	000	004
AIRCRAFT GROSS WEIGHT (lbs x 1000)	365	363	357	356	354	353	350	347	345	344	342	341
GEAR (UP OR DOWN)	UP											→
AIRCRAFT CONFIGURATION (NOTE 3)	LDG							→	TO/APP			→
LEADING EDGE SLAT POS. (DEGREES)												
FLAP SETTING (DEGREES)	42							→	22			→
WING SPOILER DEFLECTION (DEGREES)	OUT							→	IN			→
ENGINE PRESSURE RATIO	128	126	127	130	127	124	126	124	116	119	119	119
ENGINE RPM (%) N_1 N_2	70 / 85	70 / 85	72 / 85	75 / 85	70 / 84	70 / 85	74 / 86	72 / 85	63 / 85	65 / 83	65 / 82	65 / 83
FUEL FLOW/ENGINE (lbs/hr)	810	800	790	820	700	700	800	750	660	660	600	600
PHOTOTHEODOLITE (YES/NO)	YES											→
VDS OPERATING (YES/NO)	NO											→
VORTEX HIT AT TOWER: AGE (SEC), V_{MAX} (Ft/SEC), TWR LEVEL (Ft) — STBD. WING	60/82/81	40/109/72	O/T 17/50/142	19/107/141	O/T 15/59/142	23/95/126	O/T 19/78/142	24/108/139	24/116/110	19/122/131	24/135/97	31/103/74
PORT WING	AWAY FROM TOWER	AWAY FROM TOWER	30/124/102	32/111/95	27/119/100	43/106/73	31/121/90	36/119/81	45/129/71	35/134/84	55/106/73	57/109/74
VORTEX CHARACTERISTICS/REMARKS												

NOTE 1: A/C C/L LATERAL OFFSET (FEET) FROM TOWER (P = TO PORT OF TOWER; S = TO STARBOARD OF TOWER). (BY PHOTOTHEODOLITE, WHEN AVAILABLE.) **NOTE 2:** ABREAST OF TEST TOWER. (BY PHOTOTHEODOLITE; OTHERWISE AIRCRAFT RADAR ALTITUDE.) **NOTE 3:** TO = TAKEOFF, HLDG = HOLDING, LDG = LANDING, APP = APPROACH. **NOTE 4** NR = NOT REQUIRED/RECORDED. N = MISSED TOWER.

*1 SEE APPENDIX "G" FOR COMPUTED DATA; *2 PHOTOTHEODOLITE DATA PROVIDES GROUNDSPEED.

Originator	Date	Quantity	APPROVED
ANA-430	9/22/72	500	FORM

TABLE C-7 REVISED: 1/30/75

SUMMARY FLIGHT TEST DATA SHEET - VORTEX INVESTIGATION
PAGE 2 OF 2

DATE Oct. 31, 1972 AIRCRAFT L1011 COMPANY LOCKHEED (EASTERN AIRLINES) REGISTRATION N305EA

AIRCRAFT CREW ______ FIELD ELEVATION ______ ATM TURB LEVEL AT TEST ALT NONE

TEST LOCATION ______

RUN NUMBER	13	14	15	16	17	18	19					
TIME (LOCAL)	0705	0710	0715	0720	0725	0729	0733					
AIRCRAFT POSITION (NOTE 1)	451P	501P	600P	492P	388P	403P	400P					
PRESSURE ALTITUDE Hp (Ft) ALTIMETER SET AT 29.92	210	230	230	220	240	290	0					
A/C HEIGHT ABOVE GROUND (Ft) (NOTE 2)	245	220	205	213	230	239	170					
RELATIVE HUMIDITY (140 Ft)	NR	NR	81	81	NR	90	NR					
OUTSIDE AIR TEMP. (°C) (TEST ALT)	21	—	—	—	—	—	→					
AMBIENT PRESSURE (INCHES Hg)	NR	—	—	—	—	—	→					
WIND DIR./LEVEL (°TRUE) (AVE) #1	26?/140	/	/	/	/	→	273/	/	/	/	/	/
WIND VEL./LEVEL (MPH) (AVE) #1	7/140	/	/	/	/	→	7/	/	/	/	/	/
EQUIVALENT AIRSPEED (KNOTS)	158 153	167 170	165 170	166 170	136 143	136 143	305 29?					
GLIDE PATH ANGLE (DEGREES)	0 (LEVEL)	—	—	—	—	—	→					
AIRCRAFT TRACK, MAGNETIC (DEGREES)	003	003	224	006	008	207	007					
AIRCRAFT GROSS WEIGHT (lbs x 1000)	333	337	336	334	331	329	328					
GEAR (UP OR DOWN)	UP	—	—	—	—	—	→					
AIRCRAFT CONFIGURATION (NOTE 3)	TO/APP	TO	TO	TO	LDG	LDG	CRUISE					
LEADING EDGE SLAT POS. (DEGREES)	EXTENDED	—	—	—	—	→	RETRACTED					
FLAP SETTING (DEGREES)	22	10	10	10	42	42	0					
WING SPOILER DEFLECTION (DEGREES)	IN	—	—	→	OUT	OUT	IN					
ENGINE PRESSURE RATIO	115	113	115	116	123	121	116					
ENGINE RPM (%) N_1 N_2	58 | 80	58 | 80	60 | 80	62 | 82	72 | 85	60 | 84	65 | 83					
FUEL FLOW/ENGINE (lbs/hr)	530	410	520	575	780	730	650					
PHOTOTHEODOLITE (YES/NO)	YES	—	—	—	—	—	→					
VDS OPERATING (YES/NO)	NO	—	—	—	—	—	→					
VORTEX HIT AT TOWER: AGE (SEC), V_θ MAX (Ft/SEC), TWR LEVEL (Ft) STBD. WING	OFF 17.5/-/142	28/177/106	35/145/92	28/134/125	23/136/112	21.5/158/131	27/61/108					
PORT WING	31.5/1?0/??	?/207/61	71/224/78	48/222/83	6?/?/56	39/125/70	36/1??/67					
VORTEX CHARACTERISTICS/REMARKS												

NOTE 1: A/C C/L LATERAL OFFSET (FEET) FROM TOWER (P = TO PORT OF TOWER; S = TO STARBOARD OF TOWER). (BY PHOTOTHEODOLITE, WHEN AVAILABLE.) NOTE 2: ABREAST OF TEST TOWER. (BY PHOTOTHEODOLITE; OTHERWISE AIRCRAFT RADAR ALTITUDE.) NOTE 3: TO = TAKEOFF, HLDG = HOLDING, LDG = LANDING, APP = APPROACH. NOTE 4 NR = NOT REQUIRED/RECORDED. M = MISSED TOWER.

Originator	Date	Quantity	APPROVED FORM
ANA-430	9/22/72	500	

TABLE C-2. VORTEX CORE RADIUS DETERMINATION

Run No.	Vortex	Average y_v (ft/s)	Average y_v (ft/s)	Photo Coverage y_v (ft) (Approx)	Expanded Plots r_c (ft) (Approx)	Plots r_c (ft)	Logarithmic Curve Fit r_c	C_L*
1	STBD	4.9	2.8	2-3	2	--	1.5	
	PORT	--	--	--	--	--	--	1.54
2	STBD	7.2	4.0	2-3	4.0	--	2.3	
	PORT	--	--	--	--	--	--	1.53
3	STBD	15.9	5.5(E)	O/T	O/T	--	--	
	PORT	13.0	5.0	No smoke at Hit	4.0	--	2.3	
4	STBD	16.0	5.3	2-3	4.0	--	2.8	
	PORT	13.6	4.6	5-6	4.0	--	2.3	1.54
5	STBD	18.9	5.5(E)	O/T	O/T	--	--	1.48
	PORT	15.0	5.1	5-6	5.0	--	2.5	
6	STBD	17.5	5.0	3	4.0	--	2.8	1.47
	PORT	12.2	4.0	6-7	3.0	--	2.5	
7	STBD	21.7	5.4(E)	5	O/T	--	--	1.54
	PORT	17.2	5.2	4-5	3.0	2.23	2.3	
8	STDB	21.8	4.5	2-3	--	--	2.3	1.51
	PORT	16.1	4.3	2 cyl.: 1 and 5 ft	--	--	2.5	
9	STBD	18.6	3.7	2-3	2.7	--	2.8	1.18
	PORT	11.4	2.7	2-3	2.5	2.03	2.3	
10	STBD	18.8	4.1	2	3.2	--	1.87	1.21
	PORT	13.7	3.6	3	2.2	--	2.1	
11	STBD	15.3	4.4	1.5	--	--	1.7	1.16
	PORT	10.2	2.7	2	--	--	2.3	
12	STBD	14.3	4.4	2.5	2.5	--	2.4	1.16
	PORT	8.4	2.1	2.5	2.3	--	2.0	
13	STBD	20.0	5.3	O/T	O/T	--	--	1.18
	PORT	16.2	4.5	1	3.5	--	2.5	
14	STBD	15.7	4.1	2	Not Possible	--	0.8	1.03
	PORT	11.0	3.0	2.5	0.5	--	0.8	
15	STBD	15.4	3.2	3	1.2	--	1.2	1.05
	PORT	9.3	1.8	3	0.8	--	0.5	
16	STBD	15.4	3.1	No Smoke	0.9	1.57	1.2	1.03
	PORT	11.5	2.7	No Smoke	0.6	0.9	0.7	
17	STBD	14.2	5.1	No Smoke	3.4	--	2.0	1.53
	PORT	7.5	2.9	No Smoke	Vortex Hit 56 Ft.AGL	--	2.3	
18	STBD	15.9	5.0	2.5	4.0	--	2.8	1.52
	PORT	11.9	4.1	1 Inner 3 Outer	2.5	--	2.6	
19	STBD	12.5	2.3	0.5	0.8	--	1.4	0.30
	PORT	12.8	2.9	1.5	0.5	--	o.5	

* $C_L = \frac{L}{\frac{1}{2}\rho V^2 S} = \frac{nW}{qS}$

APPENDIX D

VORTEX TANGENTIAL VELOCITY DISTRIBUTIONS

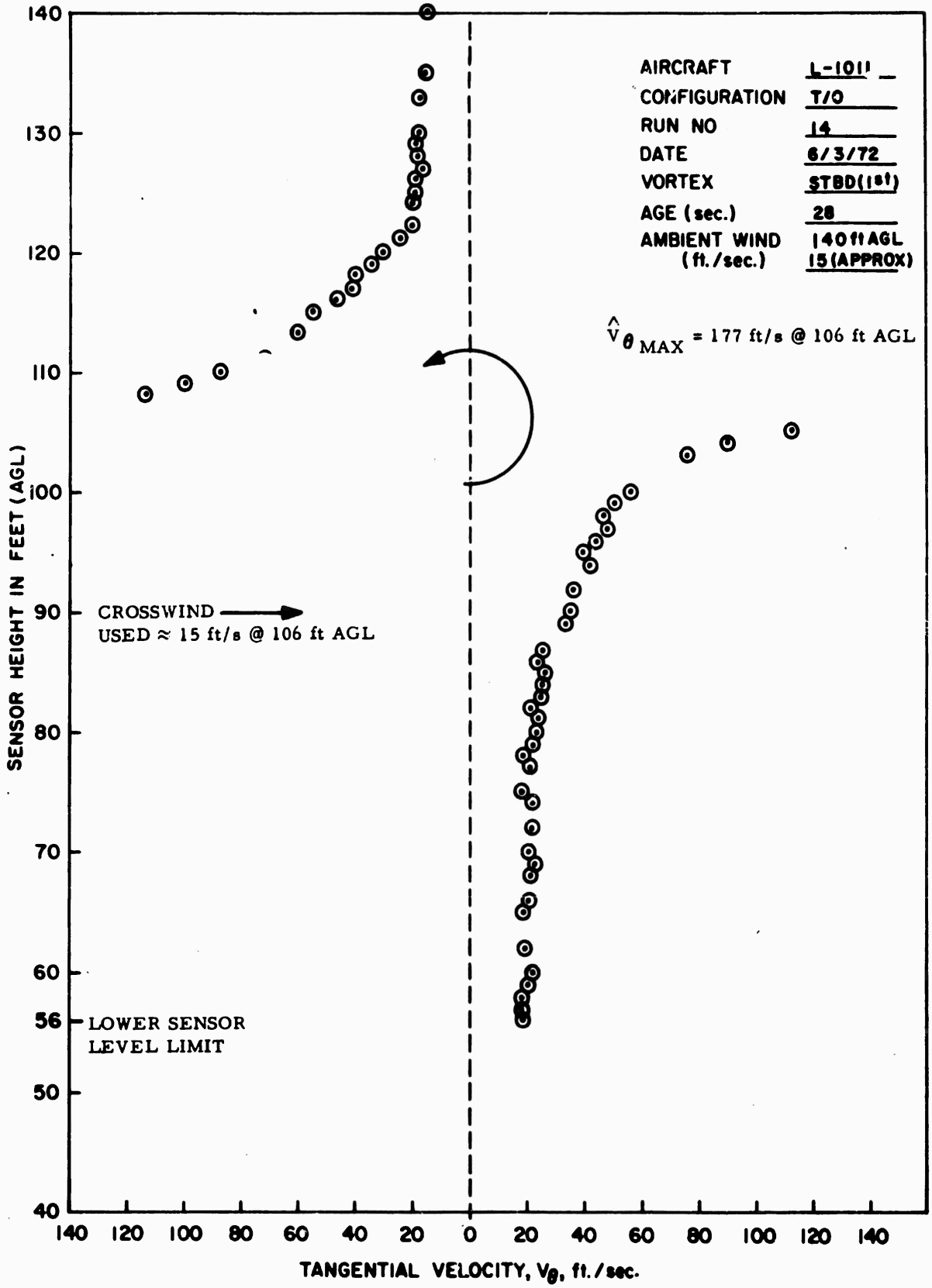
AIRCRAFT L-1011
CONFIGURATION T/O
RUN NO 14
DATE 6/3/72
VORTEX STBD(1st)
AGE (sec.) 28
AMBIENT WIND 1401t AGL
(ft./sec.) 15(APPROX)
$\hat{V}_{\theta\ MAX}$ = 177 ft/s @ 106 ft AGL
CROSSWIND
USED ≈ 15 ft/s @ 106 ft AGL
LOWER SENSOR
LEVEL LIMIT
SENSOR HEIGHT IN FEET (AGL)
140
130
120
110
100
90
80
70
60
56
50
40
140 120 100 80 60 40 20 0 20 40 60 80 100 120 140
TANGENTIAL VELOCITY, V_θ, ft./sec.

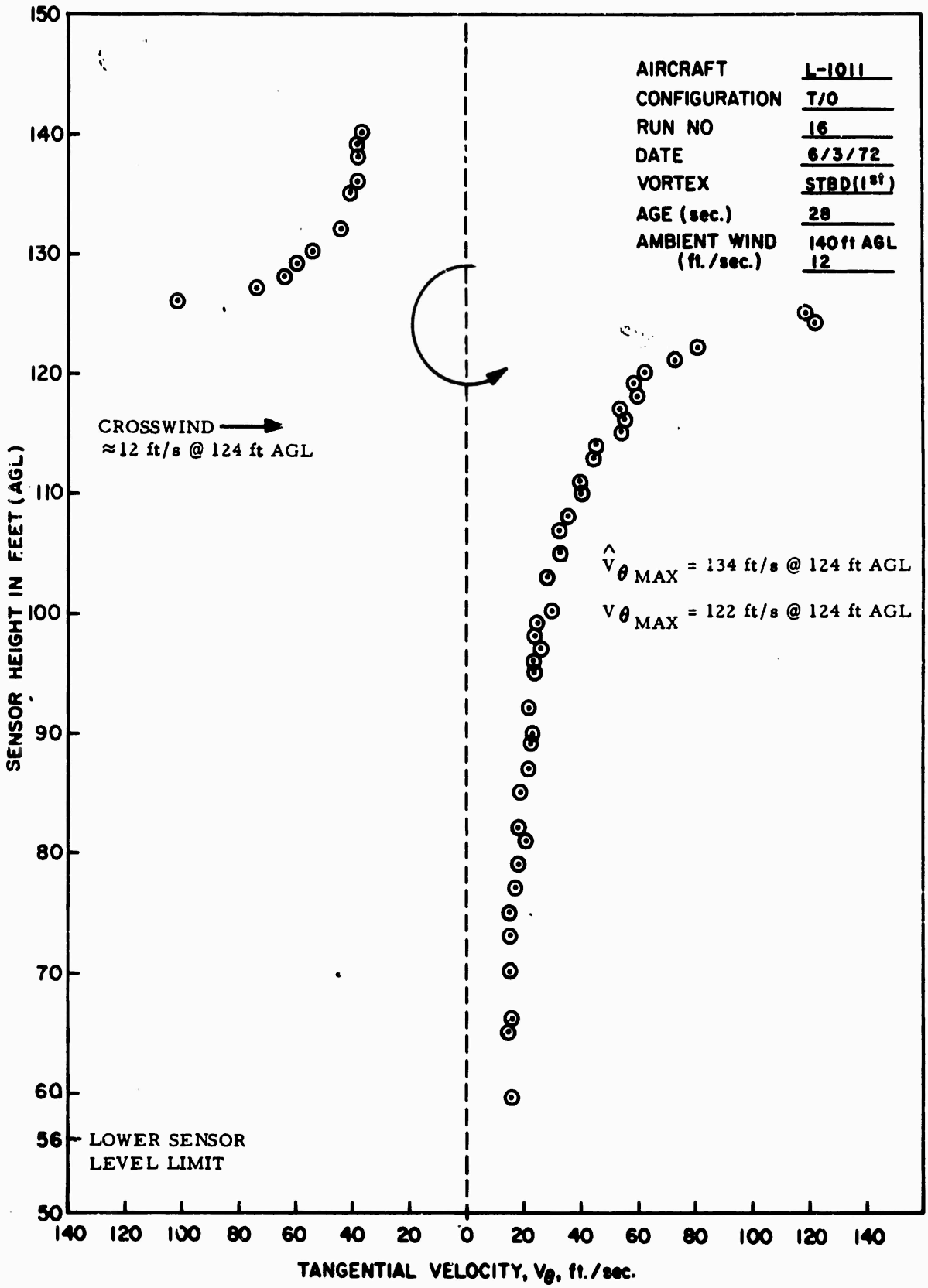
AIRCRAFT L-1011
CONFIGURATION T/O
RUN NO 16
DATE 6/3/72
VORTEX STBD(1st)
AGE (sec.) 28
AMBIENT WIND (ft./sec.) 140 ft AGL 12
CROSSWIND ≈12 ft/s @ 124 ft AGL
$\hat{V}_{\theta\,MAX}$ = 134 ft/s @ 124 ft AGL
$V_{\theta\,MAX}$ = 122 ft/s @ 124 ft AGL
LOWER SENSOR LEVEL LIMIT
SENSOR HEIGHT IN FEET (AGL)
150
140
130
120
110
100
90
80
70
60
56
50
140 120 100 80 60 40 20 0 20 40 60 80 100 120 140
TANGENTIAL VELOCITY, V_θ, ft./sec.

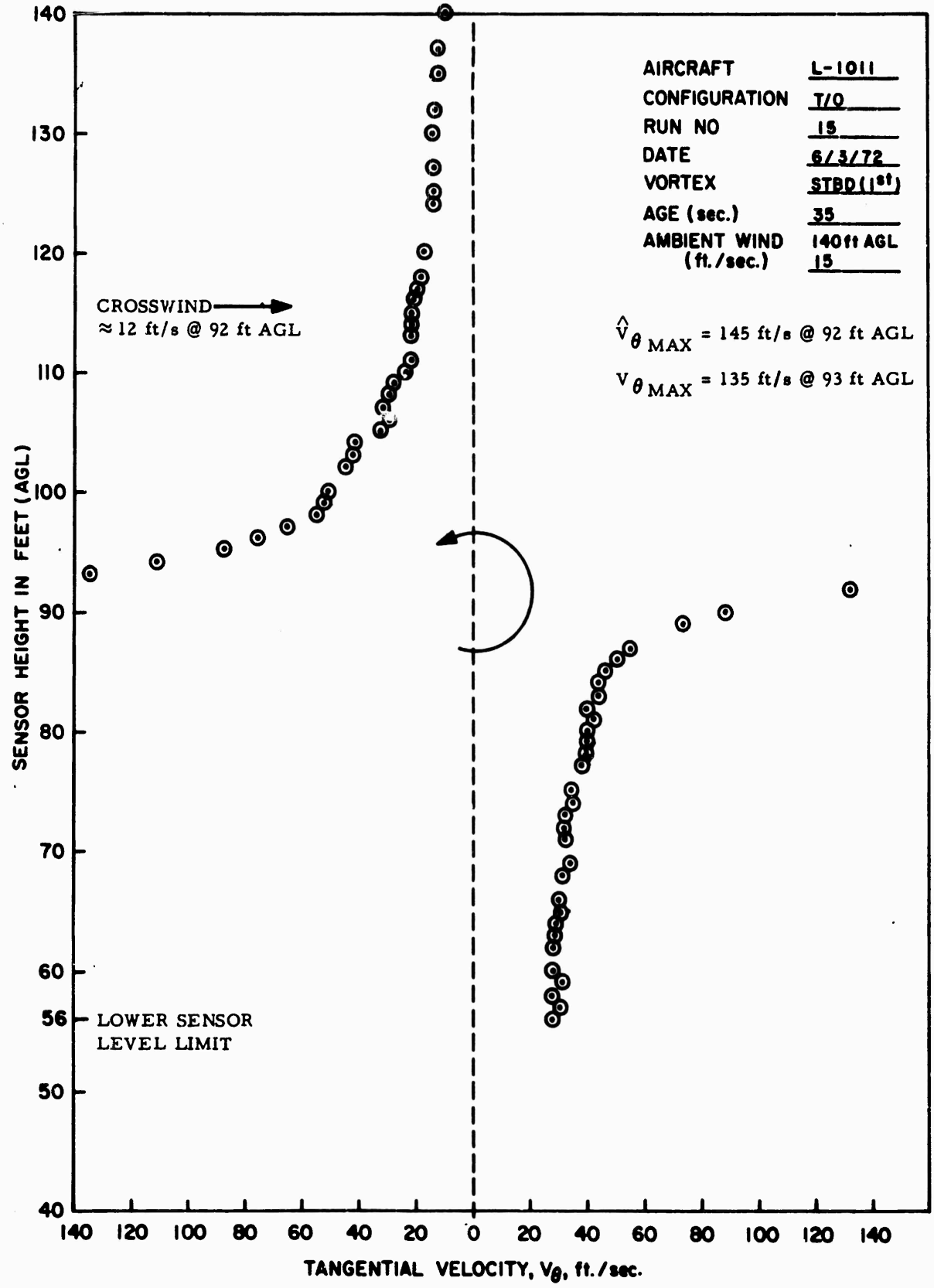
AIRCRAFT L-1011
CONFIGURATION T/O
RUN NO 15
DATE 6/3/72
VORTEX STBD(1st)
AGE (sec.) 35
AMBIENT WIND (ft./sec.) 140ft AGL 15
CROSSWIND
≈ 12 ft/s @ 92 ft AGL
$\hat{V}_{\theta\ MAX}$ = 145 ft/s @ 92 ft AGL
$V_{\theta\ MAX}$ = 135 ft/s @ 93 ft AGL
LOWER SENSOR LEVEL LIMIT
SENSOR HEIGHT IN FEET (AGL)
140
130
120
110
100
90
80
70
60
56
50
40
140 120 100 80 60 40 20 0 20 40 60 80 100 120 140
TANGENTIAL VELOCITY, V_θ, ft./sec.

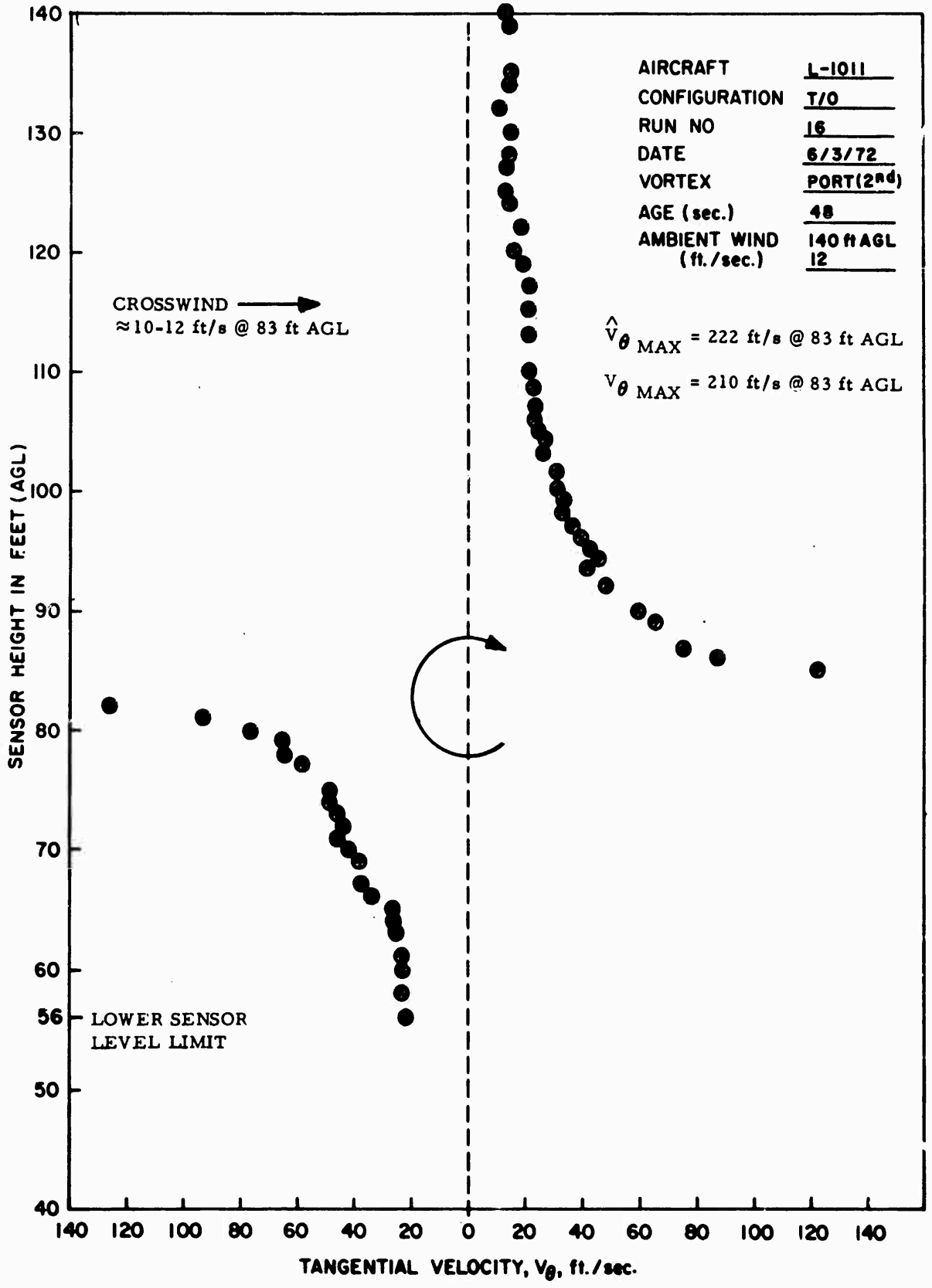
AIRCRAFT L-1011
CONFIGURATION T/O
RUN NO 16
DATE 6/3/72
VORTEX PORT(2nd)
AGE (sec.) 48
AMBIENT WIND (ft./sec.) 140 ft AGL 12
CROSSWIND
≈10-12 ft/s @ 83 ft AGL
$\hat{V}_{\theta\ MAX}$ = 222 ft/s @ 83 ft AGL
$V_{\theta\ MAX}$ = 210 ft/s @ 83 ft AGL
LOWER SENSOR LEVEL LIMIT
SENSOR HEIGHT IN FEET (AGL)
140
130
120
110
100
90
80
70
60
56
50
40
140 120 100 80 60 40 20 0 20 40 60 80 100 120 140
TANGENTIAL VELOCITY, V_θ, ft./sec.

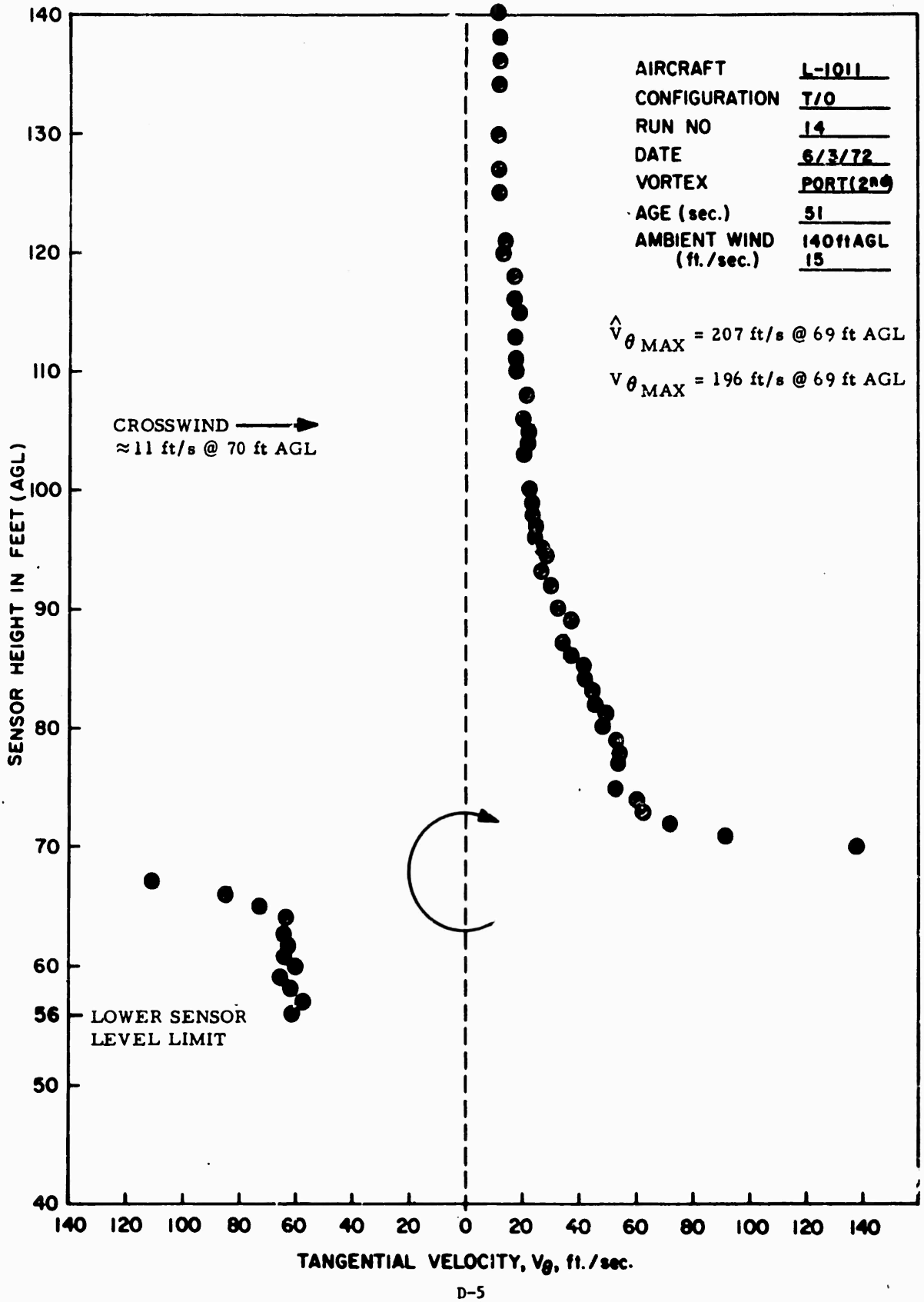
AIRCRAFT L-1011
CONFIGURATION T/O
RUN NO 14
DATE 6/3/72
VORTEX PORT(2nd)
AGE (sec.) 51
AMBIENT WIND (ft./sec.) 140ft AGL 15
$\hat{V}_{\theta\,MAX}$ = 207 ft/s @ 69 ft AGL
$V_{\theta\,MAX}$ = 196 ft/s @ 69 ft AGL
CROSSWIND ⟶
≈11 ft/s @ 70 ft AGL
LOWER SENSOR LEVEL LIMIT
SENSOR HEIGHT IN FEET (AGL)
140
130
120
110
100
90
80
70
60
56
50
40
140 120 100 80 60 40 20 0 20 40 60 80 100 120 140
TANGENTIAL VELOCITY, V_θ, ft./sec.

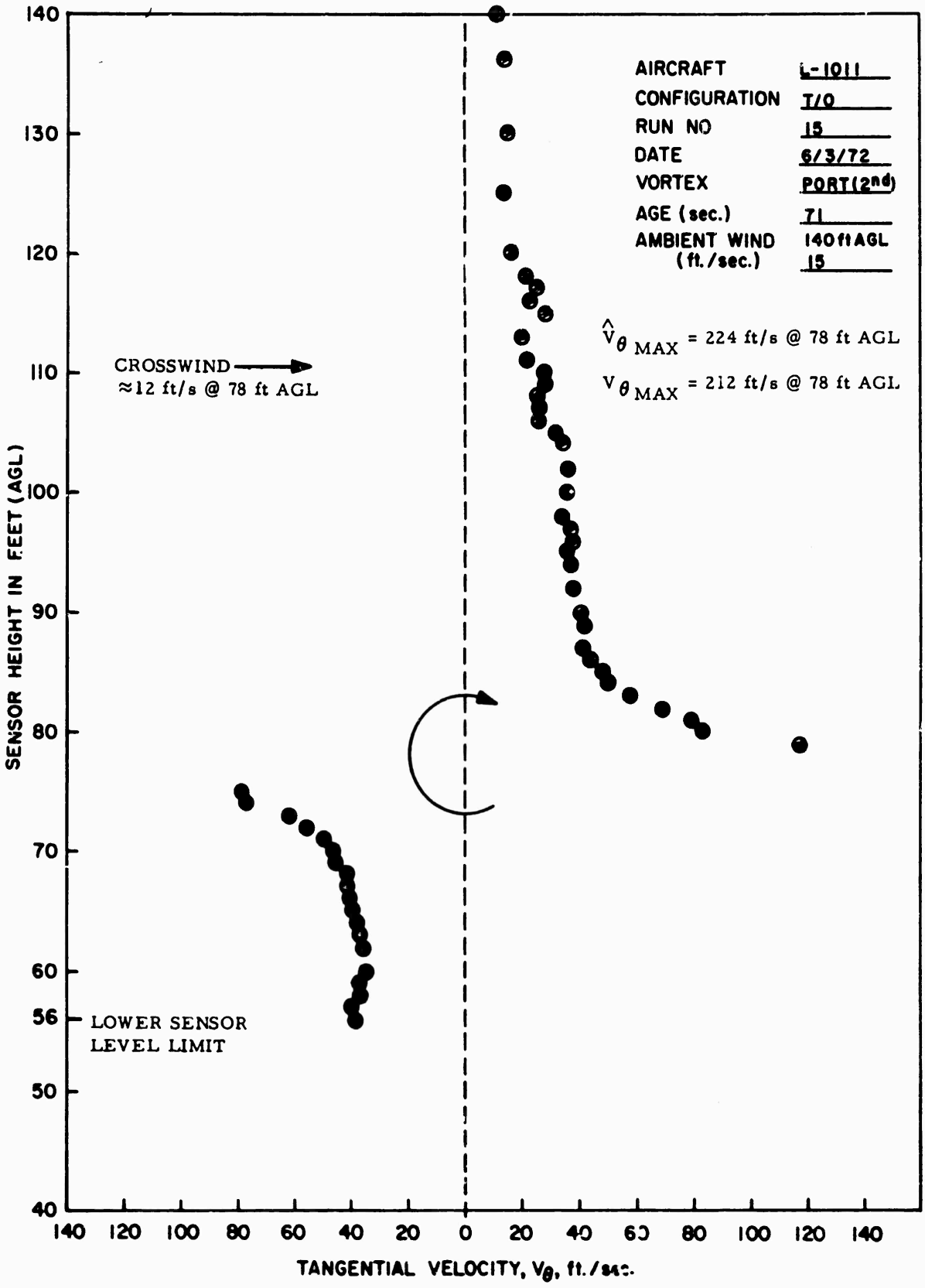
AIRCRAFT L-1011
CONFIGURATION T/O
RUN NO 15
DATE 6/3/72
VORTEX PORT(2nd)
AGE (sec.) 71
AMBIENT WIND (ft./sec.) 140 ft AGL 15
$\hat{V}_{\theta\ MAX}$ = 224 ft/s @ 78 ft AGL
$V_{\theta\ MAX}$ = 212 ft/s @ 78 ft AGL
CROSSWIND ≈12 ft/s @ 78 ft AGL
LOWER SENSOR LEVEL LIMIT
SENSOR HEIGHT IN FEET (AGL)
140
130
120
110
100
90
80
70
60
56
50
40
140 120 100 80 60 40 20 0 20 40 60 80 100 120 140
TANGENTIAL VELOCITY, V_θ, ft./sec.

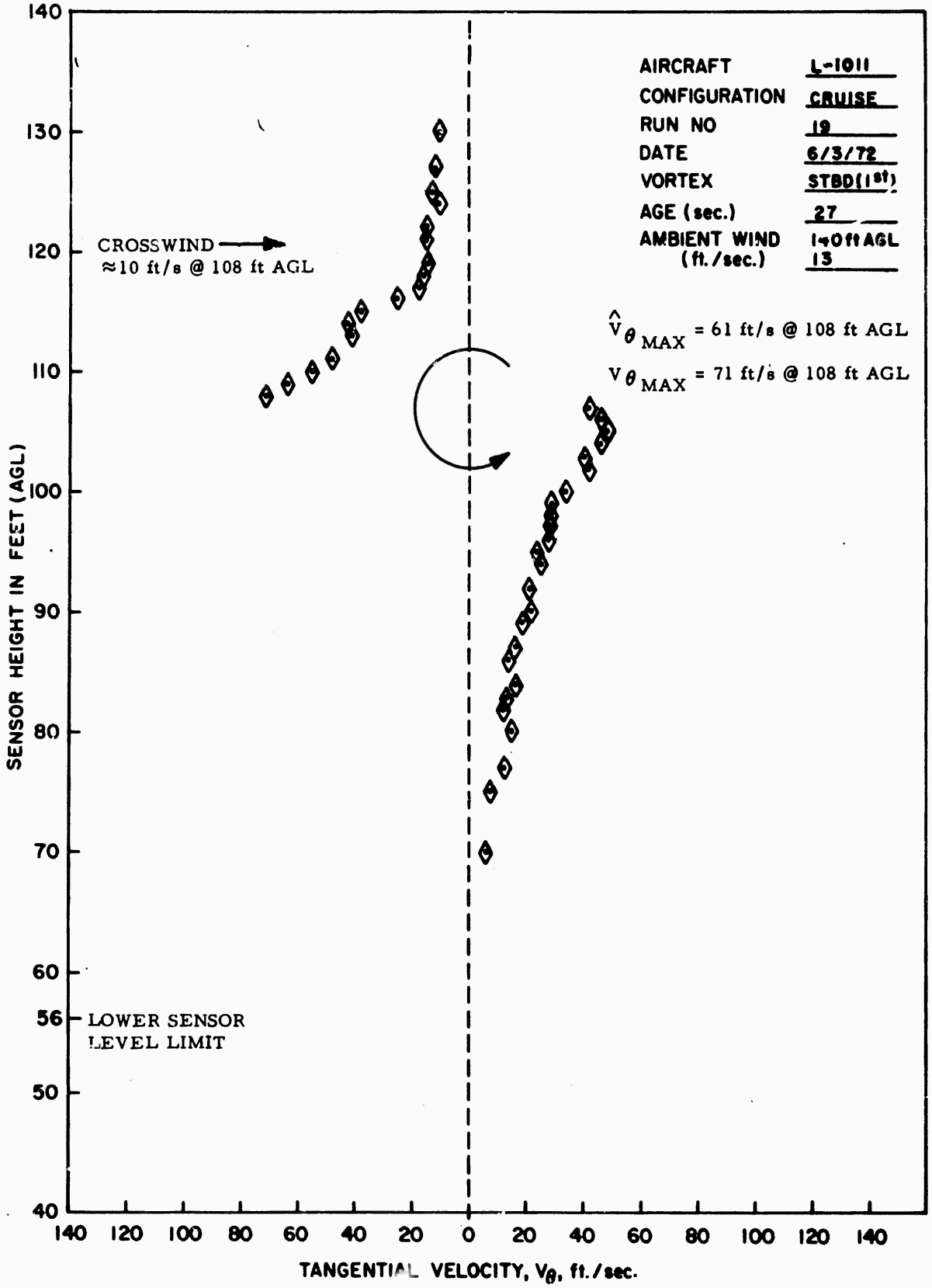
AIRCRAFT L-1011
CONFIGURATION CRUISE
RUN NO 19
DATE 6/3/72
VORTEX STBD(1ST)
AGE (sec.) 27
AMBIENT WIND (ft./sec.) 140ft AGL 13
CROSSWIND
≈10 ft/s @ 108 ft AGL
$\hat{V}_{\theta\ MAX}$ = 61 ft/s @ 108 ft AGL
$V_{\theta\ MAX}$ = 71 ft/s @ 108 ft AGL
LOWER SENSOR LEVEL LIMIT
SENSOR HEIGHT IN FEET (AGL)
140
130
120
110
100
90
80
70
60
56
50
40
140 120 100 80 60 40 20 0 20 40 60 80 100 120 140
TANGENTIAL VELOCITY, V_θ, ft./sec.

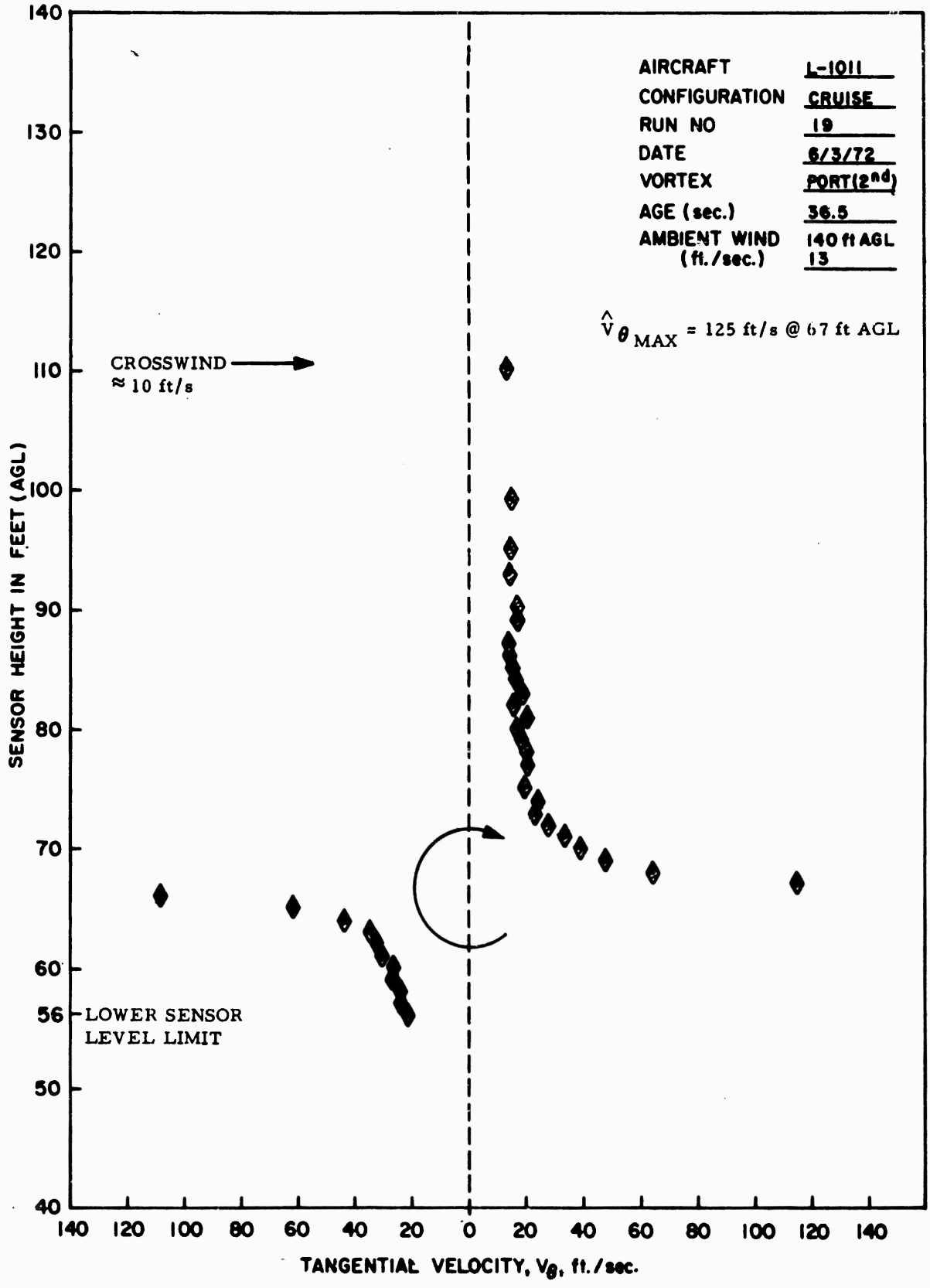
AIRCRAFT L-1011
CONFIGURATION CRUISE
RUN NO 19
DATE 6/3/72
VORTEX PORT(2nd)
AGE (sec.) 36.5
AMBIENT WIND (ft./sec.) 140 ft AGL 13
$\hat{V}_{\theta\,MAX}$ = 125 ft/s @ 67 ft AGL
CROSSWIND ≈ 10 ft/s
LOWER SENSOR LEVEL LIMIT
SENSOR HEIGHT IN FEET (AGL)
140
130
120
110
100
90
80
70
60
56
50
40
140 120 100 80 60 40 20 0 20 40 60 80 100 120 140
TANGENTIAL VELOCITY, V_θ, ft./sec.

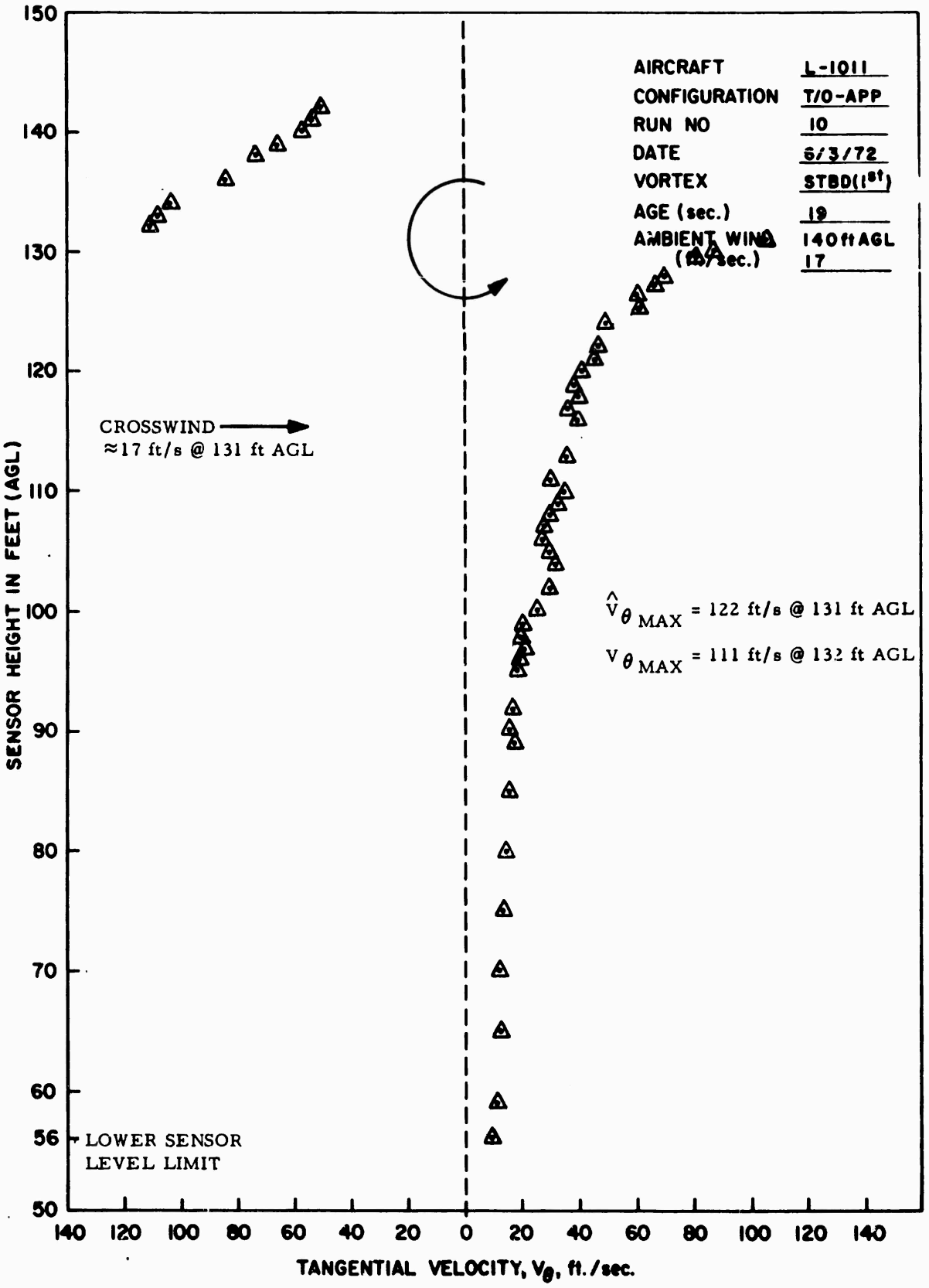
AIRCRAFT L-1011
CONFIGURATION T/O-APP
RUN NO 10
DATE 6/3/72
VORTEX STBD(1ST)
AGE (sec.) 19
AMBIENT WIND 140 ft AGL
(ft/sec.) 17
CROSSWIND
≈17 ft/s @ 131 ft AGL
$\hat{V}_{\theta\,MAX}$ = 122 ft/s @ 131 ft AGL
$V_{\theta\,MAX}$ = 111 ft/s @ 132 ft AGL
LOWER SENSOR
LEVEL LIMIT
SENSOR HEIGHT IN FEET (AGL)
150
140
130
120
110
100
90
80
70
60
56
50
140 120 100 80 60 40 20 0 20 40 60 80 100 120 140
TANGENTIAL VELOCITY, V_θ, ft./sec.

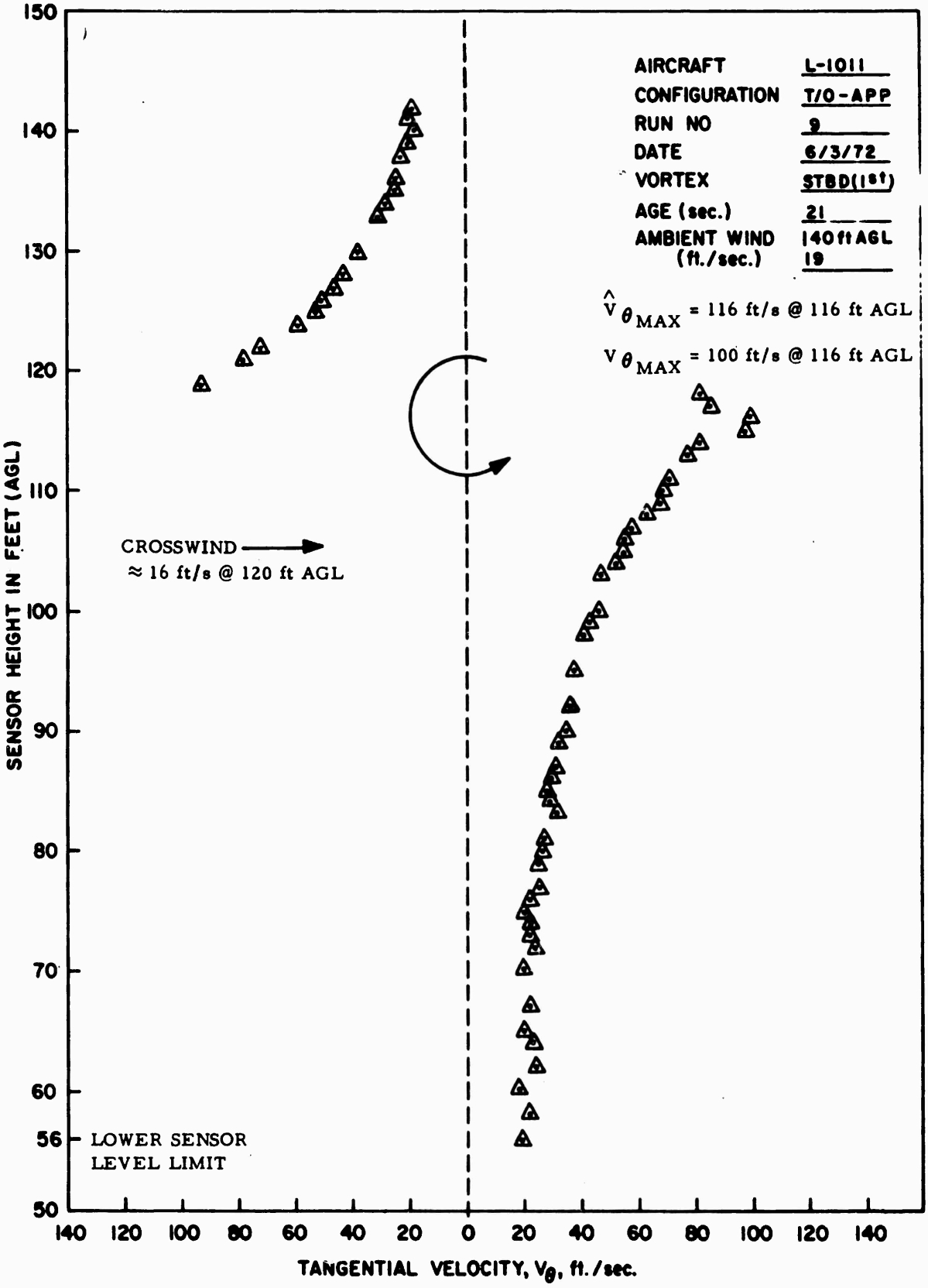
AIRCRAFT L-1011
CONFIGURATION T/O-APP
RUN NO 9
DATE 6/3/72
VORTEX STBD(1ST)
AGE (sec.) 21
AMBIENT WIND (ft./sec.) 140 ft AGL 19
$\hat{V}_{\theta MAX}$ = 116 ft/s @ 116 ft AGL
$V_{\theta MAX}$ = 100 ft/s @ 116 ft AGL
CROSSWIND
≈ 16 ft/s @ 120 ft AGL
LOWER SENSOR LEVEL LIMIT
SENSOR HEIGHT IN FEET (AGL)
150
140
130
120
110
100
90
80
70
60
56
50
140 120 100 80 60 40 20 0 20 40 60 80 100 120 140
TANGENTIAL VELOCITY, V_θ, ft./sec.

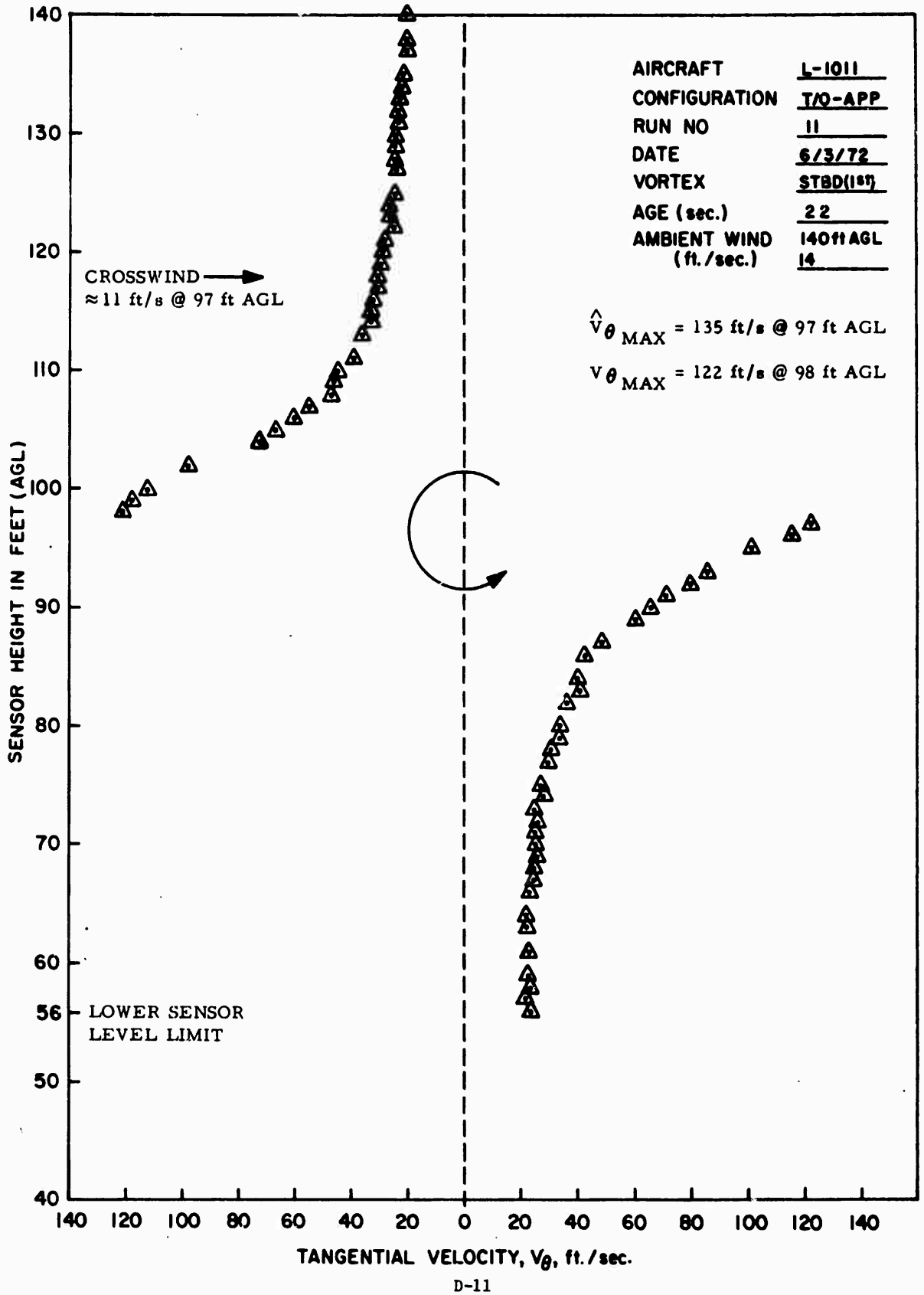
AIRCRAFT L-1011
CONFIGURATION T/O-APP
RUN NO 11
DATE 6/3/72
VORTEX STBD(1ST)
AGE (sec.) 22
AMBIENT WIND (ft./sec.) 140ft AGL 14
$\hat{V}_{\theta\ MAX}$ = 135 ft/s @ 97 ft AGL
$V_{\theta\ MAX}$ = 122 ft/s @ 98 ft AGL
CROSSWIND
≈11 ft/s @ 97 ft AGL
LOWER SENSOR LEVEL LIMIT
SENSOR HEIGHT IN FEET (AGL)
140
130
120
110
100
90
80
70
60
56
50
40
140 120 100 80 60 40 20 0 20 40 60 80 100 120 140
TANGENTIAL VELOCITY, V_θ, ft./sec.

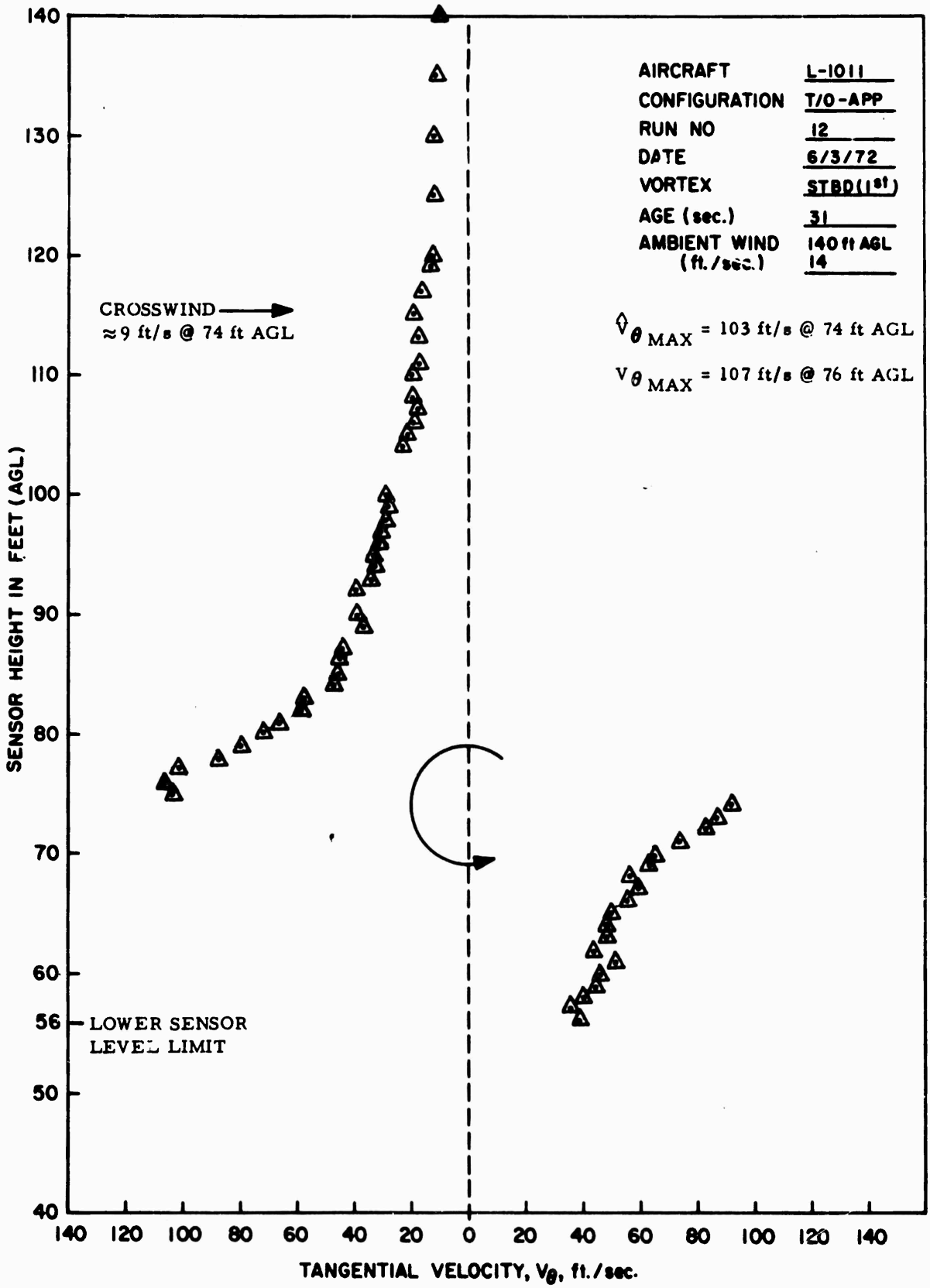
AIRCRAFT L-1011
CONFIGURATION T/O-APP
RUN NO 12
DATE 6/3/72
VORTEX STBD(1st)
AGE (sec.) 31
AMBIENT WIND (ft./sec.) 140 ft AGL 14
CROSSWIND
≈9 ft/s @ 74 ft AGL
$V_{\theta\ MAX}$ = 103 ft/s @ 74 ft AGL
$V_{\theta\ MAX}$ = 107 ft/s @ 76 ft AGL
LOWER SENSOR LEVEL LIMIT
SENSOR HEIGHT IN FEET (AGL)
140
130
120
110
100
90
80
70
60
56
50
40
140 120 100 80 60 40 20 0 20 40 60 80 100 120 140
TANGENTIAL VELOCITY, V_θ, ft./sec.

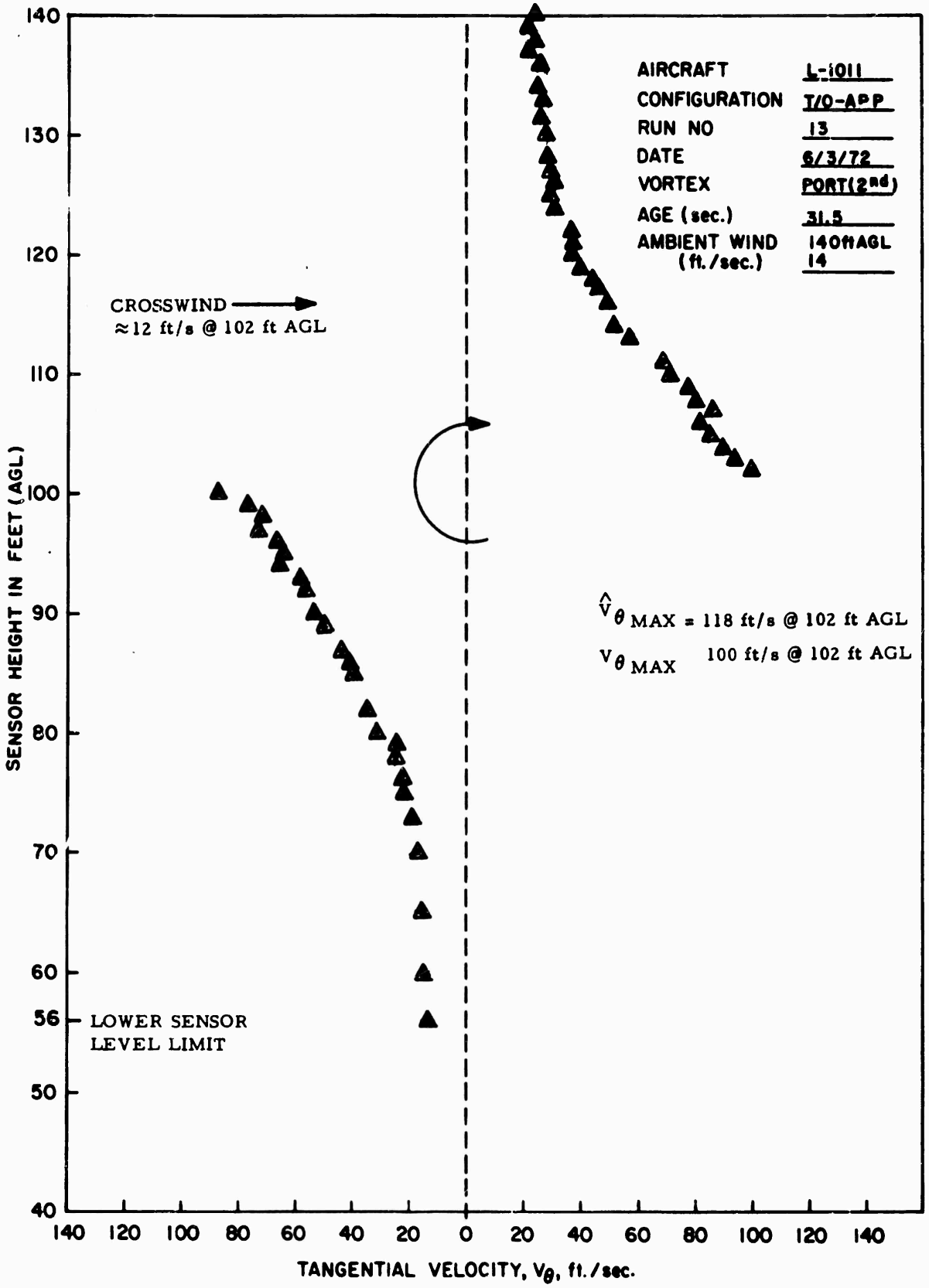
AIRCRAFT L-1011
CONFIGURATION T/O-APP
RUN NO 13
DATE 6/3/72
VORTEX PORT(2nd)
AGE (sec.) 31.5
AMBIENT WIND (ft./sec.) 140ftAGL 14
CROSSWIND ≈12 ft/s @ 102 ft AGL
$\hat{V}_{\theta\,MAX}$ = 118 ft/s @ 102 ft AGL
$V_{\theta\,MAX}$ 100 ft/s @ 102 ft AGL
LOWER SENSOR LEVEL LIMIT
SENSOR HEIGHT IN FEET (AGL)
140
130
120
110
100
90
80
70
60
56
50
40
140 120 100 80 60 40 20 0 20 40 60 80 100 120 140
TANGENTIAL VELOCITY, V_θ, ft./sec.

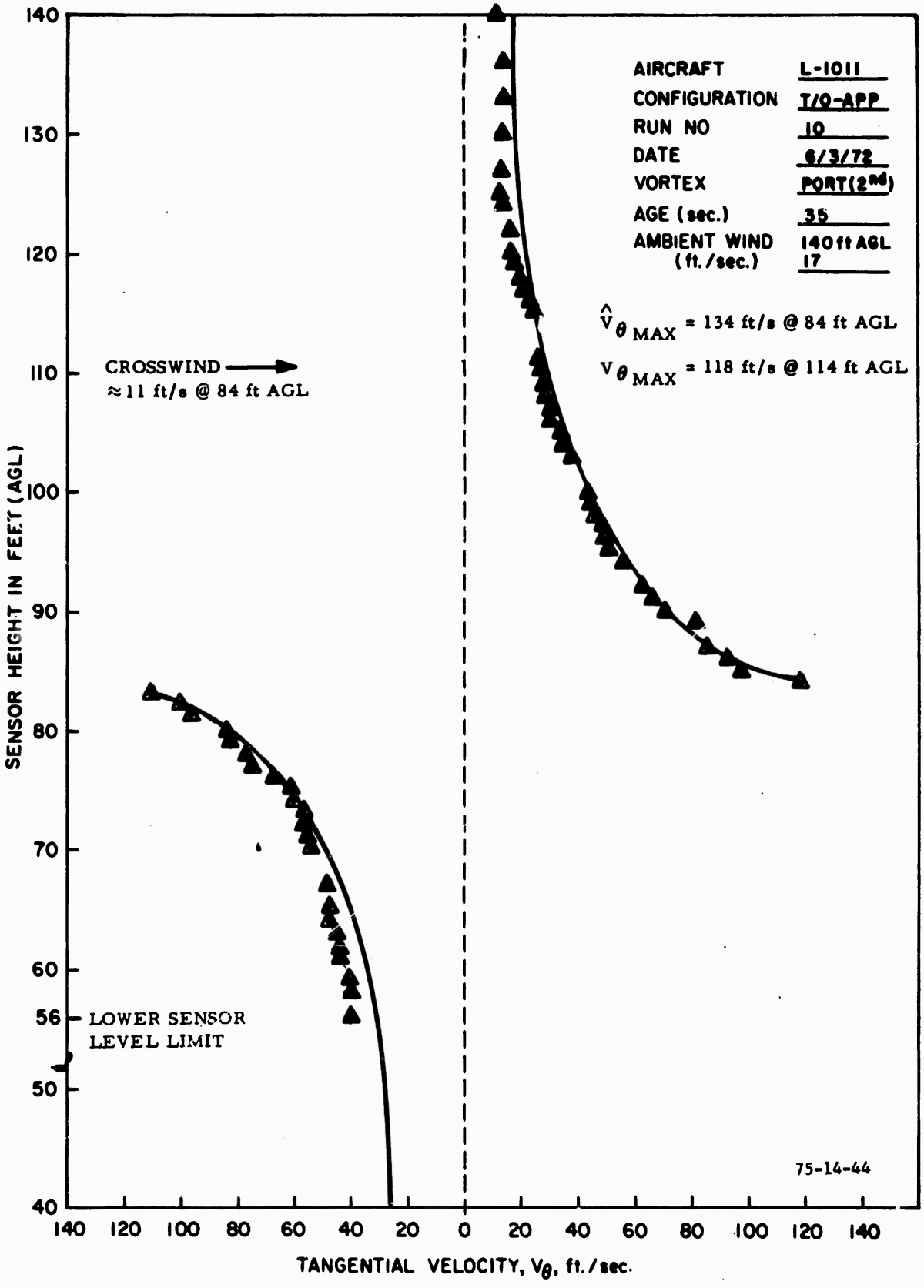
AIRCRAFT L-1011
CONFIGURATION T/O-APP
RUN NO 10
DATE 6/3/72
VORTEX PORT(2nd)
AGE (sec.) 35
AMBIENT WIND (ft./sec.) 140 ft AGL 17
$\hat{V}_{\theta\ MAX}$ = 134 ft/s @ 84 ft AGL
$V_{\theta\ MAX}$ = 118 ft/s @ 114 ft AGL
CROSSWIND
≈11 ft/s @ 84 ft AGL
LOWER SENSOR LEVEL LIMIT
75-14-44
SENSOR HEIGHT IN FEET (AGL)
TANGENTIAL VELOCITY, V_θ, ft./sec.
140
130
120
110
100
90
80
70
60
56
50
40
140 120 100 80 60 40 20 0 20 40 60 80 100 120 140

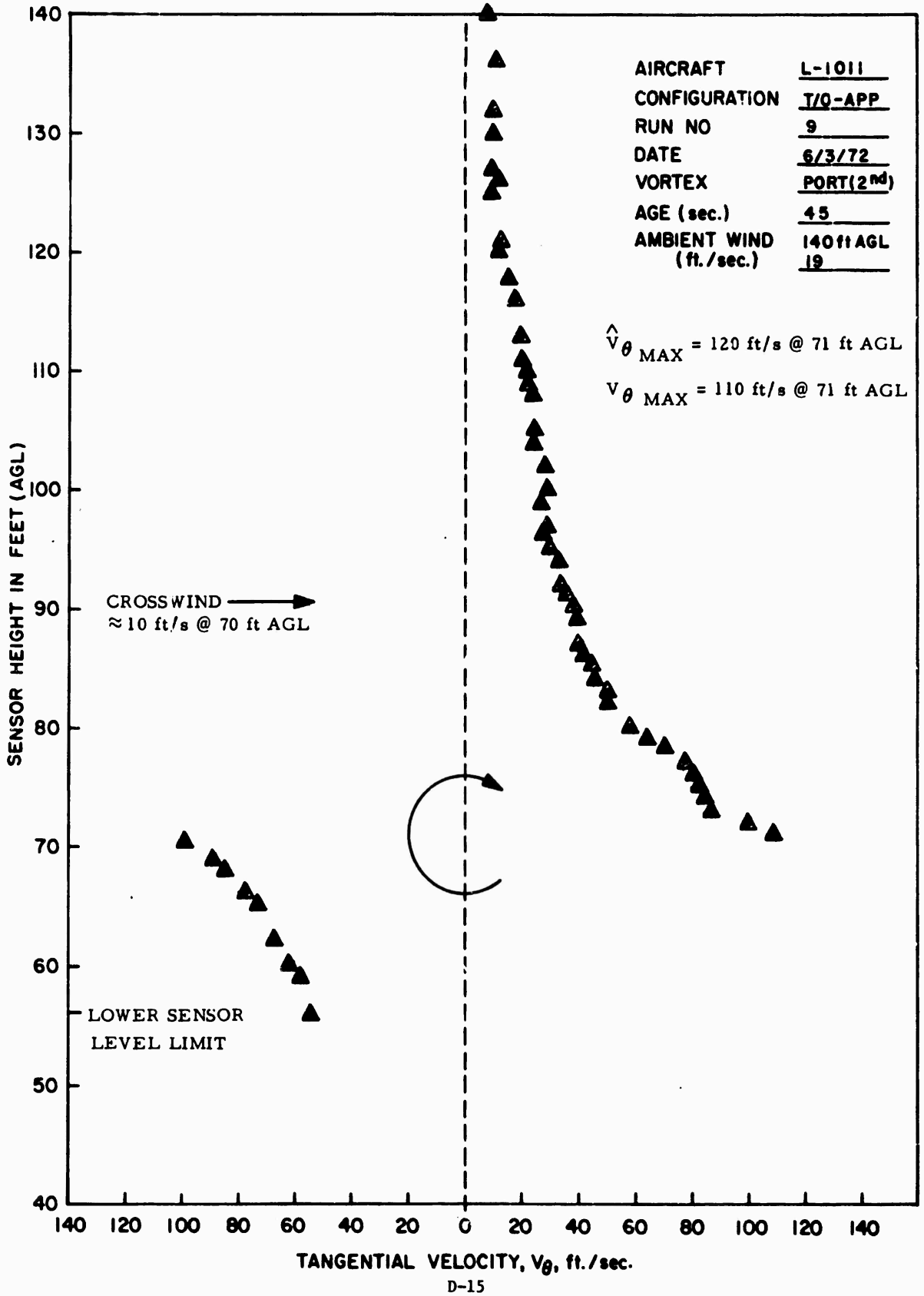
AIRCRAFT L-1011
CONFIGURATION T/O-APP
RUN NO 9
DATE 6/3/72
VORTEX PORT(2nd)
AGE (sec.) 45
AMBIENT WIND (ft./sec.) 140 ft AGL 19
$\hat{V}_{\theta\ MAX}$ = 120 ft/s @ 71 ft AGL
$V_{\theta\ MAX}$ = 110 ft/s @ 71 ft AGL
CROSSWIND ≈10 ft/s @ 70 ft AGL
LOWER SENSOR LEVEL LIMIT
SENSOR HEIGHT IN FEET (AGL)
140
130
120
110
100
90
80
70
60
50
40
140 120 100 80 60 40 20 0 20 40 60 80 100 120 140
TANGENTIAL VELOCITY, V_θ, ft./sec.

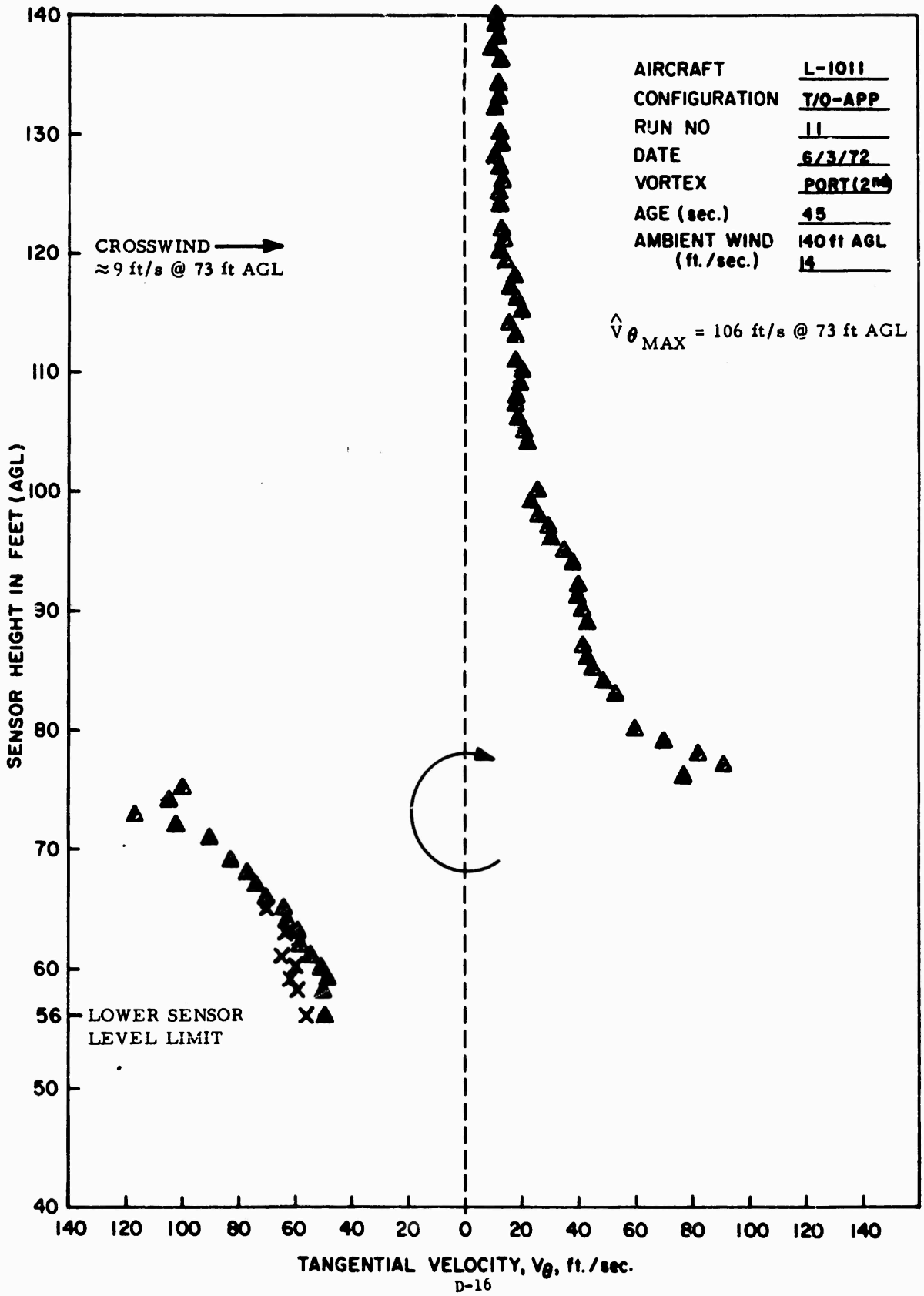
AIRCRAFT L-1011
CONFIGURATION T/O-APP
RUN NO 11
DATE 6/3/72
VORTEX PORT(2nd)
AGE (sec.) 45
AMBIENT WIND (ft./sec.) 140 ft AGL 14
$\hat{V}_{\theta_{MAX}}$ = 106 ft/s @ 73 ft AGL
CROSSWIND ⟶
≈9 ft/s @ 73 ft AGL
LOWER SENSOR LEVEL LIMIT
SENSOR HEIGHT IN FEET (AGL)
140
130
120
110
100
90
80
70
60
56
50
40
140 120 100 80 60 40 20 0 20 40 60 80 100 120 140
TANGENTIAL VELOCITY, V_θ, ft./sec.

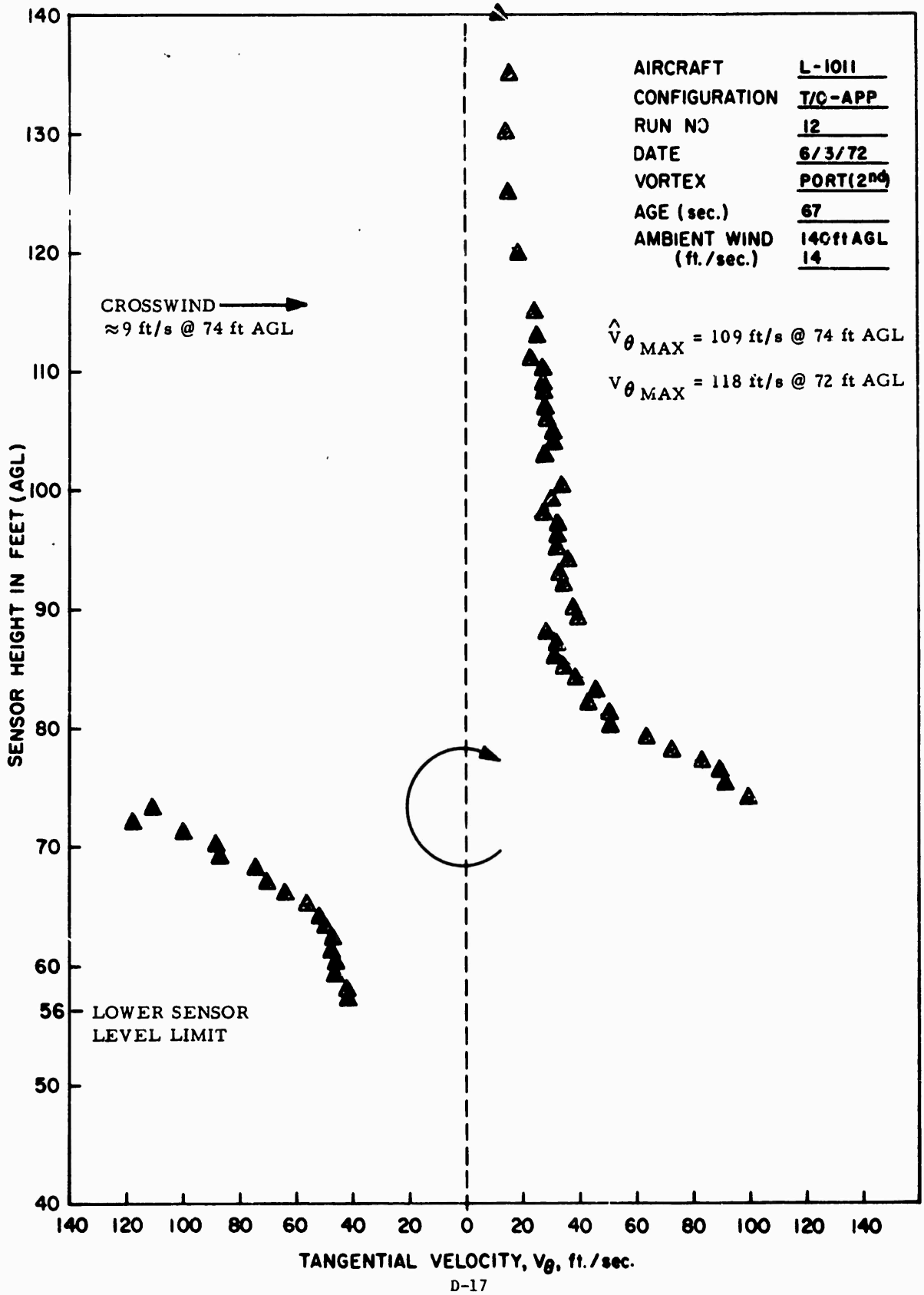
AIRCRAFT L-1011
CONFIGURATION T/O-APP
RUN NO 12
DATE 6/3/72
VORTEX PORT(2nd)
AGE (sec.) 67
AMBIENT WIND (ft./sec.) 140ft AGL 14
CROSSWIND
≈9 ft/s @ 74 ft AGL
$\hat{V}_{\theta\,MAX}$ = 109 ft/s @ 74 ft AGL
$V_{\theta\,MAX}$ = 118 ft/s @ 72 ft AGL
LOWER SENSOR LEVEL LIMIT
SENSOR HEIGHT IN FEET (AGL)
140
130
120
110
100
90
80
70
60
56
50
40
140 120 100 80 60 40 20 0 20 40 60 80 100 120 140
TANGENTIAL VELOCITY, V_θ, ft./sec.

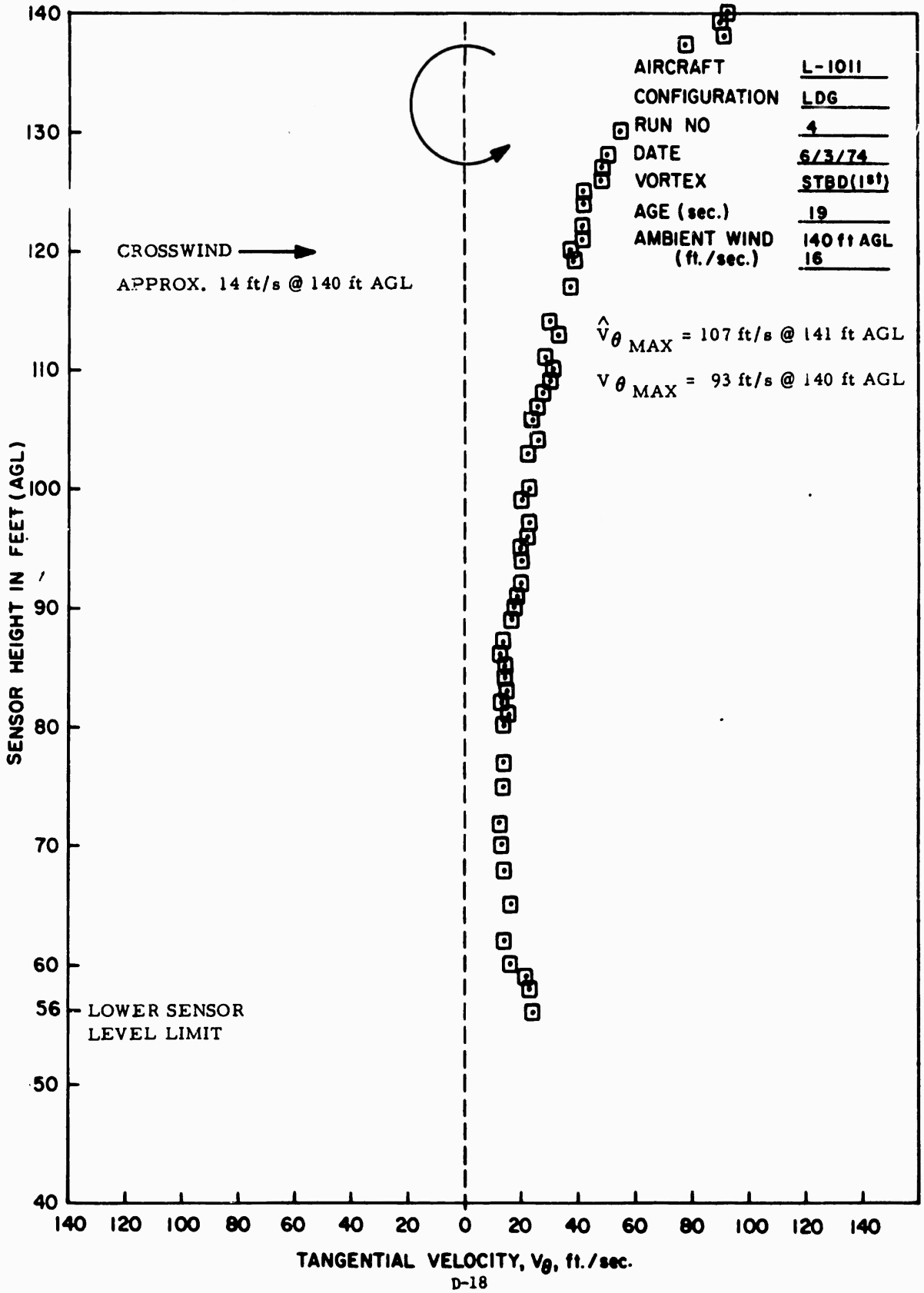
AIRCRAFT L-1011
CONFIGURATION LDG
RUN NO 4
DATE 6/3/74
VORTEX STBD(1st)
AGE (sec.) 19
AMBIENT WIND (ft./sec.) 140 ft AGL 16
CROSSWIND
APPROX. 14 ft/s @ 140 ft AGL
$\hat{V}_{\theta\ MAX}$ = 107 ft/s @ 141 ft AGL
$V_{\theta\ MAX}$ = 93 ft/s @ 140 ft AGL
LOWER SENSOR LEVEL LIMIT
SENSOR HEIGHT IN FEET (AGL)
140
130
120
110
100
90
80
70
60
56
50
40
140 120 100 80 60 40 20 0 20 40 60 80 100 120 140
TANGENTIAL VELOCITY, V_θ, ft./sec.

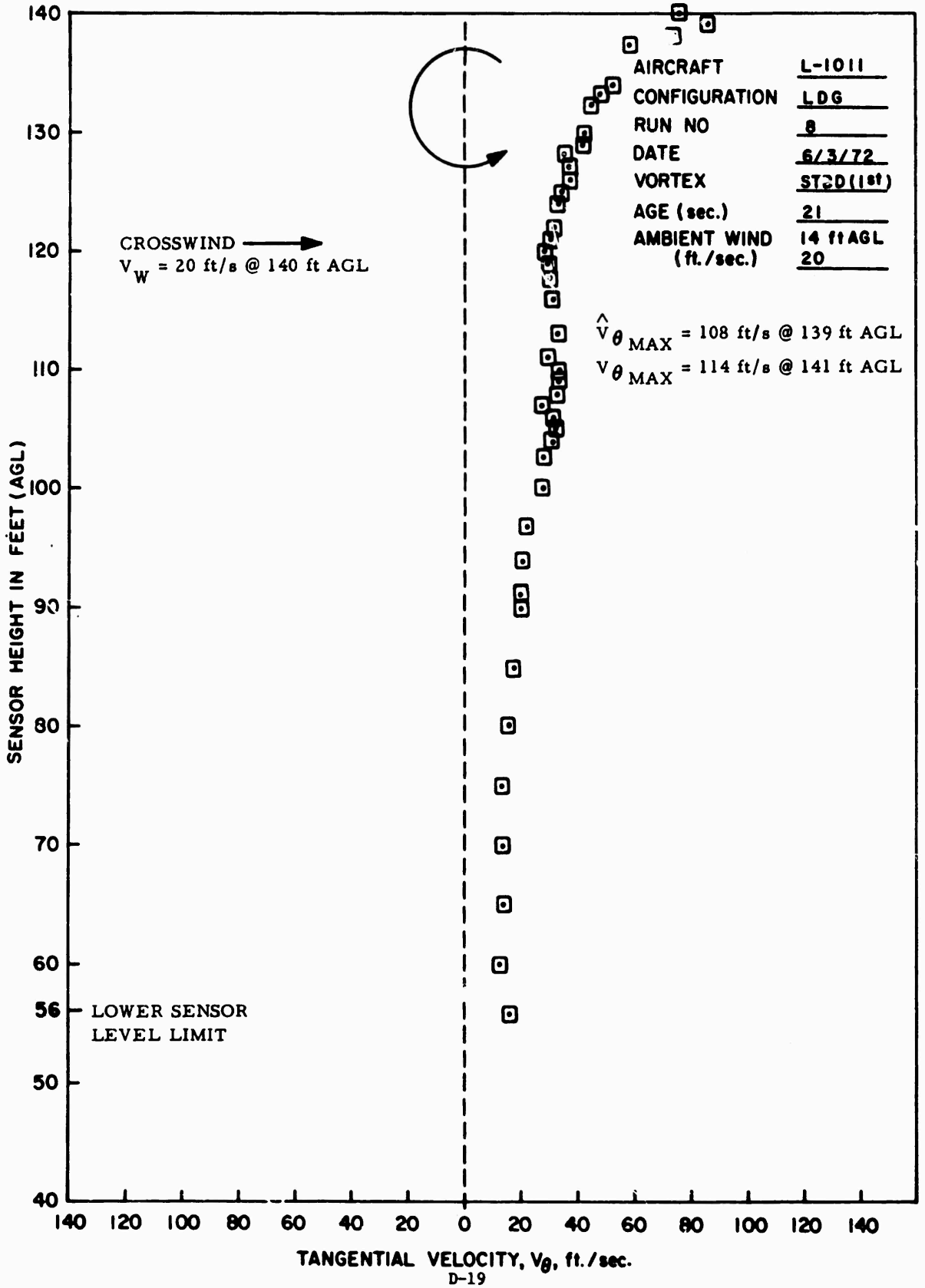
AIRCRAFT L-1011
CONFIGURATION LDG
RUN NO 8
DATE 6/3/72
VORTEX STBD (1st)
AGE (sec.) 21
AMBIENT WIND (ft./sec.) 14 ft AGL 20
CROSSWIND
V_W = 20 ft/s @ 140 ft AGL
$\hat{V}_{\theta\ MAX}$ = 108 ft/s @ 139 ft AGL
$V_{\theta\ MAX}$ = 114 ft/s @ 141 ft AGL
LOWER SENSOR LEVEL LIMIT
SENSOR HEIGHT IN FEET (AGL)
140
130
120
110
100
90
80
70
60
56
50
40
140 120 100 80 60 40 20 0 20 40 60 80 100 120 140
TANGENTIAL VELOCITY, V_θ, ft./sec.

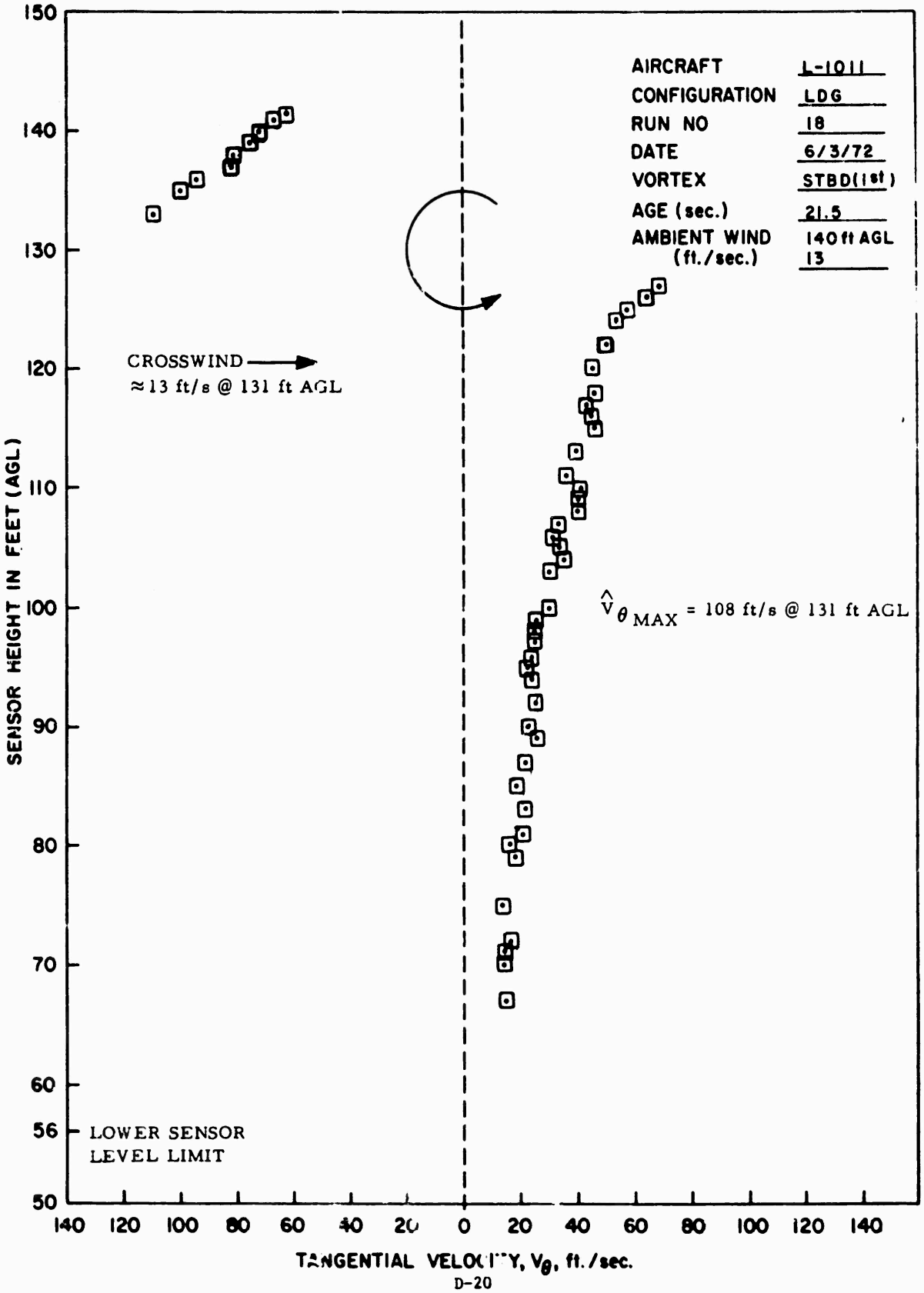
AIRCRAFT L-1011
CONFIGURATION LDG
RUN NO 18
DATE 6/3/72
VORTEX STBD(1st)
AGE (sec.) 21.5
AMBIENT WIND (ft./sec.) 140 ft AGL 13
CROSSWIND
≈13 ft/s @ 131 ft AGL
$\hat{V}_{\theta\,MAX}$ = 108 ft/s @ 131 ft AGL
LOWER SENSOR LEVEL LIMIT
SENSOR HEIGHT IN FEET (AGL)
150
140
130
120
110
100
90
80
70
60
56
50
140 120 100 80 60 40 20 0 20 40 60 80 100 120 140
TANGENTIAL VELOCITY, V_θ, ft./sec.

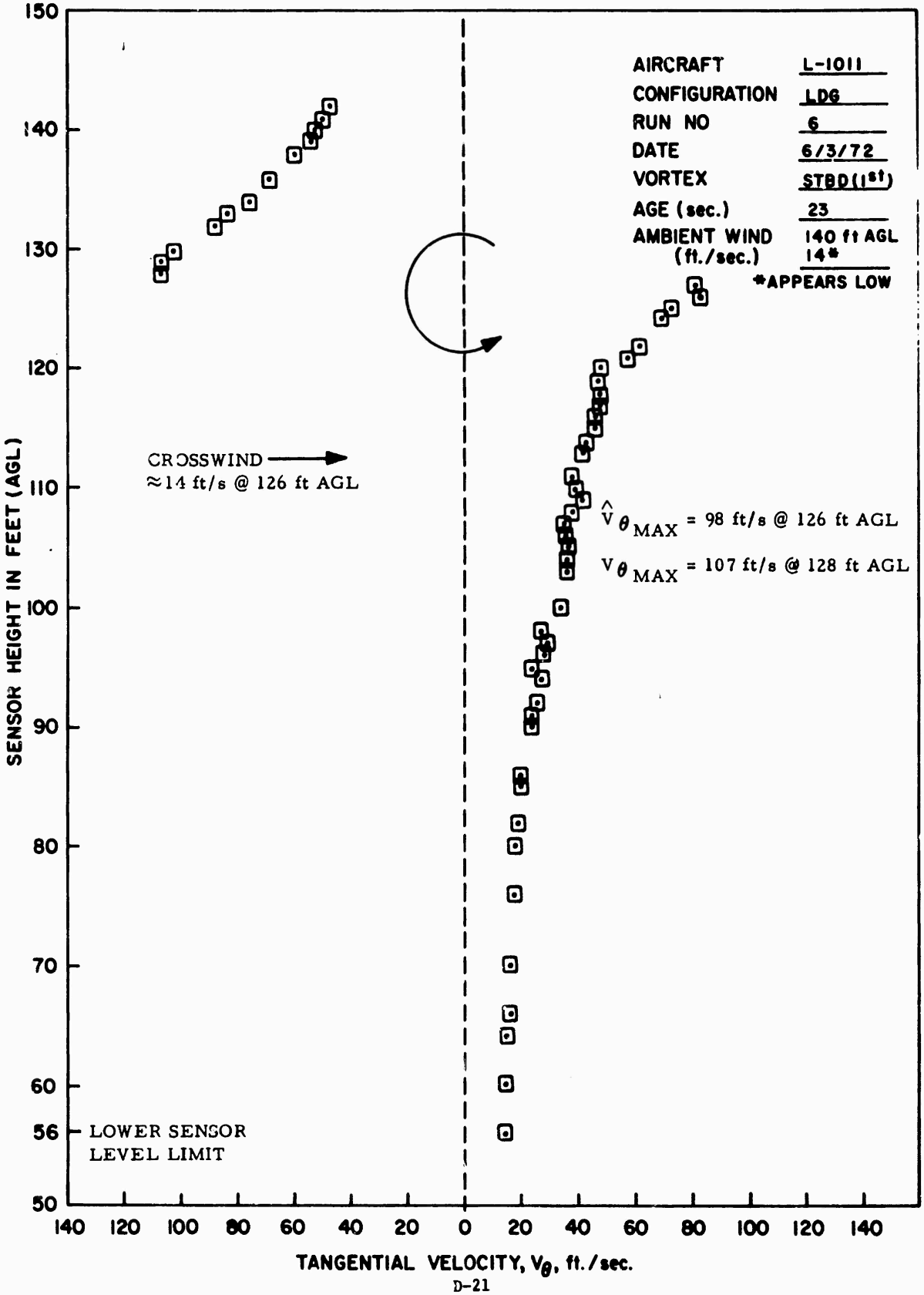
AIRCRAFT L-1011
CONFIGURATION LDG
RUN NO 6
DATE 6/3/72
VORTEX STBD(1st)
AGE (sec.) 23
AMBIENT WIND (ft./sec.) 140 ft AGL 14*
*APPEARS LOW
CROSSWIND
≈14 ft/s @ 126 ft AGL
$\hat{V}_{\theta\,MAX}$ = 98 ft/s @ 126 ft AGL
$V_{\theta\,MAX}$ = 107 ft/s @ 128 ft AGL
LOWER SENSOR LEVEL LIMIT
SENSOR HEIGHT IN FEET (AGL)
150
140
130
120
110
100
90
80
70
60
56
50
140 120 100 80 60 40 20 0 20 40 60 80 100 120 140
TANGENTIAL VELOCITY, V_θ, ft./sec.

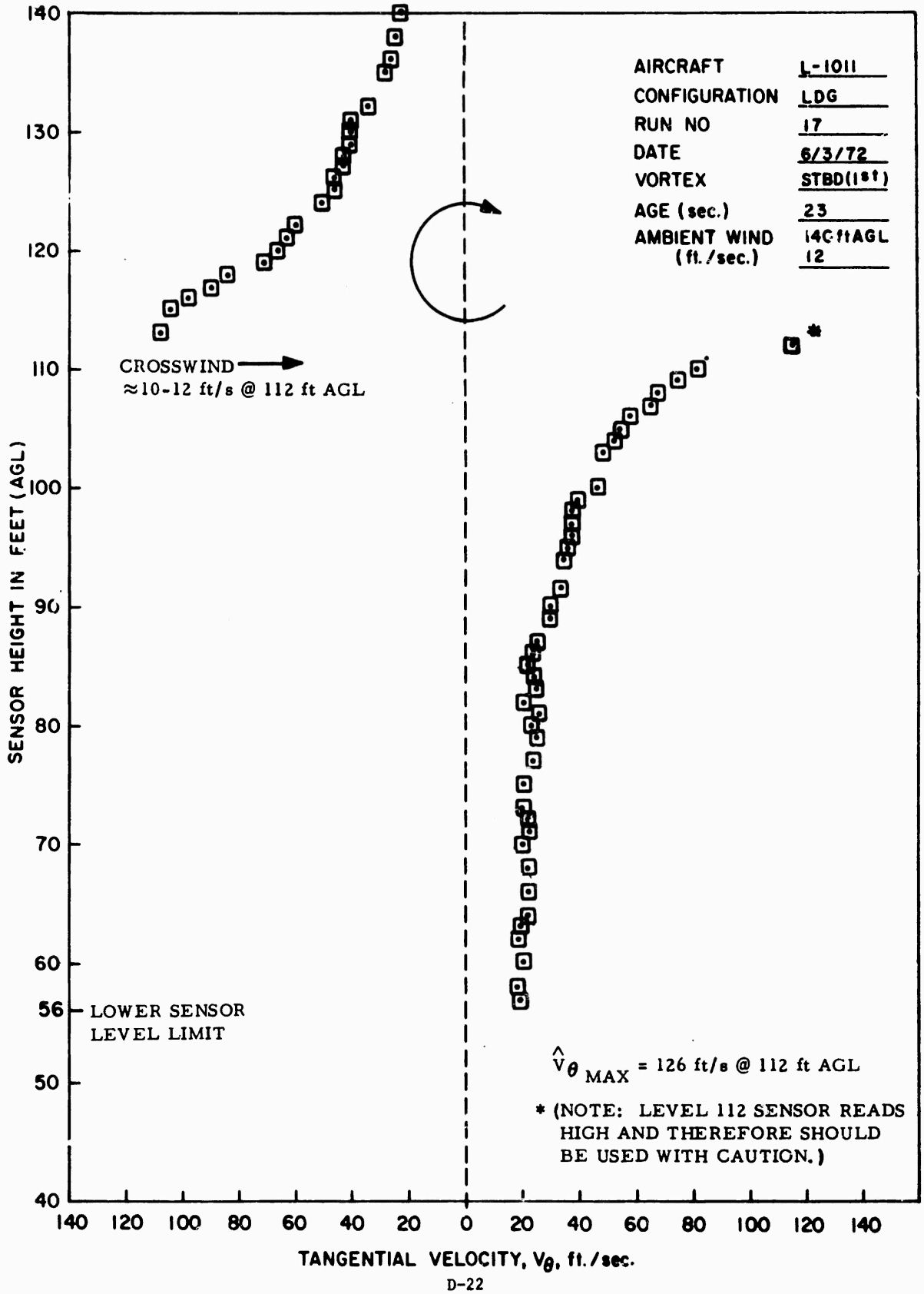
AIRCRAFT L-1011
CONFIGURATION LDG
RUN NO 17
DATE 6/3/72
VORTEX STBD(1st)
AGE (sec.) 23
AMBIENT WIND (ft./sec.) 14C ft AGL 12
CROSSWIND
≈10-12 ft/s @ 112 ft AGL
LOWER SENSOR LEVEL LIMIT
$\hat{V}_{\theta\ MAX}$ = 126 ft/s @ 112 ft AGL
* (NOTE: LEVEL 112 SENSOR READS HIGH AND THEREFORE SHOULD BE USED WITH CAUTION.)
SENSOR HEIGHT IN FEET (AGL)
140
130
120
110
100
90
80
70
60
56
50
40
140 120 100 80 60 40 20 0 20 40 60 80 100 120 140
TANGENTIAL VELOCITY, V_θ, ft./sec.

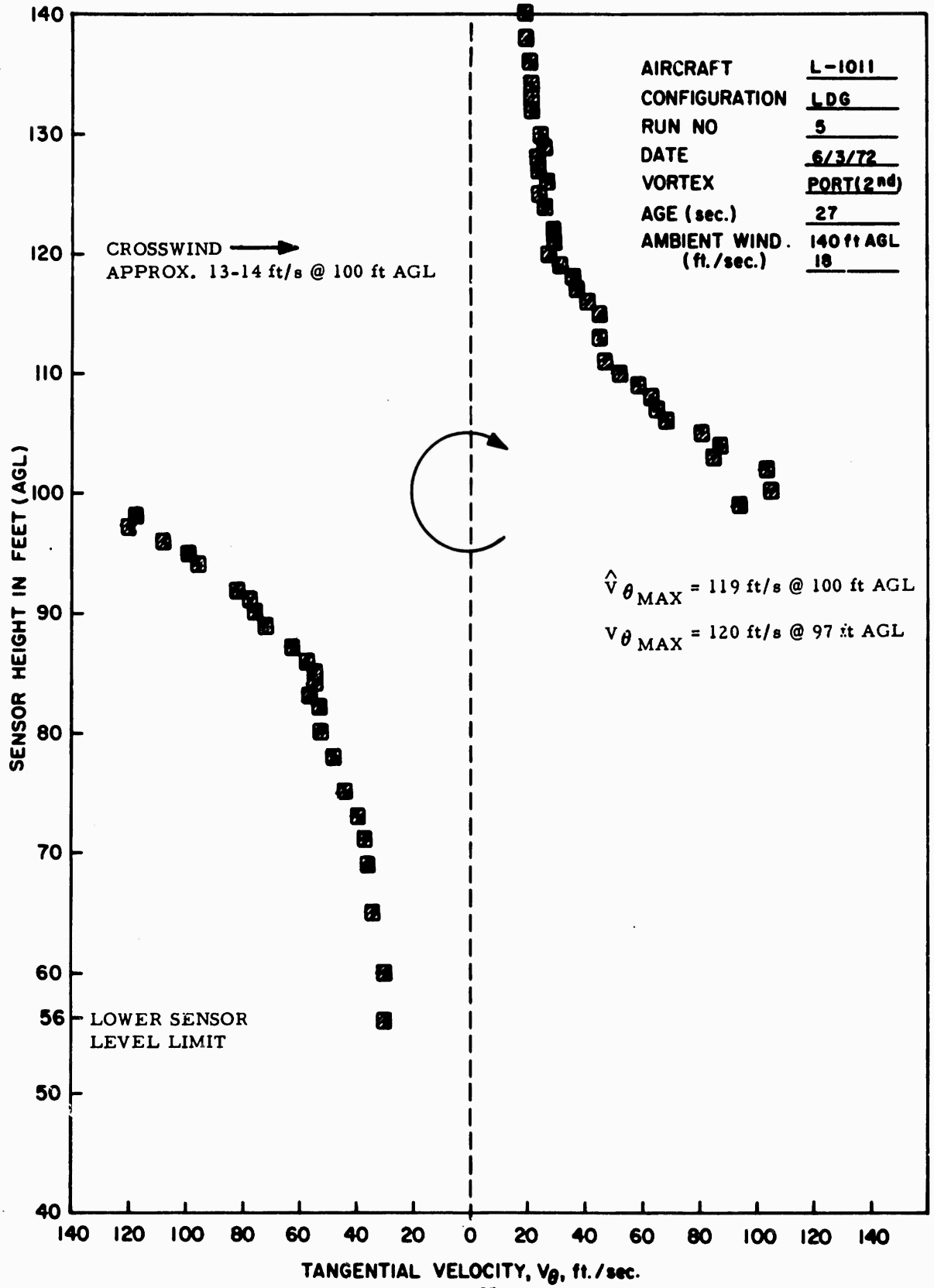
AIRCRAFT L-1011
CONFIGURATION LDG
RUN NO 5
DATE 6/3/72
VORTEX PORT(2nd)
AGE (sec.) 27
AMBIENT WIND. (ft./sec.) 140 ft AGL 18
CROSSWIND
APPROX. 13-14 ft/s @ 100 ft AGL
$\hat{V}_{\theta MAX}$ = 119 ft/s @ 100 ft AGL
$V_{\theta MAX}$ = 120 ft/s @ 97 ft AGL
LOWER SENSOR LEVEL LIMIT
SENSOR HEIGHT IN FEET (AGL)
140
130
120
110
100
90
80
70
60
56
50
40
140 120 100 80 60 40 20 0 20 40 60 80 100 120 140
TANGENTIAL VELOCITY, V_θ, ft./sec.

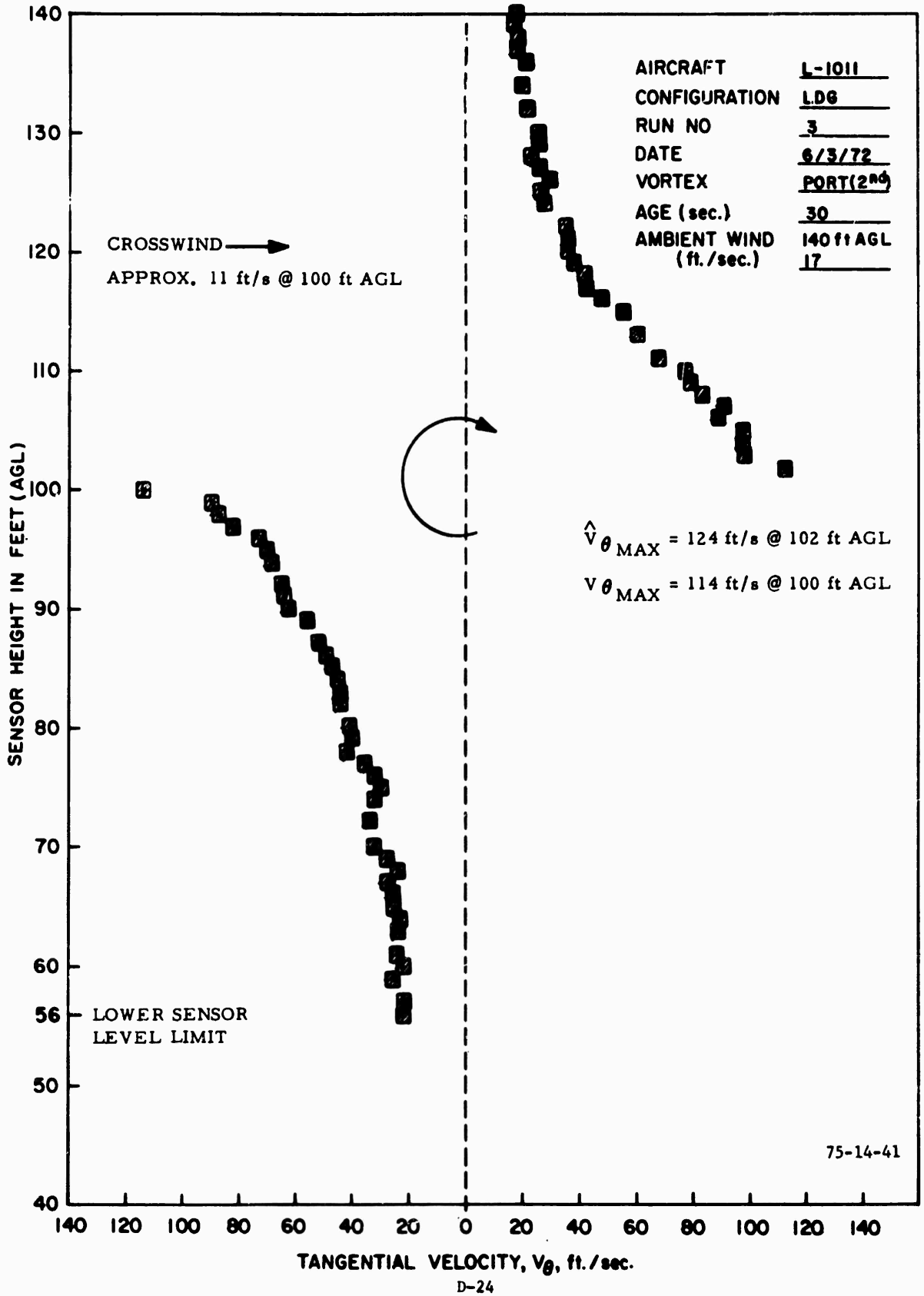
AIRCRAFT L-1011
CONFIGURATION LDG
RUN NO 3
DATE 6/3/72
VORTEX PORT(2ND)
AGE (sec.) 30
AMBIENT WIND (ft./sec.) 140 ft AGL 17
CROSSWIND
APPROX. 11 ft/s @ 100 ft AGL
$\hat{V}_{\theta\,MAX}$ = 124 ft/s @ 102 ft AGL
$V_{\theta\,MAX}$ = 114 ft/s @ 100 ft AGL
LOWER SENSOR LEVEL LIMIT
75-14-41
SENSOR HEIGHT IN FEET (AGL)
140
130
120
110
100
90
80
70
60
56
50
40
140 120 100 80 60 40 20 0 20 40 60 80 100 120 140
TANGENTIAL VELOCITY, V_θ, ft./sec.

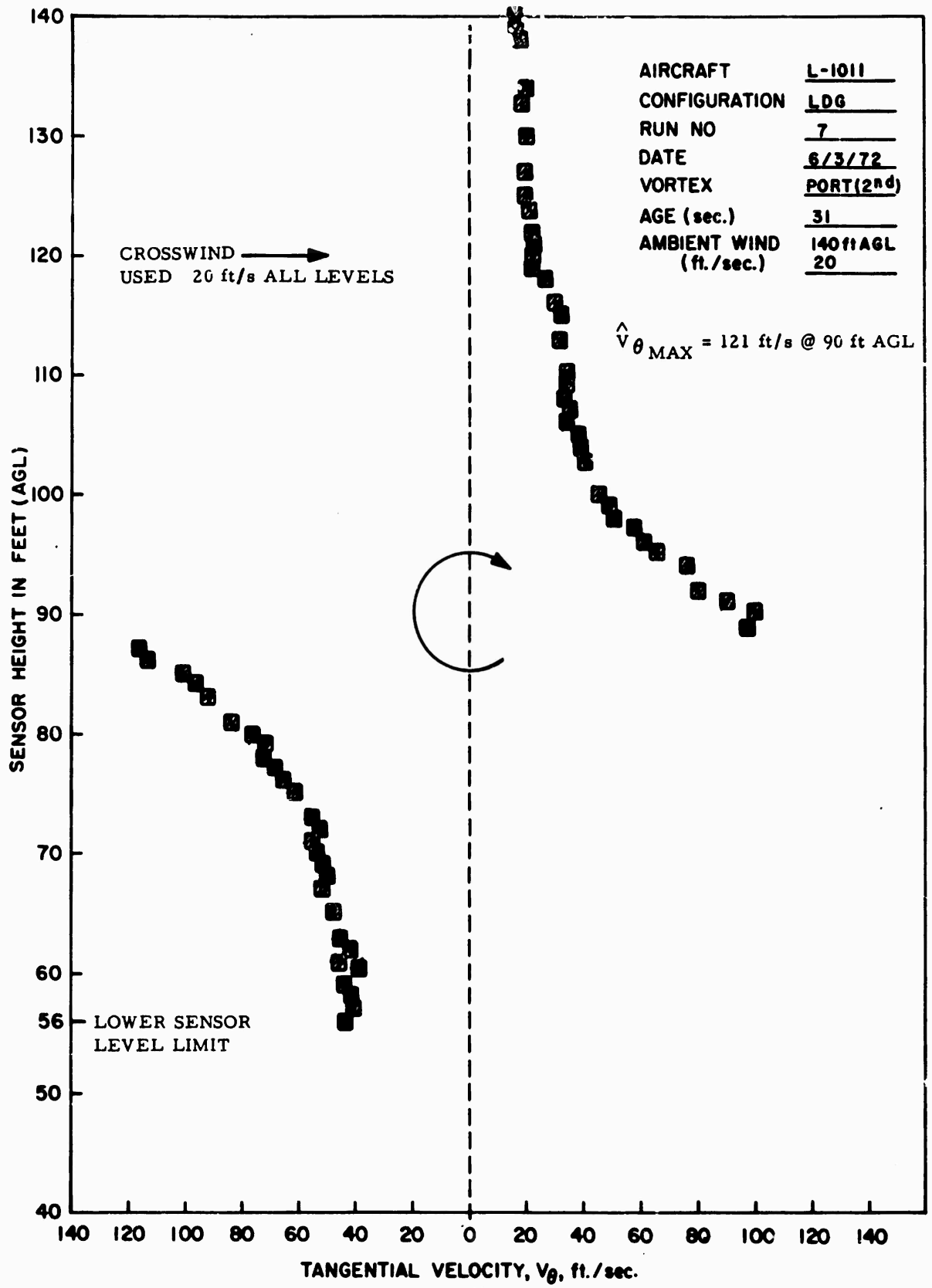
AIRCRAFT L-1011
CONFIGURATION LDG
RUN NO 7
DATE 6/3/72
VORTEX PORT(2nd)
AGE (sec.) 31
AMBIENT WIND (ft./sec.) 140 ft AGL 20
CROSSWIND
USED 20 ft/s ALL LEVELS
$\hat{V}_{\theta\,MAX}$ = 121 ft/s @ 90 ft AGL
LOWER SENSOR LEVEL LIMIT
SENSOR HEIGHT IN FEET (AGL)
140
130
120
110
100
90
80
70
60
56
50
40
140 120 100 80 60 40 20 0 20 40 60 80 100 120 140
TANGENTIAL VELOCITY, V_θ, ft./sec.

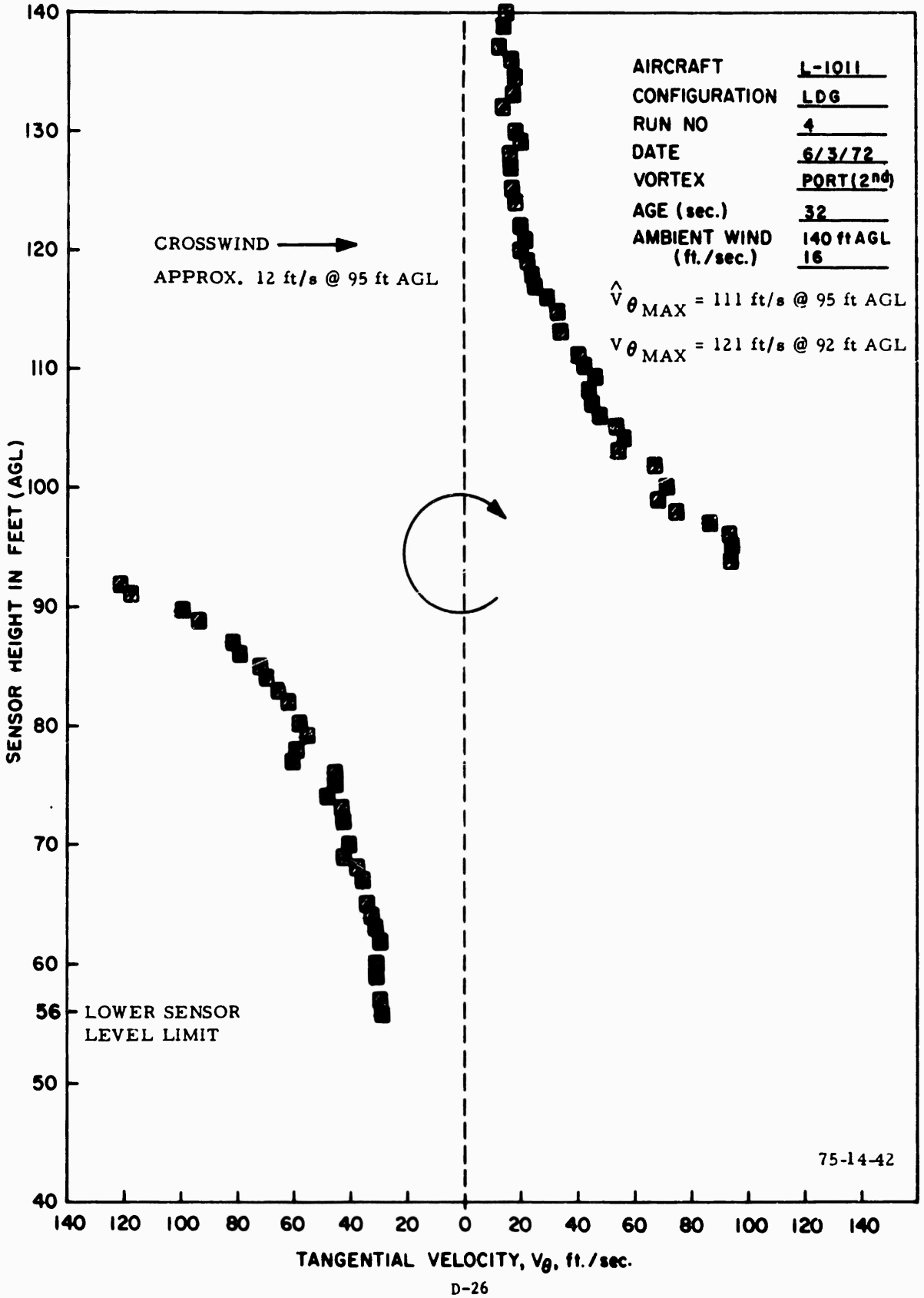
AIRCRAFT L-1011
CONFIGURATION LDG
RUN NO 4
DATE 6/3/72
VORTEX PORT(2nd)
AGE (sec.) 32
AMBIENT WIND (ft./sec.) 140 ft AGL 16
$\hat{V}_{\theta MAX}$ = 111 ft/s @ 95 ft AGL
$V_{\theta MAX}$ = 121 ft/s @ 92 ft AGL
CROSSWIND
APPROX. 12 ft/s @ 95 ft AGL
LOWER SENSOR LEVEL LIMIT
75-14-42
SENSOR HEIGHT IN FEET (AGL)
140 130 120 110 100 90 80 70 60 56 50 40
140 120 100 80 60 40 20 0 20 40 60 80 100 120 140
TANGENTIAL VELOCITY, V_θ, ft./sec.

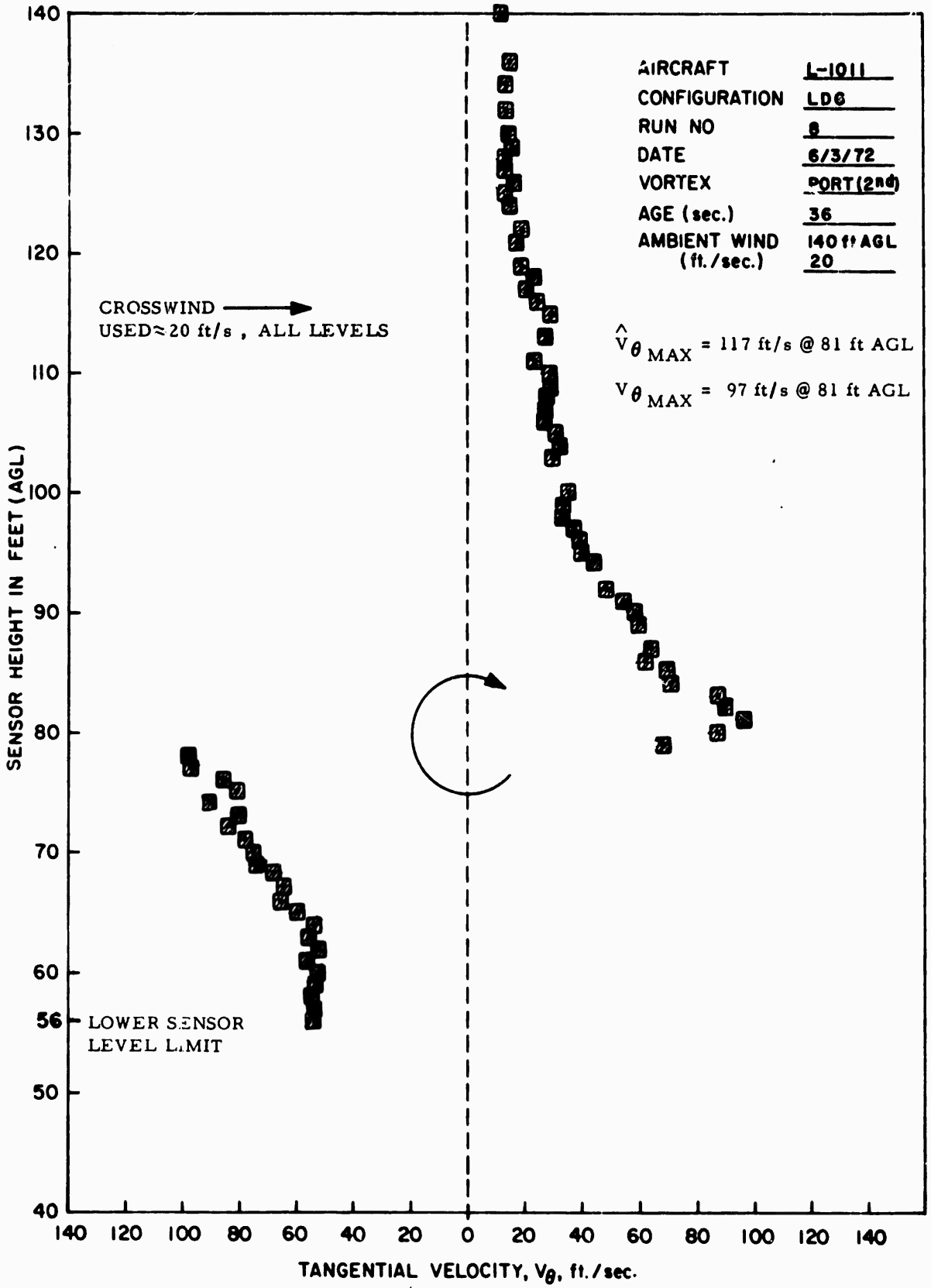
AIRCRAFT L-1011
CONFIGURATION LDG
RUN NO 8
DATE 6/3/72
VORTEX PORT (2nd)
AGE (sec.) 36
AMBIENT WIND (ft./sec.) 140 ft AGL 20
CROSSWIND → USED ≈ 20 ft/s, ALL LEVELS
$\hat{V}_{\theta\,MAX}$ = 117 ft/s @ 81 ft AGL
$V_{\theta\,MAX}$ = 97 ft/s @ 81 ft AGL
LOWER SENSOR LEVEL LIMIT
SENSOR HEIGHT IN FEET (AGL)
140
130
120
110
100
90
80
70
60
56
50
40
140 120 100 80 60 40 20 0 20 40 60 80 100 120 140
TANGENTIAL VELOCITY, V_θ, ft./sec.

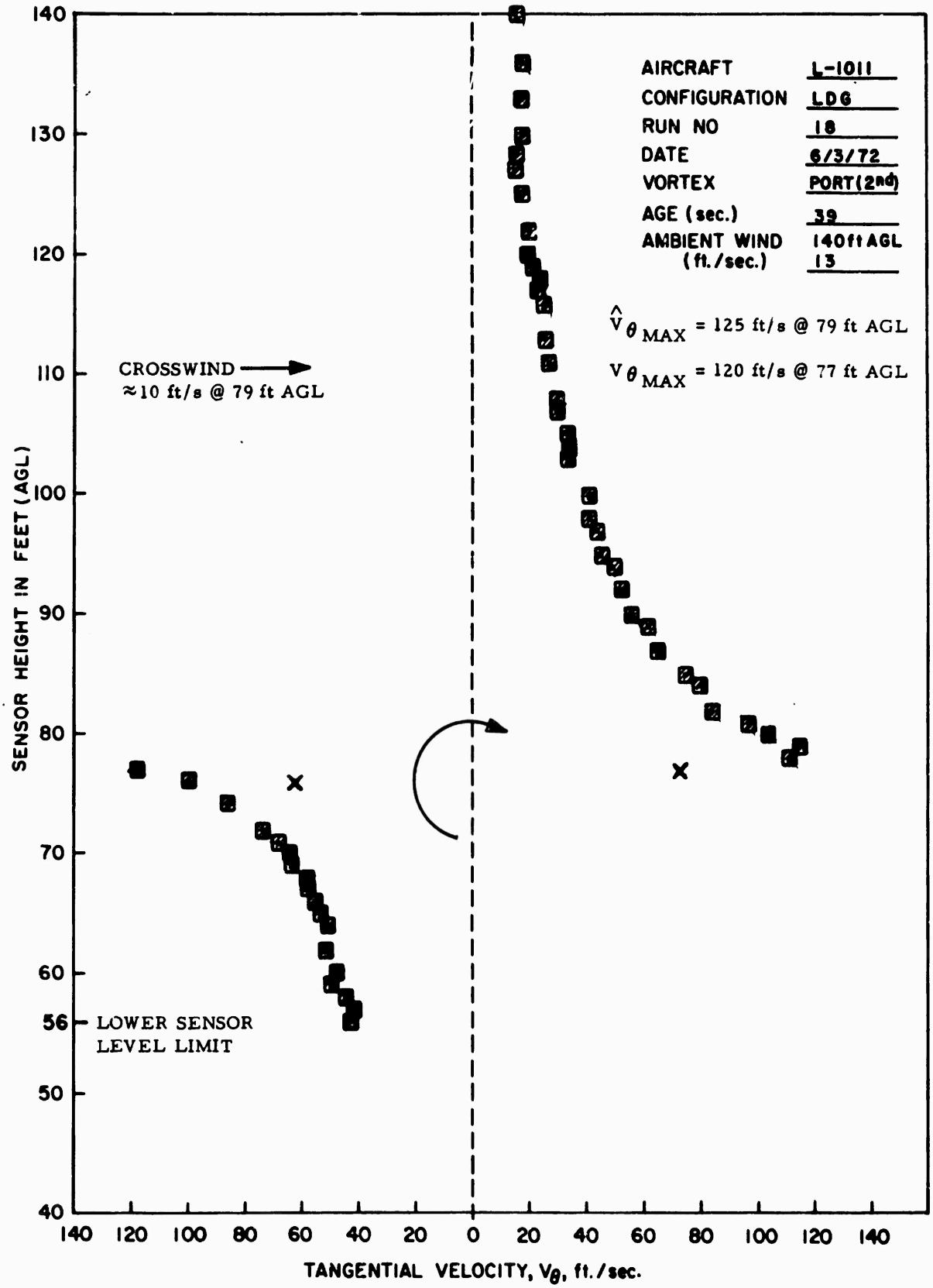
AIRCRAFT L-1011
CONFIGURATION LDG
RUN NO 18
DATE 6/3/72
VORTEX PORT(2nd)
AGE (sec.) 39
AMBIENT WIND (ft./sec.) 140ft AGL 13
$\hat{V}_{\theta\,MAX}$ = 125 ft/s @ 79 ft AGL
$V_{\theta\,MAX}$ = 120 ft/s @ 77 ft AGL
CROSSWIND
≈10 ft/s @ 79 ft AGL
LOWER SENSOR LEVEL LIMIT
SENSOR HEIGHT IN FEET (AGL)
140
130
120
110
100
90
80
70
60
56
50
40
140 120 100 80 60 40 20 0 20 40 60 80 100 120 140
TANGENTIAL VELOCITY, V_θ, ft./sec.

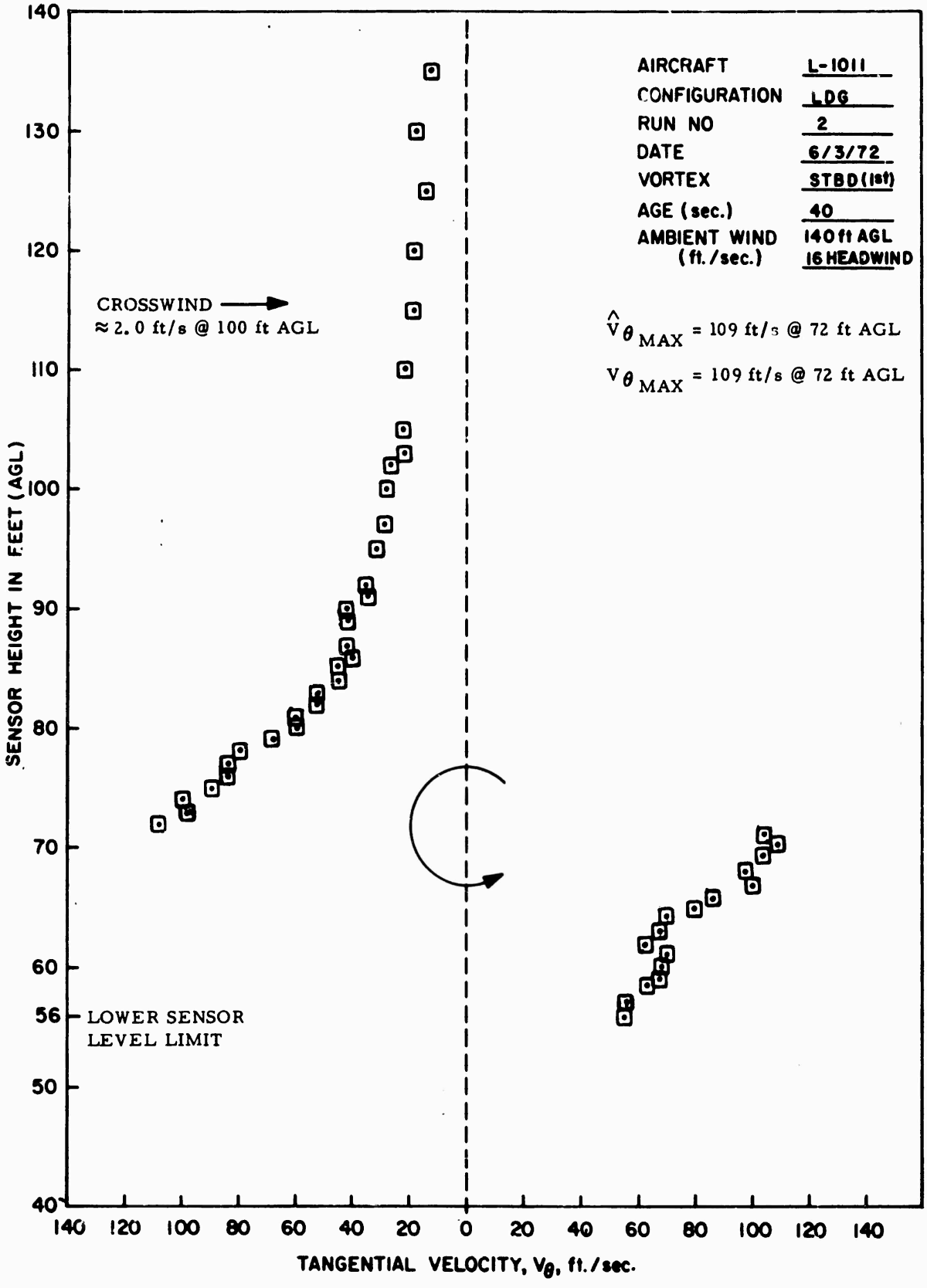
AIRCRAFT L-1011
CONFIGURATION LDG
RUN NO 2
DATE 6/3/72
VORTEX STBD (1st)
AGE (sec.) 40
AMBIENT WIND (ft./sec.) 140 ft AGL 16 HEADWIND
CROSSWIND ⟶
≈ 2.0 ft/s @ 100 ft AGL
$\hat{V}_{\theta\ MAX}$ = 109 ft/s @ 72 ft AGL
$V_{\theta\ MAX}$ = 109 ft/s @ 72 ft AGL
LOWER SENSOR LEVEL LIMIT
SENSOR HEIGHT IN FEET (AGL)
140
130
120
110
100
90
80
70
60
56
50
40
140 120 100 80 60 40 20 0 20 40 60 80 100 120 140
TANGENTIAL VELOCITY, V_θ, ft./sec.

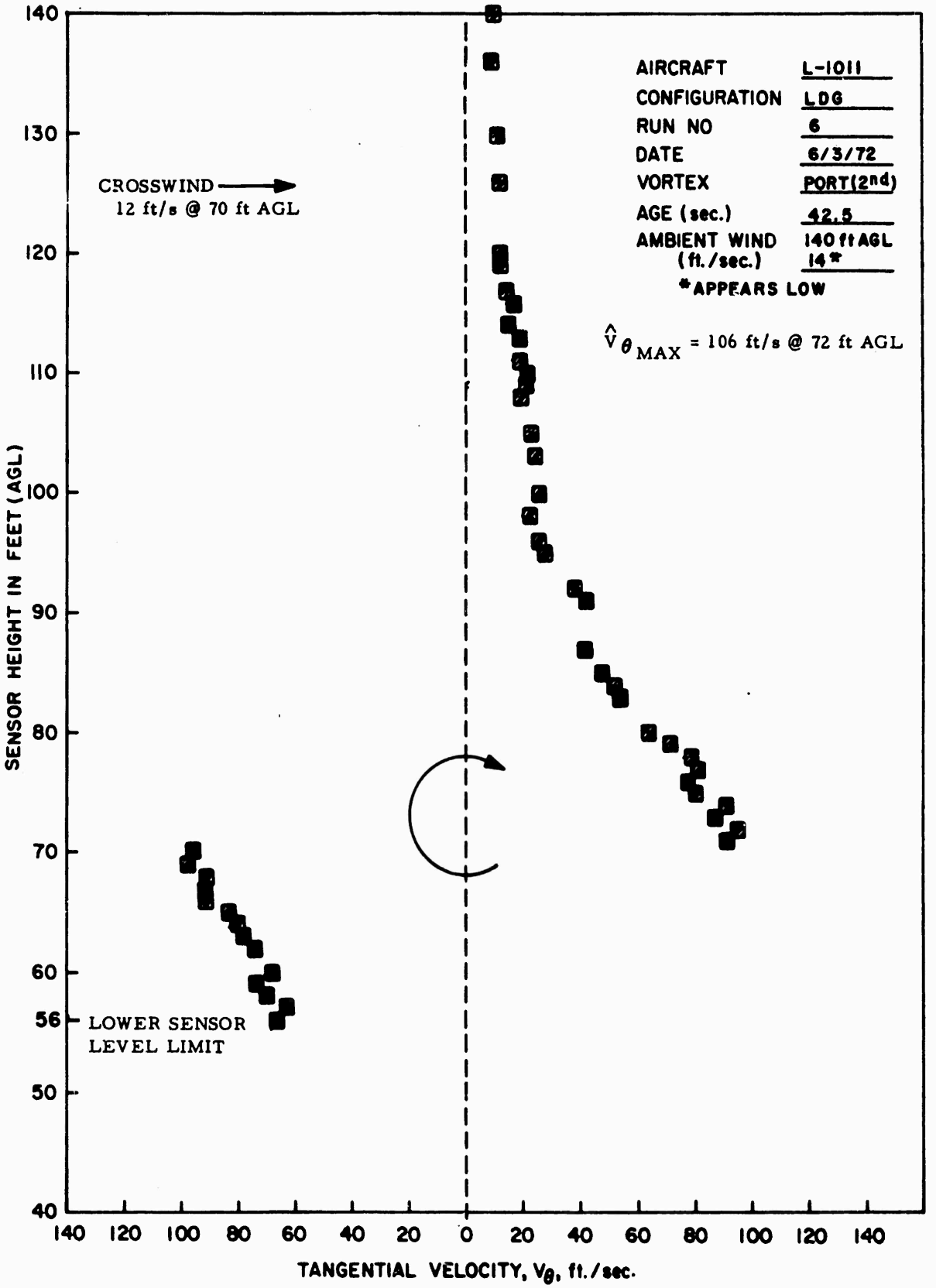
AIRCRAFT L-1011
CONFIGURATION LDG
RUN NO 6
DATE 6/3/72
VORTEX PORT(2nd)
AGE (sec.) 42.5
AMBIENT WIND (ft./sec.) 140 ft AGL 14*
*APPEARS LOW
$\hat{V}_{\theta_{MAX}}$ = 106 ft/s @ 72 ft AGL
CROSSWIND
12 ft/s @ 70 ft AGL
LOWER SENSOR LEVEL LIMIT
SENSOR HEIGHT IN FEET (AGL)
140
130
120
110
100
90
80
70
60
56
50
40
140 120 100 80 60 40 20 0 20 40 60 80 100 120 140
TANGENTIAL VELOCITY, V_θ, ft./sec.

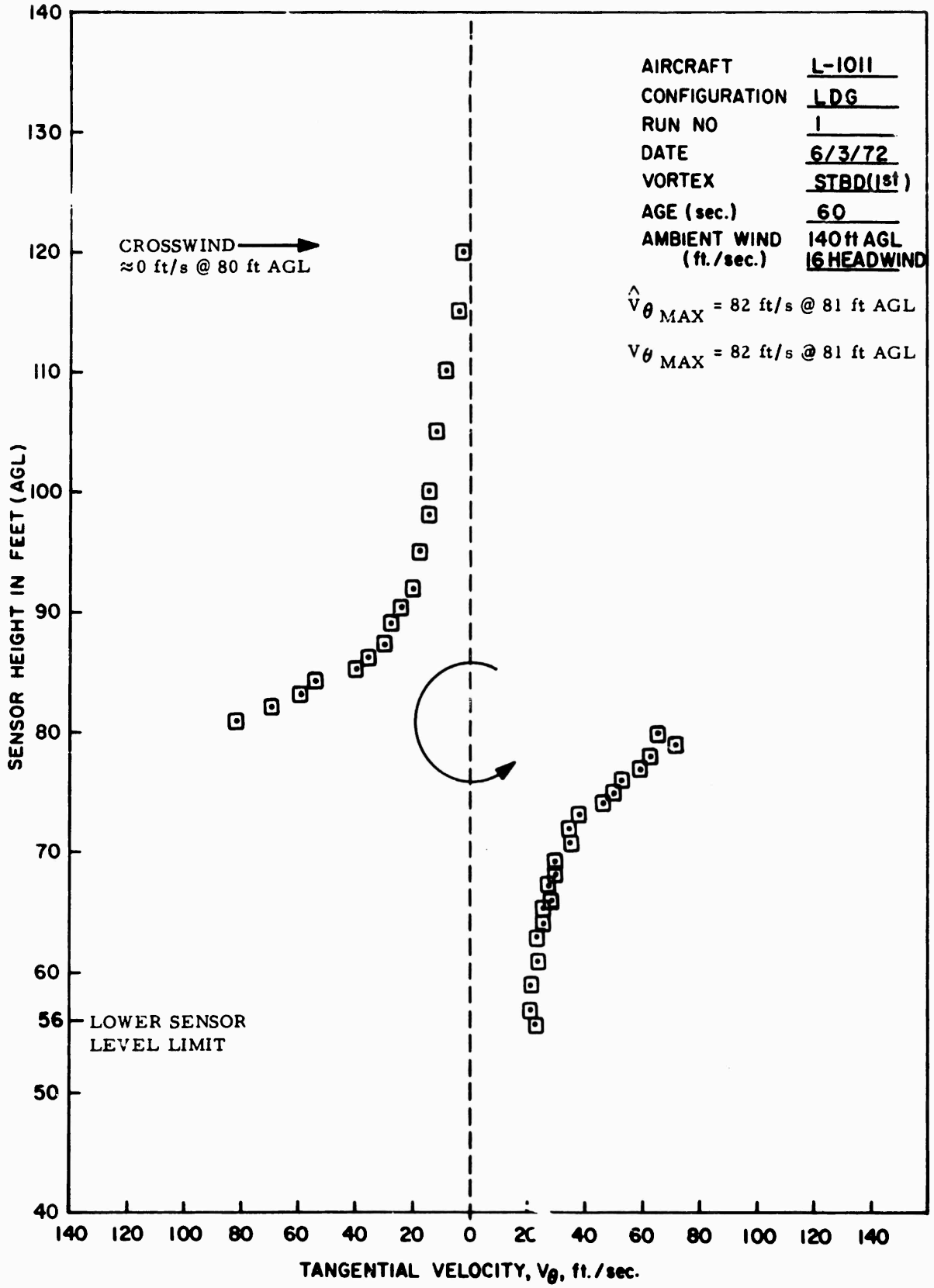
AIRCRAFT L-1011
CONFIGURATION LDG
RUN NO 1
DATE 6/3/72
VORTEX STBD(1st)
AGE (sec.) 60
AMBIENT WIND (ft./sec.) 140 ft AGL 16 HEADWIND
$\hat{V}_{\theta\ MAX}$ = 82 ft/s @ 81 ft AGL
$V_{\theta\ MAX}$ = 82 ft/s @ 81 ft AGL
CROSSWIND ≈0 ft/s @ 80 ft AGL
LOWER SENSOR LEVEL LIMIT
SENSOR HEIGHT IN FEET (AGL)
140
130
120
110
100
90
80
70
60
56
50
40
140 120 100 80 60 40 20 0 20 40 60 80 100 120 140
TANGENTIAL VELOCITY, V_θ, ft./sec.

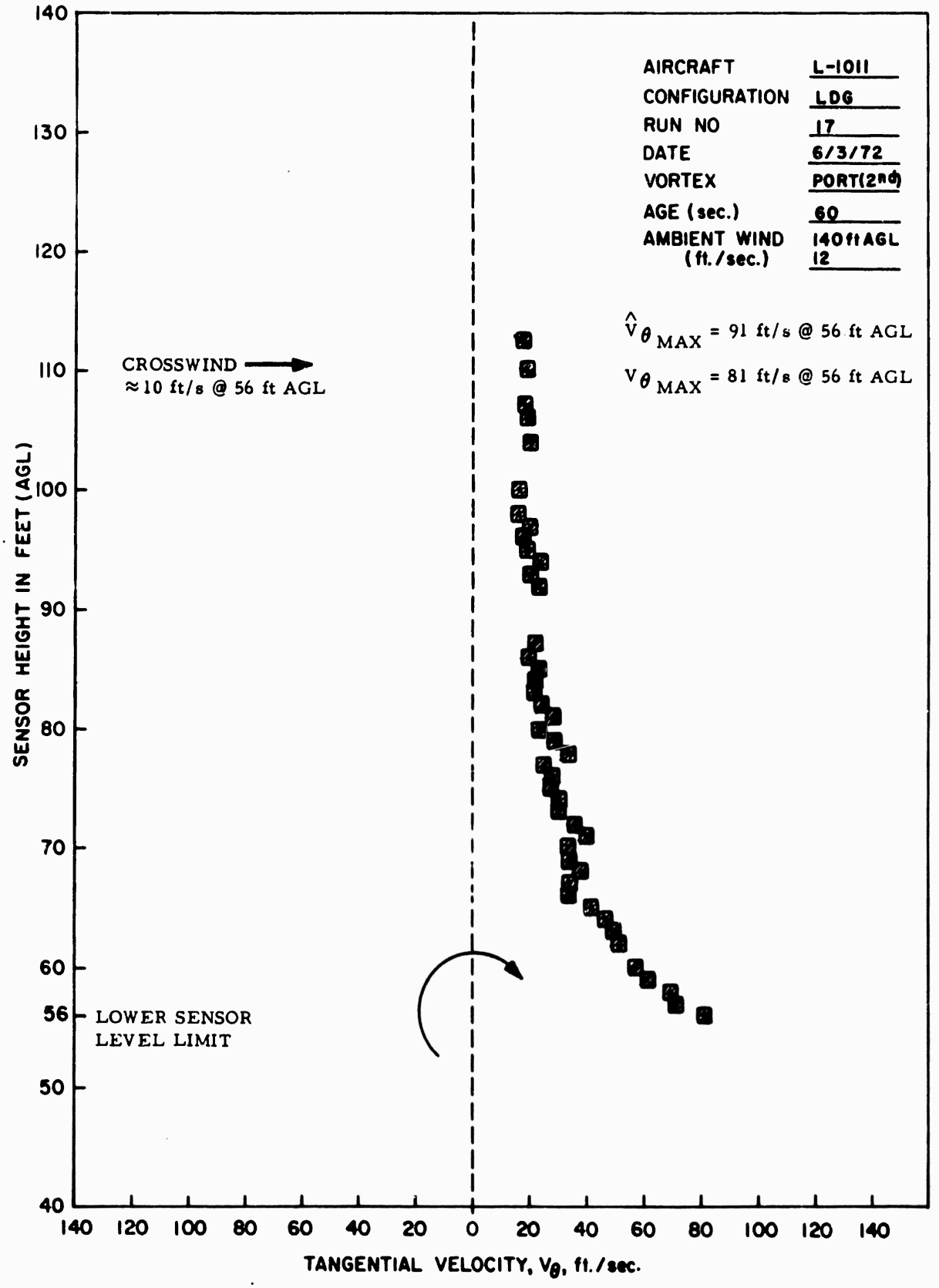
AIRCRAFT L-1011
CONFIGURATION LDG
RUN NO 17
DATE 6/3/72
VORTEX PORT(2nd)
AGE (sec.) 60
AMBIENT WIND (ft./sec.) 140 ft AGL 12
$\hat{V}_{\theta\,MAX}$ = 91 ft/s @ 56 ft AGL
$V_{\theta\,MAX}$ = 81 ft/s @ 56 ft AGL
CROSSWIND
≈10 ft/s @ 56 ft AGL
LOWER SENSOR LEVEL LIMIT
SENSOR HEIGHT IN FEET (AGL)
140
130
120
110
100
90
80
70
60
56
50
40
140 120 100 80 60 40 20 0 20 40 60 80 100 120 140
TANGENTIAL VELOCITY, V_θ, ft./sec.

APPENDIX E

RECORDED VORTEX TANGENTIAL VELOCITY VERSUS TIME--COMPUTER GENERATED EXPANDED PLOTS (Selected Plots)

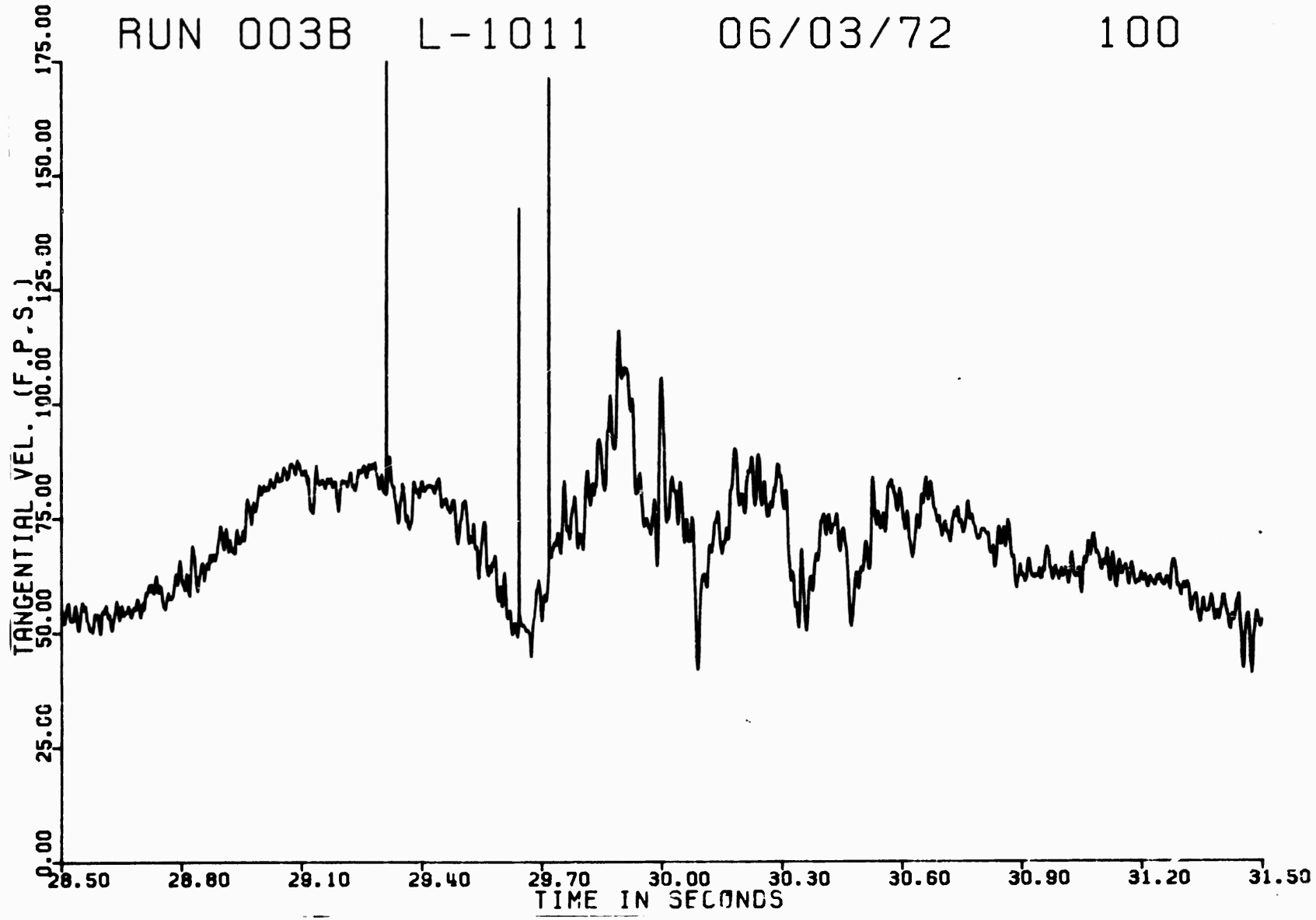
RUN 003B L-1011 06/03/72 100
TANGENTIAL VEL. (F.P.S.)
0.00
25.00
50.00
75.00
100.00
125.00
150.00
175.00
28.50
28.80
29.10
29.40
29.70
30.00
30.30
30.60
30.90
31.20
31.50
TIME IN SECONDS

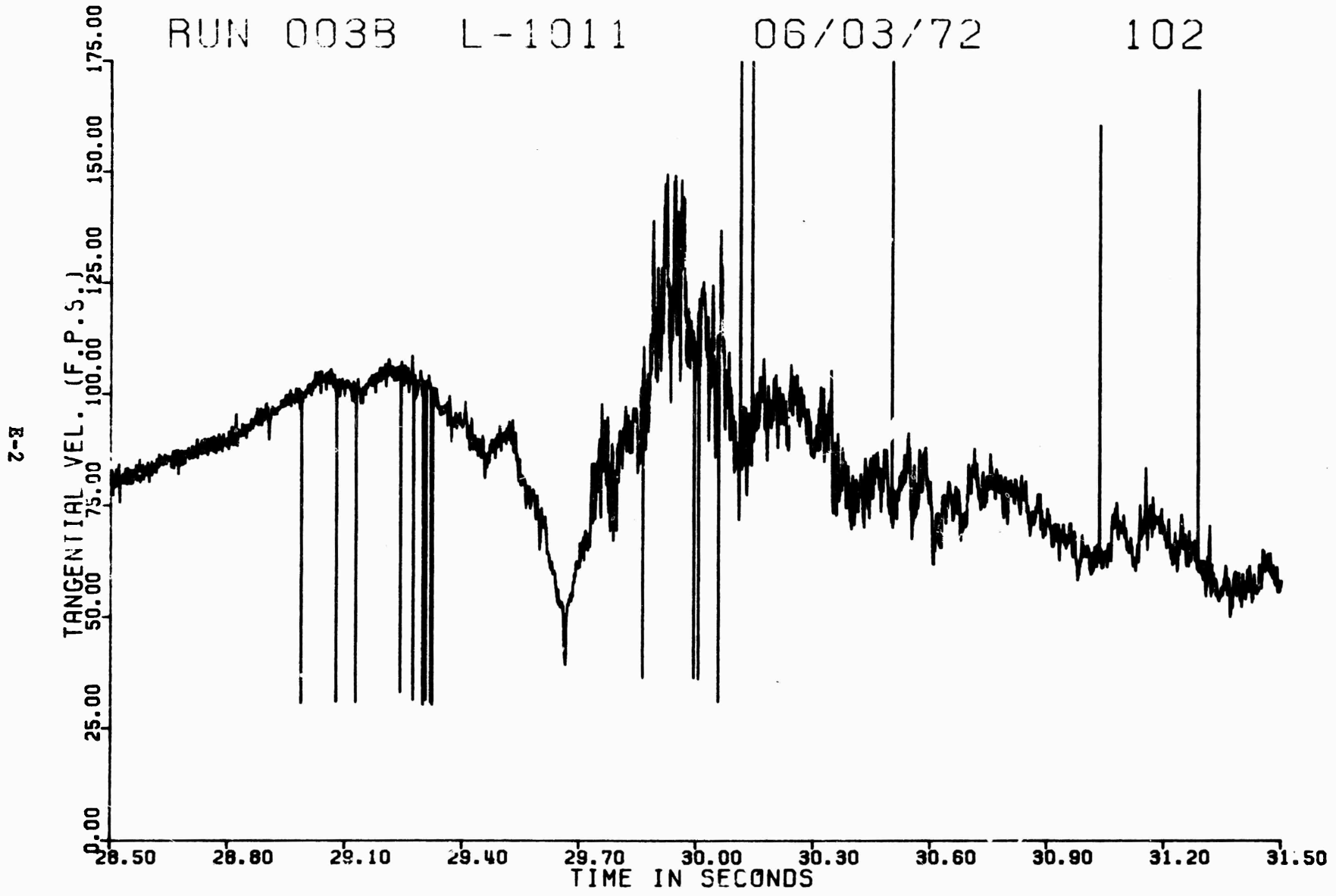
RUN 003B L-1011 06/03/72 102
TANGENTIAL VEL. (F.P.S.)
0.00
25.00
50.00
75.00
100.00
125.00
150.00
175.00
28.50
28.80
29.10
29.40
29.70
30.00
30.30
30.60
30.90
31.20
31.50
TIME IN SECONDS

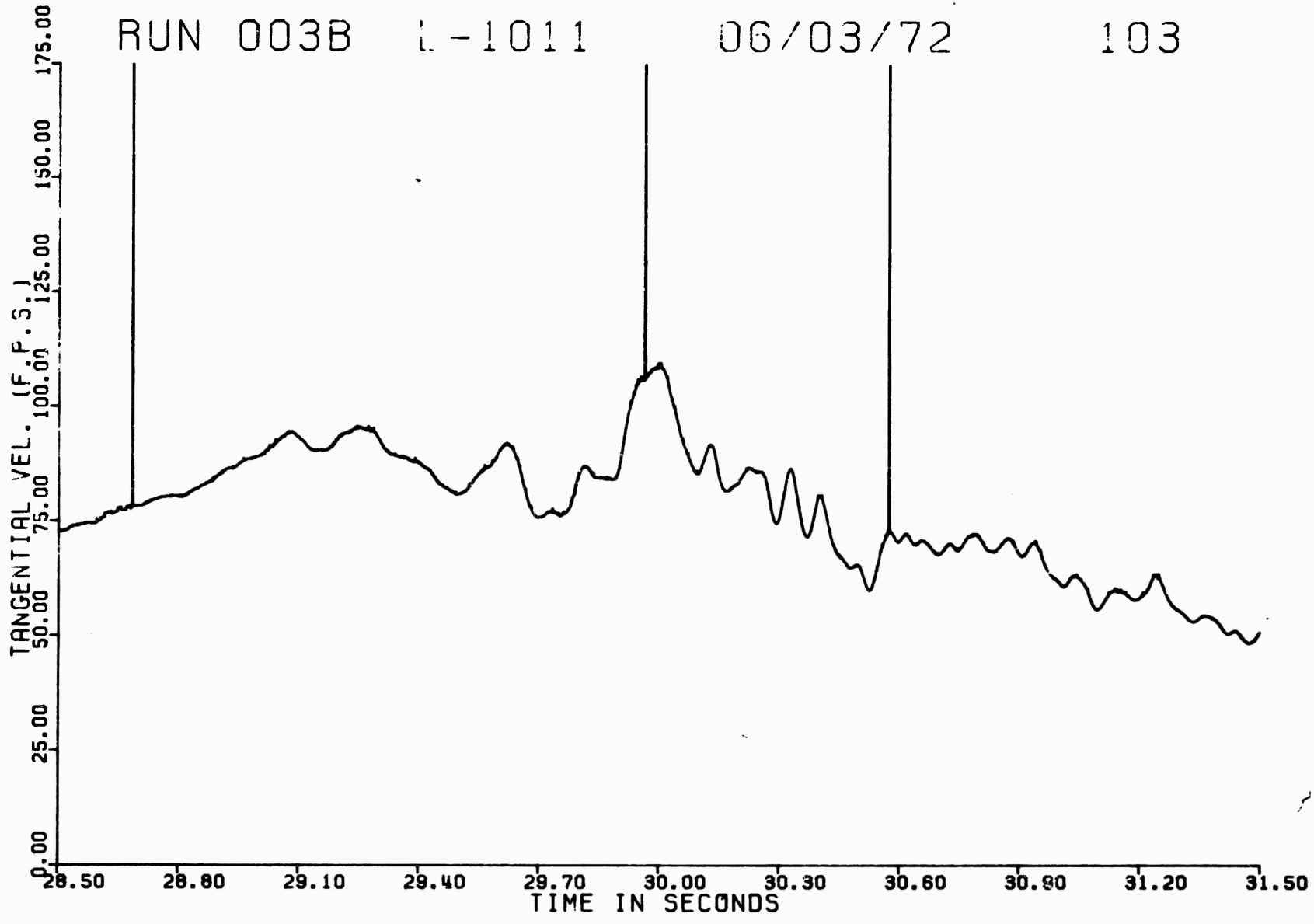
RUN 003B L-1011 06/03/72 103
TANGENTIAL VEL. (F.P.S.)
0.00
25.00
50.00
75.00
100.00
125.00
150.00
175.00
28.50
28.80
29.10
29.40
29.70
30.00
30.30
30.60
30.90
31.20
31.50
TIME IN SECONDS

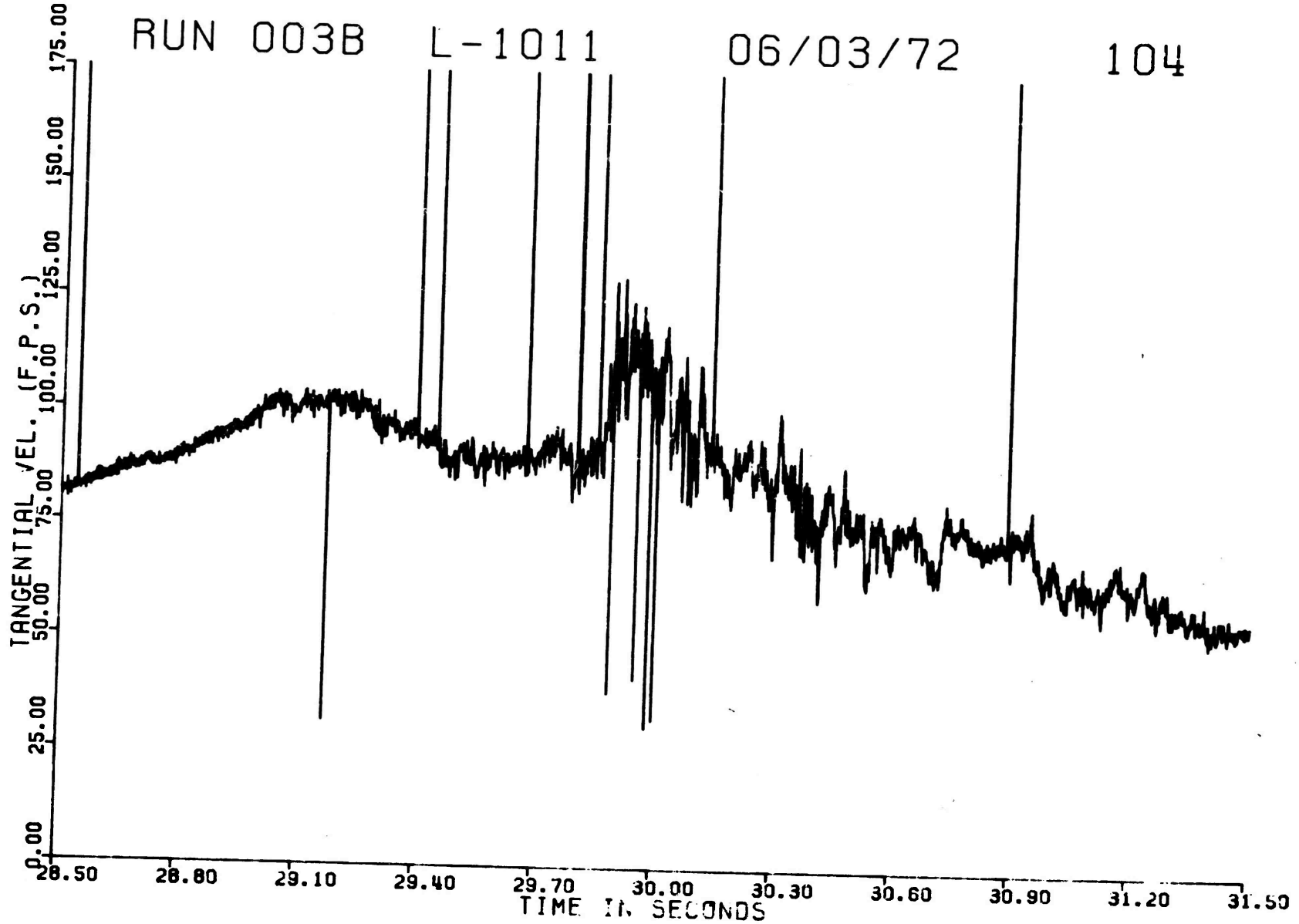
RUN 003B L-1011 06/03/72 104
TANGENTIAL VEL. (F.P.S.)
0.00
25.00
50.00
75.00
100.00
125.00
150.00
175.00
28.50
28.80
29.10
29.40
29.70
30.00
30.30
30.60
30.90
31.20
31.50
TIME IN SECONDS

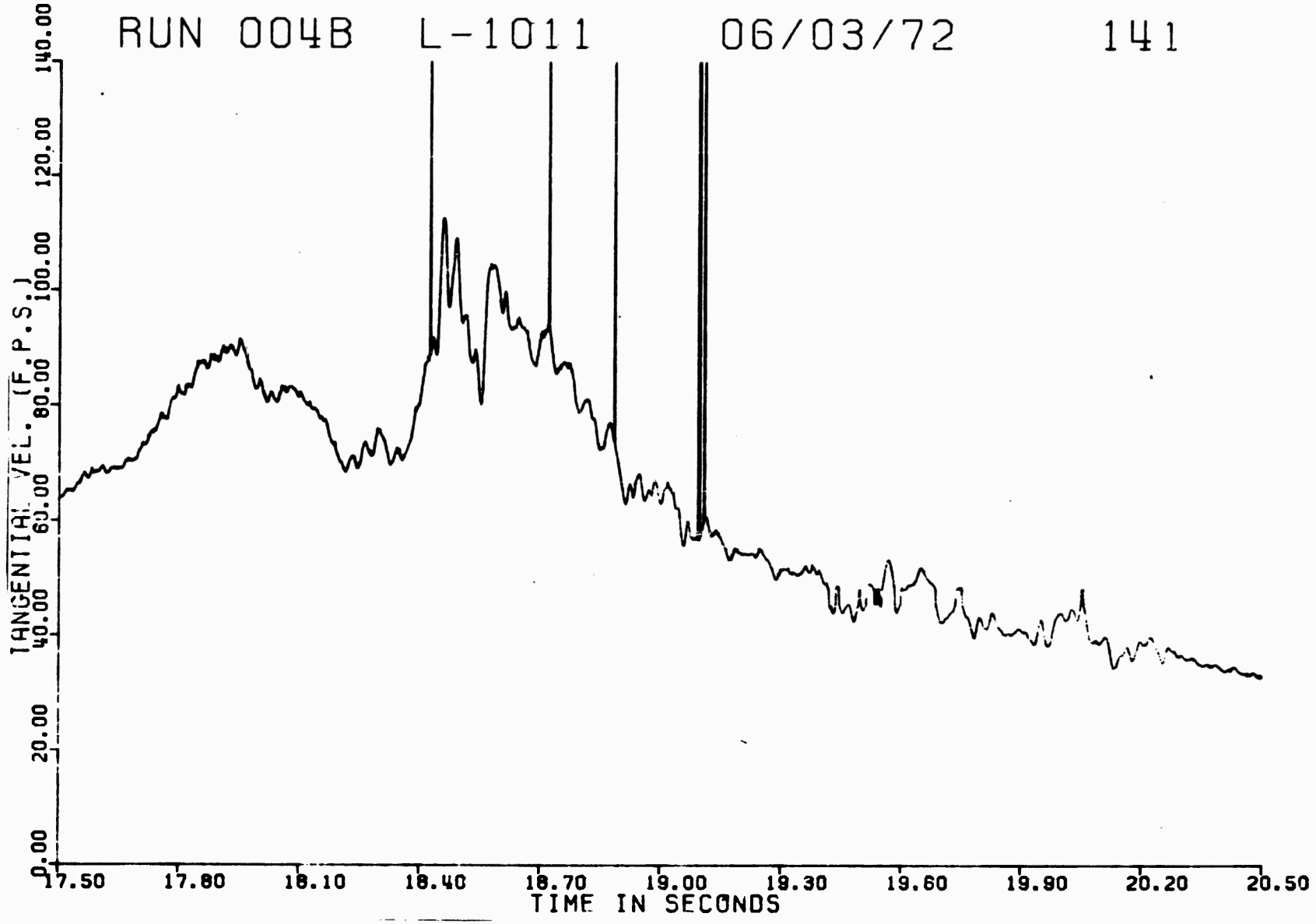
RUN 004B L-1011 06/03/72 141
TANGENTIAL VEL. (F.P.S.)
0.00
20.00
40.00
60.00
80.00
100.00
120.00
140.00
17.50
17.80
18.10
18.40
18.70
19.00
19.30
19.60
19.90
20.20
20.50
TIME IN SECONDS

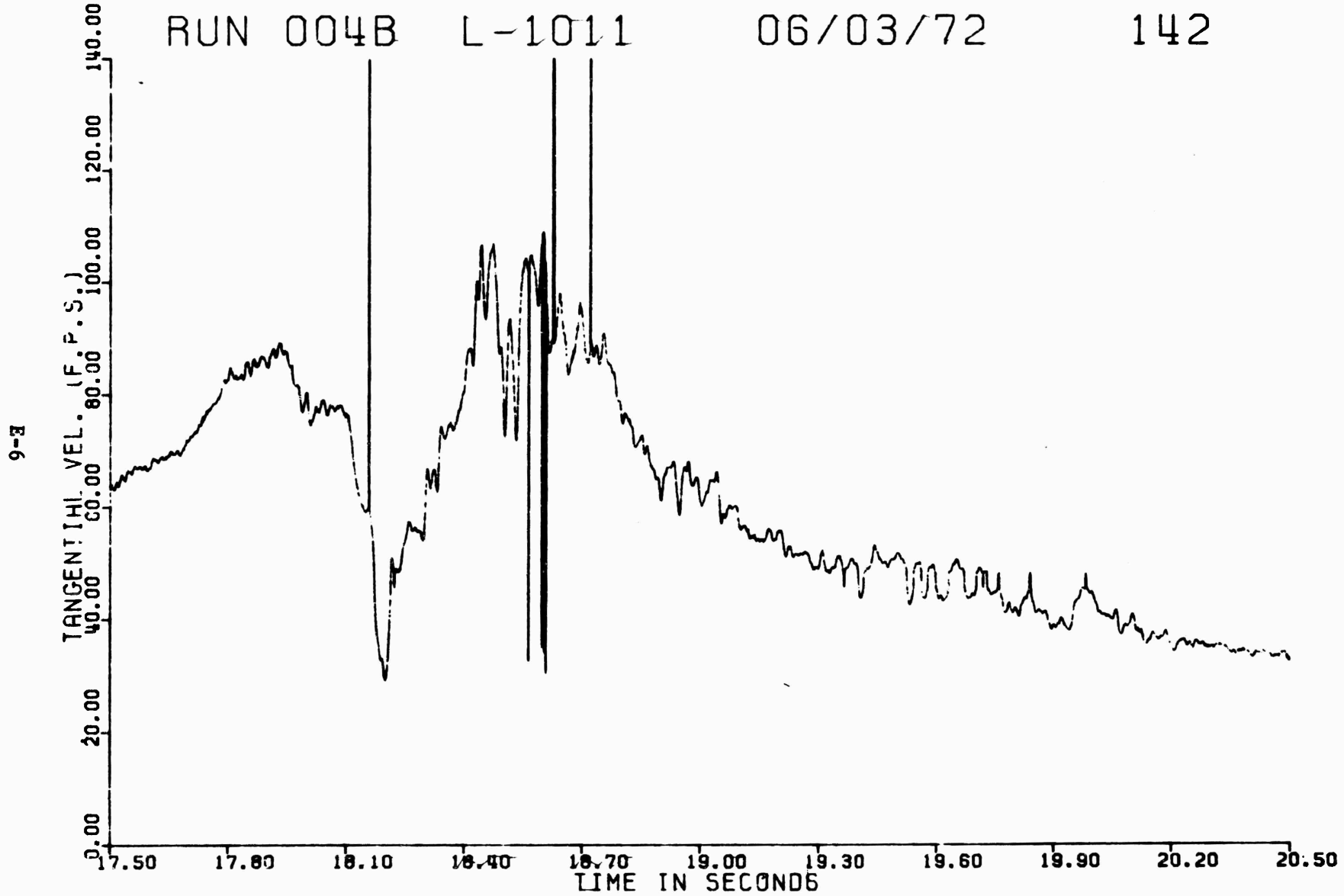
RUN 004B L-1011 06/03/72 142
TANGENTIAL VEL. (F.P.S.)
0.00
20.00
40.00
60.00
80.00
100.00
120.00
140.00
17.50
17.80
18.10
18.40
18.70
19.00
19.30
19.60
19.90
20.20
20.50
TIME IN SECONDS

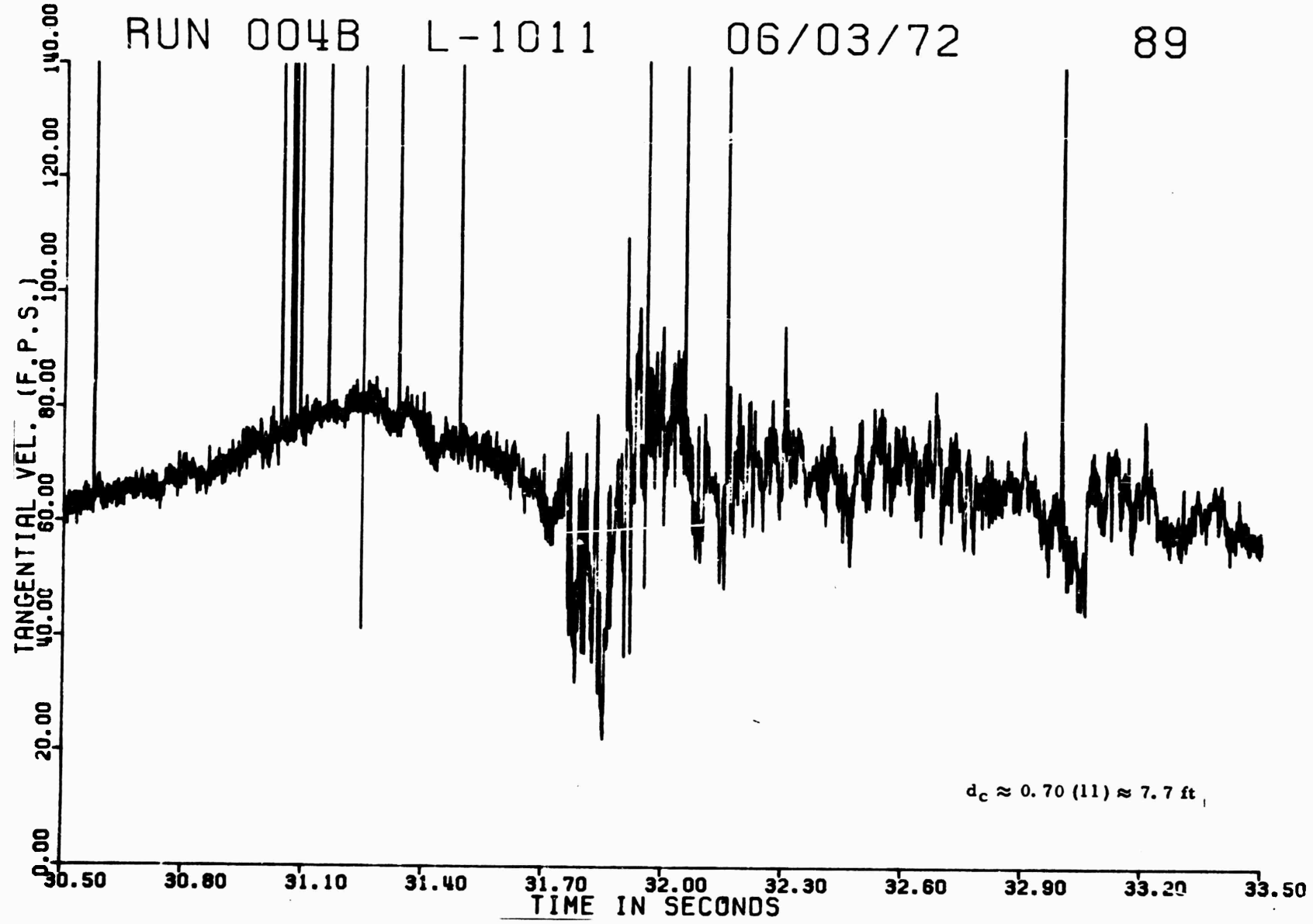
RUN 004B L-1011 06/03/72 89
TANGENTIAL VEL. (F.P.S.)
0.00
20.00
40.00
60.00
80.00
100.00
120.00
140.00
30.50
30.80
31.10
31.40
31.70
32.00
32.30
32.60
32.90
33.20
33.50
TIME IN SECONDS
$d_c \approx 0.70\,(11) \approx 7.7$ ft

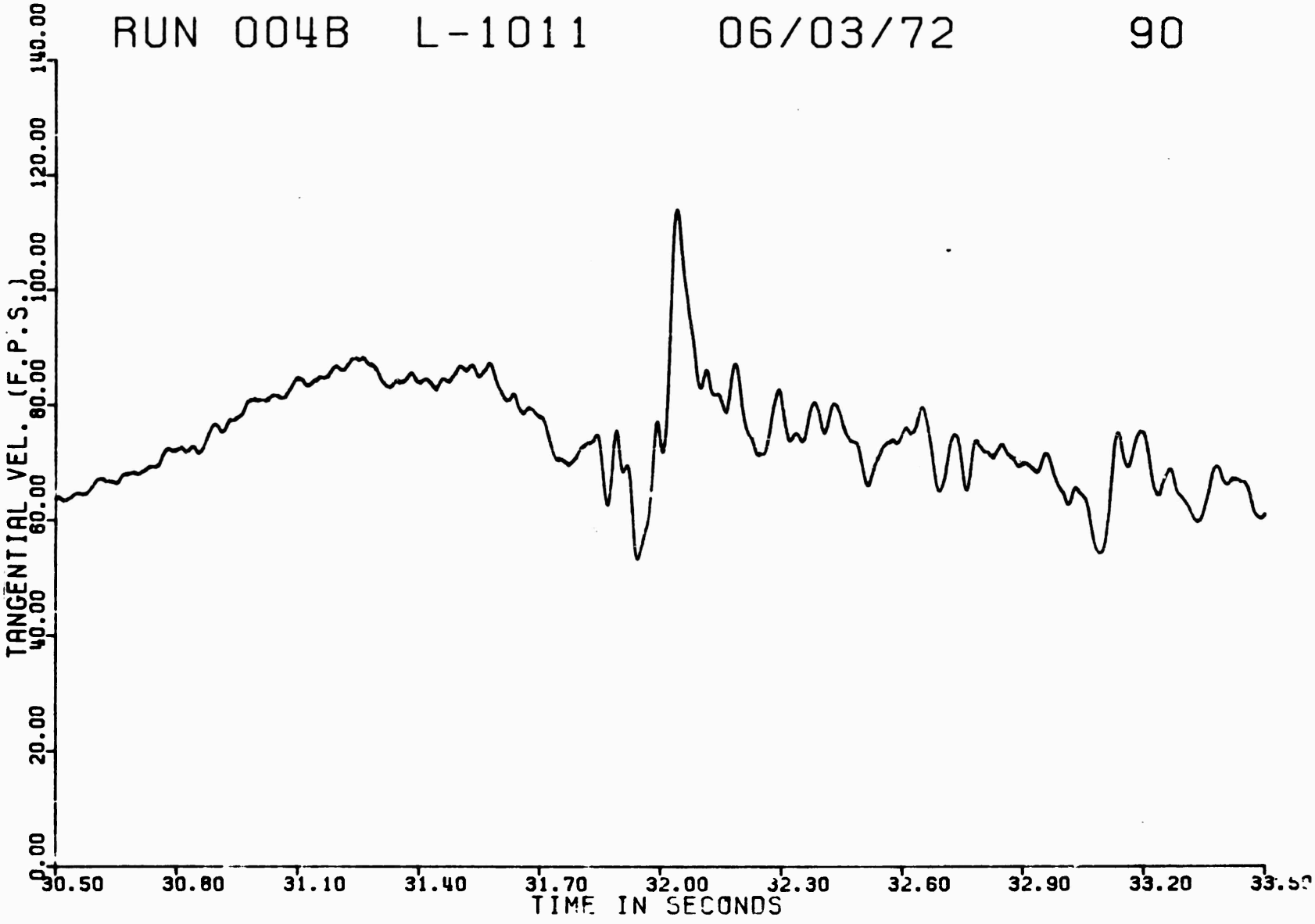
RUN 004B L-1011 06/03/72 90
TANGENTIAL VEL. (F.P.S.)
0.00
20.00
40.00
60.00
80.00
100.00
120.00
140.00
30.50
30.80
31.10
31.40
31.70
32.00
32.30
32.60
32.90
33.20
TIME IN SECONDS

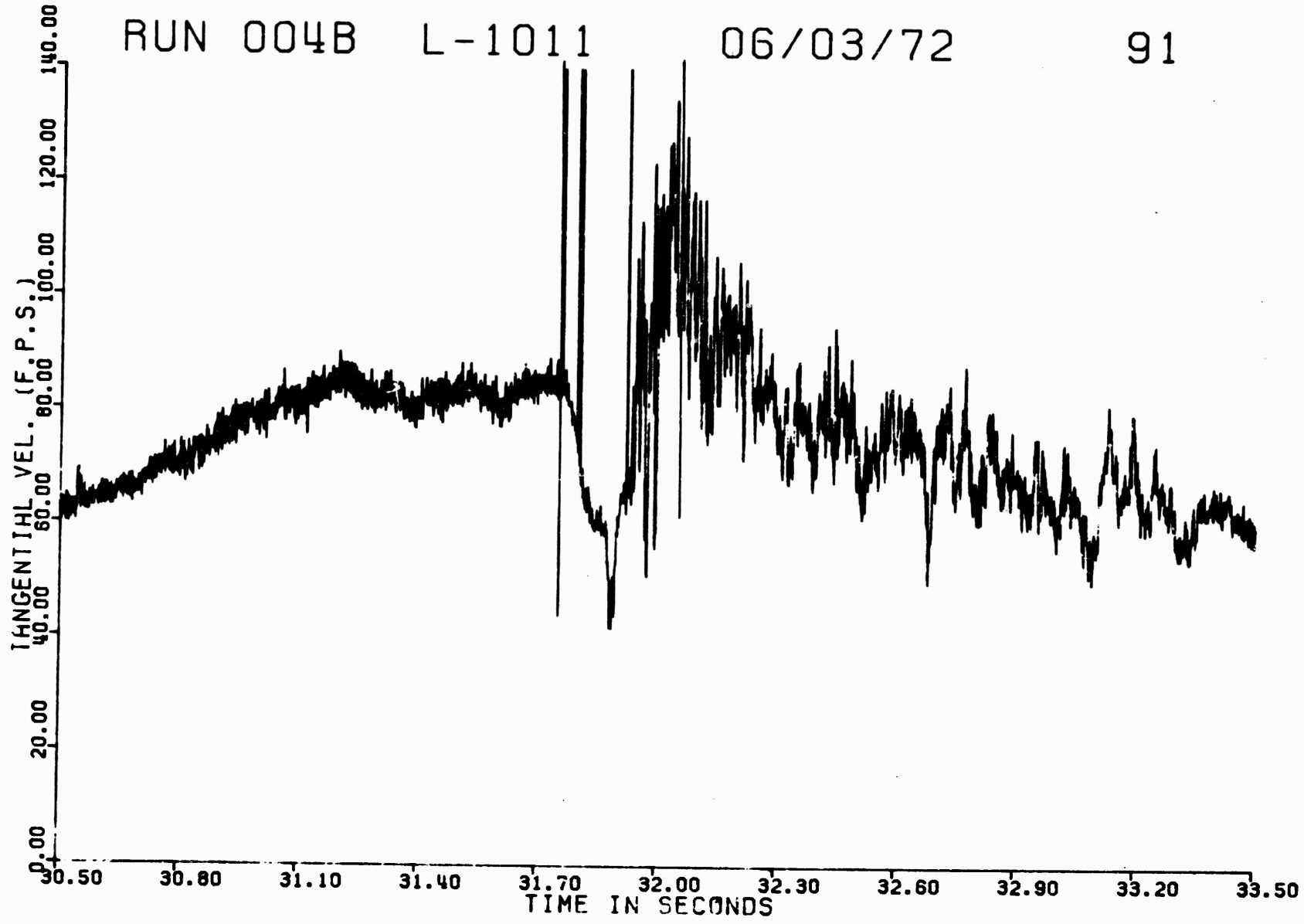
RUN 004B L-1011 06/03/72 91
TANGENTIAL VEL. (F.P.S.)
0.00
20.00
40.00
60.00
80.00
100.00
120.00
140.00
30.50
30.80
31.10
31.40
31.70
32.00
32.30
32.60
32.90
33.20
33.50
TIME IN SECONDS

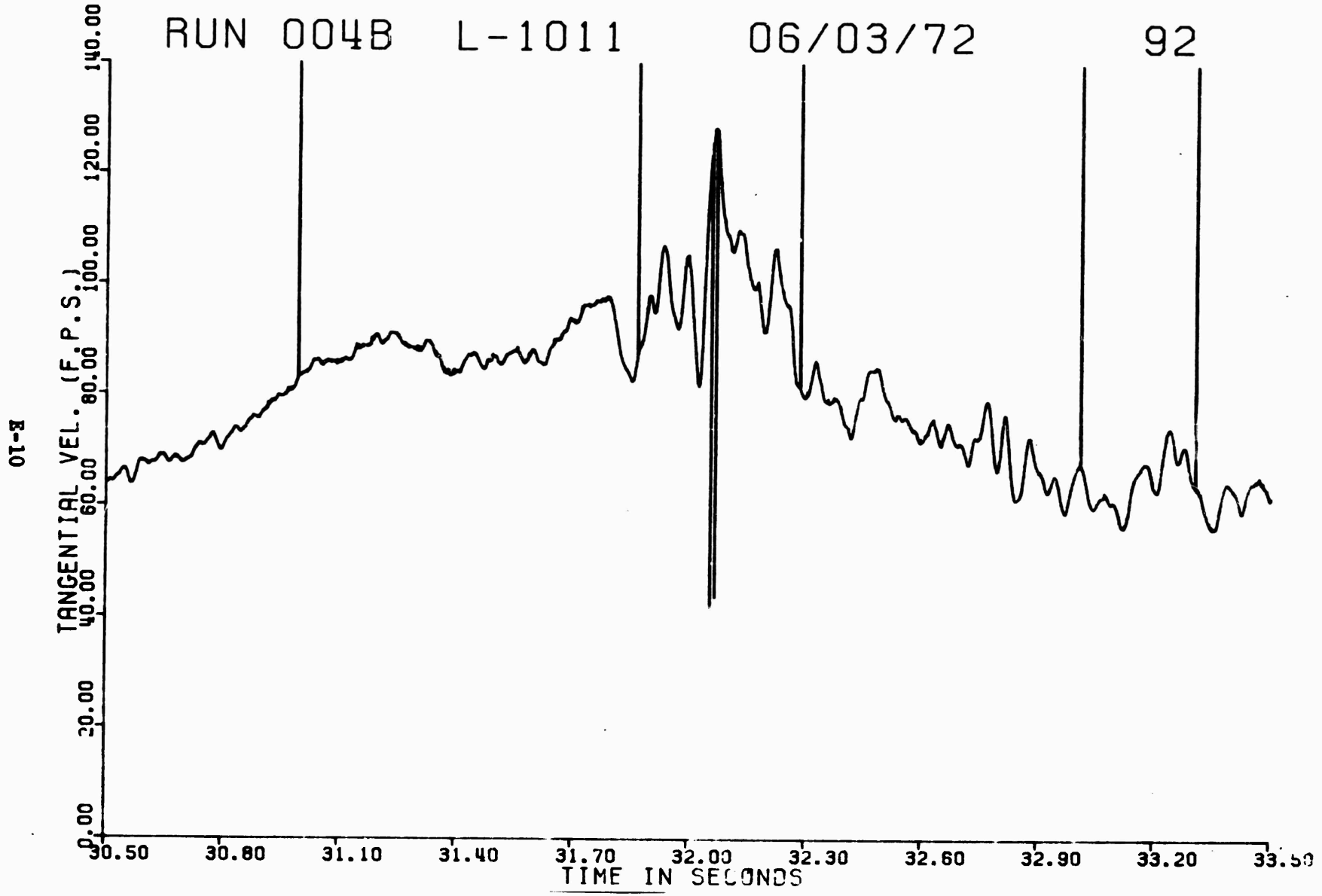
RUN 004B L-1011 06/03/72 92
TANGENTIAL VEL. (F.P.S.)
0.00
20.00
40.00
60.00
80.00
100.00
120.00
140.00
30.50
30.80
31.10
31.40
31.70
32.00
32.30
32.60
32.90
33.20
33.50
TIME IN SECONDS

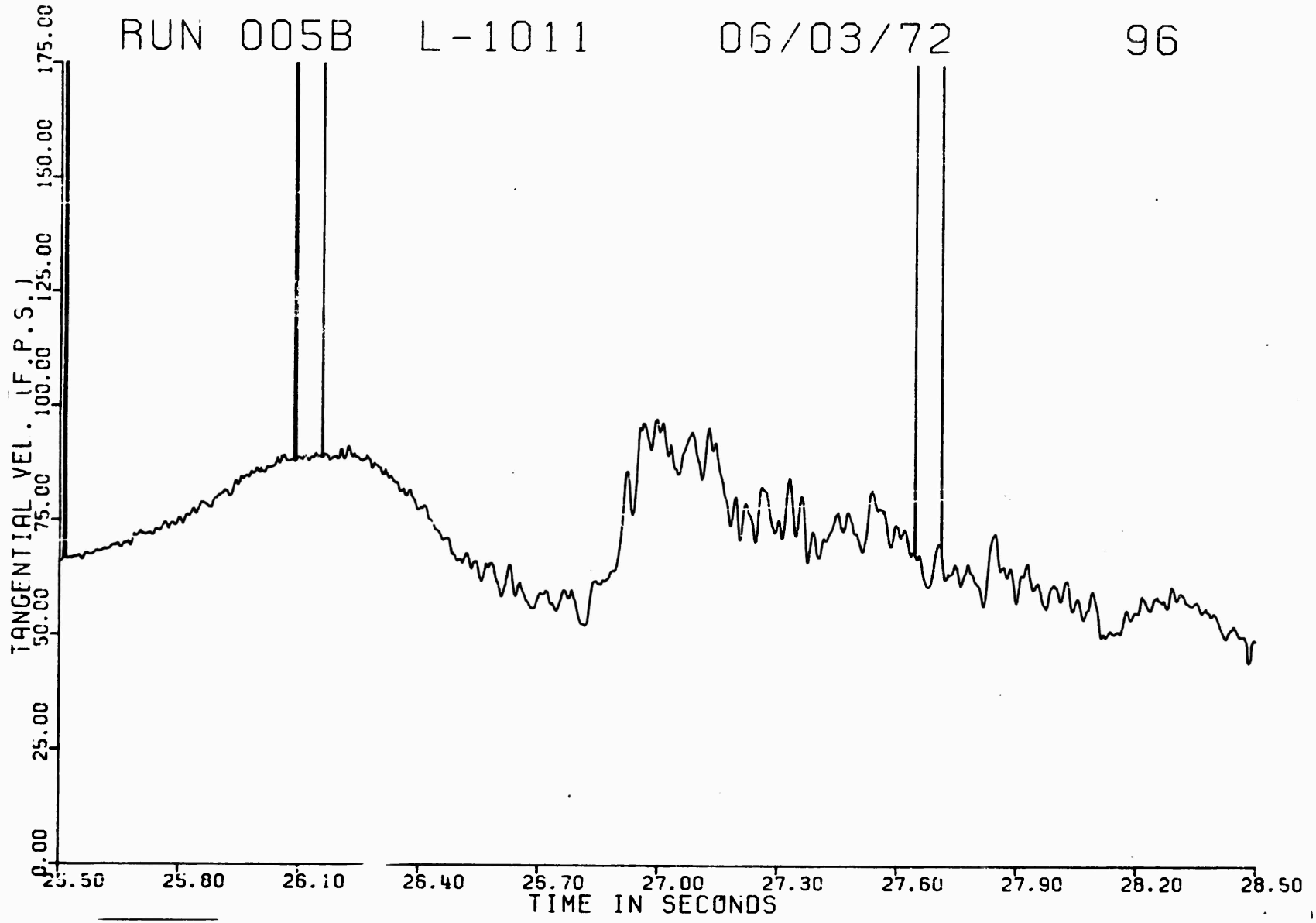
RUN 005B L-1011 06/03/72 96
TANGENTIAL VEL. (F.P.S.)
0.00
25.00
50.00
75.00
100.00
125.00
150.00
175.00
25.50
25.80
26.10
26.40
26.70
27.00
27.30
27.60
27.90
28.20
28.50
TIME IN SECONDS

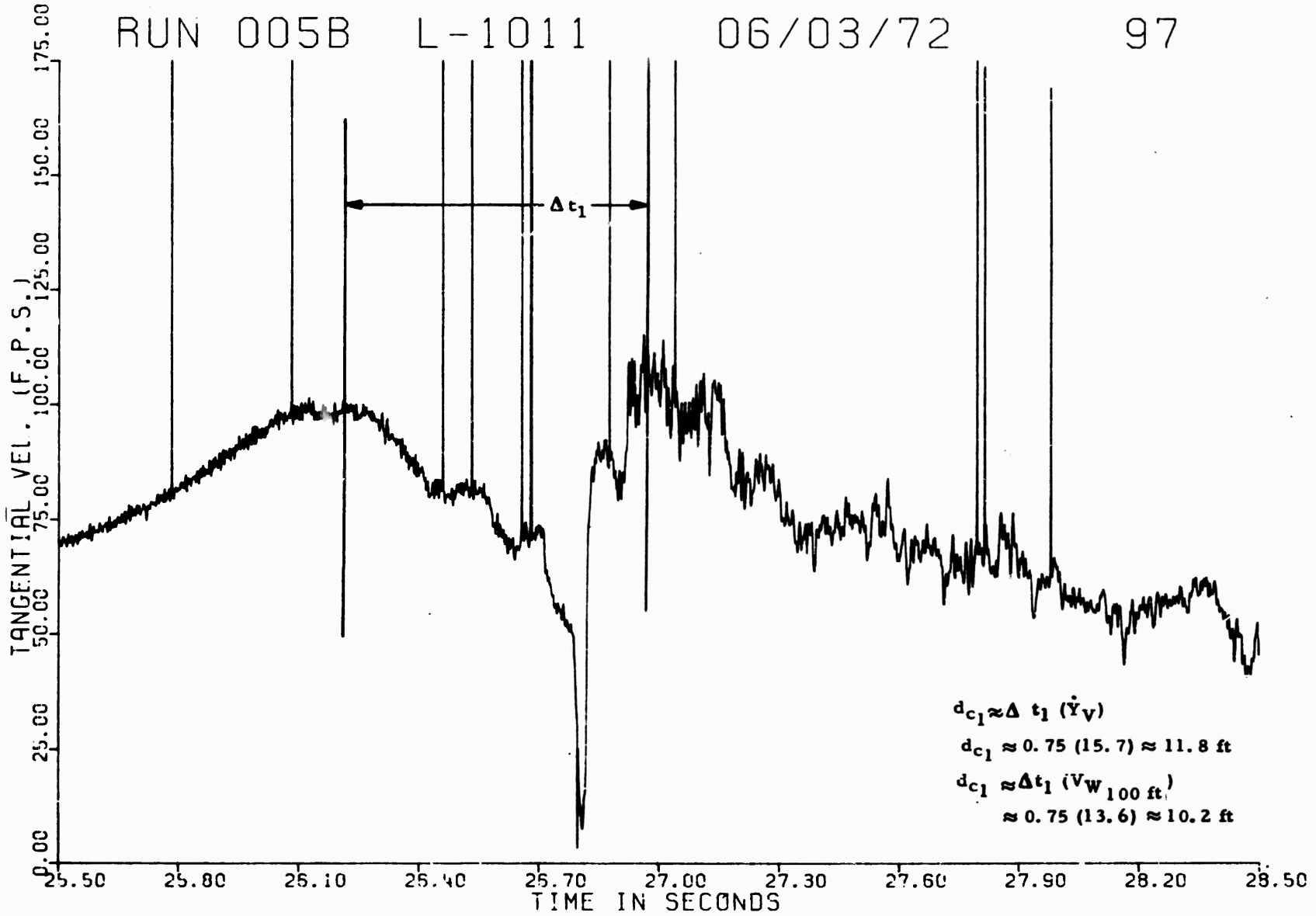
RUN 005B L-1011 06/03/72 97
TANGENTIAL VEL. (F.P.S.)
0.00
25.00
50.00
75.00
100.00
125.00
150.00
175.00
Δt_1
25.50
25.80
26.10
26.40
26.70
27.00
27.30
27.60
27.90
28.20
28.50
TIME IN SECONDS
$d_{c_1} \approx \Delta t_1 (\dot{Y}_V)$
$d_{c_1} \approx 0.75 (15.7) \approx 11.8$ ft
$d_{c_1} \approx \Delta t_1 (V_{W_{100\ ft}})$
$\approx 0.75 (13.6) \approx 10.2$ ft

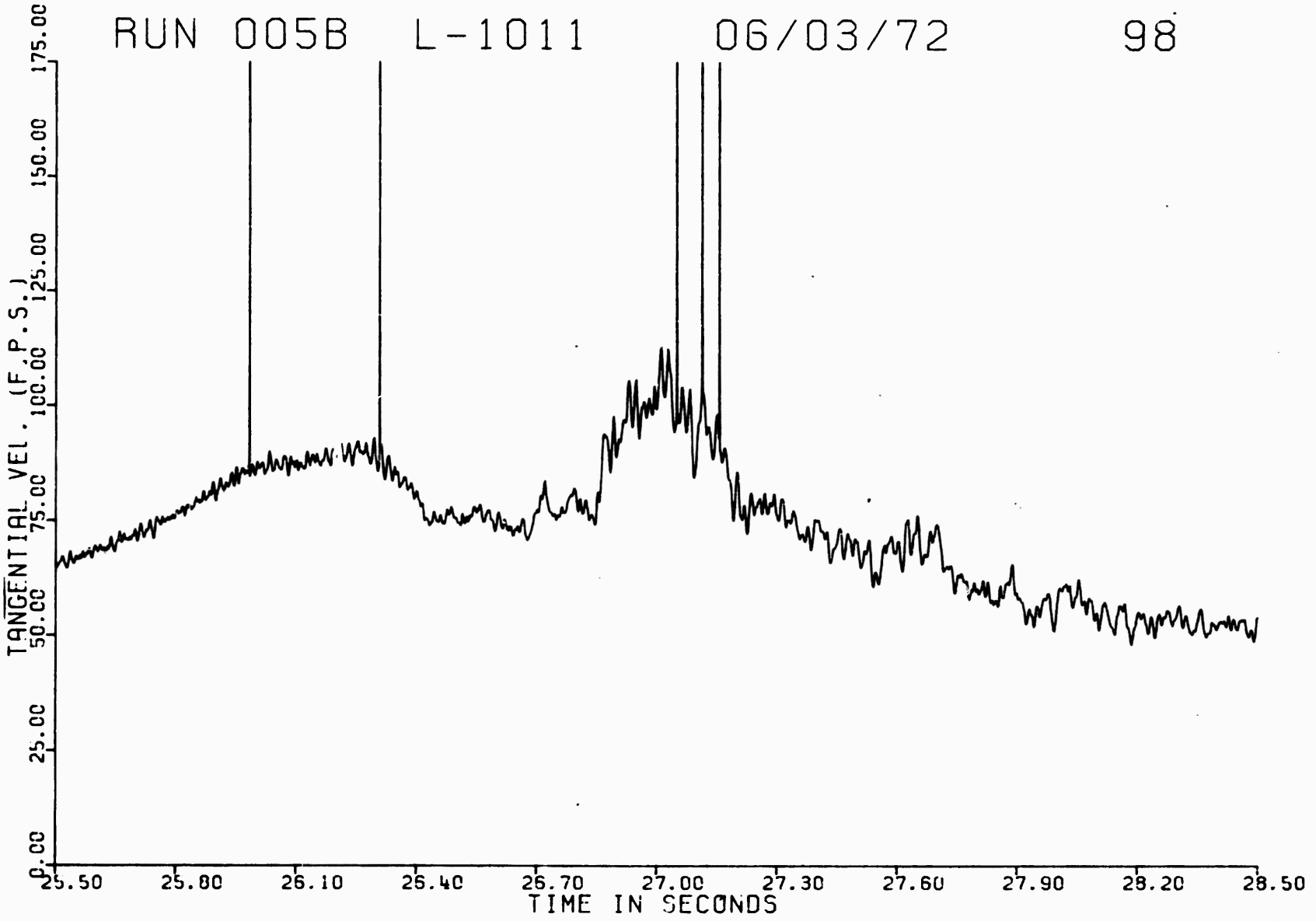
RUN 005B L-1011 06/03/72 98
TANGENTIAL VEL. (F.P.S.)
0.00
25.00
50.00
75.00
100.00
125.00
150.00
175.00
25.50
25.80
26.10
26.40
26.70
27.00
27.30
27.60
27.90
28.20
28.50
TIME IN SECONDS

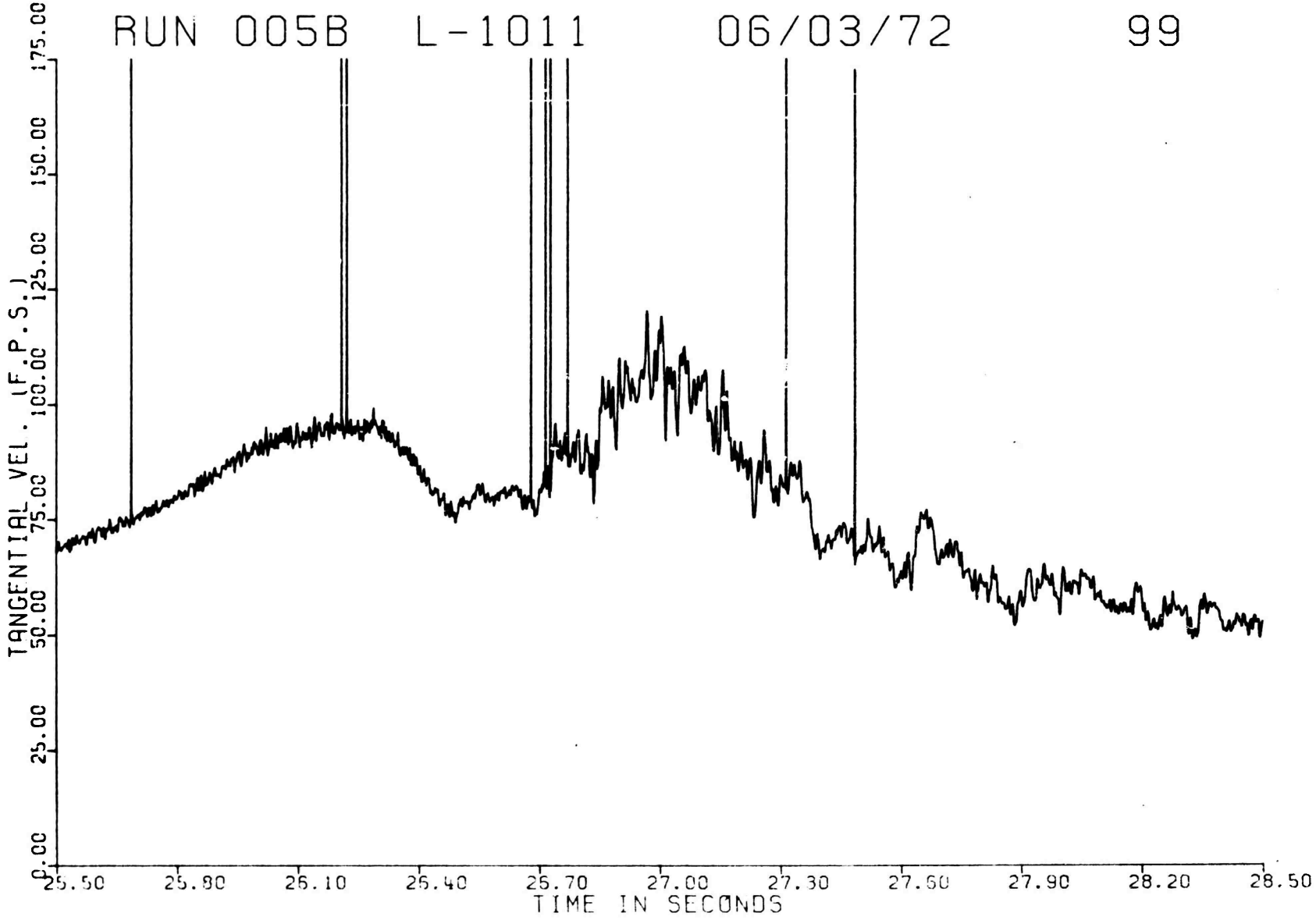
RUN 005B L-1011 06/03/72 99
TANGENTIAL VEL. (F.P.S.)
0.00
25.00
50.00
75.00
100.00
125.00
150.00
175.00
25.50
25.80
26.10
26.40
26.70
27.00
27.30
27.60
27.90
28.20
28.50
TIME IN SECONDS

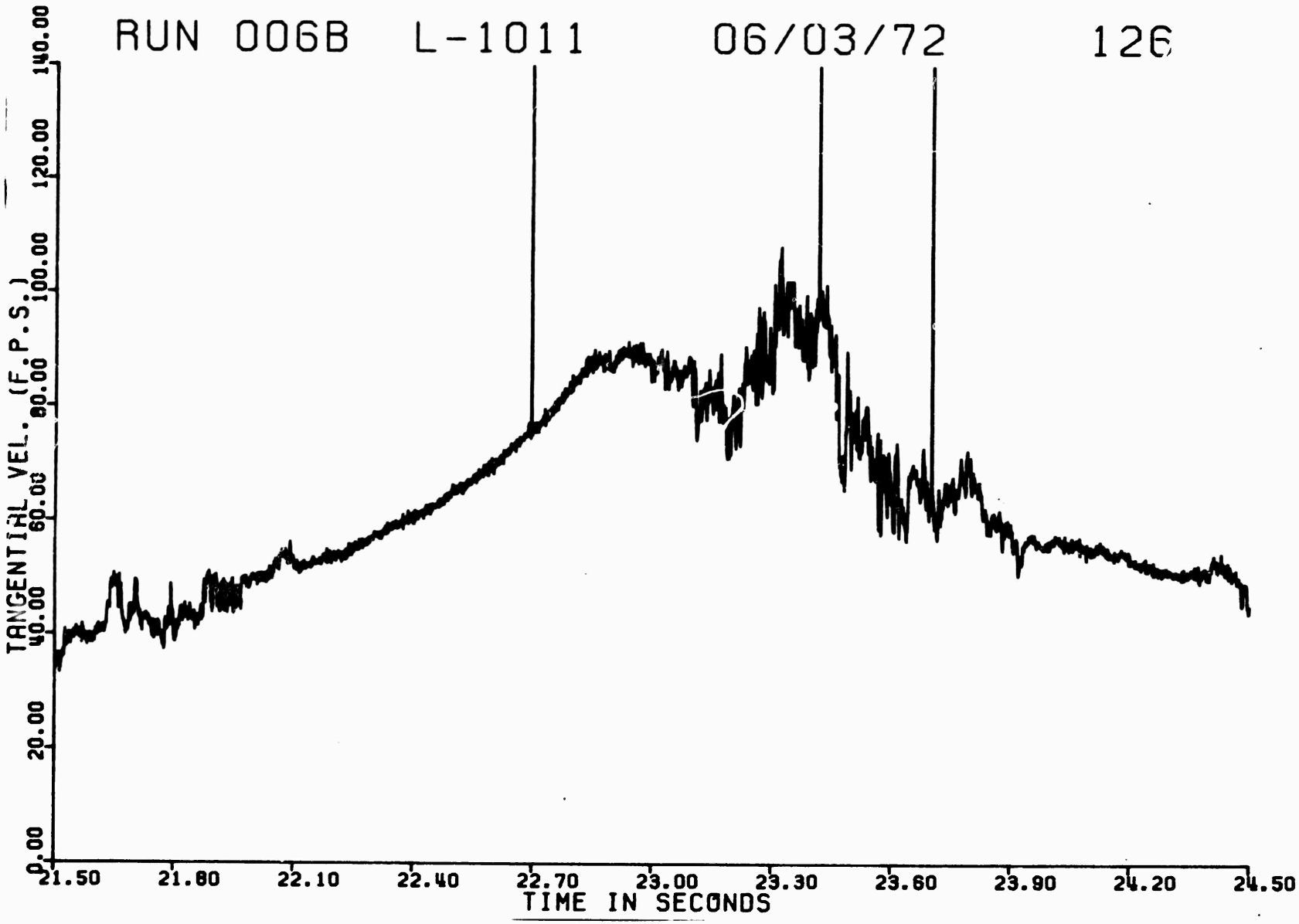
RUN 006B L-1011 06/03/72 126
TANGENTIAL VEL. (F.P.S.)
0.00
20.00
40.00
60.00
80.00
100.00
120.00
140.00
21.50
21.80
22.10
22.40
22.70
23.00
23.30
23.60
23.90
24.20
24.50
TIME IN SECONDS

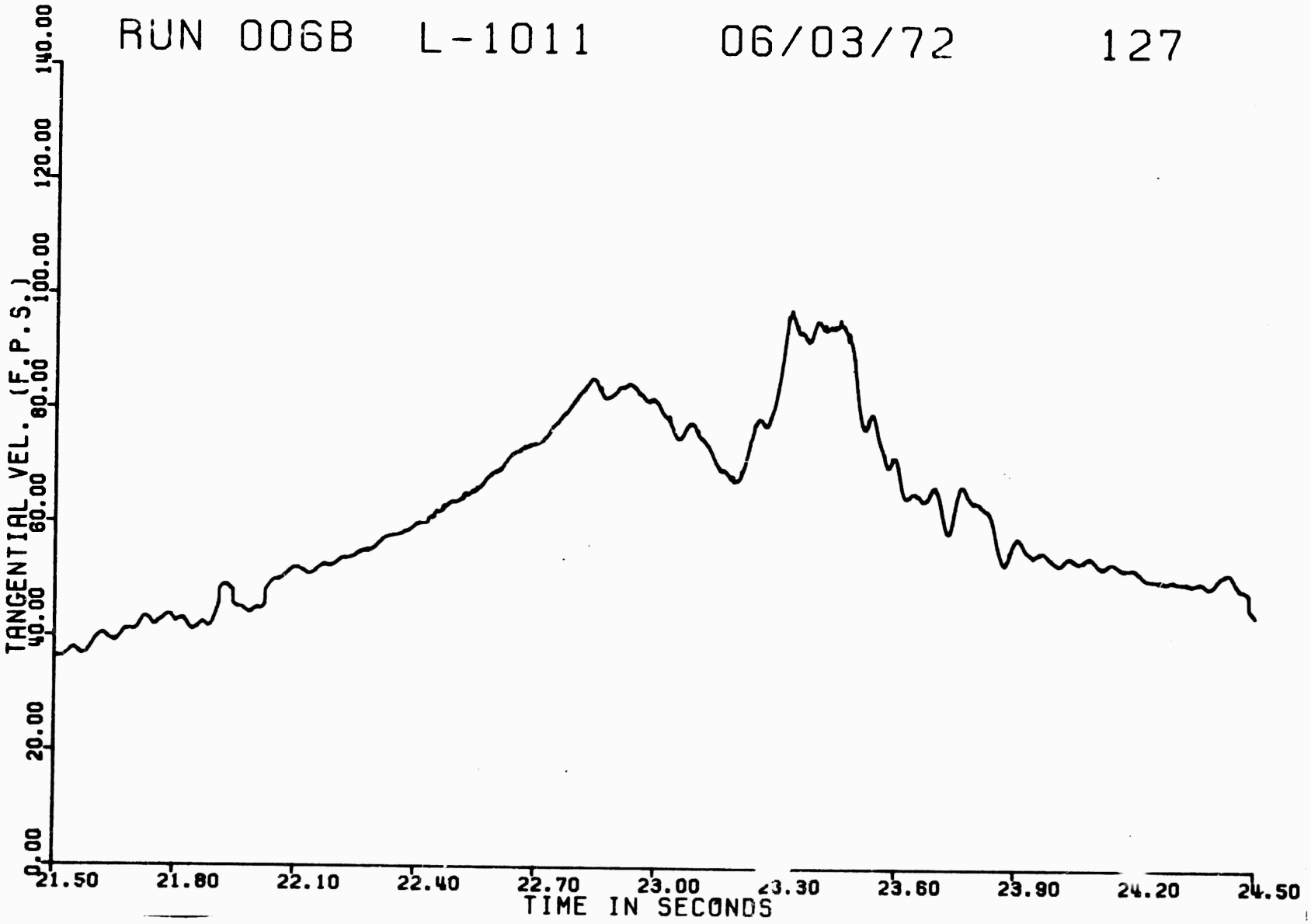
RUN 006B L-1011 06/03/72 127
TANGENTIAL VEL. (F.P.S.)
0.00
20.00
40.00
60.00
80.00
100.00
120.00
140.00
21.50
21.80
22.10
22.40
22.70
23.00
23.30
23.60
23.90
24.20
24.50
TIME IN SECONDS

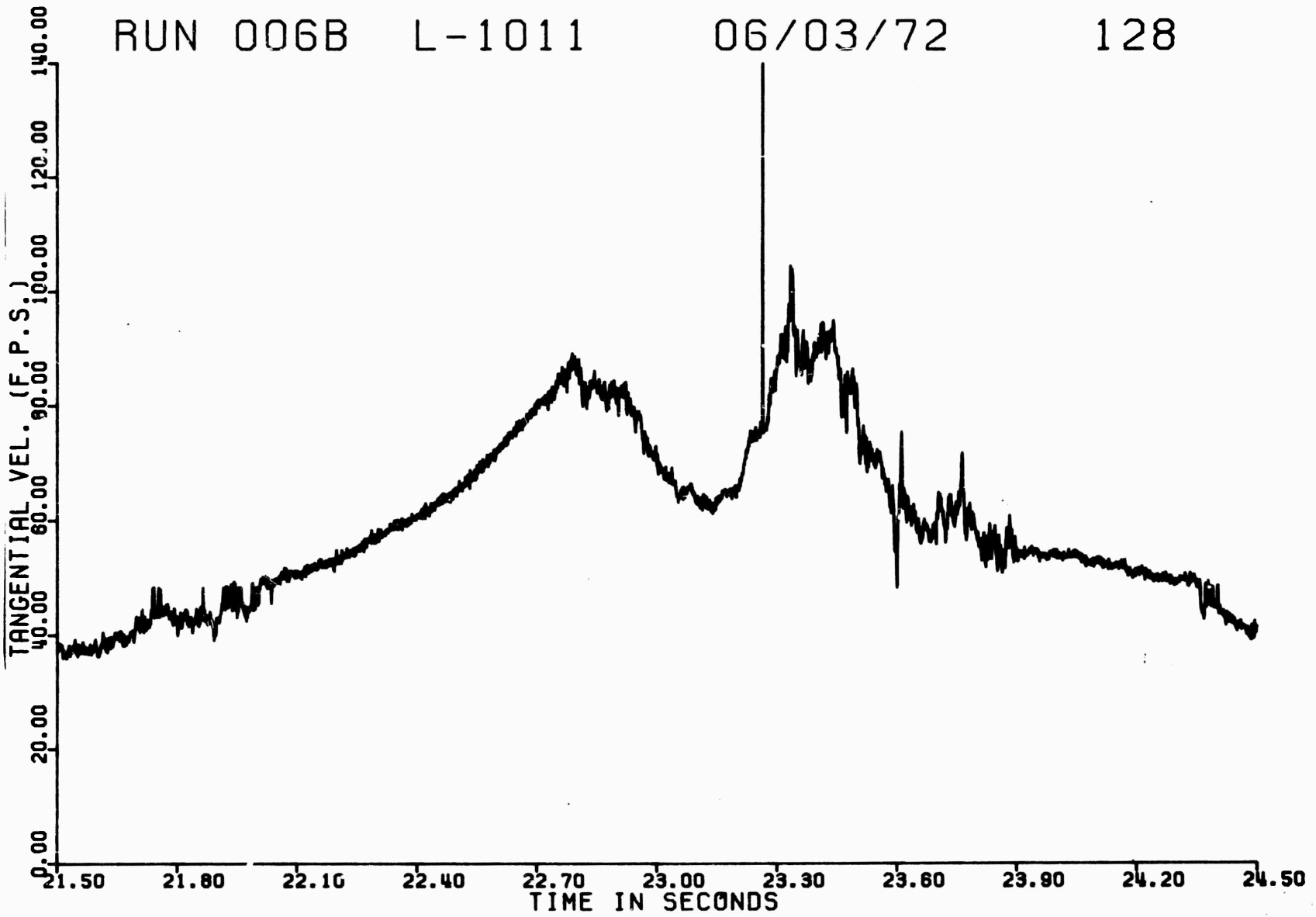
RUN 006B L-1011 06/03/72 128
TANGENTIAL VEL. (F.P.S.)
0.00
20.00
40.00
60.00
80.00
100.00
120.00
140.00
21.50
21.80
22.10
22.40
22.70
23.00
23.30
23.60
23.90
24.20
24.50
TIME IN SECONDS

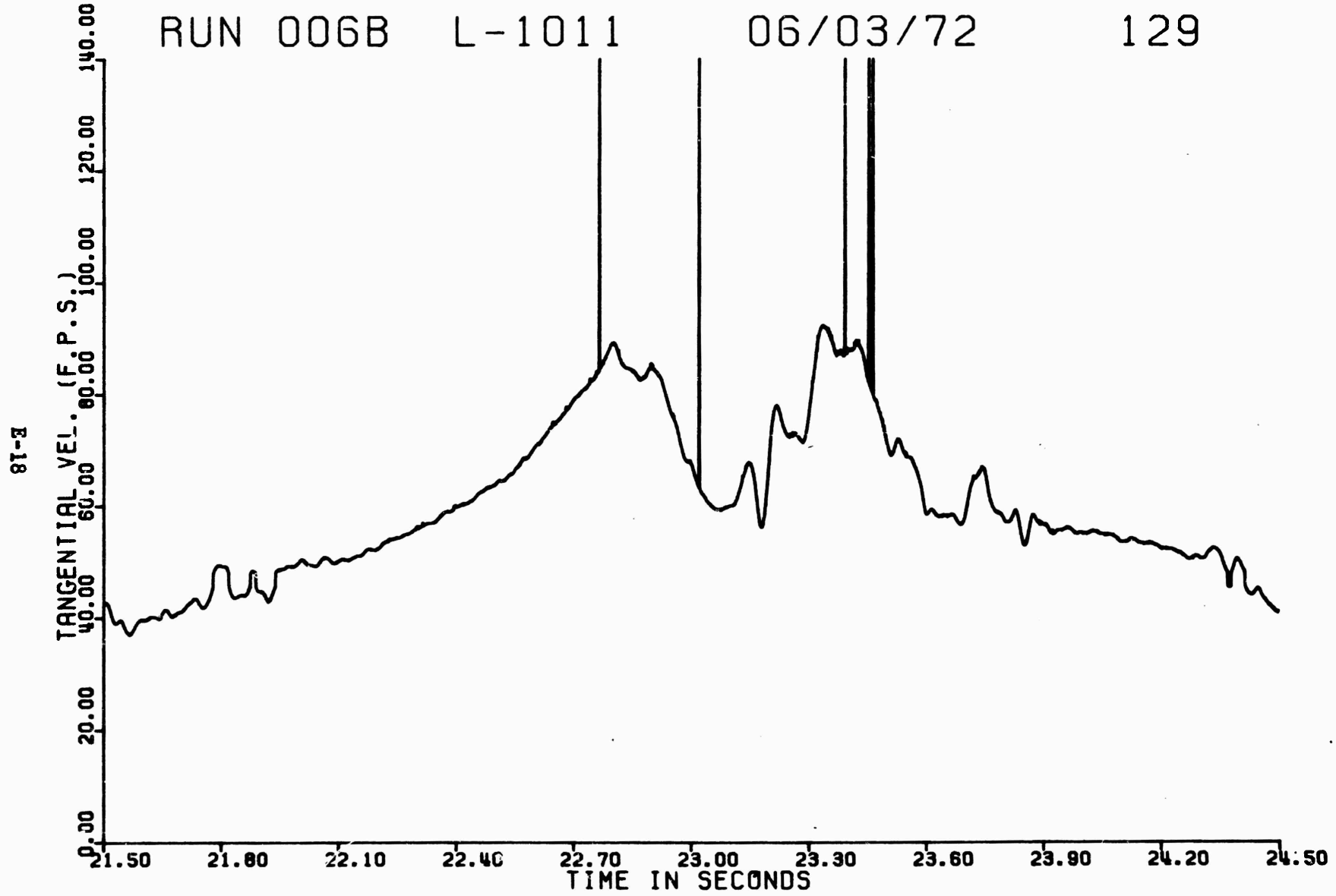
RUN 006B L-1011 06/03/72 129
TANGENTIAL VEL. (F.P.S.)
0.00
20.00
40.00
60.00
80.00
100.00
120.00
140.00
21.50
21.80
22.10
22.40
22.70
23.00
23.30
23.60
23.90
24.20
24.50
TIME IN SECONDS

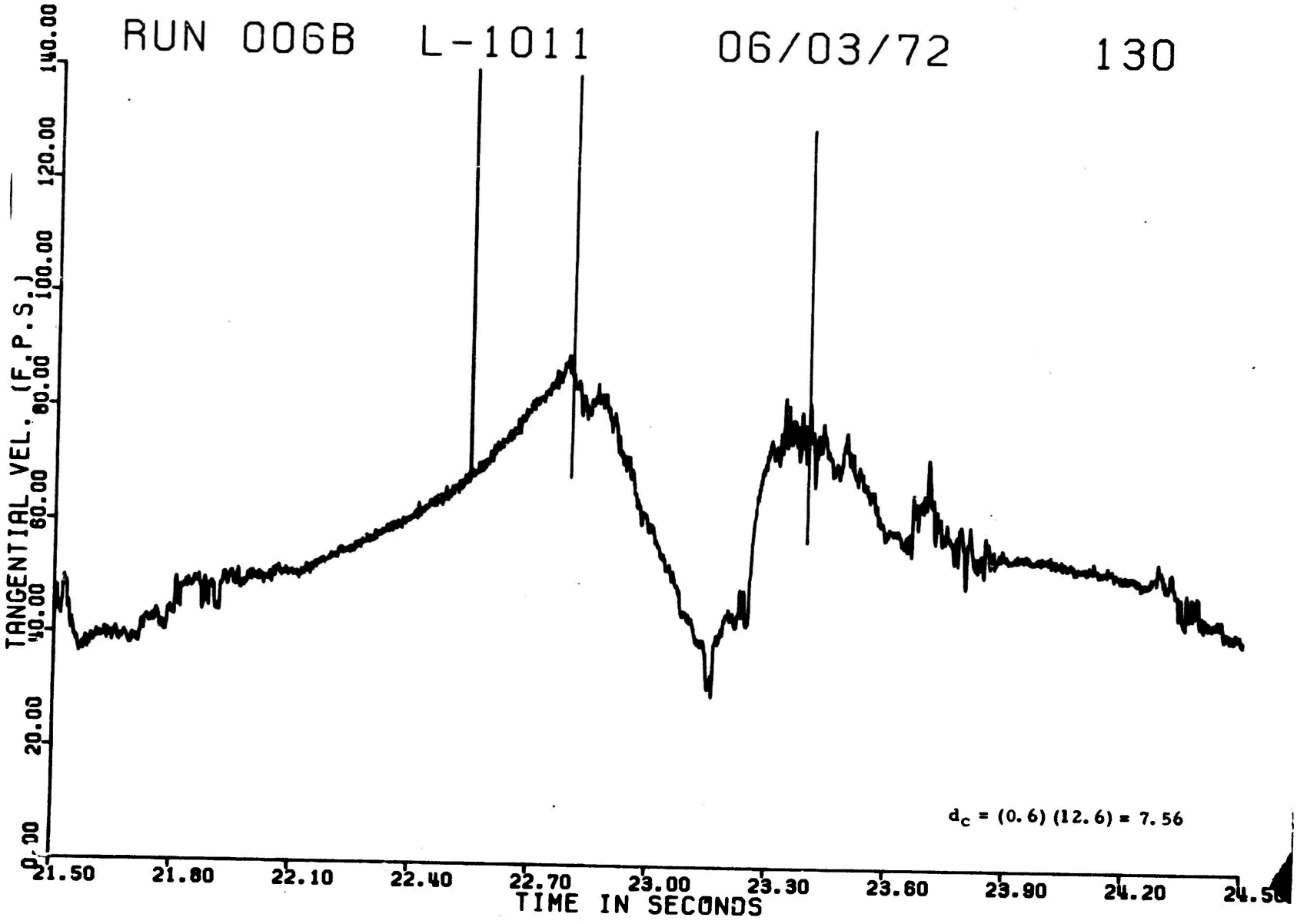
RUN 006B L-1011 06/03/72 130
TANGENTIAL VEL. (F.P.S.)
0.00
20.00
40.00
60.00
80.00
100.00
120.00
140.00
21.50
21.80
22.10
22.40
22.70
23.00
23.30
23.60
23.90
24.20
TIME IN SECONDS
$d_c = (0.6)(12.6) = 7.56$

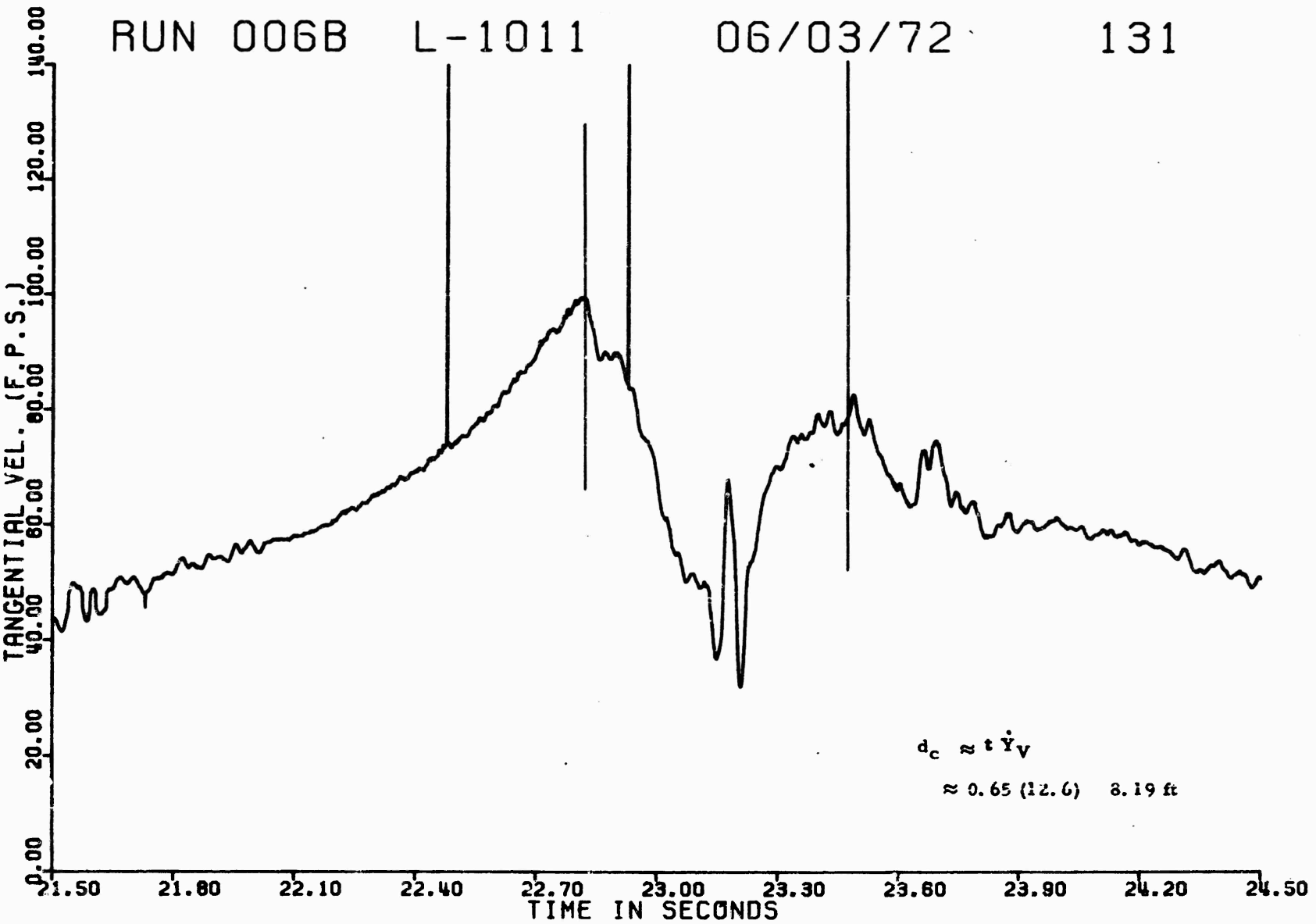
RUN 006B L-1011 06/03/72 131
TANGENTIAL VEL. (F.P.S.)
0.00
20.00
40.00
60.00
80.00
100.00
120.00
140.00
21.50
21.80
22.10
22.40
22.70
23.00
23.30
23.60
23.90
24.20
24.50
TIME IN SECONDS
$d_c \approx t \dot{Y}_V$
$\approx 0.65\ (12.6)$ 8.19 ft

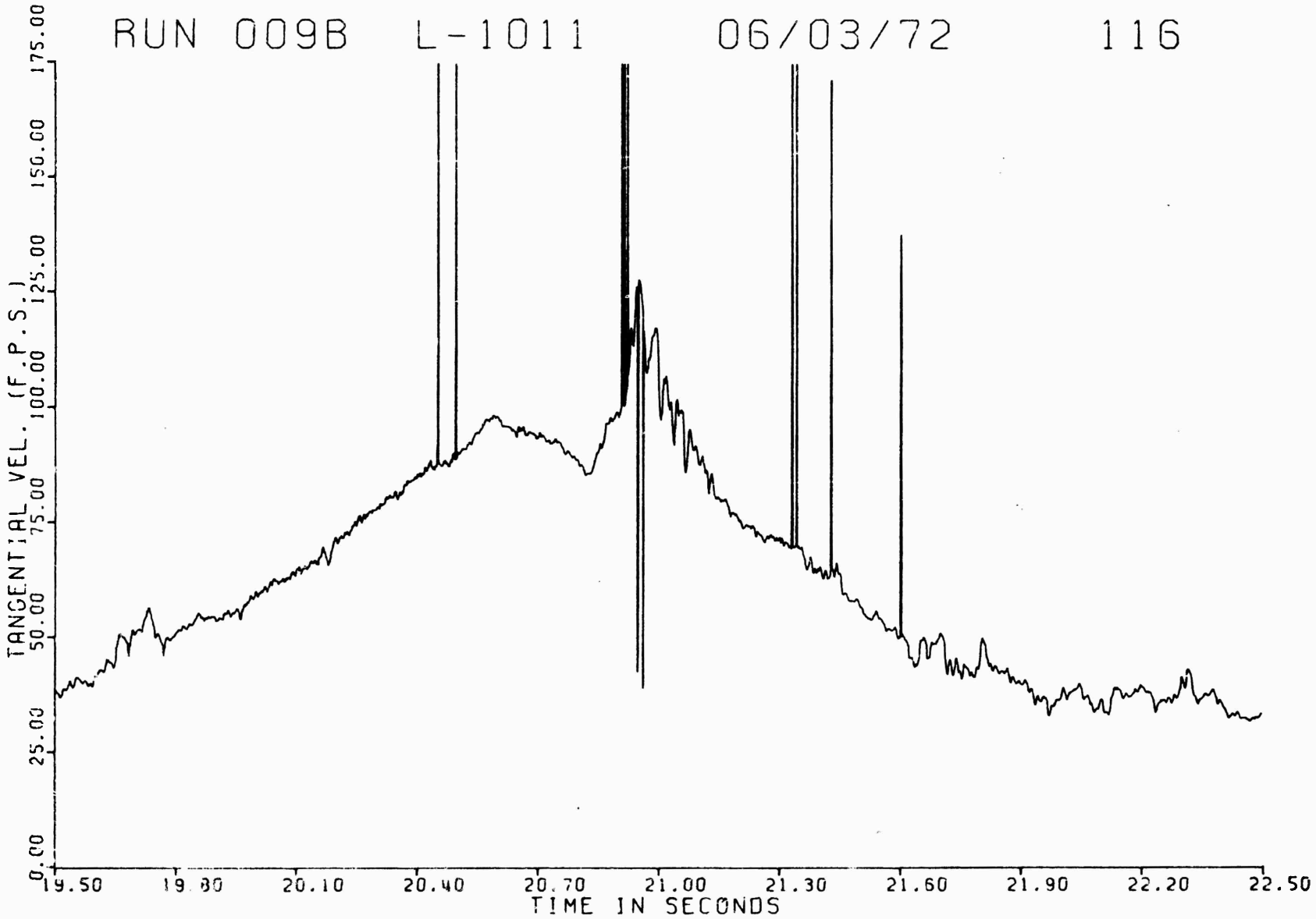
RUN 009B L-1011 06/03/72 116
TANGENTIAL VEL. (F.P.S.)
0.00
25.00
50.00
75.00
100.00
125.00
150.00
175.00
19.50
19.80
20.10
20.40
20.70
21.00
21.30
21.60
21.90
22.20
22.50
TIME IN SECONDS

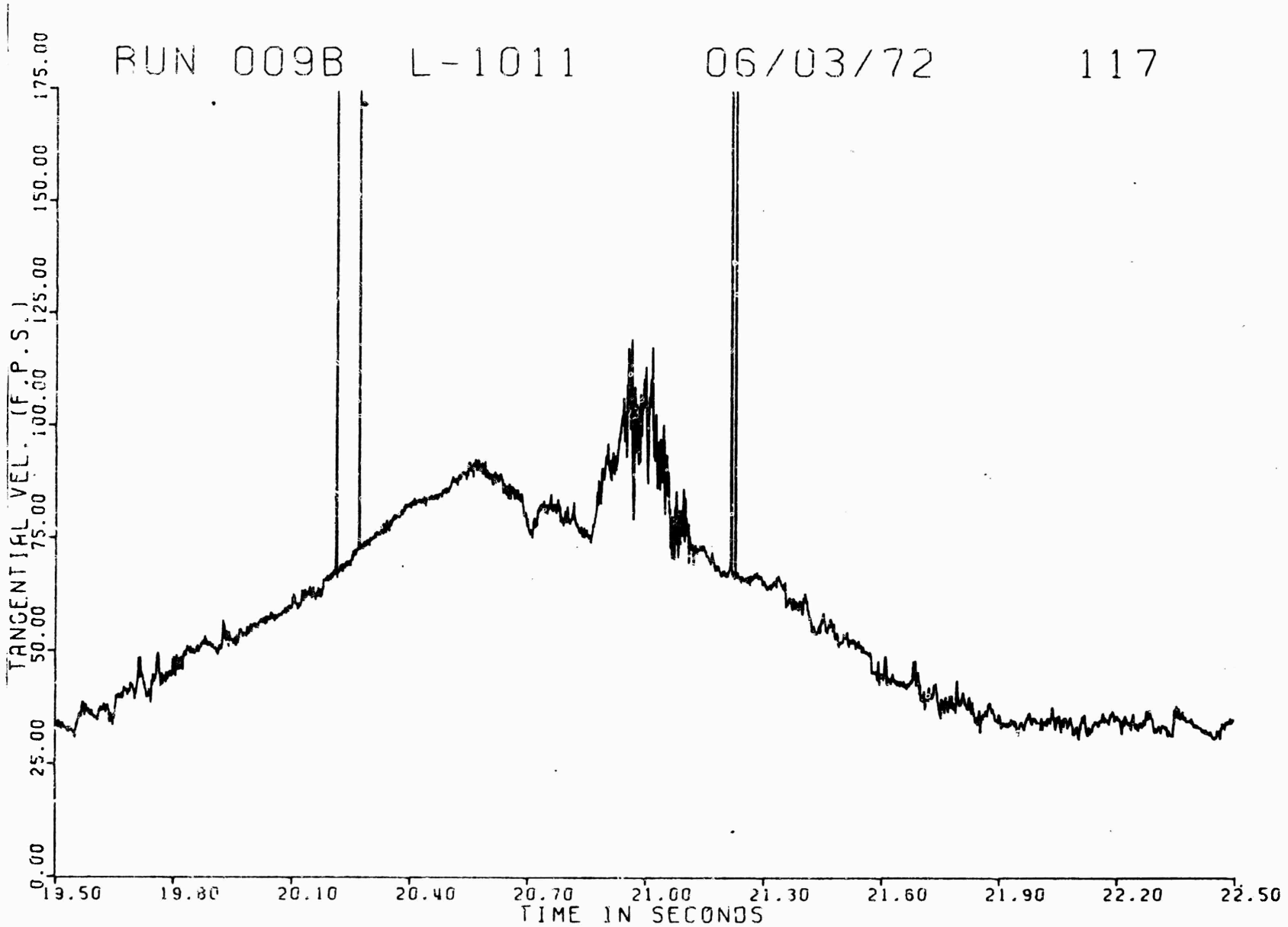
RUN 009B L-1011 06/03/72 117
TANGENTIAL VEL. (F.P.S.)
0.00
25.00
50.00
75.00
100.00
125.00
150.00
175.00
19.50
19.80
20.10
20.40
20.70
21.00
21.30
21.60
21.90
22.20
22.50
TIME IN SECONDS

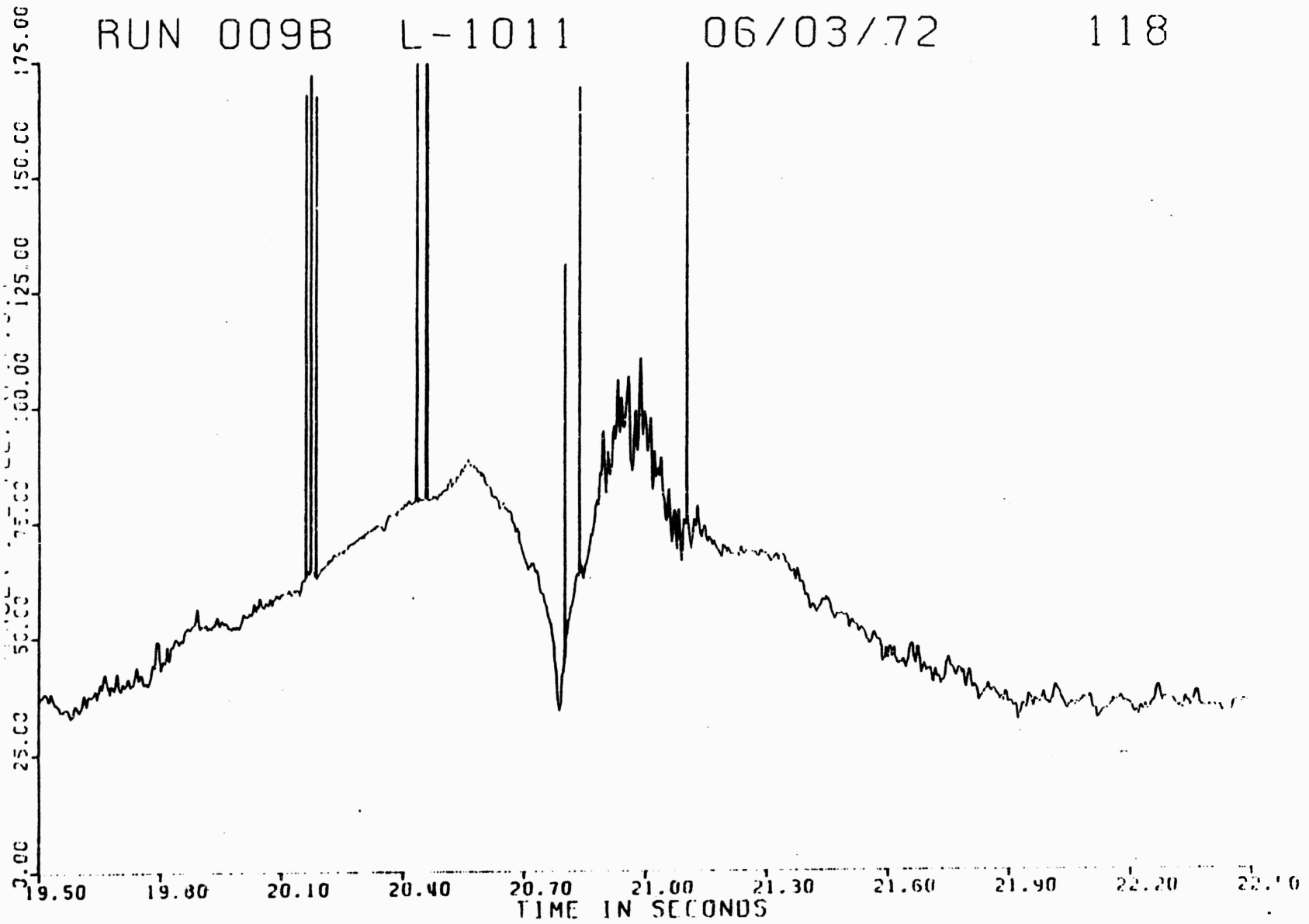
RUN 009B L-1011 06/03/72 118
175.00
150.00
125.00
100.00
75.00
50.00
25.00
0.00
19.50
19.80
20.10
20.40
20.70
21.00
21.30
21.60
21.90
22.20
TIME IN SECONDS

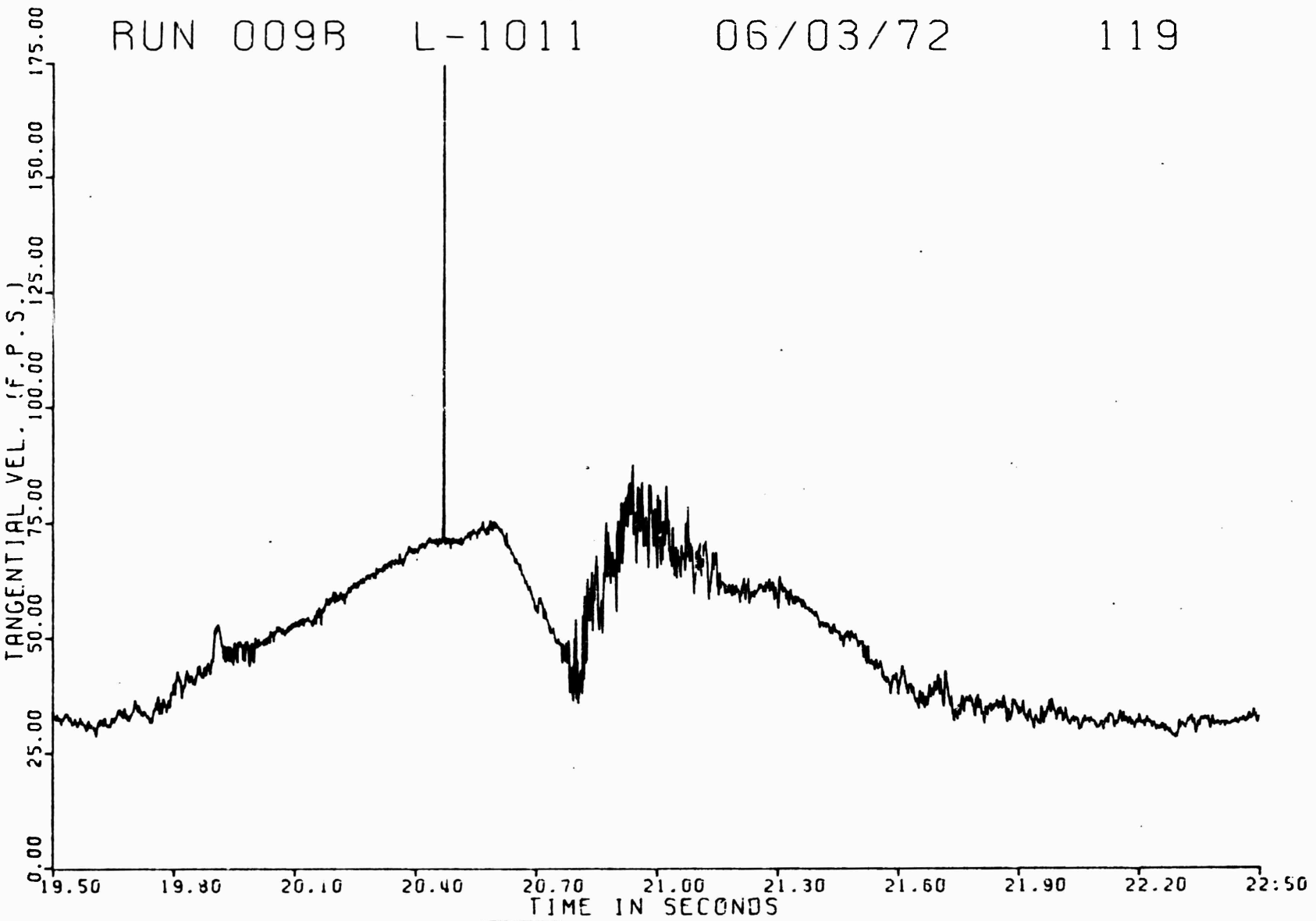
RUN 009B L-1011 06/03/72 119
TANGENTIAL VEL. (F.P.S.)
0.00
25.00
50.00
75.00
100.00
125.00
150.00
175.00
19.50
19.80
20.10
20.40
20.70
21.00
21.30
21.60
21.90
22.20
22:50
TIME IN SECONDS

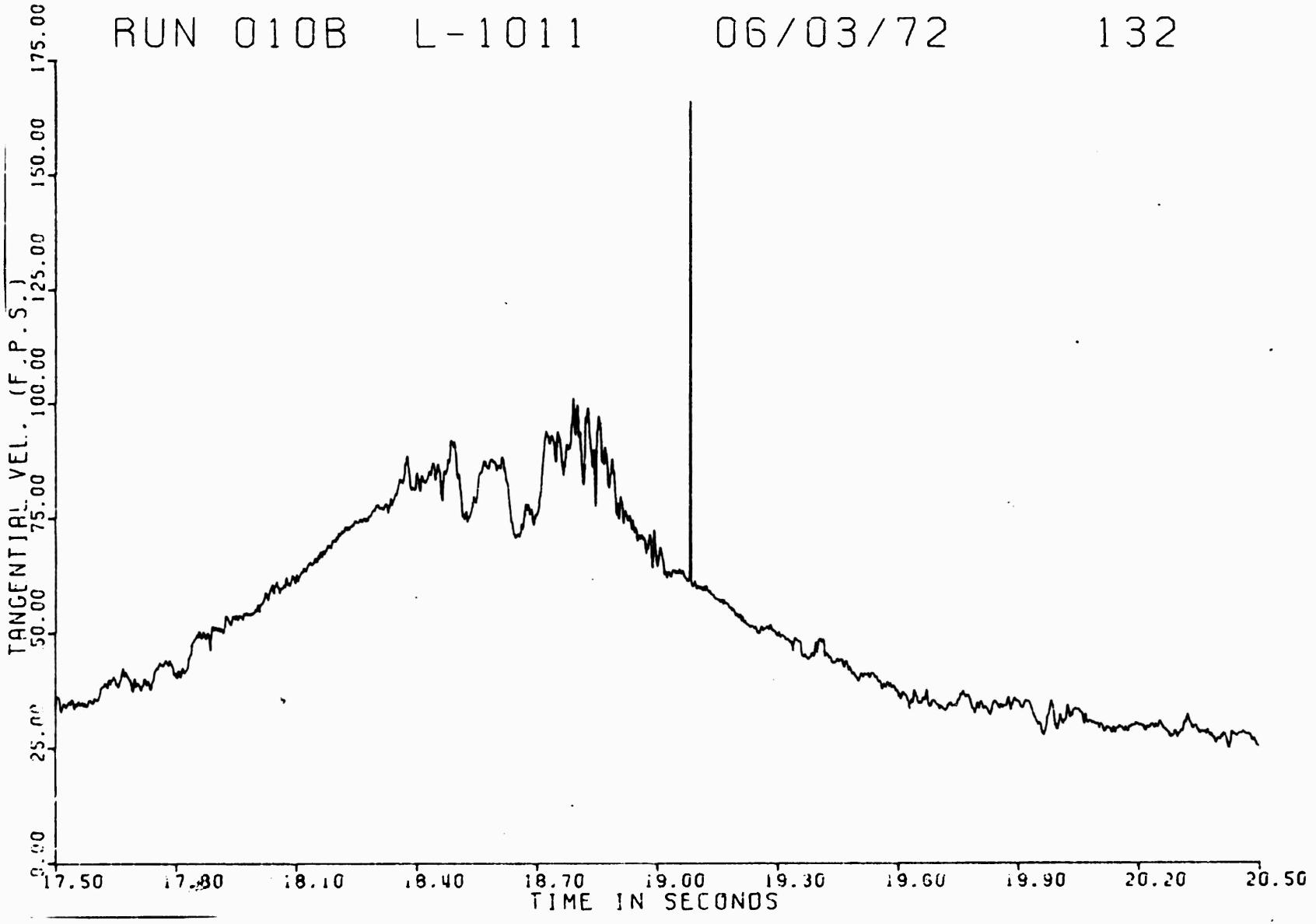
RUN 010B L-1011 06/03/72 132
TANGENTIAL VEL. (F.P.S.)
175.00
150.00
125.00
100.00
75.00
50.00
25.00
0.00
17.50
17.80
18.10
18.40
18.70
19.00
19.30
19.60
19.90
20.20
20.50
TIME IN SECONDS

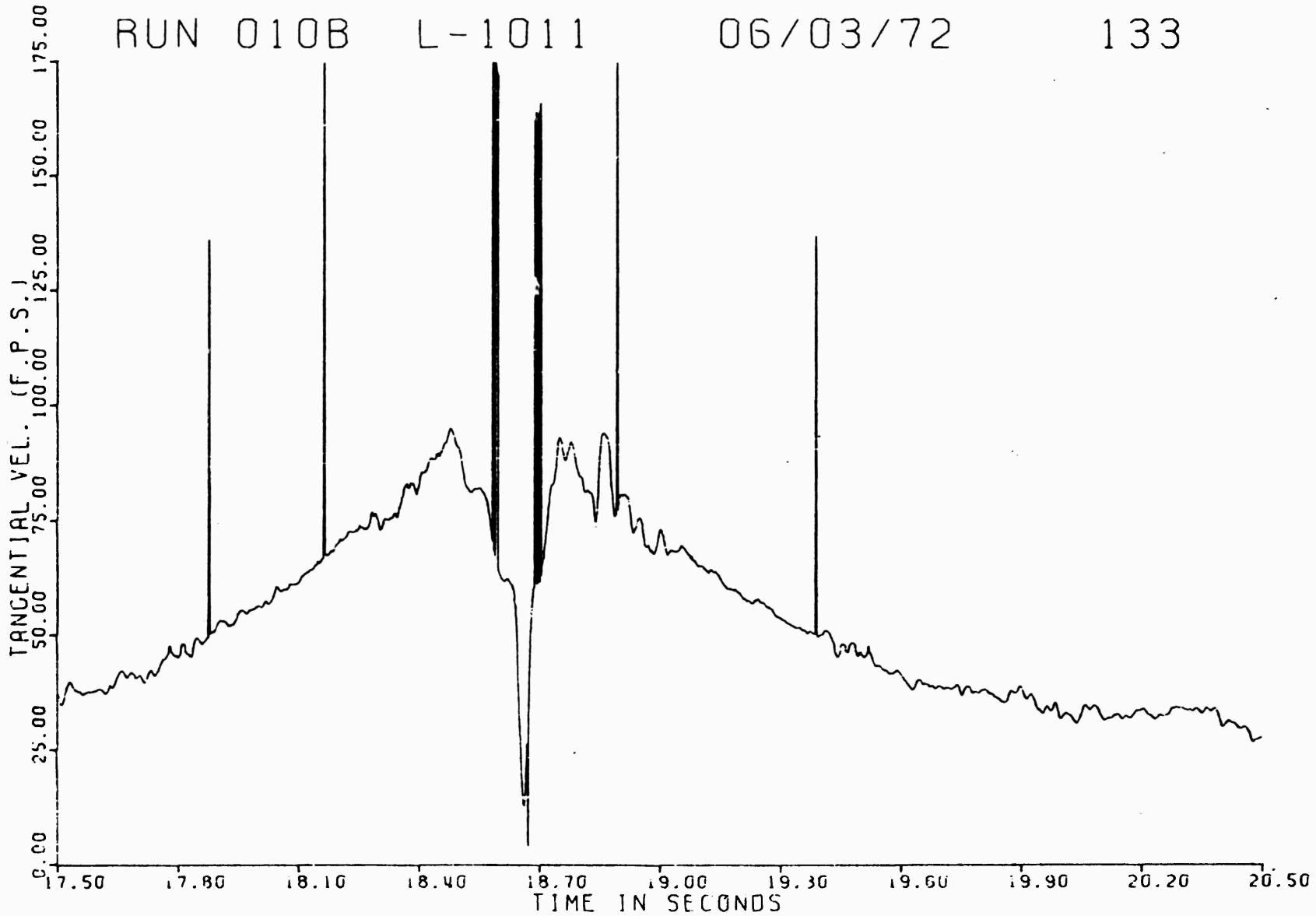
RUN 010B L-1011 06/03/72 133
TANGENTIAL VEL. (F.P.S.)
0.00
25.00
50.00
75.00
100.00
125.00
150.00
175.00
17.50
17.80
18.10
18.40
18.70
19.00
19.30
19.60
19.90
20.20
20.50
TIME IN SECONDS

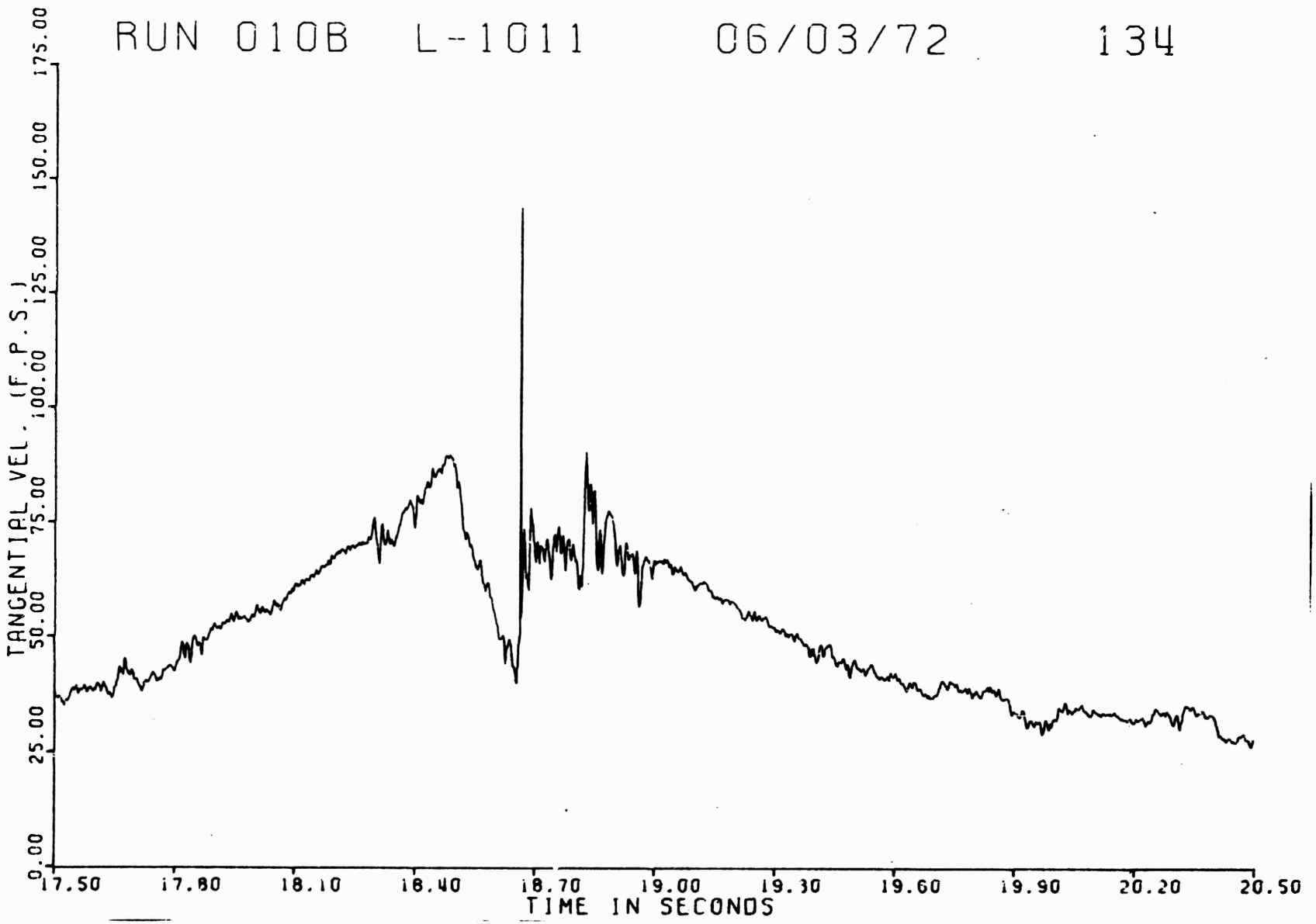
RUN 010B L-1011 06/03/72 134
TANGENTIAL VEL. (F.P.S.)
0.00
25.00
50.00
75.00
100.00
125.00
150.00
175.00
17.50
17.80
18.10
18.40
18.70
19.00
19.30
19.60
19.90
20.20
20.50
TIME IN SECONDS

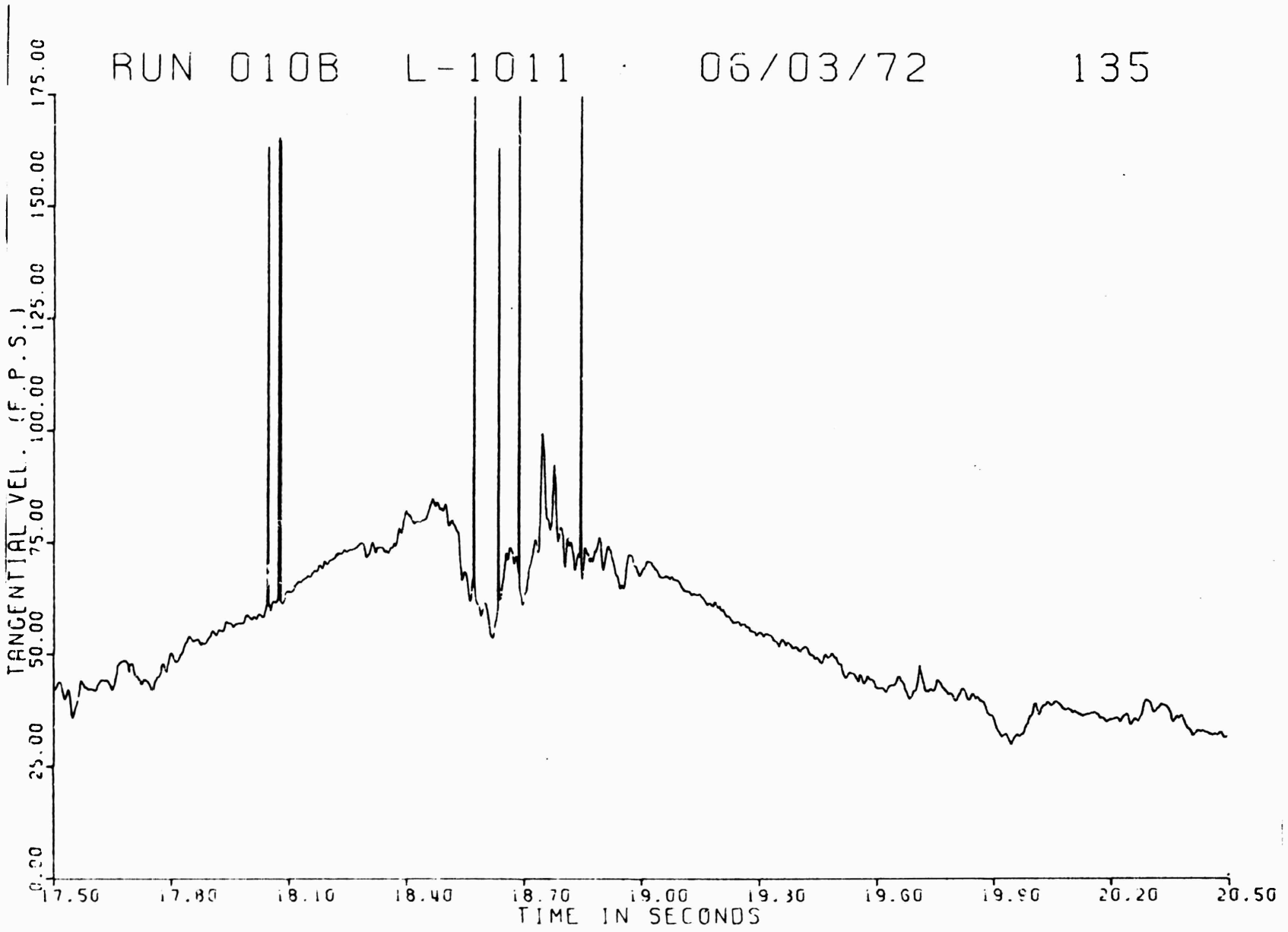
RUN 010B L-1011 06/03/72 135
TANGENTIAL VEL. (F.P.S.)
175.00
150.00
125.00
100.00
75.00
50.00
25.00
0.00
17.50
17.80
18.10
18.40
18.70
19.00
19.30
19.60
19.90
20.20
20.50
TIME IN SECONDS

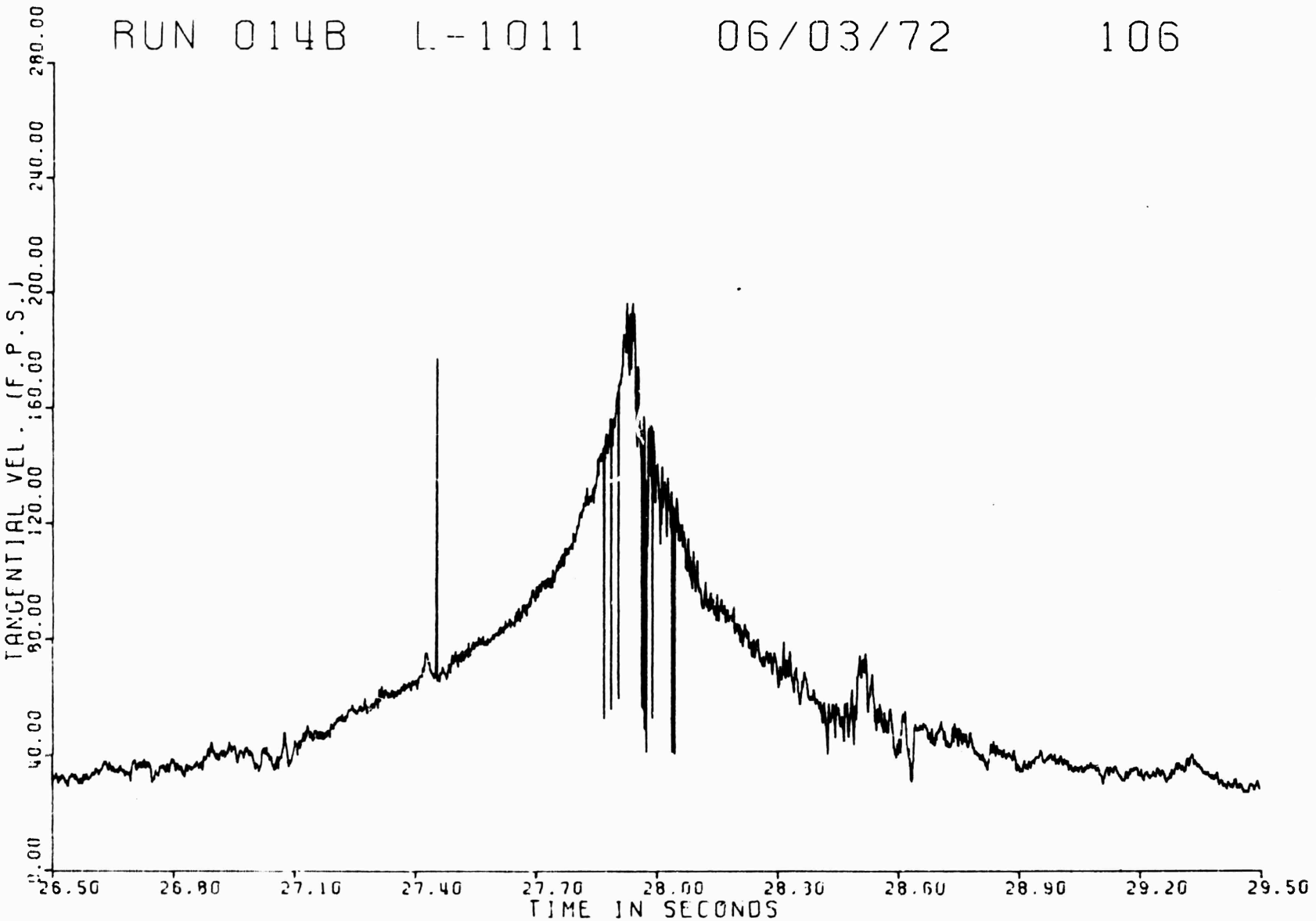
RUN 014B L-1011 06/03/72 106
TANGENTIAL VEL. (F.P.S.)
0.00
40.00
80.00
120.00
160.00
200.00
240.00
280.00
26.50
26.80
27.10
27.40
27.70
28.00
28.30
28.60
28.90
29.20
29.50
TIME IN SECONDS

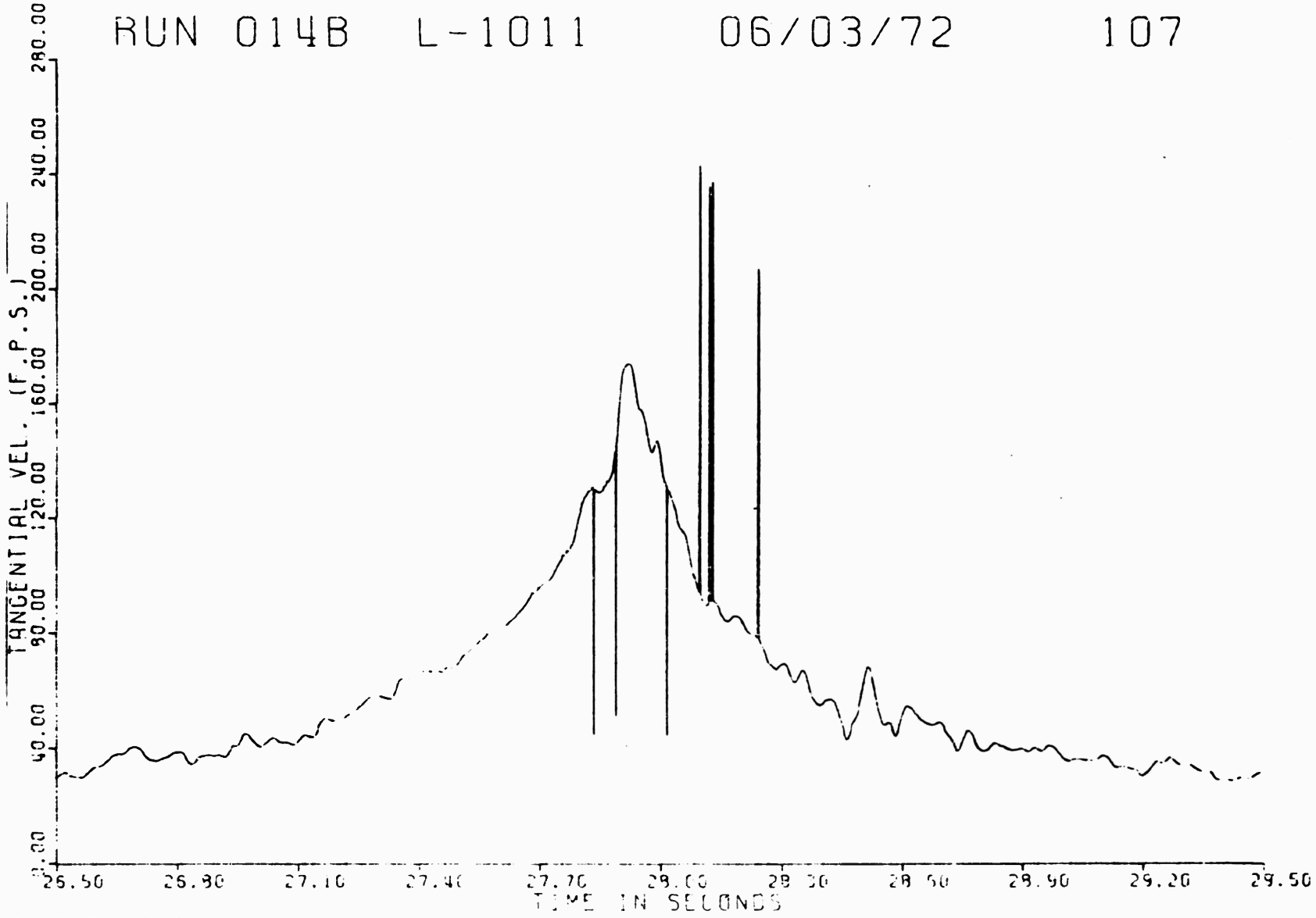
RUN 014B L-1011 06/03/72 107
TANGENTIAL VEL. (F.P.S.)
280.00
240.00
200.00
160.00
120.00
80.00
40.00
26.50
26.80
27.10
27.40
27.70
28.00
28.30
28.60
28.90
29.20
29.50
TIME IN SECONDS

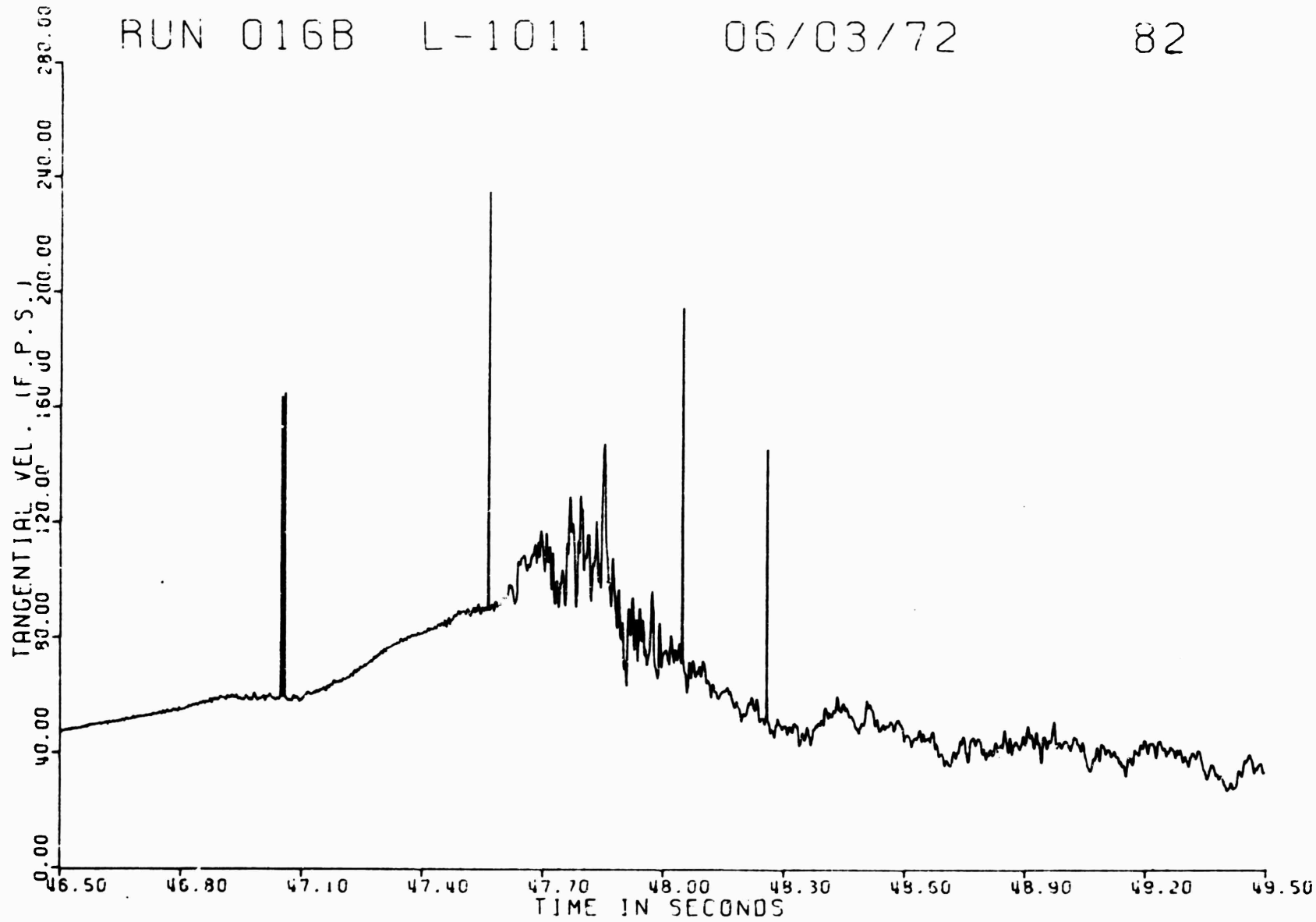
RUN 016B L-1011 06/03/72 82
TANGENTIAL VEL. (F.P.S.)
0.00
40.00
80.00
120.00
160.00
200.00
240.00
280.00
46.50
46.80
47.10
47.40
47.70
48.00
48.30
48.60
48.90
49.20
49.50
TIME IN SECONDS

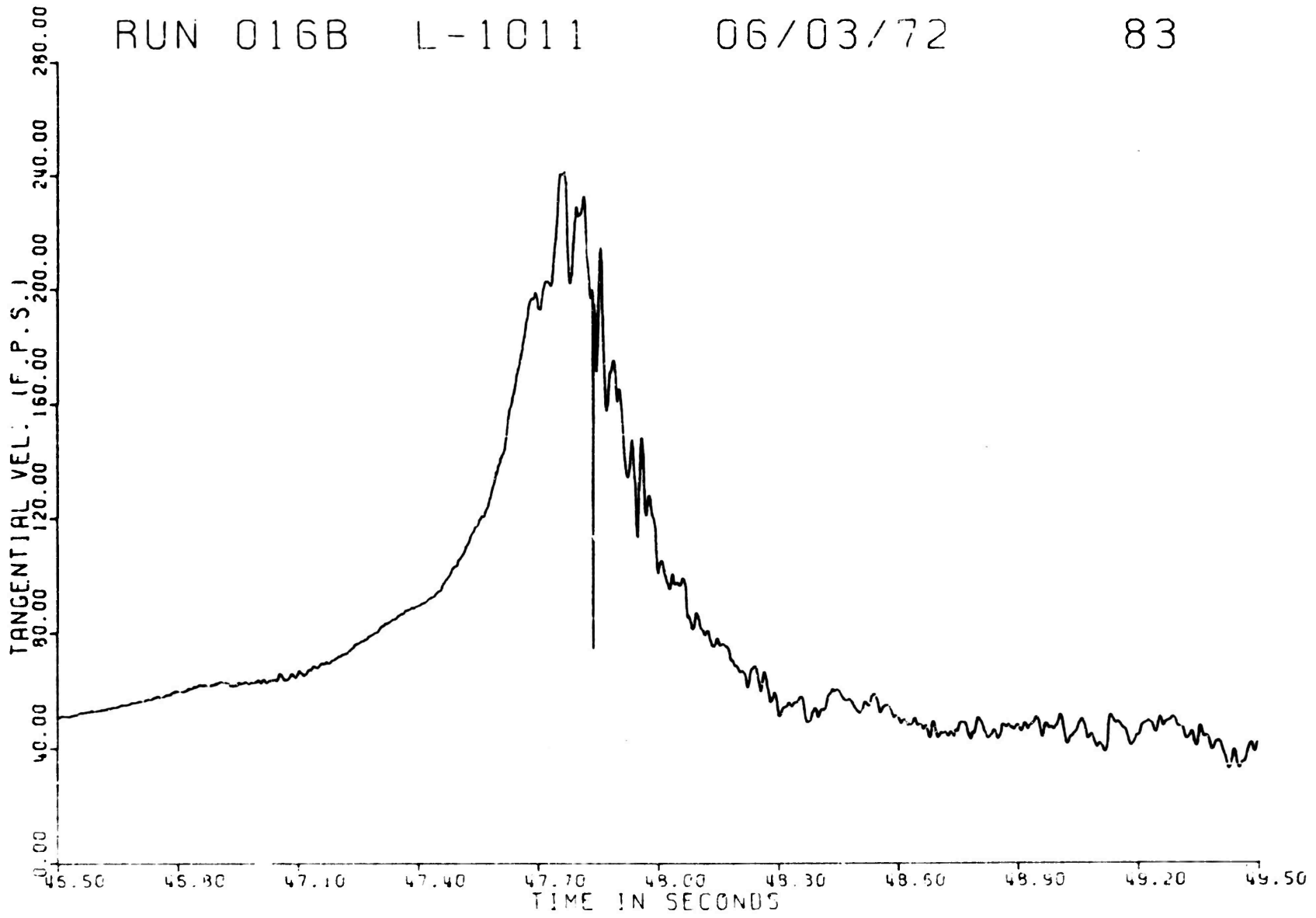
RUN 016B L-1011 06/03/72 83
TANGENTIAL VEL. (F.P.S.)
0.00
40.00
80.00
120.00
160.00
200.00
240.00
280.00
45.50
45.80
47.10
47.40
47.70
48.00
48.30
48.60
48.90
49.20
49.50
TIME IN SECONDS

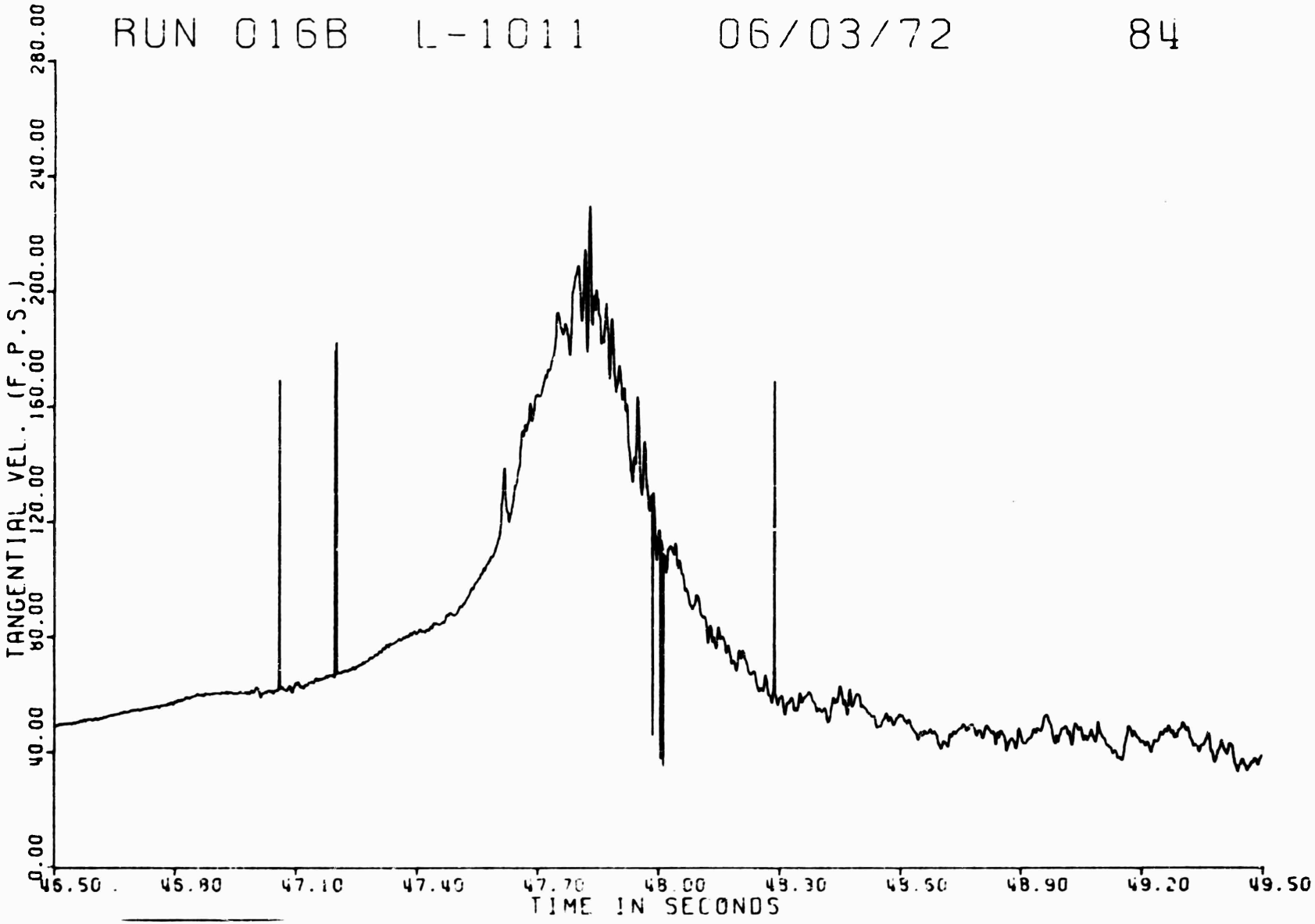
RUN 016B L-1011 06/03/72 84
TANGENTIAL VEL. (F.P.S.)
0.00
40.00
80.00
120.00
160.00
200.00
240.00
280.00
46.50
46.80
47.10
47.40
47.70
48.00
48.30
48.60
48.90
49.20
49.50
TIME IN SECONDS

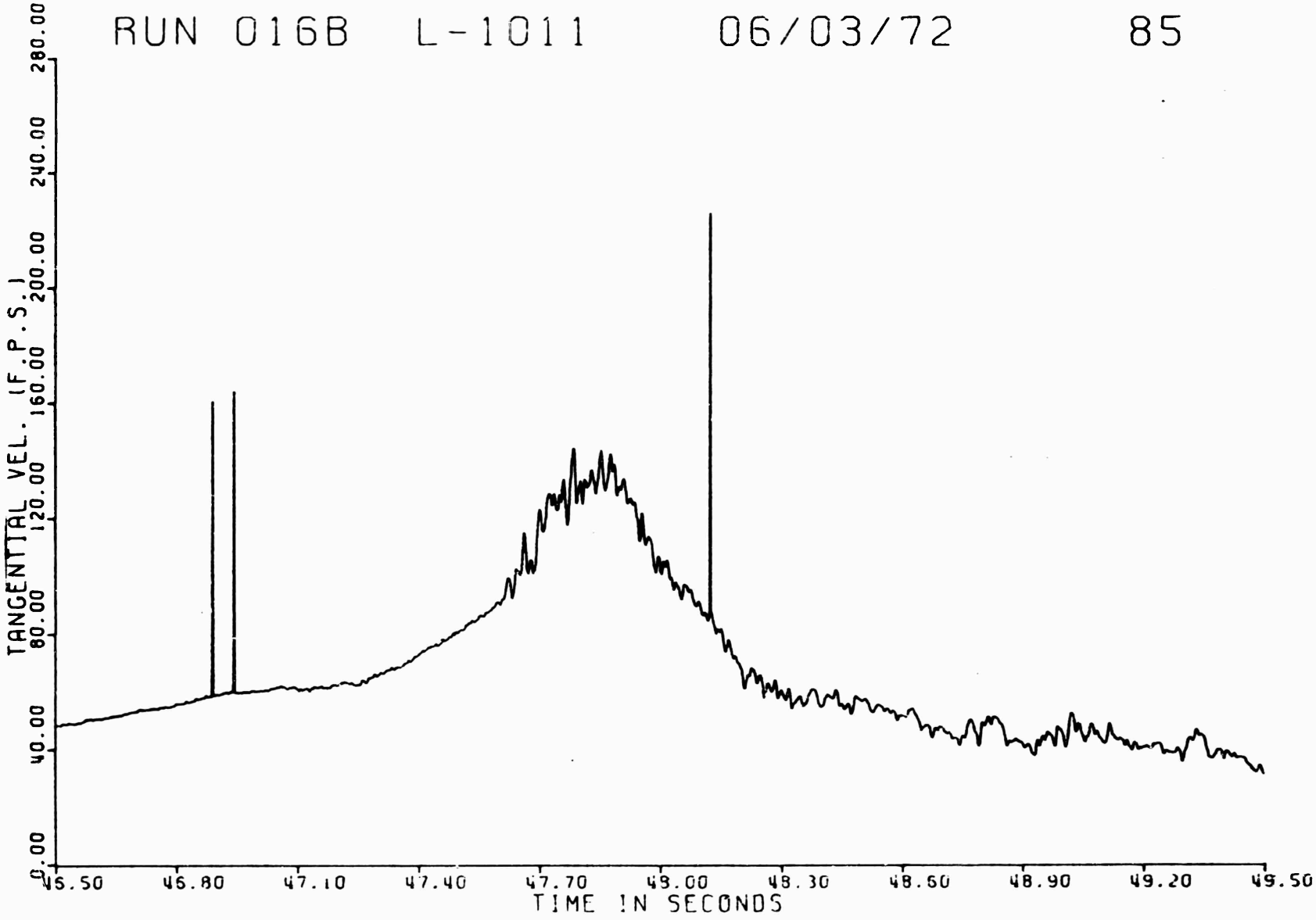
RUN 016B L-1011 06/03/72 85
TANGENTTAL VEL. (F.P.S.)
0.00
40.00
80.00
120.00
160.00
200.00
240.00
280.00
46.50
46.80
47.10
47.40
47.70
48.00
48.30
48.60
48.90
49.20
49.50
TIME IN SECONDS

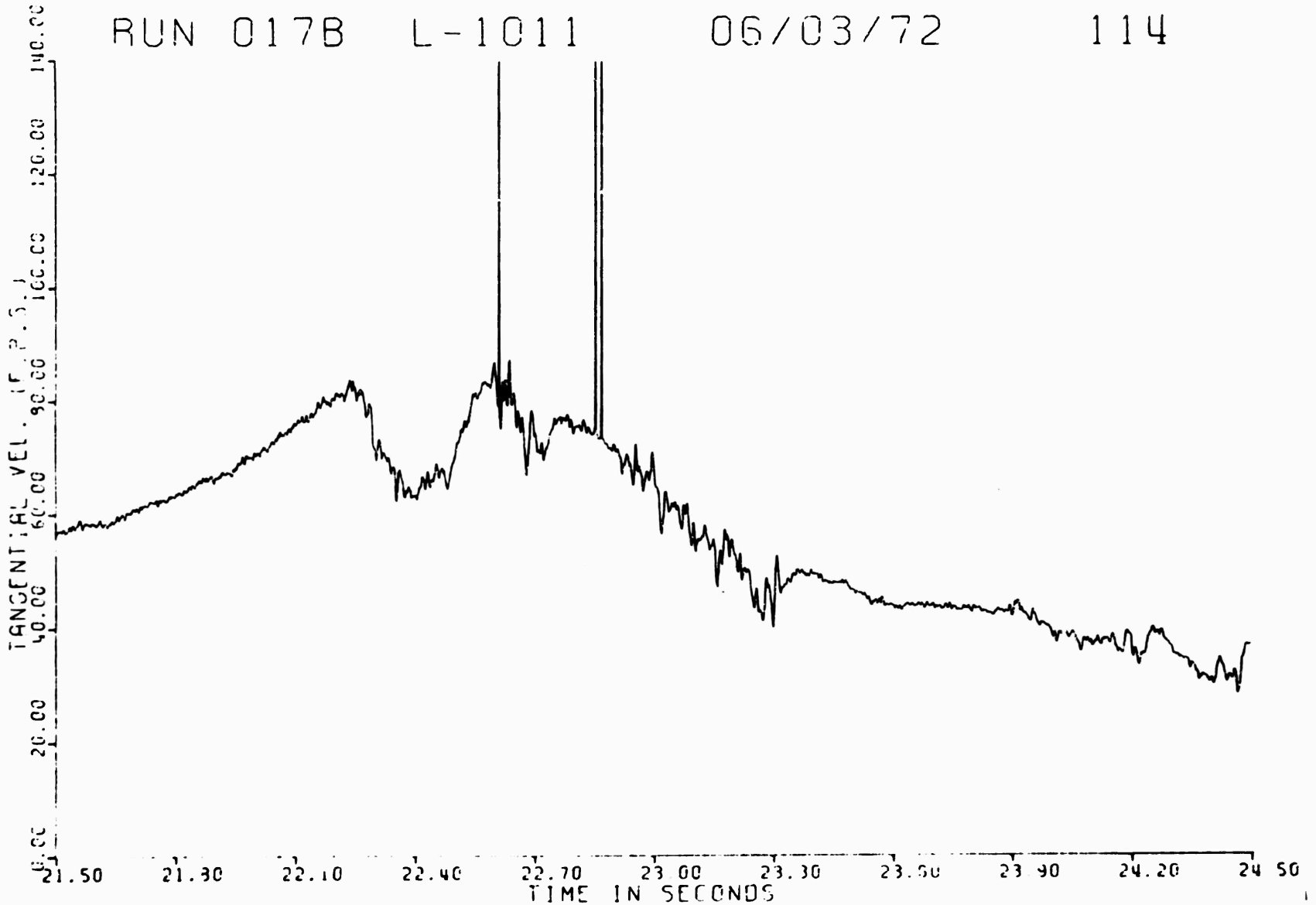
RUN 017B L-1011 06/03/72 114
TANGENTIAL VEL.
120.00
100.00
80.00
60.00
40.00
20.00
21.50
21.80
22.10
22.40
22.70
23.00
23.30
23.90
24.20
TIME IN SECONDS

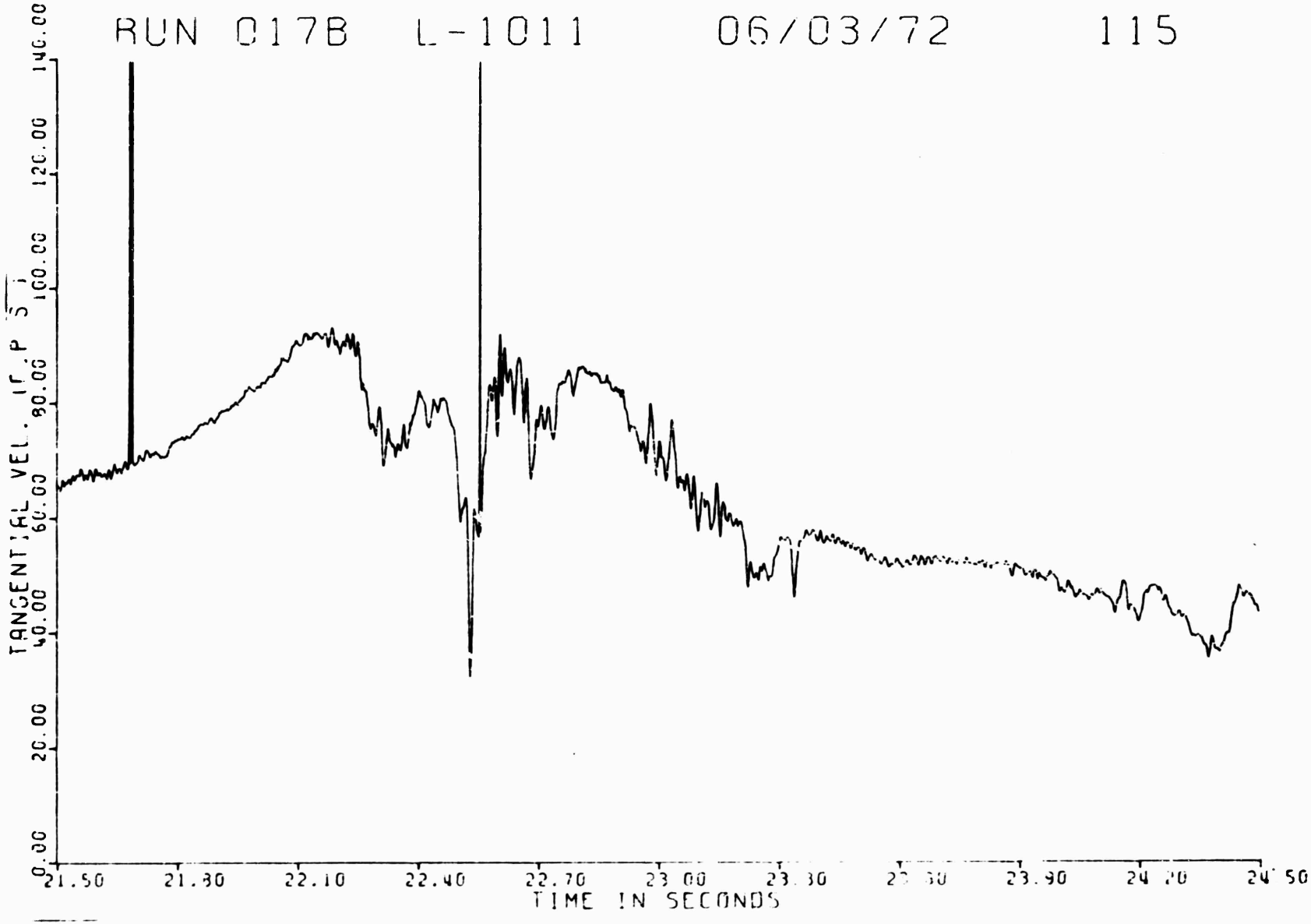
RUN 017B L-1011 06/03/72 115
TANGENTIAL VEL., FPS
0.00
20.00
40.00
60.00
80.00
100.00
120.00
140.00
21.50
21.80
22.10
22.40
22.70
23.00
23.30
23.60
23.90
24.20
24.50
TIME IN SECONDS

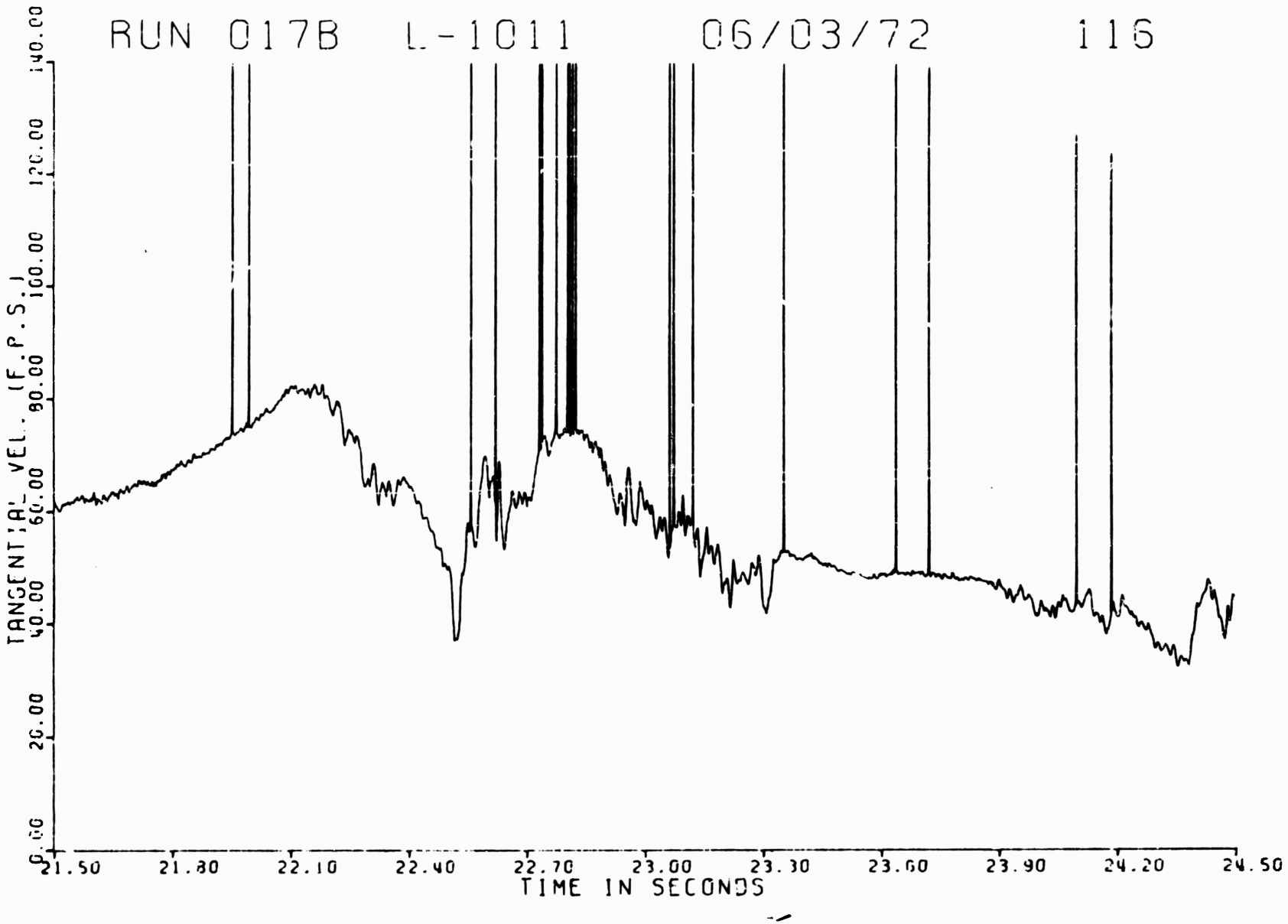
RUN 017B L-1011 06/03/72 116
TANGENTIAL VEL. (F.P.S.)
0.00
20.00
40.00
60.00
80.00
100.00
120.00
140.00
21.50
21.80
22.10
22.40
22.70
23.00
23.30
23.60
23.90
24.20
24.50
TIME IN SECONDS

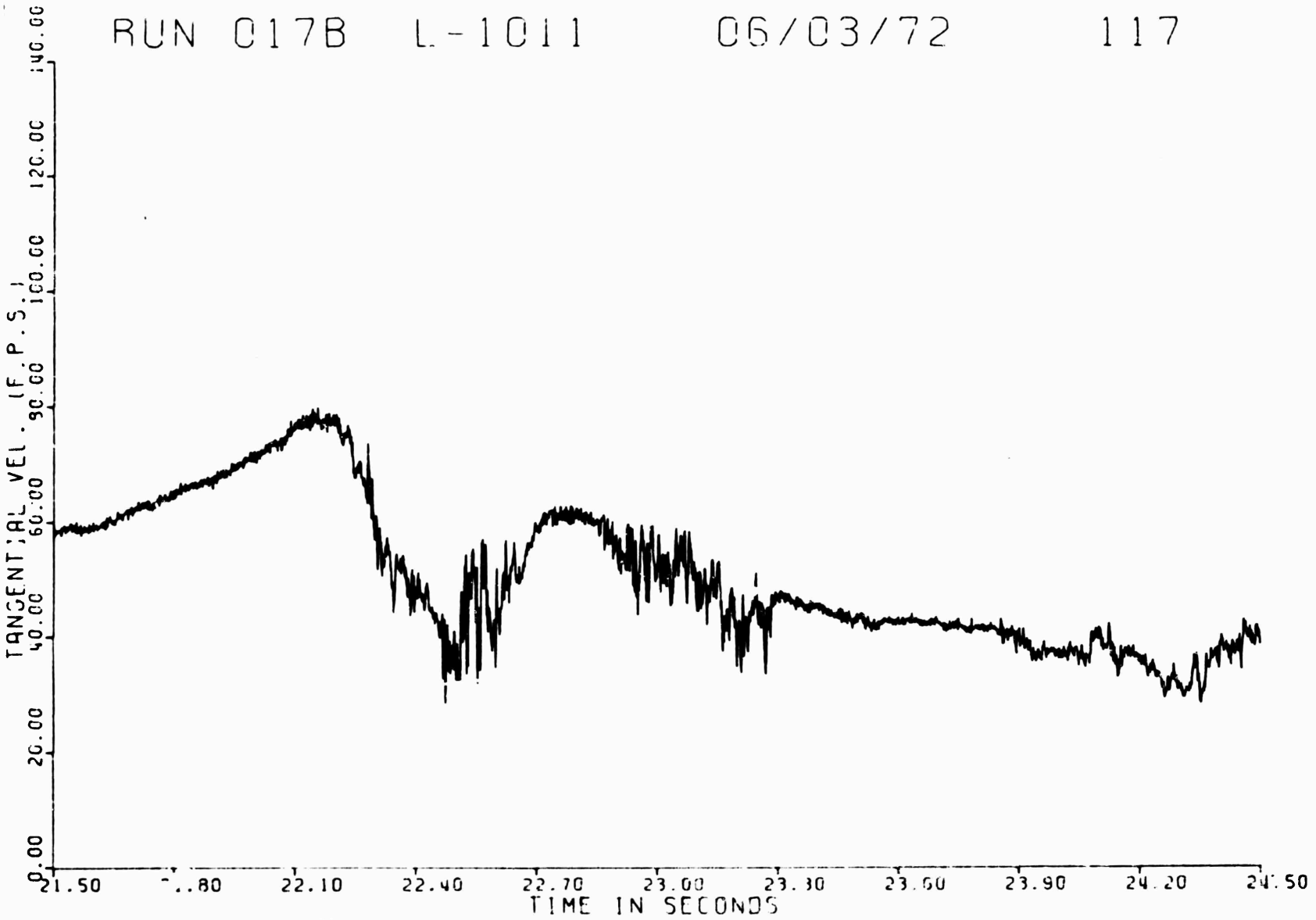
RUN 017B L-1011 06/03/72 117
TANGENTIAL VEL. (F.P.S.)
0.00
20.00
40.00
60.00
80.00
100.00
120.00
140.00
21.50
21.80
22.10
22.40
22.70
23.00
23.30
23.60
23.90
24.20
24.50
TIME IN SECONDS

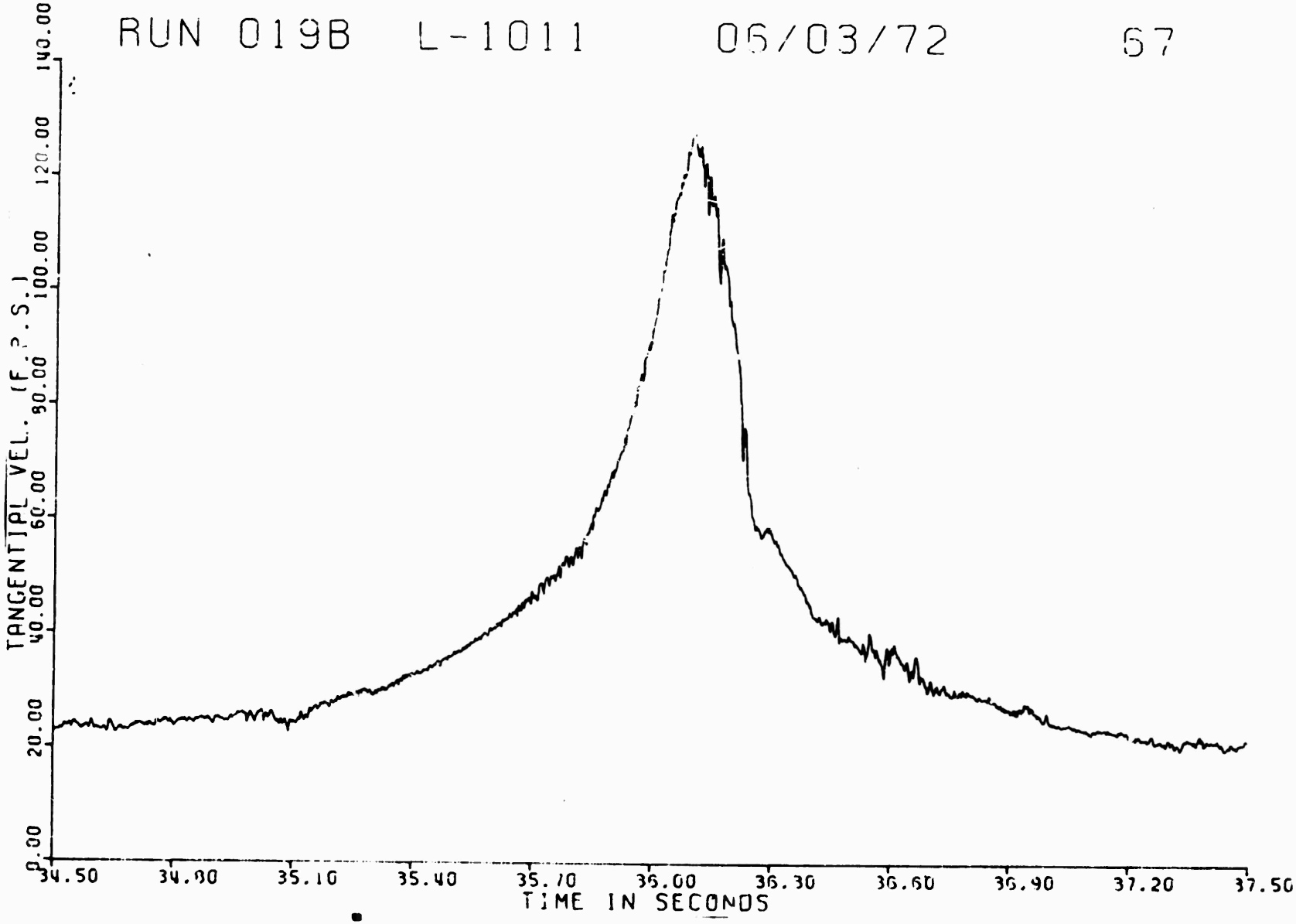
RUN 019B L-1011 06/03/72 67
TANGENTIAL VEL. (F.P.S.)
0.00
20.00
40.00
60.00
80.00
100.00
120.00
140.00
34.50
34.80
35.10
35.40
35.70
36.00
36.30
36.60
36.90
37.20
37.50
TIME IN SECONDS

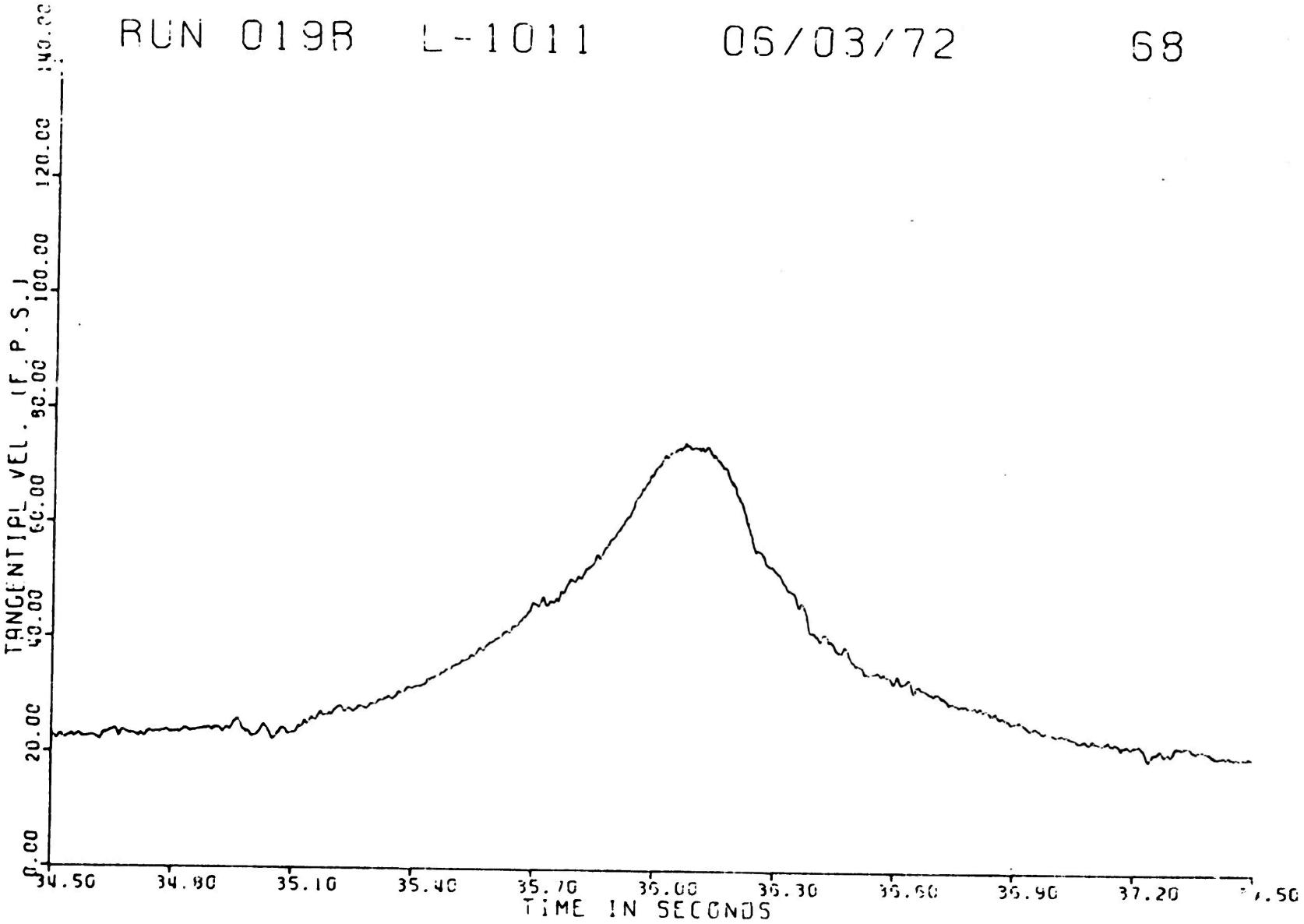
RUN 019B L-1011 06/03/72 68
TANGENTIAL VEL. IF.P.S.)
0.00
20.00
40.00
60.00
80.00
100.00
120.00
34.50
34.80
35.10
35.40
35.70
36.00
36.30
36.60
36.90
37.20
TIME IN SECONDS

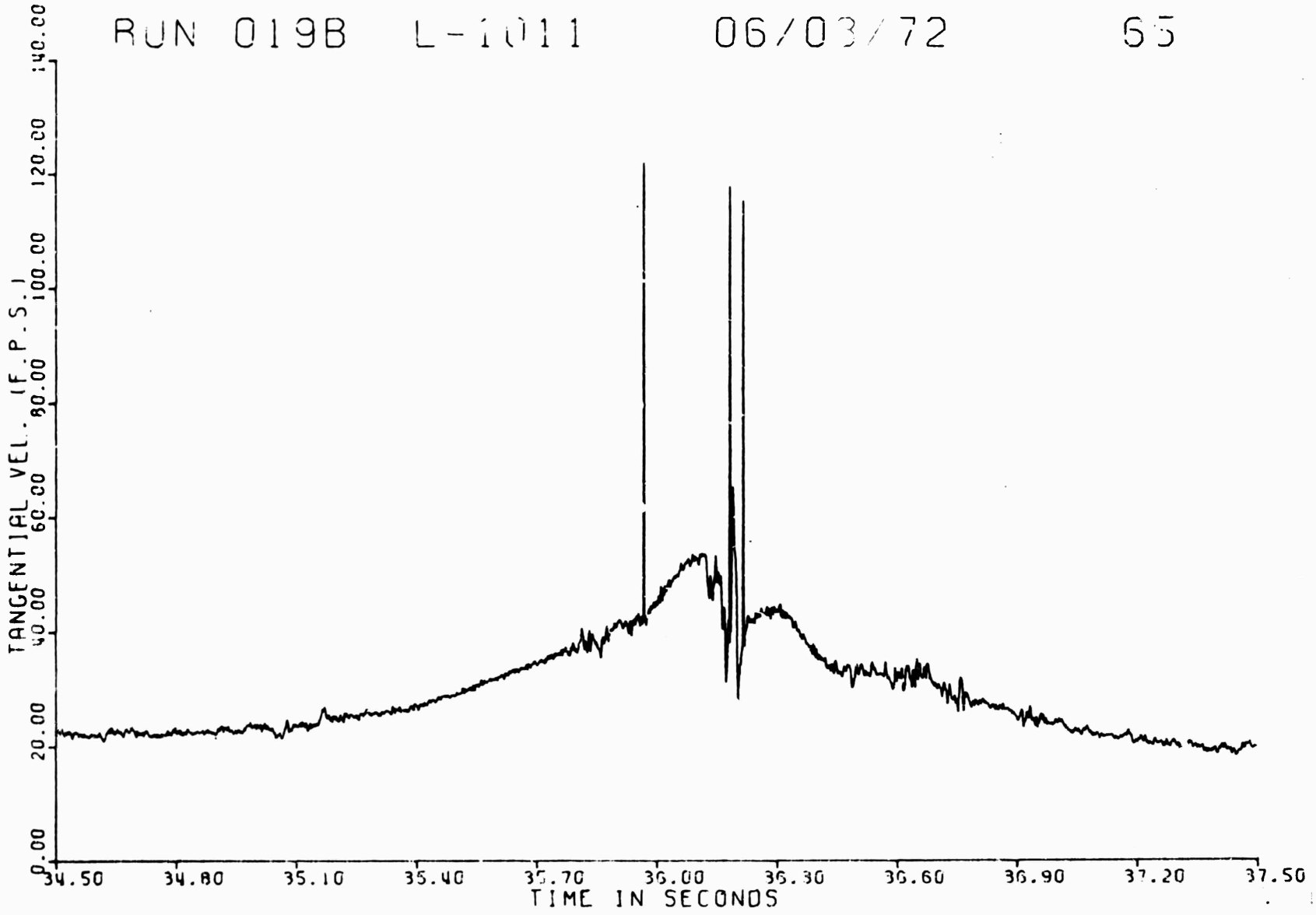
RUN 019B L-1011 06/03/72 65
TANGENTIAL VEL. (F.P.S.)
0.00
20.00
40.00
60.00
80.00
100.00
120.00
140.00
34.50
34.80
35.10
35.40
35.70
36.00
36.30
36.60
36.90
37.20
37.50
TIME IN SECONDS

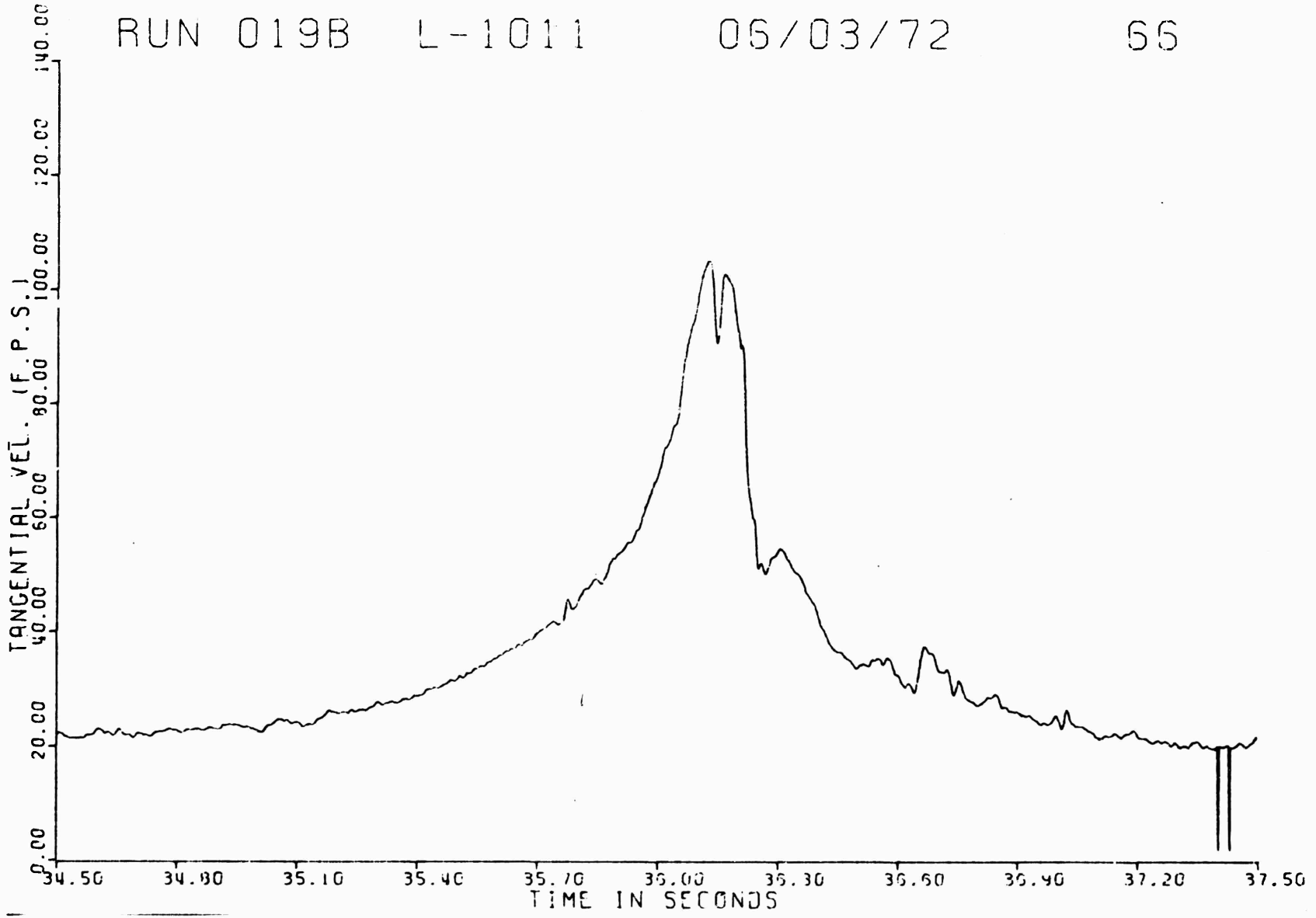
RUN 019B L-1011 06/03/72 66
TANGENTIAL VEL. (F.P.S.)
0.00
20.00
40.00
60.00
80.00
100.00
120.00
140.00
34.50
34.80
35.10
35.40
35.70
36.00
36.30
36.60
36.90
37.20
37.50
TIME IN SECONDS

APPENDIX F

RECORDED VORTEX TANGENTIAL VELOCITY VERSUS TIME--COMPOSITE PLOTS

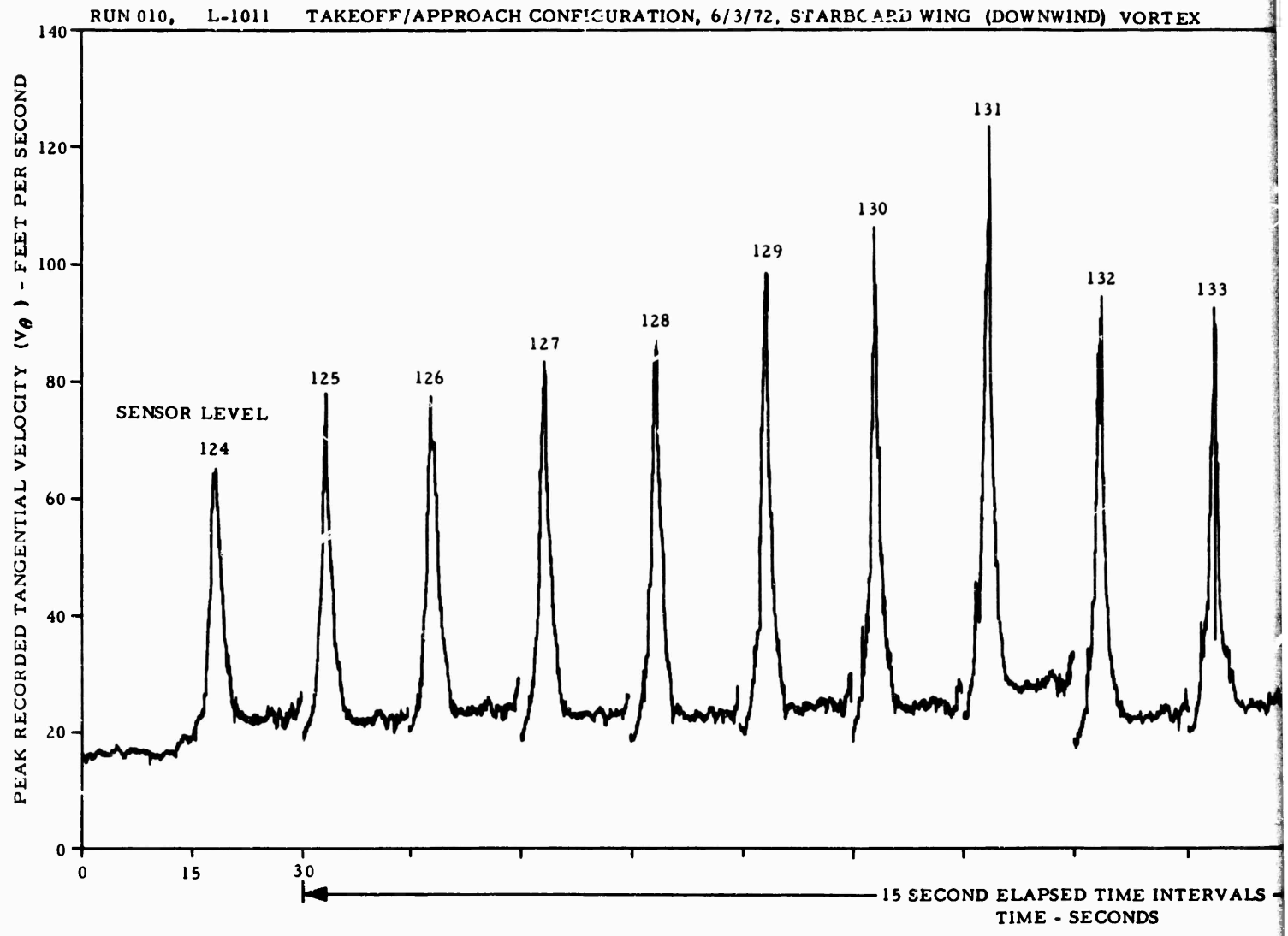
RUN 010, L-1011 TAKEOFF/APPROACH CONFIGURATION, 6/3/72, STARBOARD WING (DOWNWIND) VORTEX
PEAK RECORDED TANGENTIAL VELOCITY (V_θ) - FEET PER SECOND
140
120
100
80
60
40
20
0
SENSOR LEVEL
124
125
126
127
128
129
130
131
132
133
0
15
30
15 SECOND ELAPSED TIME INTERVALS
TIME - SECONDS

D WING (DOWNWIND) VORTEX

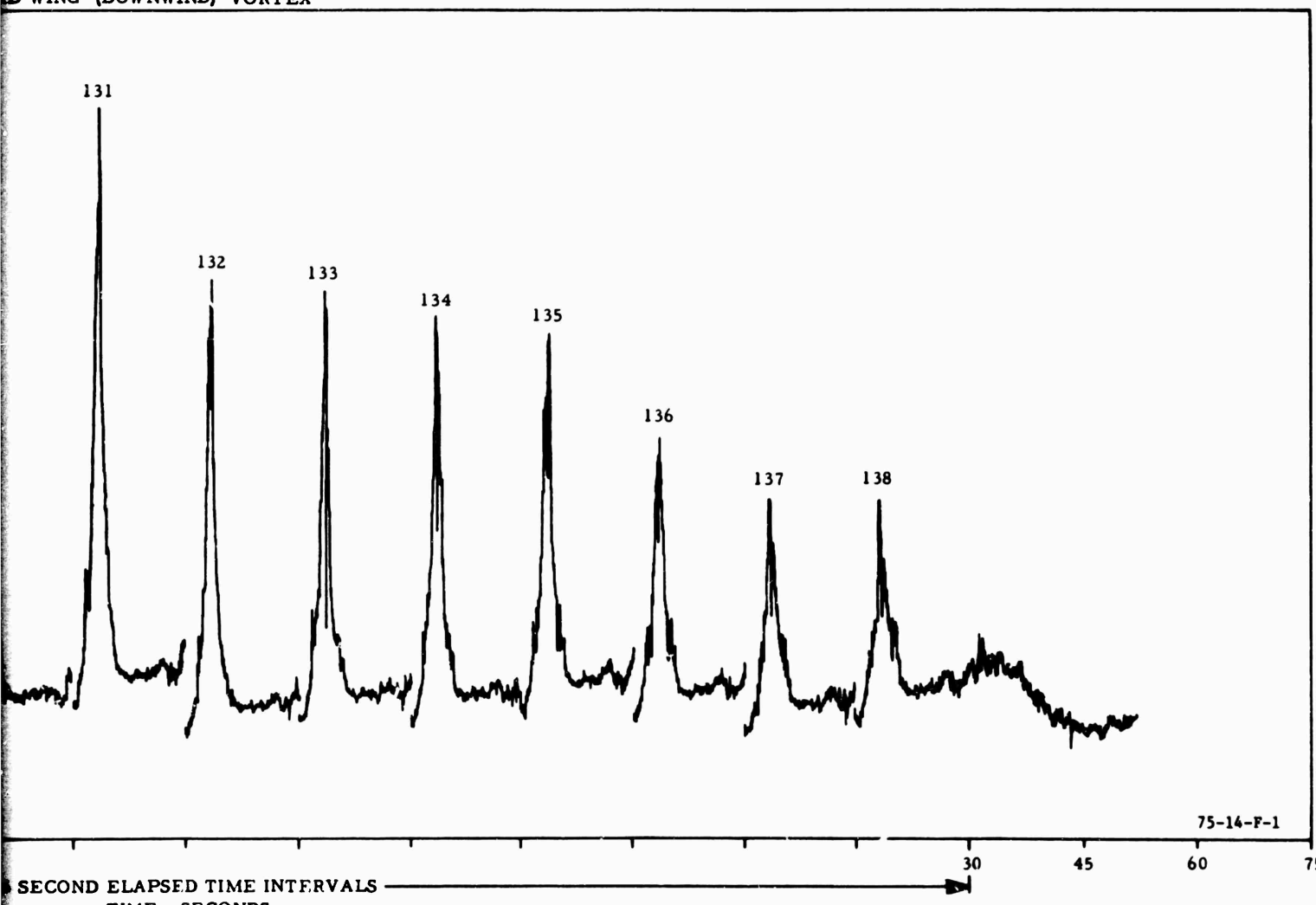

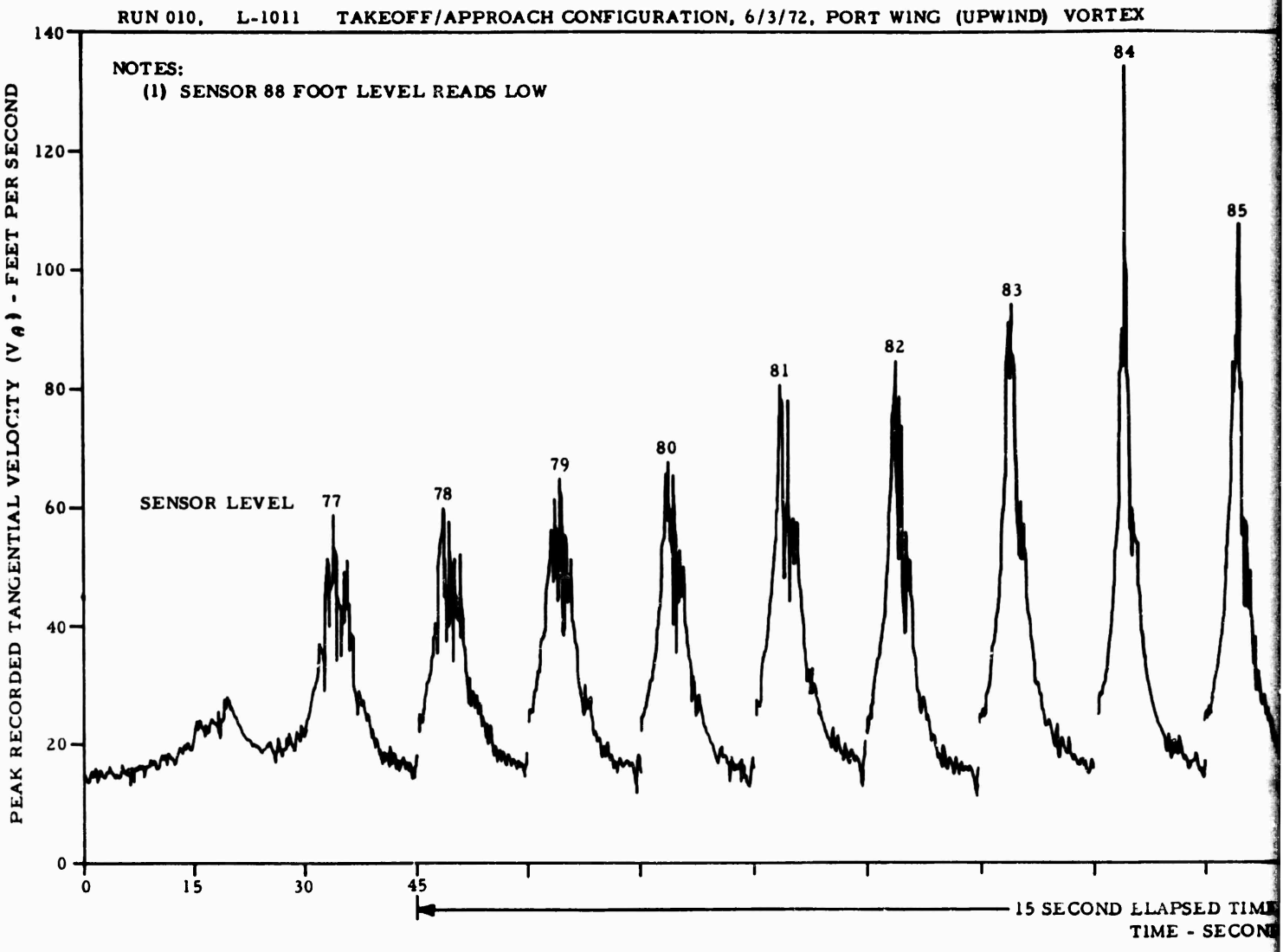
RUN 010, L-1011 TAKEOFF/APPROACH CONFIGURATION, 6/3/72, PORT WING (UPWIND) VORTEX
NOTES:
(1) SENSOR 88 FOOT LEVEL READS LOW
PEAK RECORDED TANGENTIAL VELOCITY (V θ) - FEET PER SECOND
SENSOR LEVEL
77
78
79
80
81
82
83
84
85
0
20
40
60
80
100
120
140
0
15
30
45
15 SECOND ELAPSED TIME
TIME - SECOND

NG (UPWIND) VORTEX

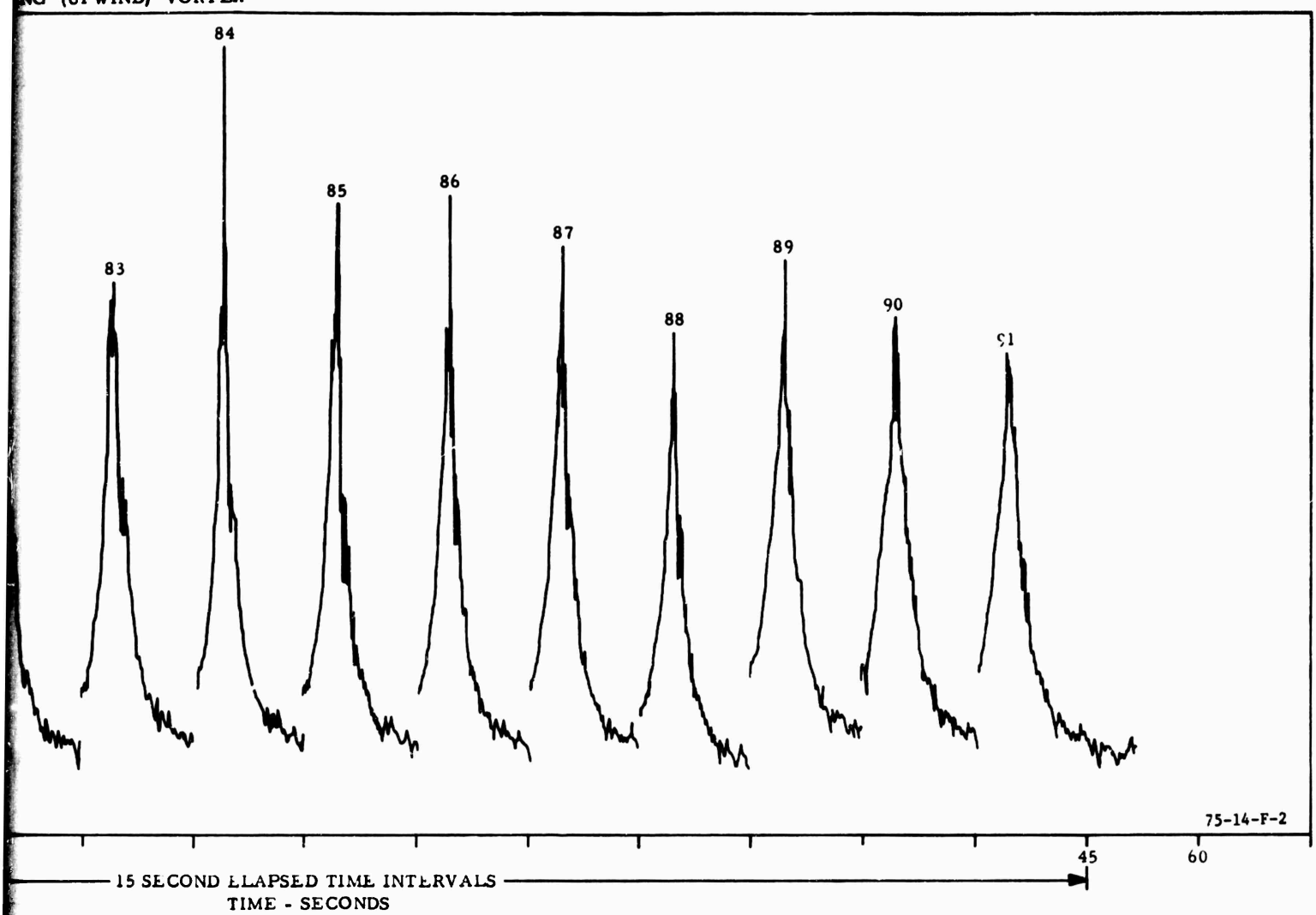

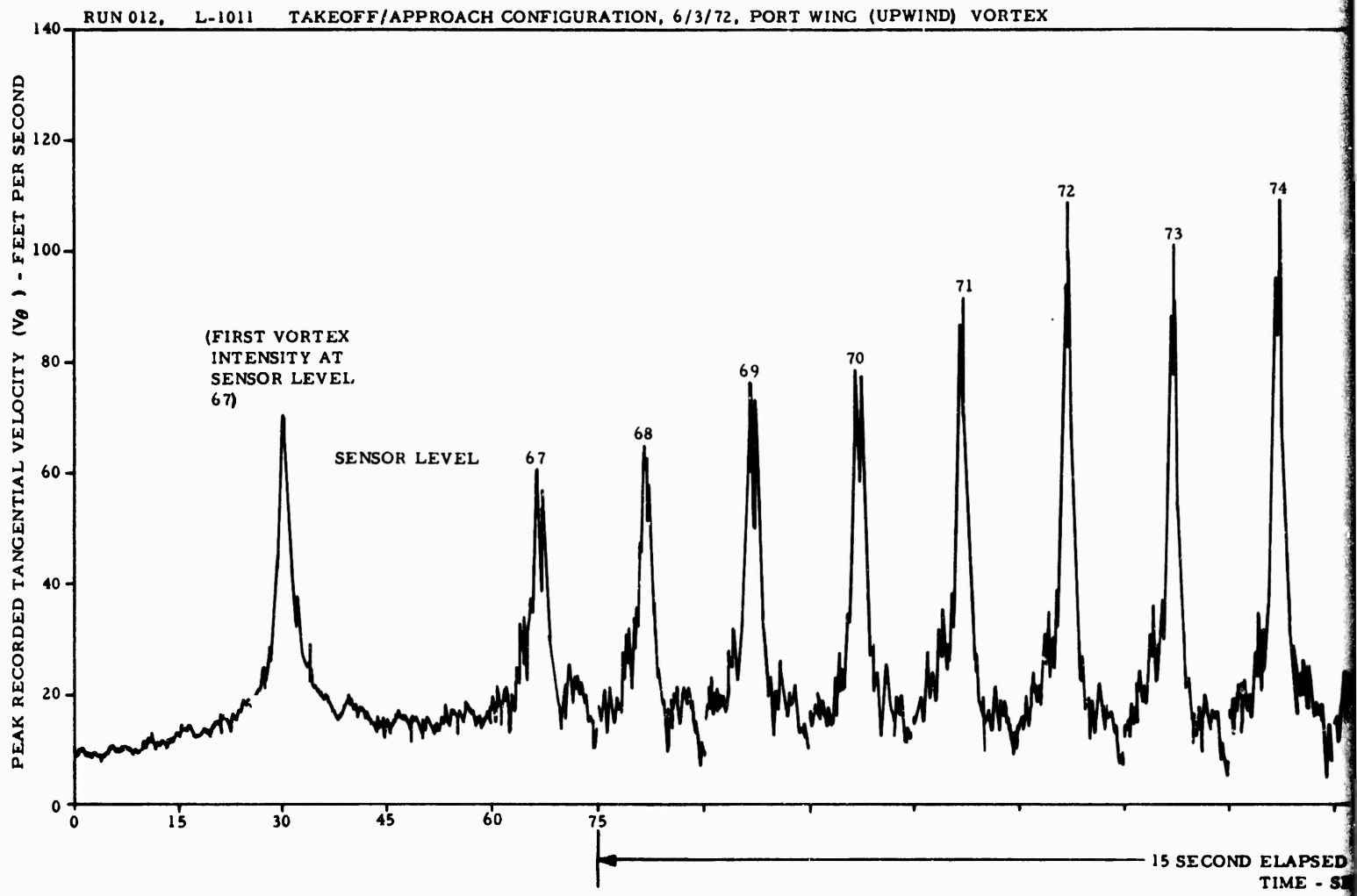
RUN 012, L-1011 TAKEOFF/APPROACH CONFIGURATION, 6/3/72, PORT WING (UPWIND) VORTEX
PEAK RECORDED TANGENTIAL VELOCITY (Vθ) - FEET PER SECOND
140
120
100
80
60
40
20
0
0
15
30
45
60
75
(FIRST VORTEX INTENSITY AT SENSOR LEVEL 67)
SENSOR LEVEL
67
68
69
70
71
72
73
74
15 SECOND ELAPSED
TIME - SE

ORTEX

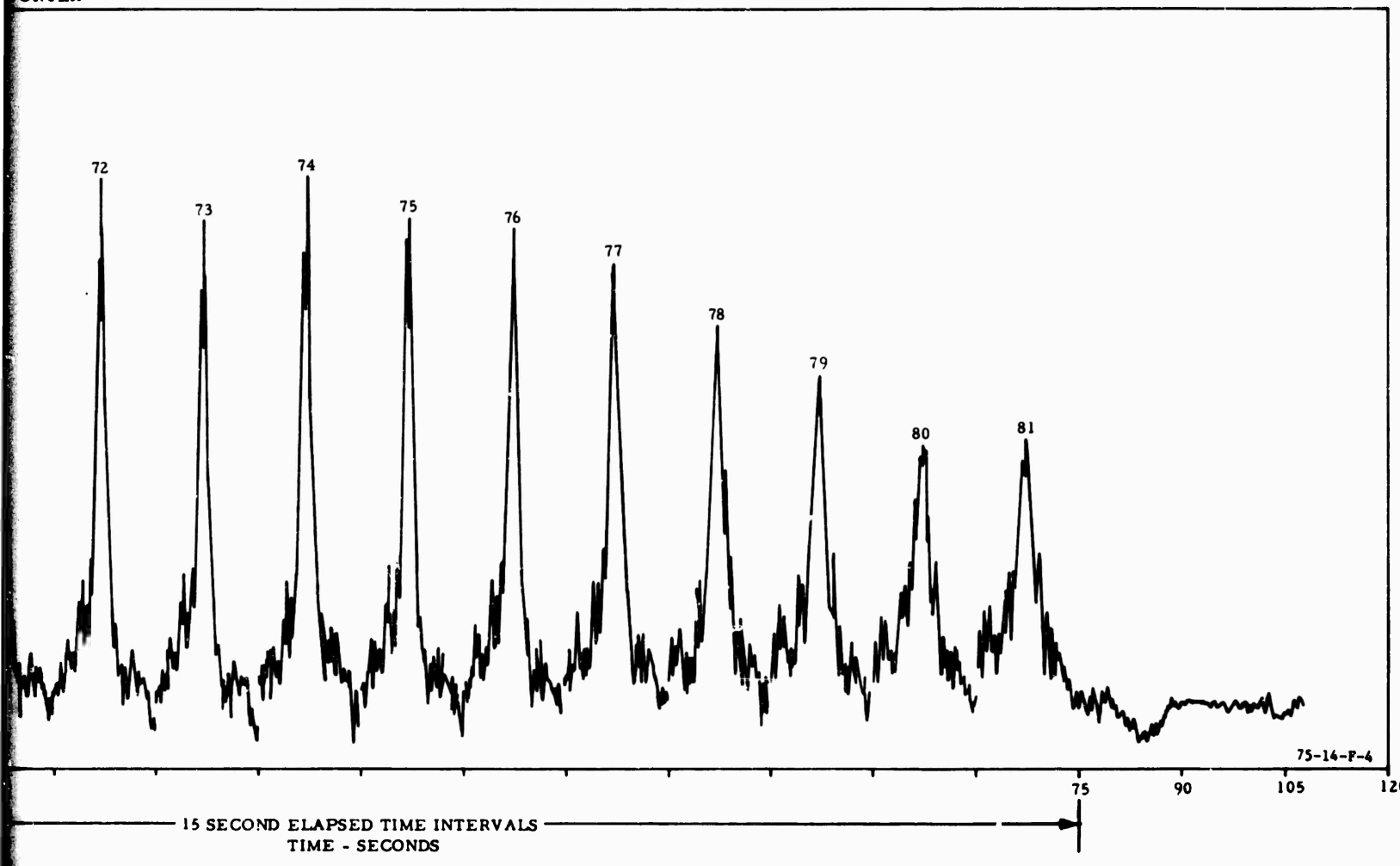
72
73
74
75
76
77
78
79
80
81
75-14-F-4
75
90
105
120
15 SECOND ELAPSED TIME INTERVALS
TIME - SECONDS

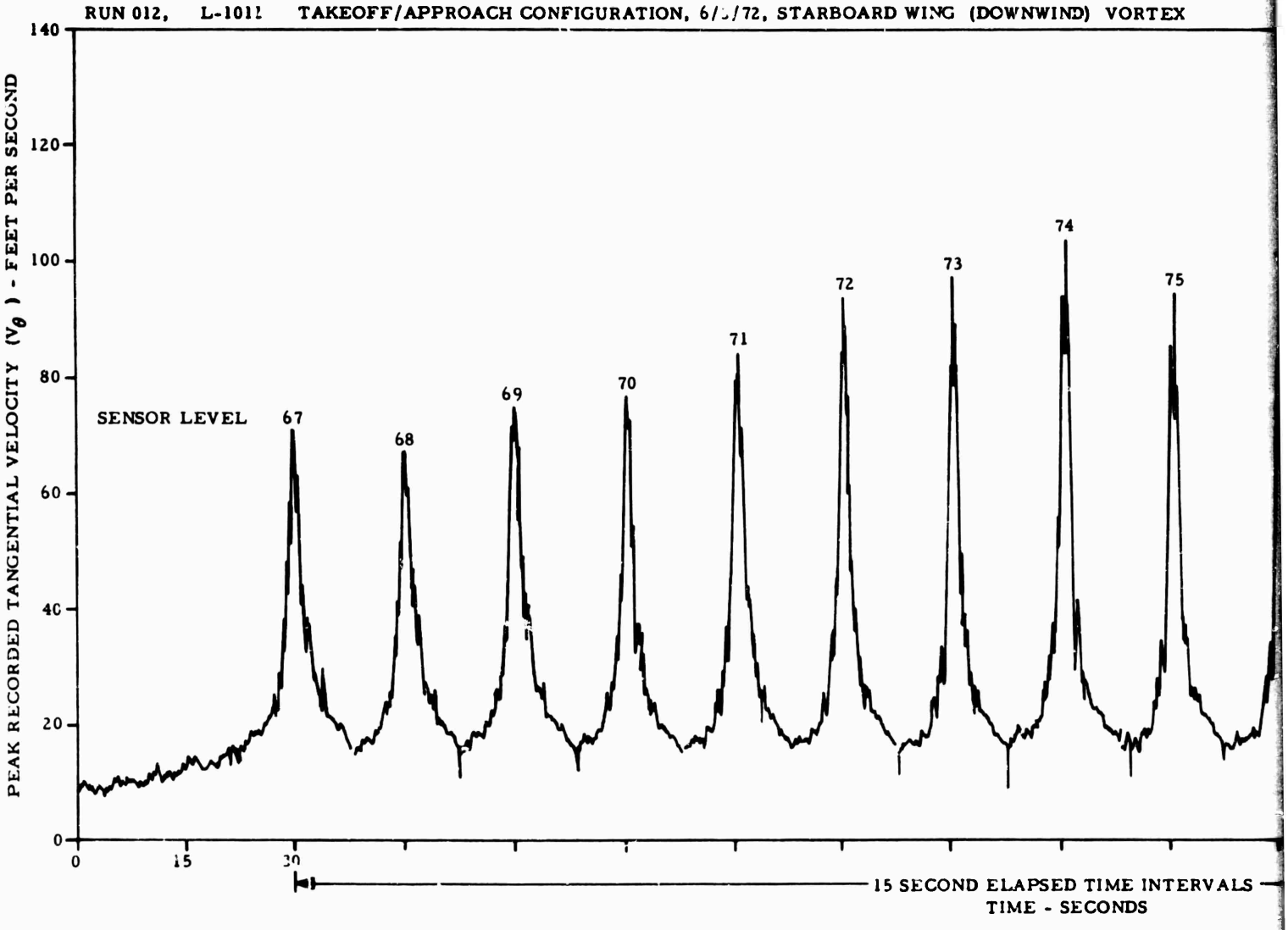
RUN 012, L-1011 TAKEOFF/APPROACH CONFIGURATION, 6/2/72, STARBOARD WING (DOWNWIND) VORTEX
PEAK RECORDED TANGENTIAL VELOCITY (V_θ) - FEET PER SECOND
140
120
100
80
60
40
20
0
SENSOR LEVEL
67
68
69
70
71
72
73
74
75
0
15
30
15 SECOND ELAPSED TIME INTERVALS
TIME - SECONDS

RD WING (DOWNWIND) VORTEX

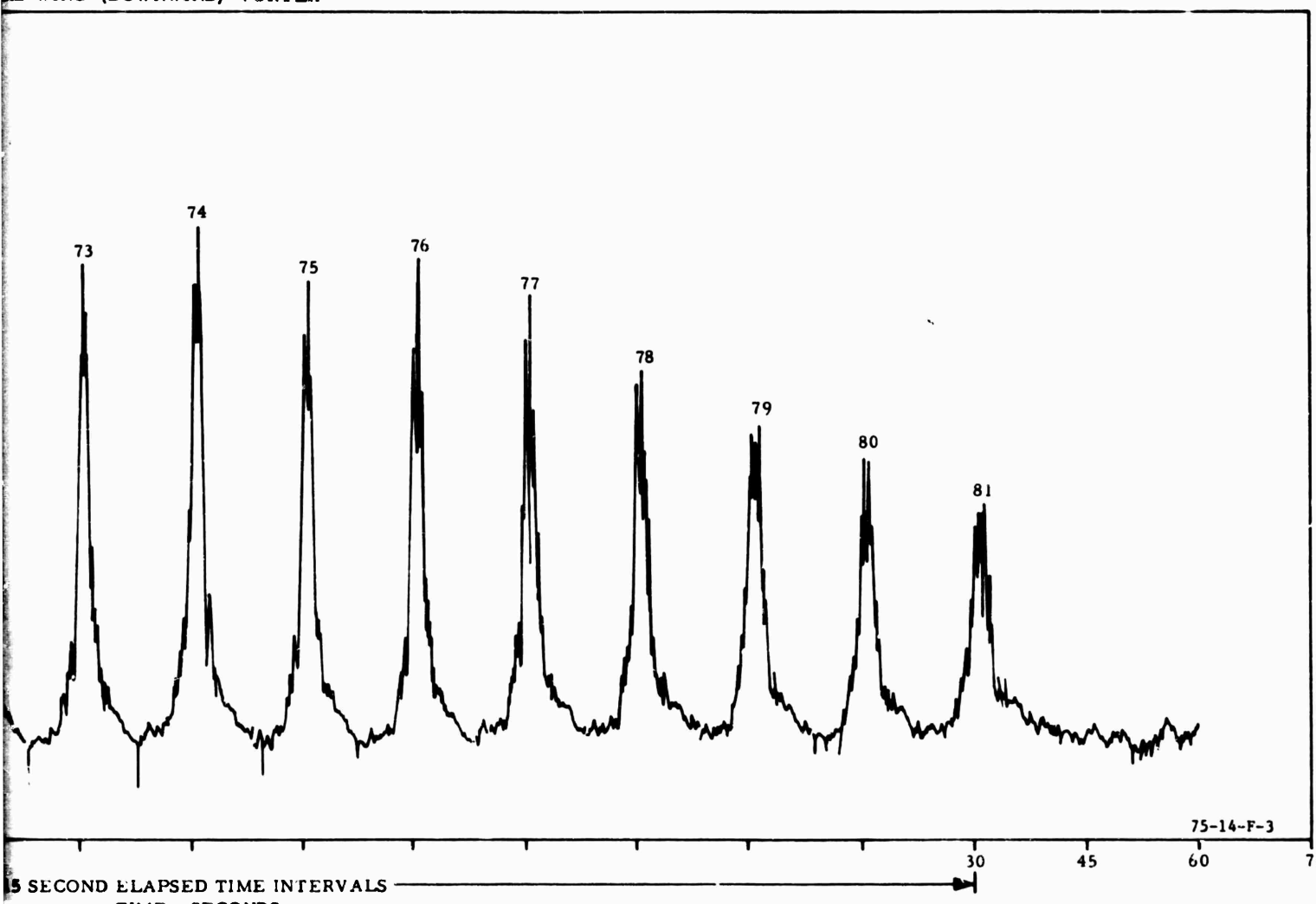

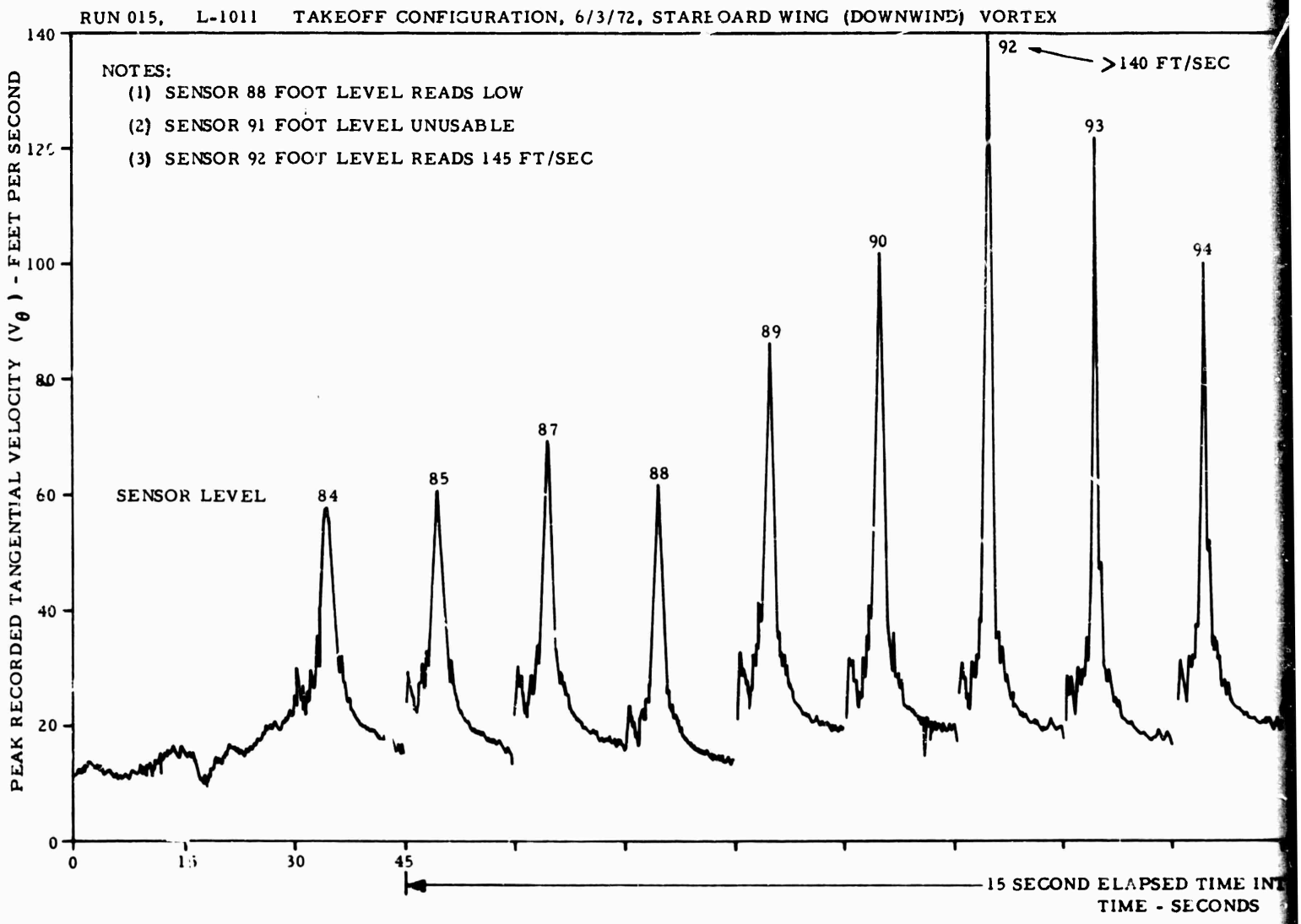
RUN 015, L-1011 TAKEOFF CONFIGURATION, 6/3/72, STARBOARD WING (DOWNWIND) VORTEX
NOTES:
(1) SENSOR 88 FOOT LEVEL READS LOW
(2) SENSOR 91 FOOT LEVEL UNUSABLE
(3) SENSOR 92 FOOT LEVEL READS 145 FT/SEC
PEAK RECORDED TANGENTIAL VELOCITY (V_θ) - FEET PER SECOND
140
120
100
80
60
40
20
0
SENSOR LEVEL
84
85
87
88
89
90
92
>140 FT/SEC
93
94
0
15
30
45
15 SECOND ELAPSED TIME INT
TIME - SECONDS

IND) VORTEX

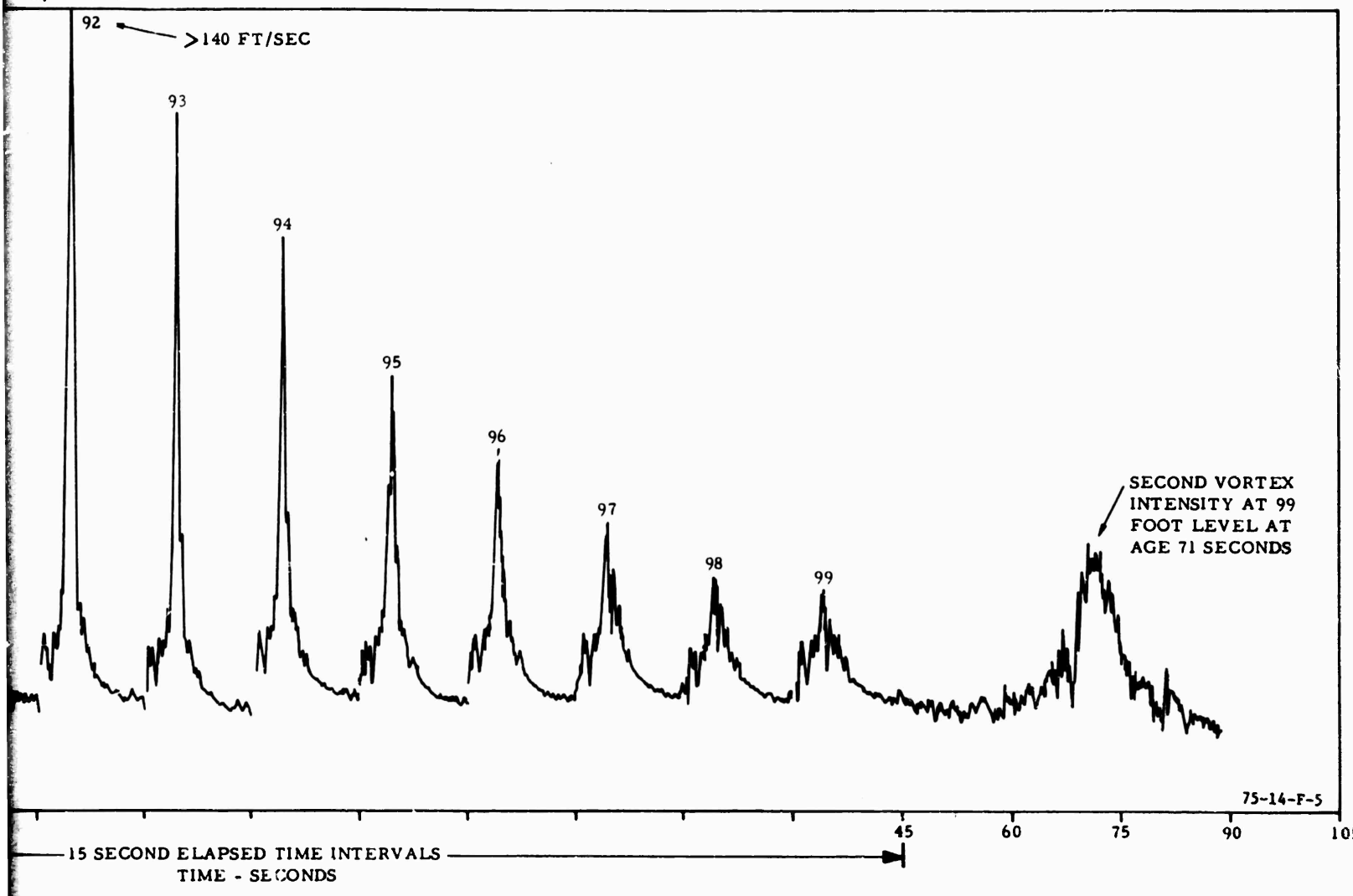
92
>140 FT/SEC
93
94
95
96
97
98
99
SECOND VORTEX INTENSITY AT 99 FOOT LEVEL AT AGE 71 SECONDS
75-14-F-5
45
60
75
90
105
15 SECOND ELAPSED TIME INTERVALS
TIME - SECONDS

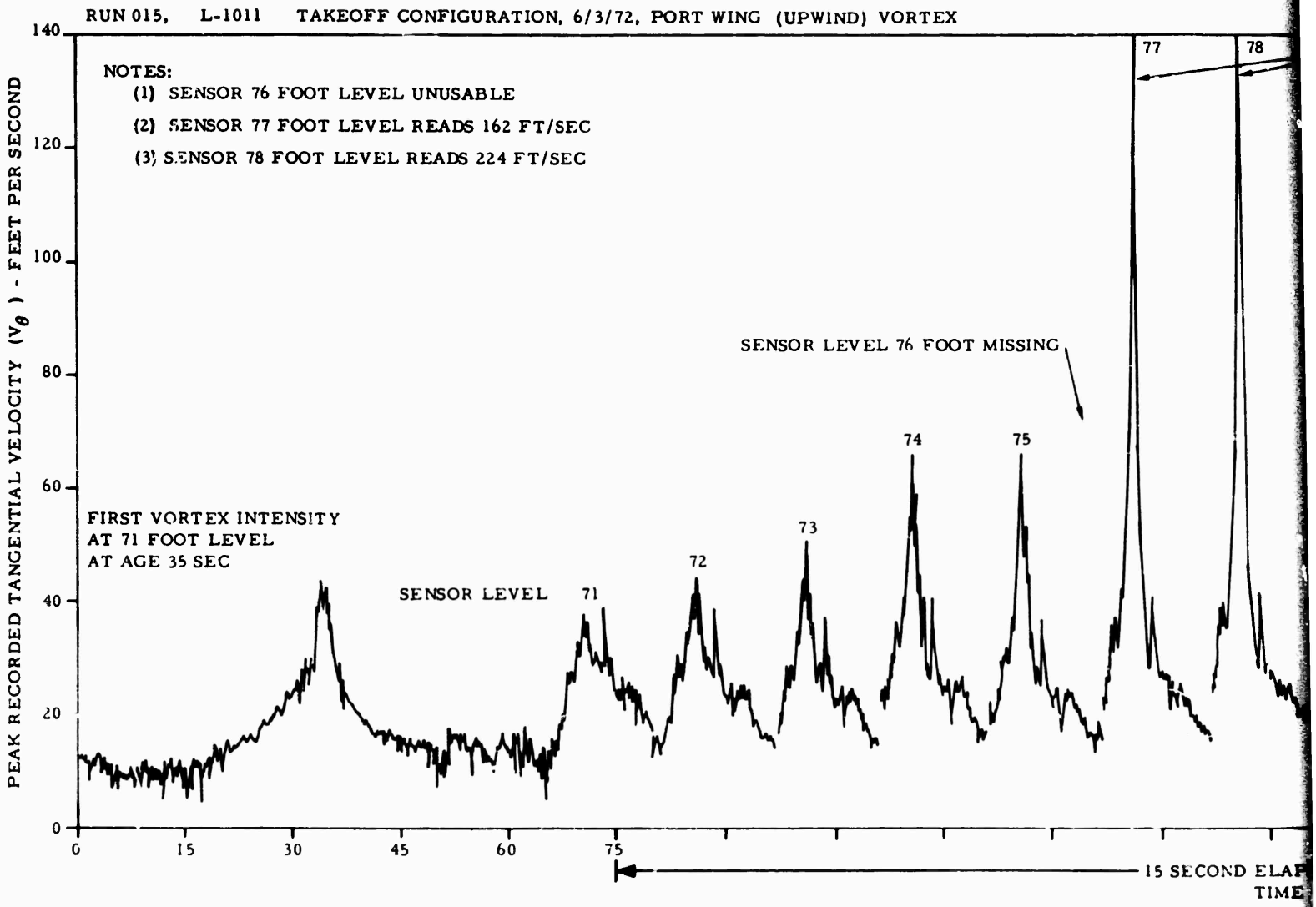
RUN 015, L-1011 TAKEOFF CONFIGURATION, 6/3/72, PORT WING (UPWIND) VORTEX
NOTES:
(1) SENSOR 76 FOOT LEVEL UNUSABLE
(2) SENSOR 77 FOOT LEVEL READS 162 FT/SEC
(3) SENSOR 78 FOOT LEVEL READS 224 FT/SEC
PEAK RECORDED TANGENTIAL VELOCITY (V_θ) - FEET PER SECOND
140
120
100
80
60
40
20
0
0
15
30
45
60
75
SENSOR LEVEL 76 FOOT MISSING
FIRST VORTEX INTENSITY
AT 71 FOOT LEVEL
AT AGE 35 SEC
SENSOR LEVEL
71
72
73
74
75
77
78
15 SECOND ELAP
TIME

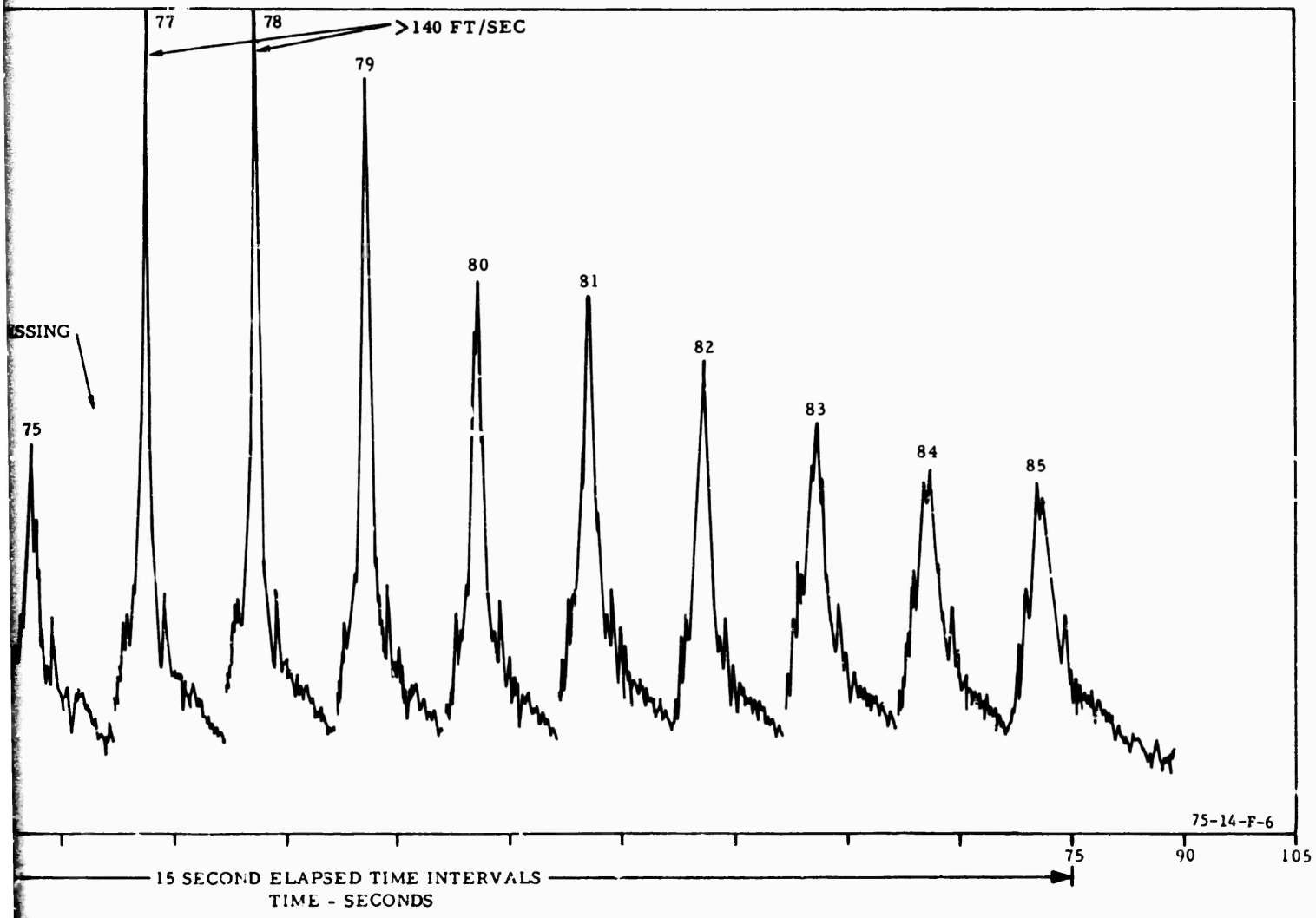
77
78
>140 FT/SEC
79
80
81
82
83
84
85
ISSING
75
75-14-F-6
75
90
105
15 SECOND ELAPSED TIME INTERVALS
TIME - SECONDS

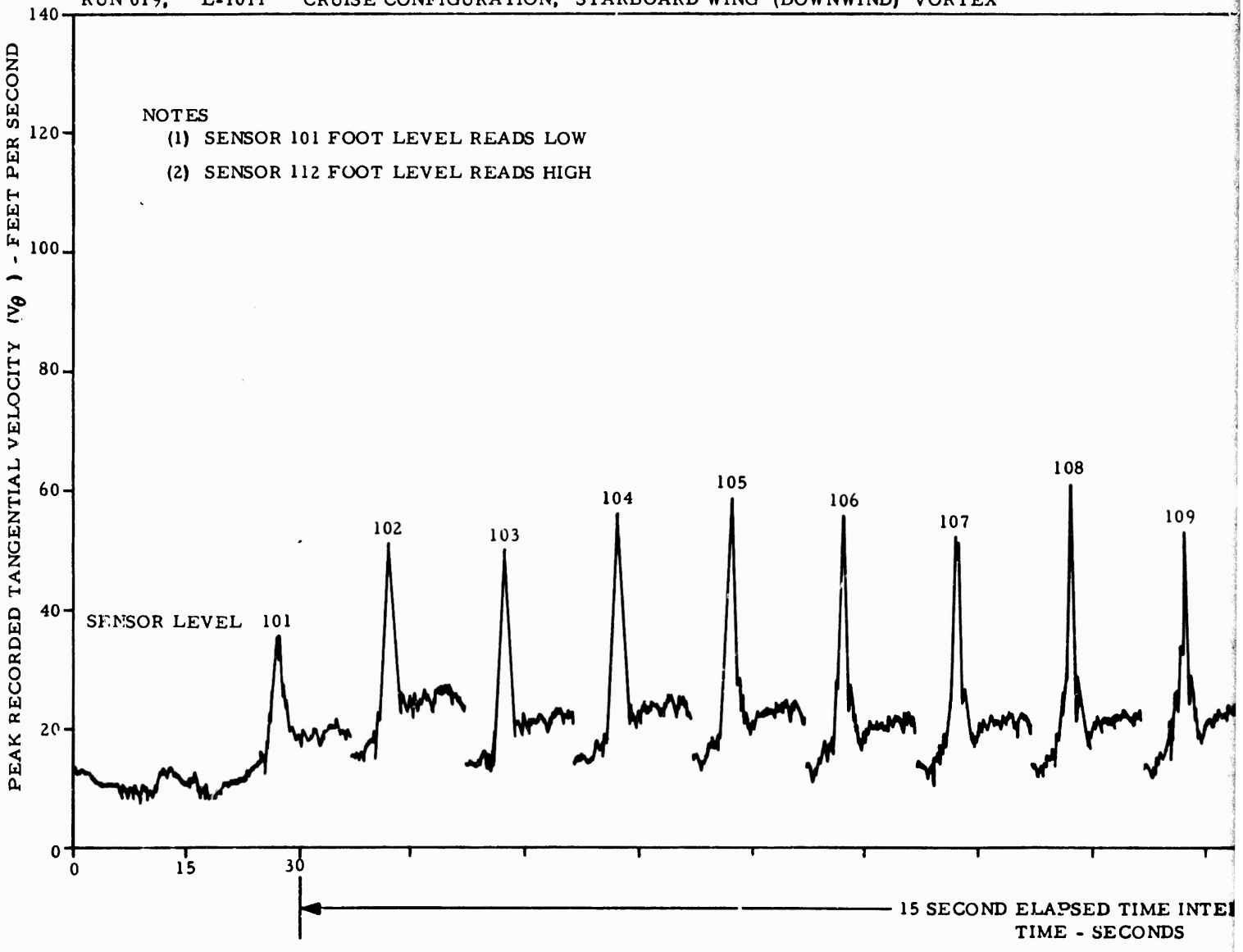
RUN 019, L-1011 CRUISE CONFIGURATION, STARBOARD WING (DOWNWIND) VORTEX
NOTES
(1) SENSOR 101 FOOT LEVEL READS LOW
(2) SENSOR 112 FOOT LEVEL READS HIGH
PEAK RECORDED TANGENTIAL VELOCITY (Vθ) - FEET PER SECOND
140
120
100
80
60
40
20
0
SENSOR LEVEL 101
102
103
104
105
106
107
108
109
0
15
30
15 SECOND ELAPSED TIME INTE
TIME - SECONDS

(IND) VORTEX

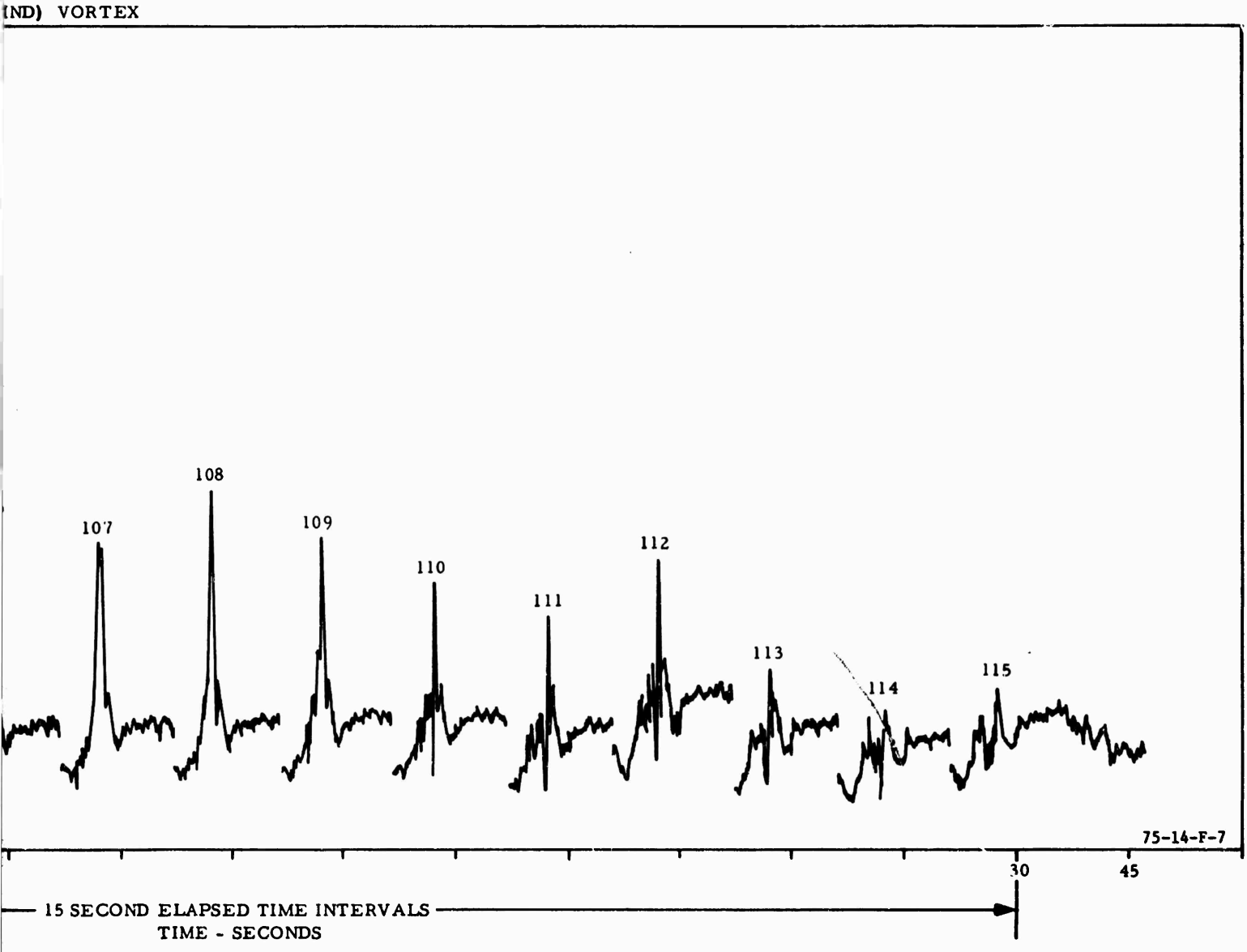
107
108
109
110
111
112
113
114
115
75-14-F-7
30
45
15 SECOND ELAPSED TIME INTERVALS
TIME - SECONDS

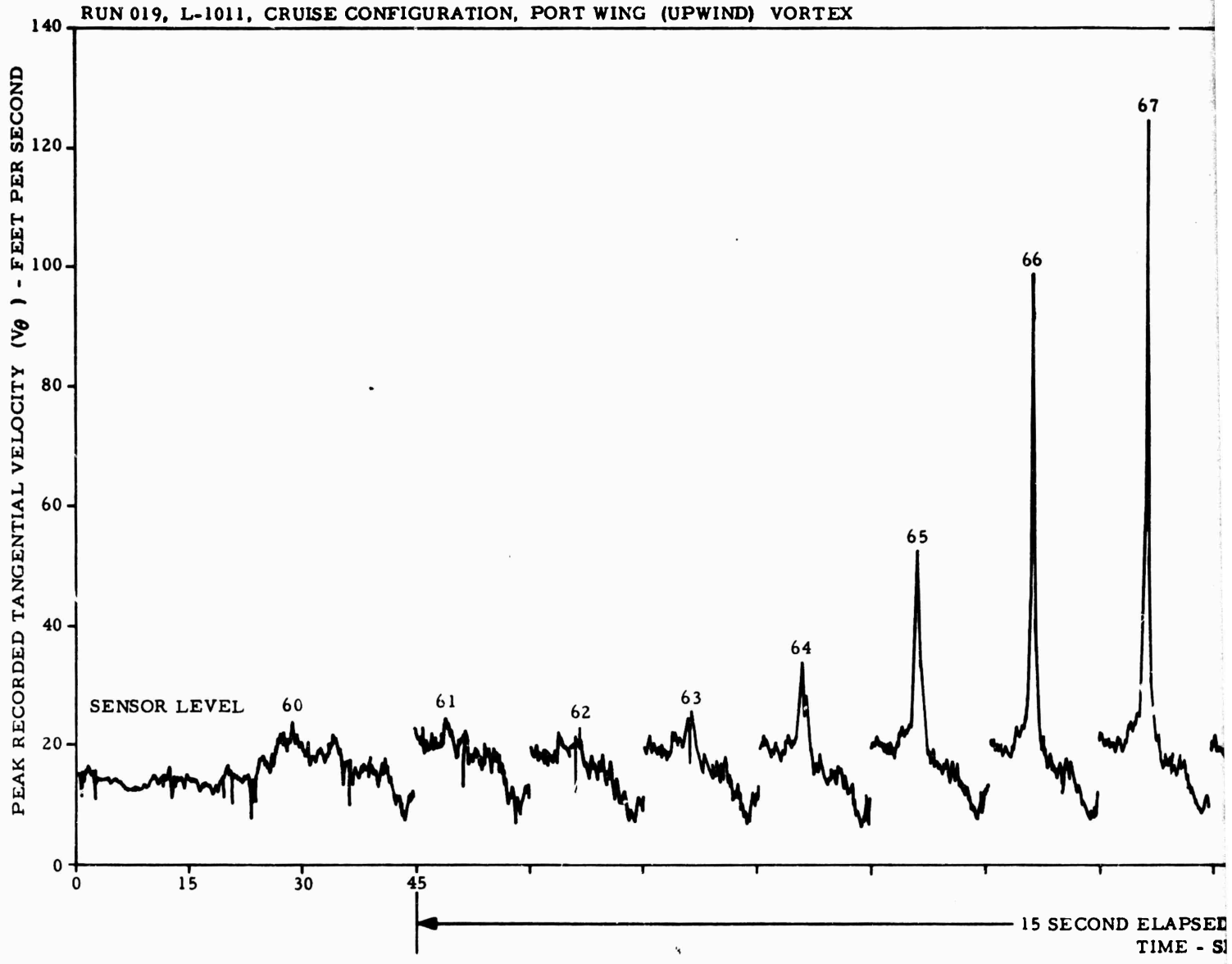
RUN 019, L-1011, CRUISE CONFIGURATION, PORT WING (UPWIND) VORTEX
PEAK RECORDED TANGENTIAL VELOCITY (Vθ) - FEET PER SECOND
140
120
100
80
60
40
20
0
SENSOR LEVEL
60
61
62
63
64
65
66
67
0
15
30
45
15 SECOND ELAPSED
TIME - SI

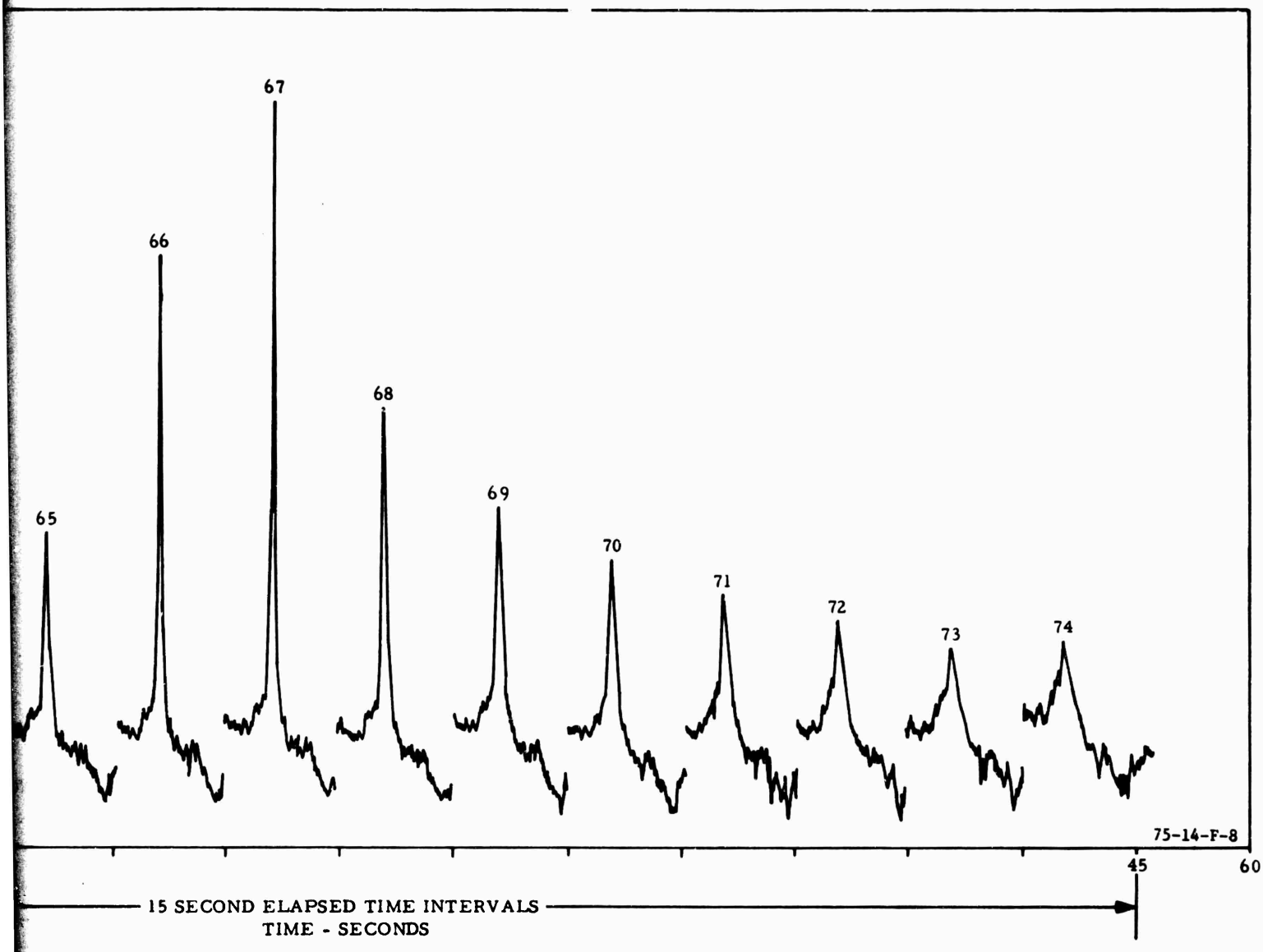
65
66
67
68
69
70
71
72
73
74
75-14-F-8
45
60
15 SECOND ELAPSED TIME INTERVALS
TIME - SECONDS

APPENDIX G

LOW-ALTITUDE METEOROLOGICAL DATA

L1011 METEOROLOGICAL DATA
Run 1, June 3, 1972

Level (Feet)	Temperature Mean (° C)	Temperature Std. Dev.	Wind Velocity Mean (ft/s)	Wind Velocity Std. Dev.	Wind Direction Mean (Mag. North)	Wind Direction Std. Dev.
23	16.0	0.1	10.8	2.3	287.6	19.0
45	16.6	0.1	10.5	2.1	307.8	13.0
70	17.2	0.1	10.5	2.2	302.7	12.0
100	16.8	0.1	12.1	2.0	309.1	13.4
140	16.9	0.1	16.0	3.2	317.5	10.9

NOTE:

Humidity at 23-foot level. Mean= 97.40, standard deviation 0.32.
Humidity at 140-foot level. Mean= 91.23, standard deviation 0.33.
Number of points used in statistical analysis 1637.

L1011 METEOROLOGICAL DATA
Run 2, June 3, 1972

23	14.5	0.4	0.8	2.2	251.3	21.8
45	14.9	1.6	1.1	2.3	283.6	24.4
70	15.9	0.9	7.7	1.1	281.0	25.1
100	15.7	3.3	10.8	3.7	297.9	22.1
140	16.4	2.8	16.4	3.5	299.9	37.9

NOTE:

Humidity at 23-foot level. Mean= 91.75, standard deviation 10.24.
Humidity at 140-foot level. Mean= 87.76, standard deviation 12.00.

L1011 METEOROLOGICAL DATA
Run 3, June 3, 1972

Level (Feet)	Temperature Mean (° C)	Temperature Std. Dev.	Wind Velocity Mean (ft/s)	Wind Velocity Std. Dev.	Wind Direction Mean (Mag. North)	Wind Direction Std. Dev.
23	14.4	0.1	1.3	0.9	262.6	9.2
45	15.4	0.1	4.6	0.7	288.5	11.0
70	16.3	0.1	7.6	0.5	283.4	4.2
100	16.5	0.1	11.3	0.5	287.3	3.5
140	17.1	0.1	17.0	2.6	295.2	1.5

NOTE:
Humidity at 23-foot level. Mean= 93.93, standard deviation 0.23.
Humidity at 140-foot level. Mean= 88.60, standard deviation 0.27.
Number of points used in statistical analysis 1203.

L1011 METEOROLOGICAL DATA
Run 4, June 3, 1972

23	15.3	0.1	1.2	0.9	261.0	3.2
45	16.0	0.1	5.4	0.5	280.9	5.9
70	16.8	0.1	8.5	0.5	272.5	5.5
100	17.0	0.1	11.6	0.5	280.0	13.1
140	17.5	0.1	15.8	3.0	293.8	1.7

L1011 METEOROLOGICAL DATA
Run 5, June 3, 1972

Level (Foot)	Temperature Mean (° C)	Temperature Std. Dev.	Wind Velocity Mean (ft/s)	Wind Velocity Std. Dev.	Wind Direction Mean (Mag. North)	Wind Direction Std. Dev.
23	15.4	0.1	5.2	0.7	249.5	3.7
45	16.2	0.1	7.8	0.6	268.3	10.2
70	17.0	0.1	10.4	0.7	262.9	5.1
100	17.3	0.1	13.6	2.2	275.8	4.3
140	17.7	0.1	18.4	2.0	284.4	22.1

NOTE:
Humidity at 23-foot level. Mean= 94.59, standard deviation 0.28.
Humidity at 140-foot level. Mean= 84.45, standard deviation 0.49.
Number of points used in statistical analysis 1227.

L1011 METEOROLOGICAL DATA
Run 6, June 3, 1972

23	15.4	5.3	264.0
45	16.2	6.7	272.0
70	16.6	9.0	266.0
100	16.6	12.6	279.0
140	17.4	13.9	268.0

NOTE:
Humidity at 23-foot level. Mean= 86.00.
Humidity at 140-foot level. Mean= 76.00.
Standard deviation not calculated.

L1011 METEOROLOGICAL DATA
Run 7, June 3, 1972

Level (Feet)	Temperature Mean (° C)	Temperature Std. Dev.	Wind Velocity Mean (ft/s)	Wind Velocity Std. Dev.	Wind Direction Mean (Mag. North)	Wind Direction Std. Dev.
23	15.4	0.1	6.4	0.5	260.0	5.9
45	16.5	0.1	8.7	0.6	270.1	2.3
70	17.3	0.1	11.2	0.6	267.1	8.8
100	17.3	0.1	13.7	2.7	277.1	15.8
140	17.8	0.1	20.2	2.0	291.2	7.9

NOTE:
Humidity at 23-foot level. Mean= 91.27, standard deviation 0.31.
Humidity at 140-foot level. Mean= 80.21, standard deviation 0.29.
Number of points used in statistical analysis 1205.

L1011 METEOROLOGICAL DATA
Run 8, June 3,

23	15.7	0.1	5.8	0.9	260.4	6.6
45	16.6	0.1	9.3	0.7	272.8	3.5
70	17.3	0.1	11.7	0.7	268.1	12.9
100	17.3	0.1	14.1	2.1	276.4	14.2
140	17.8	0.1	20.4	2.2	287.6	15.7

NOTE:
Humidity at 23-foot level. Mean= 90.26, standard deviation 0.28.
Humidity at 140-foot level. Mean= 78.72, standard deviation 0.27.
Number of points used in statistical analysis, 1223.

L1011 METEOROLOGICAL DATA
Run 9, June 3, 1972

Level (Feet)	Temperature Mean (° C)	Temperature Std. Dev.	Wind Velocity Mean (ft/s)	Wind Velocity Std. Dev.	Wind Direction Mean (Mag. North)	Wind Direction Std. Dev.
23	16.1	0.1	5.8	0.6	264.2	8.1
45	16.7	0.1	8.3	0.7	274.6	7.2
70	17.4	0.1	10.1	0.8	267.9	10.8
100	17.3	0.1	13.4	2.0	277.5	12.2
140	17.6	0.1	19.1	1.9	287.7	19.1

NOTE:
Humidity at 23-foot level. Mean= 89.97, standard deviation 0.26.
Humidity at 140-foot level. Mean= 78.86, standard deviation 0.27.
Number of points used in statistical analysis, 1241.

L1011 METEOROLOGICAL DATA
Run 10, June 3, 1972

23	16.4	0.1	6.0	0.9	254.0	9.0
45	16.8	0.1	8.2	1.0	271.3	8.1
70	17.3	0.1	9.8	1.1	265.2	8.4
100	17.2	0.1	11.9	1.5	275.6	12.9
140	17.6	0.1	16.7	3.0	285.3	20.2

NOTE:
Humidity at 23-foot level. Mean= 89.81, standard deviation 0.28.
Humidity at 140-foot level. Mean= 79.44, standard deviation 0.28.
Number of points used in statistical analysis, 1217.

L1011 METEOROLOGICAL DATA
Run 11, June 3, 1972

Level (Feet)	Temperature Mean (° C)	Temperature Std. Dev.	Wind Velocity Mean (ft/s)	Wind Velocity Std. Dev.	Wind Direction Mean (Mag. North)	Wind Direction Std. Dev.
23	16.7	0.1	6.2	0.9	241.9	14.1
45	17.0	0.1	7.3	1.2	256.4	7.9
70	17.5	0.1	9.2	1.0	254.1	8.3
100	17.3	0.1	11.2	1.4	269.9	6.9
140	17.4	0.1	13.6	2.6	279.4	23.6

NOTE:
Humidity at 23-foot level. Mean= 89.19, standard deviation 0.27.
Humidity at 140-level. Mean= 80.44, standard deviation 0.28.

L1011 METEOROLOGICAL DATA
Pun 12, June 3, 1972

23	17.1	4.0	230.0
45	17.0	5.2	259.0
70	16.2	8.0	254
100	17.4	9.7	275.0
140	17.3	11.8	265.0

NOTE:
Humidity at 23-foot level. Mean= 82.0.
Humidity at 140-foot level. Mean= 74.0.

L1011 METEOROLOGICAL DATA
Run 13, June 3, 1972

Level (Feet)	Temperature Mean (° C)	Temperature Std. Dev.	Wind Velocity Mean (ft/s)	Wind Velocity Std. Dev.	Wind Direction Mean (Mag. North)	Wind Direction Std. Dev.
23	17.0		6.7		232.0	
45	17.0		7.1		262.0	
70	17.3		8.0		251.0	
100	17.1		9.9		289.0	
140	16.9		11.5		278.0	

NOTE:
Humidity at 23-foot level. Mean= 80.0.
Humidity at 140-foot level. Mean= 74.0.
Standard deviation not calculated.

L1011 METEOROLOGICAL DATA
Run 14, June 3, 1972

23	17.1		4.8		240.0	
45	17.0		4.9		266.0	
70	17.4		7.7		284.0	
100	17.2		10.7		277.0	
140	17.2		12.3		281.0	

NOTE:
Humidity at 23-foot level. Mean= 82.0.
Humidity at 140-foot level. Mean= 74.0.
Standard deviation not calculated.

L1011 METEOROLOGICAL DATA
Run 15, June 3, 1972

Level (Feet)	Temperature Mean (° C)	Temperature Std. Dev.	Wind Velocity Mean (ft/s)	Wind Velocity Std. Dev.	Wind Direction Mean (Mag. North)	Wind Direction Std. Dev.	
23	17.1	0.1	9.1	1.0	233.9	12.3	
45	17.4	0.1	10.0	1.2	248.6	7.3	
70	17.8	0.1	11.3	1.6	311.0	13.1	(Bad Signal)
100	17.5	0.1	12.8	2.6	256.9	6.3	
140	17.5	0.1	14.7	2.0	269.5	9.7	

NOTE:

Humidity at 23-foot level. Mean= 85.35, standard deviation 0.33.
Humidity at 140-foot level. Mean= 81.01, standard deviation 0.24.
Number of points used in statistical analysis,1201.

L1011 METEOROLOGICAL DATA
Run 16, June 3, 1972

23	17.2	0.1	7.0	1.2	246.8	14.9	
45	17.5	0.1	8.2	1.4	260.2	9.6	
70	17.9	0.1	9.6	1.4	146.2	158.6	(Bad Signal)
100	17.6	0.1	11.1	1.6	263.7	7.1	
140	17.5	0.1	12.4	2.2	268.9	21.0	

NOTE:

Humidity at 23-foot level. Mean= 85.07, standard deviation 0.36.
Humidity at 140-foot level. Mean= 81.14, standard deviation 0.25.
Number of points used in statistical analysis, 1207.

L1011 METEOROLOGICAL DATA
Run 17, June 3, 1972

Level (Feet)	Temperature Mean (° C)	Temperature Std. Dev.	Wind Velocity Mean (ft/s)	Wind Velocity Std. Dev.	Wind Direction (Mean (Mag. North)	Wind Direction Std. Dev.
23	17.4		8.2		248.0	
45	17.8		8.2		260.0	
70	18.2		9.2		NR*1	
100	18.1		9.1		261.0	
140	17.9		10.6		263.0	

NOTE:
Humidity at 23-foot level. Mean= 79.0.
Humidity at 140-foot level. Mean=75.0.
Standard deviation not calculated.

*1 Sensor was damaged by a direct vortex hit on earlier run 14.

L1011 METEOROLOGICAL DATA
Run 18, June 3, 1972

23	17.6	0.1	10.0	1.4	242.4	15.5
45	17.9	0.1	10.3	1.9	257.8	7.9
70	18.2	0.1	10.8	2.1	246.5	131.9 (Bad Signal)
100	18.0	0.1	12.2	2.1	267.0	6.4
140	17.9	0.1	13.0	2.0	272.5	22.4

NOTE:
Humidity at 23-foot level. Mean= 83.28, standard deviation, 0.43.
Humidity at 140-foot level. Mean= 80.07, standard deviation, 0.42
Number of points used in statistical analysis, 1201.

APPENDIX H

L1011 AIRCRAFT CHARACTERISTICS

I. FUSELAGE

Length, feet	177.7
Diameter, exterior, inches	235.0

II. WING

A. GENERAL

Span, b, feet	155.3
Area, S, feet^2	3456.0
Aspect ratio, (AR) (b/c)	6.95
Sweepback, 25 percent chord line, degrees	35.0
Wing chord, average, c, feet (=b/AR)	22.3
Wing chord, root, c_r, feet	34.3
Wing chord, tip, c_c, feet	10.3
Taper ratio	0.3

B. FLAPS (Fowler Trailing-Edge Flaps)

(Configuration)

Takeoff, degrees	4, 10, 14, 18, or 22
Holding, degrees	0 and 4
Landing, degrees	42

C. LEADING-EDGE DEVICES

Slats: four outboard of engine, three inboard.

D. SPOILERS

Six on upper surface each wing.

III. ENGINES

Manufacturer	Rolls-Royce
Designation	RB211-22F
Number of engines	3

IV. PERFORMANCE (Airspeeds) (Approximate):

Takeoff, knots	165
Approach to landing, knots	135

V. DESIGN WEIGHTS (Maximum):

Takeoff, pounds	430,000
Landing, pounds	358,000
Wing-loading, pounds/foot^2	123

BASIC EQUATIONS AND DIMENSIONS

L1011 SPANWISE LIFT DISTRIBUTION CALCULATION

$$\int_1^{\eta} \frac{C_L c}{C_{AV}} d\eta = \int_1^{\eta} \frac{C_L c}{C_{AV}} \frac{dy}{b/2} = \int_1^{\eta} \frac{C_L c\, dy}{S/2}$$

$$= \int_1^{\eta} \frac{\text{LIFT/IN}}{q\, S/2}\, dy$$

$$= \frac{S_2}{q\, S/2} \text{ AT } \eta$$

BASIC AIRLOAD $= \frac{S_2}{q\, S/2}$ AT $C_{L_{EXPOSED}} = 0$

ADDITIONAL AIRLOAD $= \frac{S_2}{q\, S/2} C_{L_{EXP.}}$

TO CONVERT FROM NON-DIMENSIONAL DISTRIBUTIONS TO RUNNING ROAD IN LB/IN:

$$S_2/_{IN} = (C_{AV})(q)\left[\frac{C_L c}{C_{L_{EXP}} C_{AV} (C_{L_{EXP}})} + \frac{C_L c}{C_{AV}} @\, C_{L_{EXP}} = 0\right]$$

where

C_{av} = S/b = 267.6 inches
S = Wing Area = 3456 ft^2
b = Wing Span = 1860 in
C_{LExp} = Exposed Wing Lift Coefficient
= $S_{Z_{EXP}}$ + (qS/2)
q = Dynamic Pressure in PSI
η_{BL} = $\frac{\text{Butt Line}}{b/2}$

APPROXIMATE RELATIONS FOR $C_{L_{Exp}}$

$$C_{L_{EXP}} = [C_{L_A} - C_{L_{A-T}}] \frac{C_{L_{EXP}}}{C_{L_{A-T}}} + \Delta C_{L_{EXP}} @\, C_{L_{A-T}} = 0$$

$\delta_F = 0°$, $M = .5$: $C_{L_{EXP}} \approx [C_{L_A} = 0](.81) = .012$

$\delta_F = 26°$, $M = .2$: $C_{L_{EXP}} \approx [C_{L_A} = .100](.75) + .020$

$\delta_F = 42°$, $M = .2$: $C_{L_{EXP}} \approx [C_{L_A} = .162](.59) + .215$